Possibilities of using the genetic algorithms to solve optimization tasks in construction projects

Marek Krajnák
Institute of Civil Engineering Technology and Management; Faculty of Civil Engineering, Technical University of Kosice, Slovakia. E-mail: marek.krajnak@tuke.sk

Summary

Article discusses the use of genetic algorithms to solve optimization problems in construction, focusing on the possibilities and limitations of their use in conditions of construction practice. The genetic algorithms bring new approaches to solutions and provide an interesting alternative to conventional optimization methods. It is an access solution with internal intelligence and ability to improvement. Contribution refers to specific application areas within construction resources optimization to increase efficiency of construction.

KEYWORDS: construction resources optimization, genetic algorithms, construction projects, effectiveness

INTRODUCTION

Currently, the increasingly frequent is use of evolutionary computing or evolutionary algorithms for solving complex mathematical, technical and non-technical problems. These methods, or rather algorithms basically simulate principles of biological evolution. As can be seen in living nature around us, evolution is basically simple, but on the other hand, very robust and powerful optimization tool. Biologists say that is valid for single-celled organisms as well as for most complex organisms consisting of thousands of billions of cells [1].

Genetic algorithms (GAs) are based on biological principles of evolution and provide an interesting alternative to "classic" gradient-based optimization methods. They are particularly useful for highly nonlinear problems and models, whose computation time is not a primary concern. Similar to other search methods they perform better than gradient-based methods in finding a global optimum if a problem is highly nonlinear and features multiple local minima. In general, GAs approach the entire design space randomly and then improve the found design points by applying genetics-based principles and probabilistic selection criteria [2], [3].

ISSN 2285-2735, Pages 212 - 219

1. HISTORICAL EVOLUTION OF THE GENETIC ALGORITHMS

Scientists started to deal with these random genetic changes and natural selection and tried to bring these principles to solve practical problems that people face every day. Simulation of thousands to millions of evolutionary cycles, that occur in nature, requiring powerful computers, which in the early development of these methods were not available. Therefore, until the second half of the 20th century began at different locations around the world to solve different problems arise by natural evolution of the different design, but in some respects similar approaches. In Germany in the mid-60th years, Rechenberg and Schwefel have developed in optimizing engineering tasks so. evolutionary strategy. Lawrence Fogel in the U.S. introduced, during modeling and design of machines, a technique called evolutionary programming. As the beginning of genetic algorithms are considered working group led by John Holland of the University of Michigan in the USA in 70s the 20th century [1].

These discoveries, or several others, now cover the concept of evolutionary algorithms. All these approaches have evolved and still evolving and simultaneously influence each other, so the boundaries between them are more and more lost. All have common features, which form the basis of stochastic optimization based on changes in the individual competition and potential solutions. The most popular representative of this group is just genetic algorithms [1].

2. PRINCIPLES OF OPERATION OF THE GENETIC ALGORITHMS

GA is an universal browser and stochastic optimization approach, which is bordered by in the space of admissible solutions to the problem or be able to find at least closer to the global optimum [3] [4]. It shall apply when the nature of the principle of survival of strongest individuals and the necessity of termination the weakest or non-viable [5].

The genetic algorithm works with a group of several potential solutions of the problem - with a population. Each potential solution (also individual) is represented by an ordered set parameters or values that fully describes the properties and of which looking for the best combination. The elements of this set are called genes and can be binary-numeric, integer-numeric, real-number, symbol or mixed type depending on the nature of the problem. They are arranged in sequence, called a string or chromosome [6].

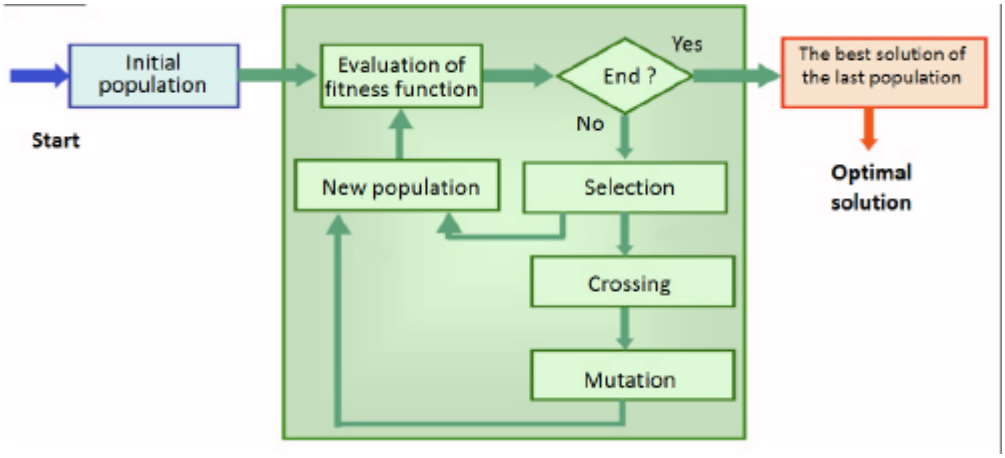

Figure 1: Block diagram of the genetic algorithm [8]

2.1 Operators of the GAs

The initial population of strings in the first calculation cycle (first generation) is obtained by randomly generating of genes within the planned boundaries. For each solution, which is decoded from the string into an existing computer model to quantify the calculation, is needed to determine value of objective function - fitness. Fitness is actually a measure of success or suitability of the string.

Another definition describes the objective function as an objective task, expressed by linear form, while the optimum form must ensure selected solution [7].

All individuals of the population compared to each other and then select a group of individuals into an unchanged new population. Also select a second group of individuals, which is designed to innovation by these operators:

- **Selection,**
- **Crossing over,**
- **Mutation.**

Operation of crossing randomly combines genes of two parents. In the ordinary way, crossing the two parent strings divided into one or more random locations and descendants receive alternately every second of the following substrings separated from each parent (Figure 2, Figure 3). Operation of mutation randomly changes the randomly selected genes randomly selected subjects (Figure. 4). Methods for selection of individuals into new populations are also several species differ in degree of preference and way the most successful individuals compared to

randomly selected individuals. The choice of all these genetic operations is influenced by the type of problem solving [5].

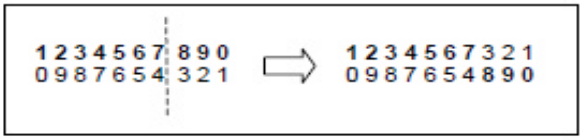

Figure 2: Example of one-point crossing of two integer strings [5]

Figure 3: Example of multi-point crossover of two strings [5]

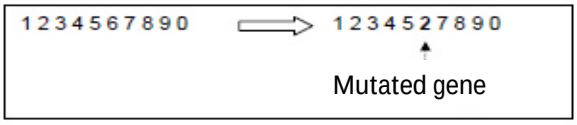

Figure 4: Example of integer string mutation [5]

2.2 Features of the GAs

As can be seen above, the primary usefulness of the GA is that it starts by sampling the entire design space, possibly enabling it to pick points close to a global optimum. It then proceeds to apply changes to the ranked individual design points, which leads to an improvement of the population fitness from one generation to another [2]:

The main advantages of GAs are:

- the nature of the optimization model does not need to be known. This makes GAs very interesting for complex problems or for users inexperienced in gradient-based optimization techniques,
- the optimization model and its constraints do not have to be continuous or even real values. No simplification of a problem is necessary to accommodate it to a particular algorithm (e.g. linearization),
- they are readily available and easily implemented.

The main disadvantages of GAs are:

- a large number of parameters need to be set. This is simplified by information from literature, but problem-specific adjustments might need to be made,
- due to the comparatively very large number of function calls, GAs require significant computational resources. This makes them unattractive for optimization problems with computationally demanding analyses.

3. APPLICATION OF THE GAS IN CONSTRUCTION PROJECTS

As indicated, genetic or evolutionary algorithms can be used to resolve a very wide range of tasks. The condition is the ability to formulate an objective function which is to be minimized or maximized. The minimization is usually to minimize the deviations (errors) from the desired state, minimizing energy consumption, fuel costs or losses, to minimize adverse effects and so on. The maximization can go to maximize efficiency, performance, profits etc. Another condition is the existence of their use of computer optimized representation of the problem. This means that for any point on the search space we can calculate the value of the objective function - evaluate it in terms of success rate in terms of meeting the desired objective [5].

3.1 Dividing of the optimization tasks in construction projects

There are several studies on distribution of optimization problems, in this paper are divided optimization problems based on economic-process model [9]:

- **resource optimization**
  - optimization sub deliveries purchasing,
  - optimization of acquisition costs of material,
  - optimization of storage costs,
  - optimizing purchasing policies,
- **process optimization**
  - optimization of continuous supply of material for construction,
  - optimization of the transfer of masses,
  - optimization of performance standards,
  - optimization of technological processes,

- optimization of organization works,
- optimization of resource consumption standards,

- **optimization of construction products**
  - optimization of the production program,
  - optimization of material composition of structures,
  - optimization of under construction,
  - optimization of construction activities in terms of production costs,
- **optimization of customer**
  - optimization of pricing policy,
  - optimization of marketing,
  - optimization of customer base.

4. ANALYSIS OF AVAILABLE SOFTWARE TOOLS

The following text gradual introduces three different software that use genetic algorithms to solve optimization problems. A common feature is the use of Excel as a workplace.

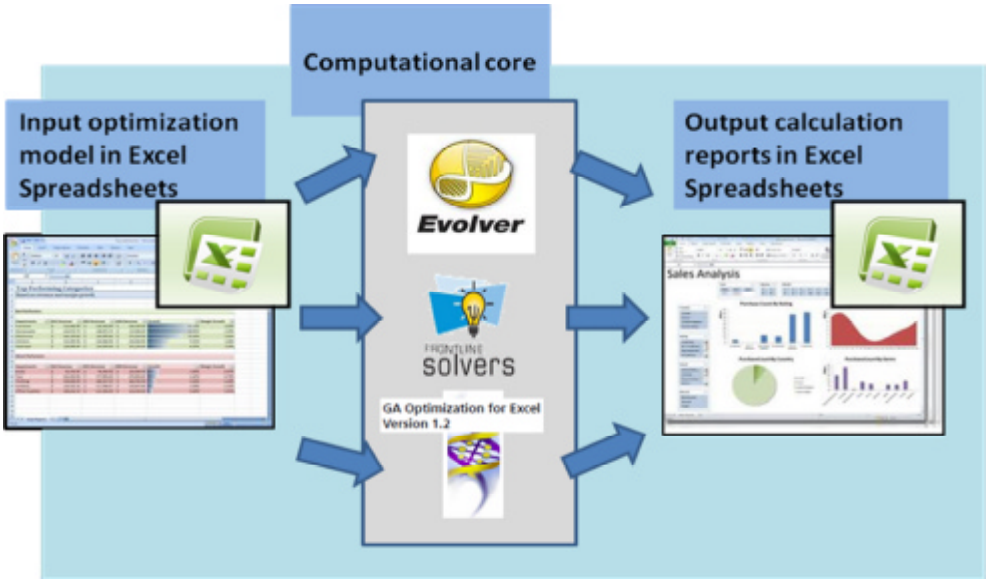

Figure 5: Optimization process using GA software (Source: Author)

4.1 Evolver (from Palisade Corporation)

Evolver is the genetic algorithm optimization add-in for Microsoft Excel. Evolver uses innovative genetic algorithms (GAs) technology to quickly solve optimization problems in finance, distribution, scheduling, resource allocation, manufacturing, budgeting, engineering, and more. Virtually any type of problem that can be modeled in Excel can be solved by Evolver, including previously unsolvable, complex nonlinear problems. Evolver is available by itself or as part of the software package - Decision Tools Suite.

Evolver is available in Professional and Industrial editions. The Professional edition allows up to 250 adjustable variables per model, while the Industrial edition allows unlimited variables. Use Evolver Industrial edition for largest models where we can control hundreds or thousands of adjustable cells [10].

4.2 Solver (from Frontline Systems)

Solver, within the software package Microsoft Office 2010, allows using a genetic algorithm, in addition linear and nonlinear algorithms that were available in earlier versions. Like Evolver uses the solver to work full compatibility with Excel. By means of solver can find the optimum (maximum or minimum) value of the formula in one cell (called the target cell) under the restrictions of values of other cells with formulas in the worksheet. Solver works with a group of cells called the decision variables or variable cell calculations involved in target cells and cells with a restriction. Solver adjusts the values in the cells of the decision variables so as to not exceed the limits in the cells with the restrictions and to obtain the desired result for the target cell [11].

4.3 GA Optimization for Excel (from A. Schreyer)

This program allows the user to take an Excel spreadsheet with any type of calculation data (no matter how complex) and optimize a calculation outcome (e.g. total cost). This is based on the selection of up to five design variables and up to five constraints. The optimization can be performed as maximization, minimization or the attempt to reach a target value. Applications for this technique lie in every field of work. If the problem can be modeled in Excel, it can be optimized using this program. The main advantage of this program is that it can solve highly nonlinear problems or problems that feature discontinuous functions. The software is the result of a term project in a class on engineering design optimization [12].

CONCLUSION

Genetic algorithms are powerful and perspective optimization tool, which uses the popularity and now clearly rising. It is a time and computationally consuming approach, but the current trend growth performance computing, this factor loses significance. In addition, GAs do not impose great demands on the user. They are quite able to solve a variety of universal problems, which can replace the need for knowledge of many other optimization methods and area of optimization of construction projects is an area where it could be the potential of these advanced methods fully exploited.

Contribution was written within the implementation of the project VEGA 1/0840/11 Multi-dimensional approaches to support integrated design and management of construction projects.

References

1. Špacek, J.: Concurrent Engineering. *Optimizing the implementation of PLM systems to companies using genetic algorithms.* Brno: Vysoké ucení technické v Brne, Fakulta strojního inženýrství, 2006. 26 s.
2. Schreyer, A.: *GA Optimization for Excel Version 1.2. Genetic Algorithm Optimization in Excel Spreadsheets. Quick Start Manual.* 2006. available on the Internet: http://www.alexschreyer.net/blog/wp-content/uploads/2006/12/ga_optimization_for_excel_1_2.pdf
3. Goldberg, D.: *Genetic Algorithms in Search, Optimization and Machine Learning*. Addison-Wesley. 1989.
4. Z.Michalewicz: *Genetic Algorithms+Data Structures=Evolutionary Programs*. Springer, 1996
5. Sekaj, I., Foltin, M.: *Matlab Toolbox – Genetické algoritmy. STU Bratislava.*
6. Sekaj, I.: *Riešenie problémov pomocou genetických algoritmov.* Automatizace, vol. 47, 2004, No. 9, p. 552-555.
7. Bašková, R.: *Modelovanie procesov výstavby. Ekonomicko-matematické metódy – cast I. Lineárna optimalizácia a sietová analýza*. Košice: SvF -TU Košice: október 2004. 150 s.
8. http://www.posterus.sk/?p=3364
9. Mesároš, F., Mesároš P.: *Process oriented approach on optimization of construction works costs.* In: Ekonomika a manažment podniku. - ISSN 1336-4103. - Roc. 5, c.1, 2007. s.74-84.
10. http://www.palisade.com/devkits/edk.asp
11. http://office.microsoft.com/sk-sk/excel-help/definovanie-a-riesenie-problemu-pouzitim-riesitela-HP010342416.aspx
12. http://www.alexschreyer.net/projects/xloptim/
13. Bašková, R., Spišáková M.: *Diagram for leveling Formwork.* In: Selected Scientific Papers: Journal of Civil Engineering. - ISSN 1336-9024. - Roc. 5, c. 1 (2010), s. 97-104
14. Bašková, R.: *Dilef method for optimization of formwork.* In: CzechSTAV 2010 : stavební systémy a technologie : sborník príspevku z mezinárodní vedecké konference : 25. - 29.října 2010, Hradec Králové, Ceská republika. - Hradec Králové : Magnanimitas, 2010. - ISBN 978-80-86703-38-1. - P. 118-125

Design of Experiment Application in Thermal Bridges Assessment

Daniel Lepadatu, Adrian Iacob, and Adrian-Alexandru Ciobanu
Department of Civil and Industrial Engineering, Faculty of Civil Engineering and Building Services,"Gheorghe Asachi" Technical University, Iasi, 700050, Romania

Summary

Implementation of Energy Performance of Buildings Directive (EPBD) in national regulations demands an enhancement in envelope thermal efficiency requirements, and implicitly a higher consideration in thermal bridges assessment.

The purpose of this paper is to emphasize the significance of different factors involved in the effect of thermal bridges, subjecting to analysis critical areas of the envelope of prefabricated concrete large-panel apartment buildings.

Values for linear thermal transmittances and temperature factors are obtained by numerical analysis of steady-state bidirectional thermal field, using a heat transfer software. The parameters of thermal bridges are computed for variable values of thermal properties of materials and geometric characteristics of building details.

In order to render guidance for a good practice in building energy audits, a great variety of thermal bridges should be solved, leading to a high amount of work.

This study consists of an analysis of results obtained by numerical simulation, by means of statistical method of investigation. The method is based on an experimental plan, defined by limit values of ranges for factors that influence the energy performance and by the corresponding values for response parameters. Through a nonlinear regression model are established equations in order to determine the response factor for intermediate values of the variable factors. Therefore, a small number of numerical simulations for a type of thermal bridge offers the possibility to solve the more wide series of its configurations.

KEYWORDS: design of experiment, building envelope, thermal bridge, prefabricated concrete large-panel, energy efficiency.

1. INTRODUCTION

Although *Directive 2010/31/EU of the European Parliament and of the Council of 19 May 2010 on the energy performance of buildings* does not include explicit indications upon thermal bridges issue, under this aspect, still proves a great impact through national building codes, which follow European perspectives on energy efficiency. Thus, implementation of Energy Performance of Buildings Directive (EPBD) in romanian national regulations demands an enhancement in envelope thermal efficiency requirements and implicitly a higher consideration in thermal bridges assessment.

A thermal bridge is defined as part of the building envelope where the otherwise uniform thermal resistance is significantly changed and which has a major effect on its thermal performance by giving rise to two- or three-dimensional heat flows (Janssens, 2007). Under the aspect of health and comfort a thermal bridge introduces an area with lower interior surface temperature, where the condensation of indoor moisture causes a high relative humidity, and furthermore the risk of mould growth (Gudum, 2008).

About 70% of apartment blocks in Romania are prefabricated concrete large-panels buildings constructed before 1989, this constructive solution being wide-spread in all eastern and central European states and also in many parts of the Soviet Union, with only a few local changes made (Ilomets *et al.*, 2011). Most of these buildings fail to meet today's energy performance standards, mainly because of low requirements for thermal performance in the previous construction standards and lack of attention to the quality of construction practices.

In energy envelope assessment there are many factors with high influence over thermal analysis results and reduced possibility of being precisely determined, thus giving rise to inaccurate calculation. In order to provide a more comprehensive evaluation of energy performance, there has to be taken into account the uncertainty of input parameters, which implies a lack of information about true value and also variability representing the heterogeneity of parameters (Jaraminiene & Juodis, 2006).

For this reason Design of Experiment method can be a useful tool in the investigation of those parameters. This method was introduced in the '20s by Sir R.A. Fisher, and the agronomists were among the first to understand its practicability. Towards the '60s, due to Taguchi's work, Design of Experiment is implemented in Japanese industry in order to take in consideration processes variance. Afterwards, this method was in the '80s assumed in U.S.A., and also in Europe in the '90s. Design of Experiment is applied to all "black box" phenomena, for which is intended an optimization (Lepadatu *et al.*, 2005; Lepadatu *et al.*, 2006) of response parameter by controlling of input factors.

2. DESIGN OF EXPERIMENT METHOD AND RESPONSE SURFACE METHODOLOGY

2.1. Design of experiments

The optimization process of different quality characteristics of a system is an essential one for every study, if the goal is to answer to the present requirements. This process refers to manipulating the most important process variables to levels or settings that result in the best obtainable set of operating conditions for the system. Response Surface Methodology (RSM) is a collection of mathematical and statistical techniques for empirical model building (Mayer & Montgomery, 1995; Cornell, 1990). The objective of experiments is to optimize a response (output variables) which is influenced by several independent variables (input variables). Originally, RSM was developed to model experimental response (Box *et al.*, 1978) and then migrated into modeling of numerical experiments which are less expensive. The difference is in the type of error generated by the response.

An important and simplified tool of RSM is the Design of Experiments (Box *et al.*, 1978), usually abbreviated as DoE. The objective of DoE is the selection of the point where the response should be evaluated. In a traditional DoE, screening experiments are performed in the early stages of the process, when it is likely that many of the design variables initially considered have little or no effect on the response. The purpose is to identify the design variables that have large effect for further investigation. To construct an approximate model that can capture interactions between N design variables, a full factorial approach (Montgomery, 2001) may be necessary to investigate all possible combinations. A factorial experiment is an experimental strategy in which design variables are varied together, instead one at a time. If the number of design variables becomes large, a fraction of a full factorial design can be used at the cost of estimating only a few combinations between variables. This is called fractional factorial design and is usually used for screening important design variables. Genichi Taguchi, a Japanese engineer, proposed several approaches to experimental designs that are sometimes called "Taguchi Methods." "Taguchi" designs (Taguchi & Konishi, 1987) are similar to our familiar fractional factorial designs. Taguchi introduced a new concept in industrial engineering that changed the way, where scientists reacting to new products. These concepts created a pragmatic approach to developing new products, namely Parameter Design and Tolerance Design (Ross, 1988).

In thermal bridges analysis an Ishikawa diagram (known also as fishbone diagram, or cause-and-effect diagram) presents in Figure 1 some possible causes that influence the response parameters of building junctions.

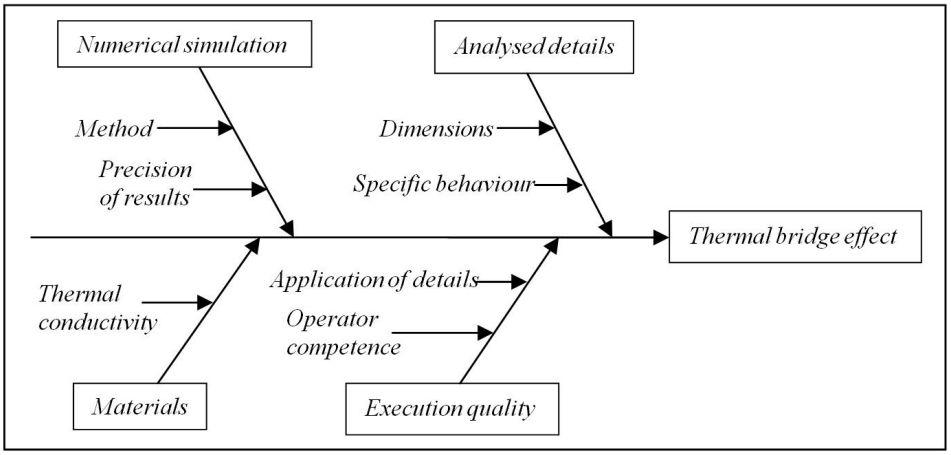

Figure 1. Fishbone diagram of factors affecting errors on thermal bridges.

2.2. Response surface methodology

The Response Surface Methodology (RSM) provides an approximate relationship between a true response *Y* and *p* design variables, which is based on the observed data from the process or system. The response is generally obtained from real experiments or computer simulations, and the true response y is the expected response. Thus, computer simulations are performed in this paper and the true response *y* can be written as:

$$Y = F\left(x_1, x_2, ..., x_p\right) \tag{1}$$

where the variables x_1, x_2, … x_p are expressed in natural units of a measurement, and are therefore called natural variables. The numerically obtained response *Y* differs from the expected value *y* due to random error, *e.*

In many cases, the approximating function F of the true response *y* is normally chosen to be either a first-order or a second-order polynomial model, which is based on Taylor series expansion. In general the second-order model is:

$$Y = b_0 + \sum_{j=1}^{p} b_j x_j + \sum_{j=1}^{p} b_{jj} x_j^2 + \sum_{i<j}^{p} b_{ij} x_i x_j + e \tag{2}$$

where $ß_0$, $ß_j$, $ß_{jj}$ and $ß_{ij}$ are regression factors. For a first-order model with interactions, only $ß_0$, $ß_j$ and $ß_{ij}$ are determined.

3. THERMAL BRIDGES ASSESSEMENT

3.1. Thermal Bridges Subjected to Analysis

Parametric studies were performed for two envelope solutions (Iacob *et al.*, 2011), with external walls (Figure 2) consisted of a load-bearing concrete inner layer, a coating concrete outer layer and autoclaved aerated concrete (AAC), respectively mineral wool (MW) in between.

Figure 2. Configurations of prefabricated concrete large panels:
a. with AAC insulation layer; b. with mineral wool layer.

Main locations of thermal bridges (Ilomets *et al.*, 2011) in apartment buildings composed of prefabricated concrete large panels, which are assessed in this study, are represented in Figure 3, for AAC solution.

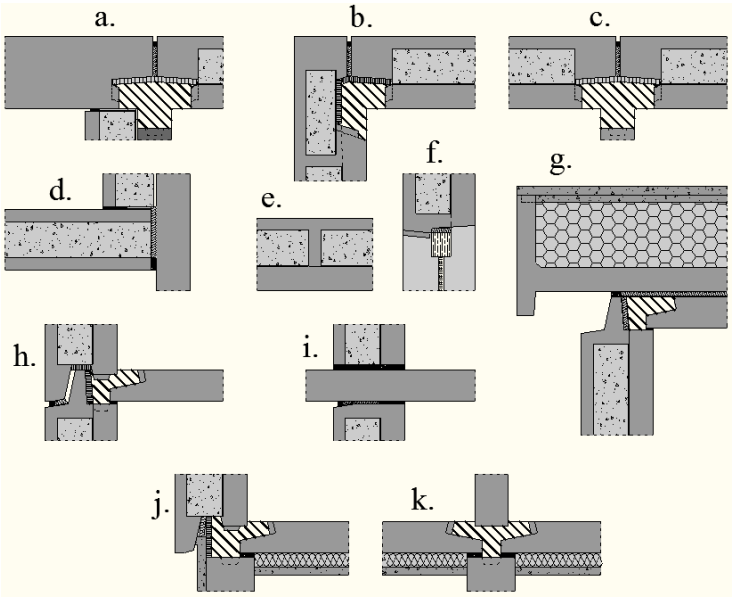

Figure 3. Specific details of thermal bridging: vertical junctions (a, b, c, d, e, f) and horizontal junctions (g, h, i, j, k).

For this configuration of external wall, there were brought a few changes (Figure 4) regarding the continuity of the insulating layer, by inserting thicker layers of polystyrene in wall junctions. The solution with mineral wool, as an improvement of the prefabricated large-panel concept, already had better design details (Figure 5.a).

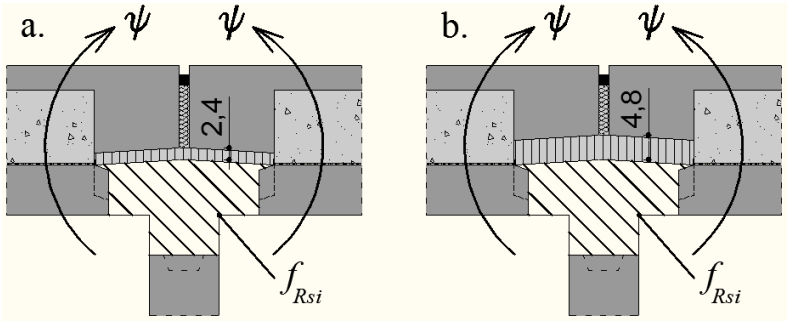

Figure 4. Initial and improved details for an external walls junction.

The major part of the existing building stock was constructed in times with lower requirements for thermal insulation. Therefore, the energy consumption for heating needs to be markedly reduced (Munch-Andersen, 2009).

The most efficient way to improve energy performance of existing buildings is applying exterior insulating layers (Figure 5). Along with hygrothermal aspects of this solution, other advantages that should be mentioned are the absence of another implication upon the interior space and the possibility to reform the aesthetic value of the building.

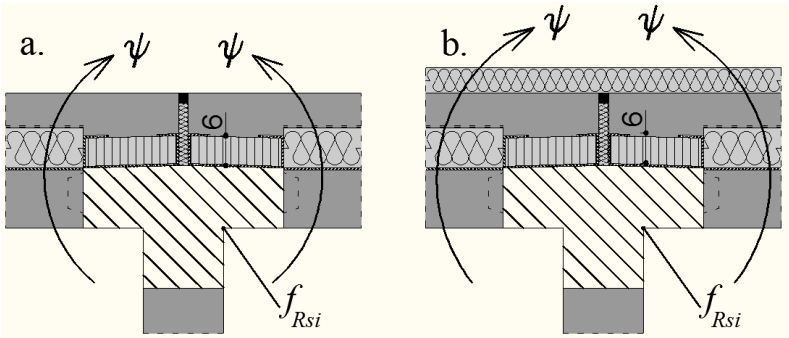

Figure 5. Walls junction details, before and after refurbishment.

3.2. Input factors: envelope design parameters

Building materials can fail meeting the heat conductivity values stated (Jaraminiene & Juodis, 2006), leading to deviations of envelope heat transfer coefficient from its design values. During the service life of a building, materials are exposed to weather conditions, as temperature and moisture, that contribute to its ageing by reductions in thermal resistance.

In Table 1 and Table 2, low and high values of the influential factors are selected for AAC solution, respectively MW solution, taking account of geometric variations from Section 3.1 and uncertainty considering thermal properties of autoclaved aerated concrete, mineral wool, polystyrene in junctions, but also of coating concrete outer layer.

Table 1. Low and high levels of factors – AAC solution

Parameter	Reduced parameter	Low	High
Polystyrene thickness, [cm]	X_1	2.4	4.8
Coating concrete thermal conductivity, [W/mK]	X_2	0.81	2.03
AAC thermal conductivity, [W/mK]	X_3	0.24	0.34
Polystyrene thermal conductivity, [W/mK]	X_4	0.04	0.05
External insulation thickness, [cm]	X_5	0	20

Table 2. Low and high levels of factors – MW solution

Parameter	Reduced parameter	Low	High
Mineral wool thermal conductivity, [W/mK]	X_1	0.042	0.052
Polystyrene thermal conductivity, [W/mK]	X_2	0.04	0.05
External insulation thickness, [cm]	X_3	0	20

The study is carried out by means of steady-state simulations, performed with ANSYS 12 program, obtaining values for surface temperature and values for heat flux corresponding to surfaces with non-adiabatic boundary conditions. With Equations (3) and (4) temperature factor and linear thermal transmittance values are obtained.

$$f_{Rsi} = (q_{si} - q_{out})/(q_{\text{int}} - q_{out}) \tag{3}$$

$$y = (f' - f_u)/l \cdot (q_{\text{int}} - q_{out}) \tag{4}$$

where $?_{si}$, $?_{out}$ and $?_{int}$ represent surface, outer and inner temperatures, measured in $°C$, F' and F_u represent bidirectional heat flux passing through the thermal bridge and unidirectional heat flux passing through the building components in the absence of a thermal bridge, measured in W, and l represents the length of the thermal bridge, measured in m.

The number of simulations depends on the number of parameters. For two levels for each parameter of 11 thermal bridges, the number of simulations is 352 ($11 \cdot 2^5$) for AAC solution and 88 ($11 \cdot 2^3$) for MW solution. In this paper only some significant results are presented.

4. RESULTS AND DISCUSSION

The responses analyzed in the study can be identified by their coded notations: Y_1 (linear thermal transmittance $?_1$), Y_2 (linear thermal transmittance $?_2$) and Y_3 (temperature factor f_{Rsi}).

A standard statistical technique to carry it out, analysis of variance (ANOVA), is currently used to provide a measure of confidence. ANOVA results are given in Tables 3 to 8. This way, the significance of interaction effect of the five factors for AAC solution is expressed through p-value (lack-of-fit probability), which has to be smaller than 0,05, as is set out in the initial assumptions. Interactions with exceeding p-values can therefore be ignored. R-sqr coefficient is a statistical measure and expresses the approximation degree of the mathematical model, which is better as R-sqr value grows to 1. A low R-sqr value indicates that important and sistematic factors where ignored in the regression model. Similarly, adjusted R-sqr coefficient indicates the adjacency between hypothetical and real models.

Table 3. Summary of ANOVA for Y_1 (linear thermal transmittance $?_1$) – horizontal junction *g*, AAC solution

Regr. Coefficients; Var.:Y1; R-sqr=,99997; Adj R-sqr:,99995						
	Regressn - Coeff.	**Std.Err.**	**t(16)**	**p**	**-95,% - Cnf.Limt**	**+95,% - Cnf.Limt**
Mean/Interc.	0,065603	0,007012	9,356	0,000000	0,050739	0,080466
(1)X1	-0,015779	0,000943	-16,734	0,000000	-0,017778	-0,013780
(2)X2	0,057851	0,001882	30,740	0,000000	0,053861	0,061841
(3)X3	0,104559	0,020218	5,172	0,000093	0,061699	0,147418
(4)X4	3,338847	0,144927	23,038	0,000000	3,031616	3,646077
(5)X5	0,001662	0,000117	14,232	0,000000	0,001415	0,001910
1 by 2	-0,000120	0,000140	-0,857	0,404267	-0,000416	0,000177
1 by 3	0,000671	0,001707	0,393	0,699419	-0,002948	0,004290
1 by 4	-0,032524	0,017070	-1,905	0,074867	-0,068710	0,003662
1 by 5	0,000816	0,000009	95,561	0,000000	0,000798	0,000834
2 by 3	-0,010396	0,003358	-3,096	0,006937	-0,017515	-0,003278
2 by 4	-0,086884	0,033580	-2,587	0,019842	-0,158070	-0,015698
2 by 5	-0,002706	0,000017	-161,167	0,000000	-0,002742	-0,002670
3 by 4	-0,130667	0,409673	-0,319	0,753888	-0,999134	0,737801
3 by 5	-0,005343	0,000205	-26,086	0,000000	-0,005778	-0,004909
4 by 5	-0,143440	0,002048	-70,027	0,000000	-0,147782	-0,139098

Table 4. Summary of ANOVA for Y_2 (linear thermal transmittance $?_2$) – horizontal junction g, AAC solution

Regr. Coefficients; Var.:Y2; R-sqr=,99971; Adj R-sqr:,99944						
	Regressn - Coeff.	**Std.Err.**	**t(16)**	**p**	**-95,% - Cnf.Limt**	**+95,% - Cnf.Limt**
Mean/Interc.	0,223924	0,027857	8,0384	0,000001	0,16487	0,282978
(1)X1	-0,023301	0,003746	-6,2197	0,000012	-0,03124	-0,015359
(2)X2	0,108280	0,007477	14,4816	0,000000	0,09243	0,124131
(3)X3	-0,387789	0,080325	-4,8278	0,000186	-0,55807	-0,217508
(4)X4	1,457049	0,575795	2,5305	0,022263	0,23642	2,677681
(5)X5	-0,011567	0,000464	-24,9265	0,000000	-0,01255	-0,010583
1 by 2	-0,000099	0,000556	-0,1776	0,861300	-0,00128	0,001080
1 by 3	0,002992	0,006782	0,4412	0,664964	-0,01138	0,017369
1 by 4	-0,009023	0,067818	-0,1330	0,895819	-0,15279	0,134745
1 by 5	0,001226	0,000034	36,1457	0,000000	0,00115	0,001298
2 by 3	-0,045136	0,013341	-3,3832	0,003792	-0,07342	-0,016854
2 by 4	-0,149352	0,133413	-1,1195	0,279462	-0,43217	0,133470
2 by 5	-0,004005	0,000067	-60,0319	0,000000	-0,00415	-0,003863
3 by 4	-0,233743	1,627635	-0,1436	0,887602	-3,68418	3,216689
3 by 5	0,023308	0,000814	28,6403	0,000000	0,02158	0,025033
4 by 5	-0,052506	0,008138	-6,4518	0,000008	-0,06976	-0,035254

Table 5. Summary of ANOVA for Y_3 (temperature factor f_{Rsi}) – horizontal junction g, AAC solution

Regr. Coefficients; Var.:Y3; R-sqr=,99997; Adj R-sqr:,99995 ual=,0000007						
	Regressn - Coeff.	**Std.Err.**	**t(16)**	**p**	**-95,% - Cnf.Limt**	**+95,% - Cnf.Limt**
Mean/Interc.	0,83913	0,010476	80,0979	0,000000	0,81692	0,861334
(1)X1	0,01142	0,001409	8,1052	0,000000	0,00843	0,014406
(2)X2	-0,05751	0,002812	-20,4505	0,000000	-0,06347	-0,051544
(3)X3	-0,11679	0,030208	-3,8661	0,001368	-0,18083	-0,052750
(4)X4	-1,38857	0,216542	-6,4125	0,000009	-1,84761	-0,929518
(5)X5	0,00693	0,000175	39,7363	0,000000	0,00656	0,007305
1 by 2	0,00028	0,000209	1,3511	0,195468	-0,00016	0,000726
1 by 3	-0,00052	0,002550	-0,2053	0,839890	-0,00593	0,004883
1 by 4	0,00565	0,025505	0,2215	0,827528	-0,04842	0,059716
1 by 5	-0,00059	0,000013	-46,1827	0,000000	-0,00062	-0,000562
2 by 3	-0,00238	0,005017	-0,4750	0,641209	-0,01302	0,008253
2 by 4	0,18254	0,050173	3,6381	0,002214	0,07617	0,288898
2 by 5	0,00232	0,000025	92,3376	0,000000	0,00226	0,002370
3 by 4	0,56517	0,612113	0,9233	0,369560	-0,73245	1,862791
3 by 5	0,00525	0,000306	17,1473	0,000000	0,00460	0,005897
4 by 5	0,03802	0,003061	12,4235	0,000000	0,03153	0,044511

Regression coefficients, obtained with the nonlinear regression model, are directly inserted in Equation (2), which gives predictions upon linear thermal transmittances and temperature factor, for any values of variable factors within the domains of definition.

Standard error of response is the average variability for the regression model at any given value of a factor, used in obtaining the t-ratio, a test statistics that gives more reliance in the regression coefficients as its value is higher.

Confidence limits are expressed in terms of confidence coefficients for the estimate. A narrow interval of ± 95% confidence limits suggests that in 95% of the time the interval will contain the true parameter value.

Pareto charts obtained from the statistical analysis are presented in Figures 6 to 11, and have the role to reveal the importance order of the variables. The charts in Figures 6, 7 and 8 shows the statistical significance of factors and their interactions upon linear thermal transmittances $?_1$ and $?_2$ and temperature factor f_{Rsi}, for AAC solution, at a wall or roof slab connection. X_5, X_2 and X_1 are leading factors in this order, whereas X_4 and X_3 have a lessened influence.

A physical interpretation of results will state that highest effects upon thermal bridges parameters are given by the additional external insulation thickness, the thermal conductivity of the outer layer of concrete and the thickness of polystyrene in the connection area. Furthermore, interactions between external insulation thickness with the other leading factors are shown as relevant, highlighting the importance of relating those three variables in thermal bridges assessment.

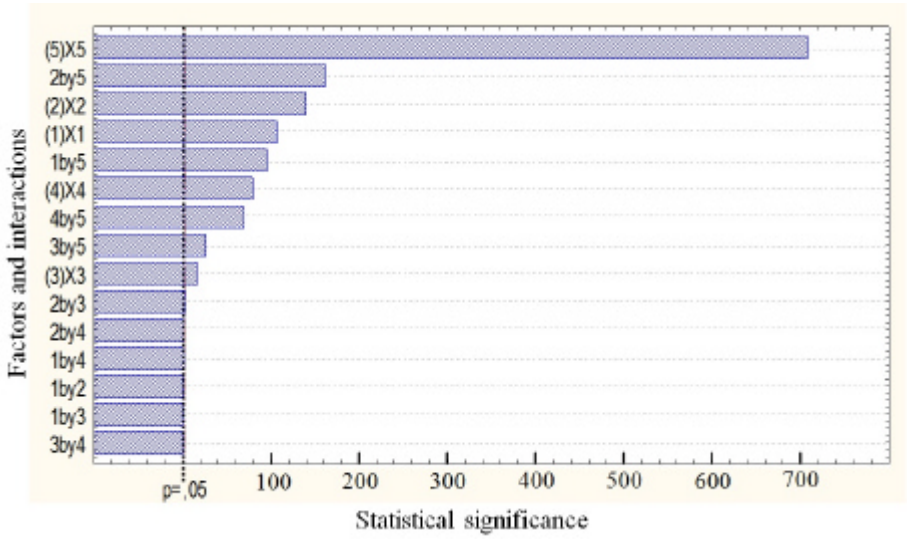

Figure 6. Pareto charts of standardized effect of Y_1 (linear thermal transmittance $?_1$), for horizontal junction *g*, AAC solution.

Although previous statement might be seen as reasonable, it would be misleading to be taken as an absolute truth. Actually, the demonstrated influences are not characteristics of factors, but they reside in their variability. In other words, the range of variance for a specific factor weights in its statistical significance.

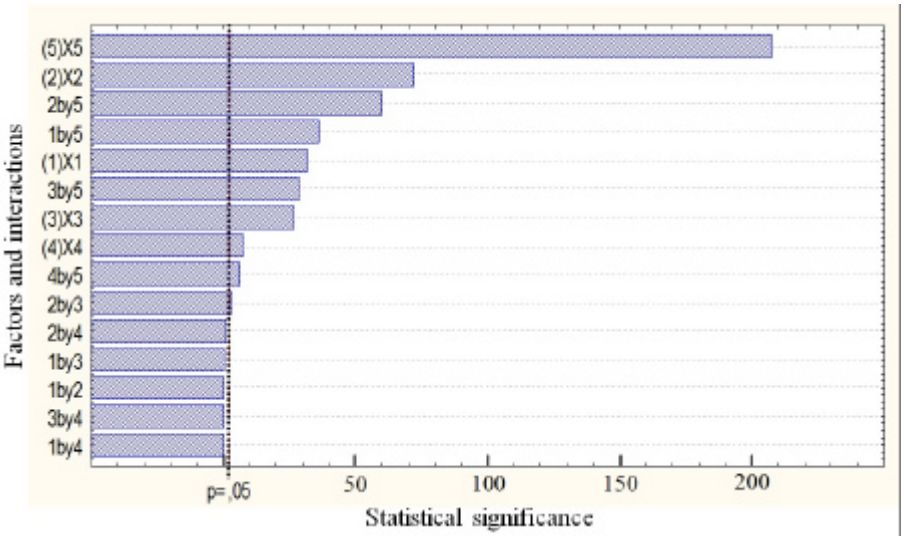

Figure 7. Pareto charts of standardized effect of Y_2 (linear thermal transmittance ? 2), for horizontal junction g, AAC solution.

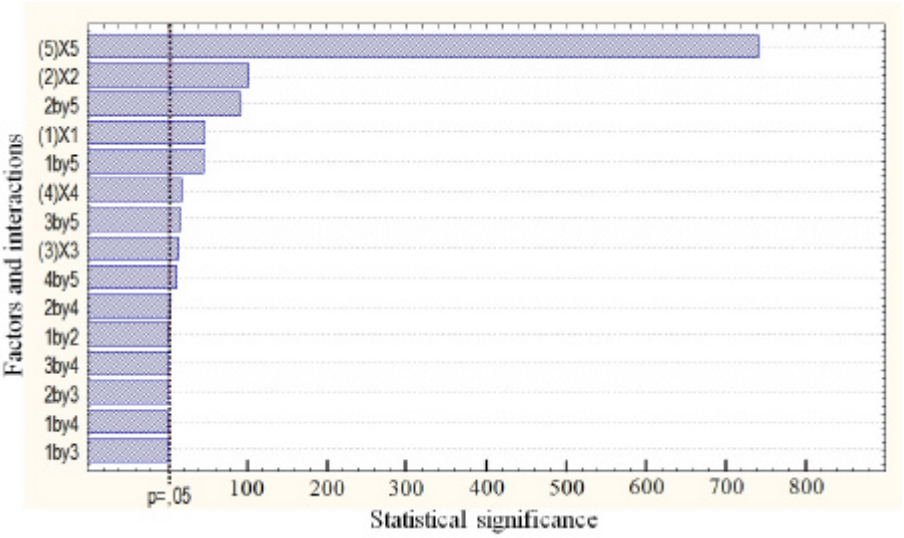

Figure 8. Pareto charts of standardized effect of Y_3 (temperature factor f_{Rsi}), for horizontal junction *g*, AAC solution.

If low-level and high-level values of variables are modified, so that wider intervals are defined for X_3 and X_4, and narrower intervals for X_1, X_2 and X_5, it is to be expected for corresponding modifications in the statistical significances. Moreover, if all factors ranges would be very narrow, it will still have a meaning making observations upon statistical significances, even though Equation (2) will have a major $ß_0$ coefficient and insignificant regression coefficients for factors.

Table 6. Summary of ANOVA for Y_1 (linear thermal transmittance $?_1$) – vertical junction *b*, MW solution

Regr. Coefficients; Var.:Y1; R-sqr=1,; Adj R-sqr:1						
	Regressn - Coeff.	**Std.Err.**	**t(1)**	**p**	**-95,% - Cnf.Limt**	**+95,% - Cnf.Limt**
Mean/Interc.	0,52535	0,002451	214,357	0,002970	0,4942	0,55649
(1)X1	-3,58998	0,051572	-69,611	0,009145	-4,2453	-2,93469
(2)X2	3,14455	0,053810	58,438	0,010893	2,4608	3,82827
(3)X3	-0,02160	0,000037	-584,813	0,001089	-0,0221	-0,02114
1 by 2	-2,02112	1,132150	-1,785	0,325064	-16,4065	12,36421
1 by 3	0,15329	0,000566	270,798	0,002351	0,1461	0,16048
2 by 3	-0,14540	0,000566	-256,855	0,002479	-0,1526	-0,13821

Table 7. Summary of ANOVA for Y_2 (linear thermal transmittance $?_2$) – vertical junction *b*, MW solution

Regr. Coefficients; Var.:Y2; R-sqr=1,; Adj R-sqr:1,						
	Regressn - Coeff.	**Std.Err.**	**t(1)**	**p**	**-95,% - Cnf.Limt**	**+95,% - Cnf.Limt**
Mean/Interc.	0,06303	0,001559	40,420	0,015747	0,0432	0,082838
(1)X1	-1,32145	0,032811	-40,275	0,015804	-1,7383	-0,904544
(2)X2	2,82536	0,034235	82,529	0,007714	2,3904	3,260351
(3)X3	-0,00275	0,000024	-117,100	0,005436	-0,0031	-0,002454
1 by 2	-4,10211	0,720293	-5,695	0,110657	-13,2543	5,050076
1 by 3	0,07719	0,000360	214,329	0,002970	0,0726	0,081766
2 by 3	-0,11843	0,000360	-328,833	0,001936	-0,1230	-0,113852

Table 8. Summary of ANOVA for Y_3 (temperature factor f_{Rsi}) – vertical junction *b*, MW solution

Regr. Coefficients; Var.:Y3; R-sqr=1,; Adj R-sqr:1						
	Regressn - Coeff.	**Std.Err.**	**t(1)**	**p**	**-95,% - Cnf.Limt**	**+95,% - Cnf.Limt**
Mean/Interc.	0,845066	0,001357	622,6941	0,001022	0,82782	0,862310
(1)X1	-0,389573	0,028557	-13,6419	0,046583	-0,75243	-0,026720
(2)X2	-0,519775	0,029796	-17,4442	0,036455	-0,89837	-0,141175
(3)X3	0,005438	0,000020	265,8154	0,002395	0,00518	0,005698
1 by 2	0,626912	0,626912	1,0000	0,500000	-7,33876	8,592582
1 by 3	0,024437	0,000313	77,9585	0,008166	0,02045	0,028419
2 by 3	0,024858	0,000313	79,3017	0,008027	0,02087	0,028840

The charts in Figures 9, 10 and 11 shows the statistical significance of factors and interactions upon linear thermal transmittances $?_1$ and $?_2$ and temperature factor f_{Rsi}, for MW solution, at a walls corner connection. While MW thermal conductivity proves a sufficient influence upon the two linear transmittances, f_{Rsi} factor is solely dependent on variance of external insulation thermal resistance.

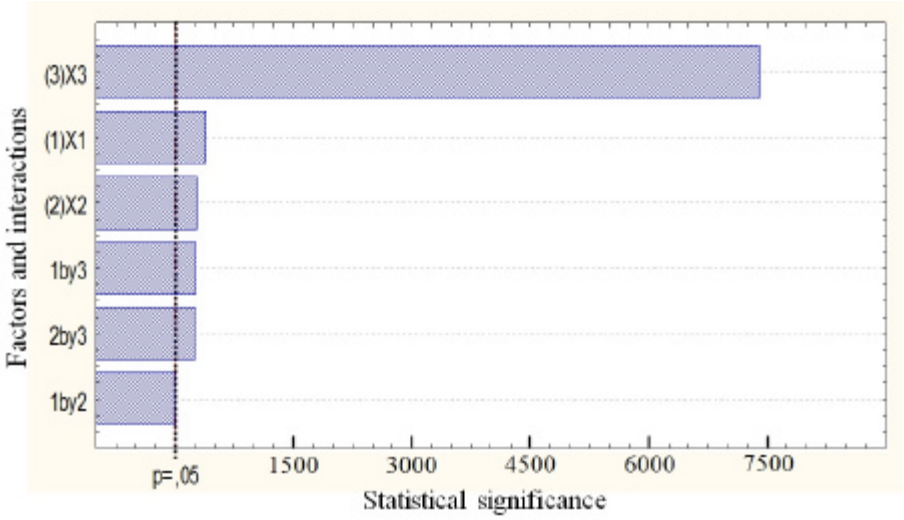

Figure 9. Pareto charts of standardized effect of Y_1 (linear thermal transmittance $?_1$), for vertical junction *b*, MW solution.

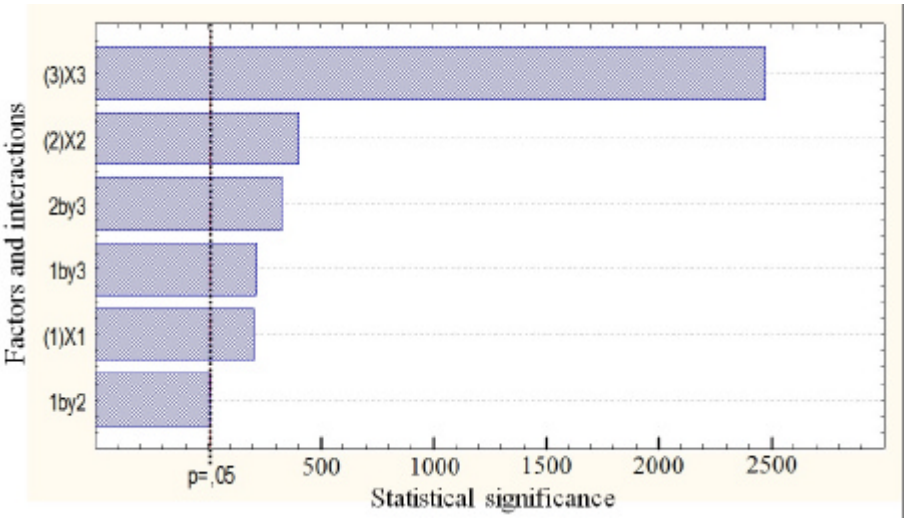

Figure 10. Pareto charts of standardized effect of Y_2 (linear thermal transmittance $?_2$), for vertical junction *b*, MW solution.

Same as for AAC solution, a high f_{Rsi} value for MW solution is conditioned by a continuous insulation layer in thermal bridges areas, in order to minimize variations in inner surface temperature field. For linear thermal transmittances, in both cases, the geometric characteristic of thermal bridges renders a certain relevance also to minor factors.

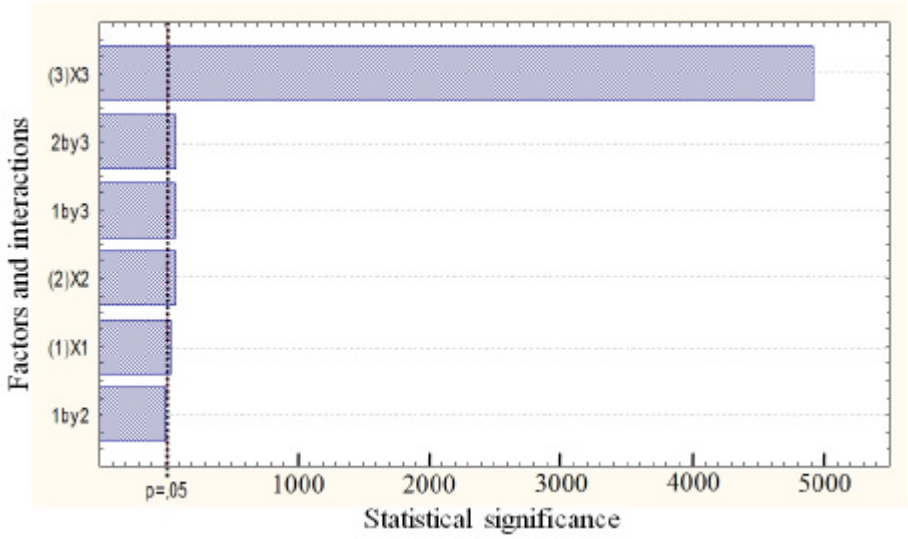

Figure 11. Pareto charts of standardized effect of Y_3 (temperature factor f_{Rsi}), for vertical junction *b*, MW solution.

5. CONCLUSIONS

In this paper a statistical analysis method was presented by applying it in a thermal bridges study. All factors were proved to be significant, but not for all the parameters of response studied. Thus, continuous insulation layer in thermal bridges areas, determined mainly by the additional external polystyrene layer and secondary by the coating concrete external layer, has a great influence upon linear thermal transmittances and temperature factor. AAC and mineral wool layers, being interrupted in thermal bridges area, have very low statistical significances for temperature factor, because of the low impact upon the variations in inner surface temperature fields.

This study reveals the possibility of obtaining a mathematical model to predict values for linear thermal transmittance and temperature factor, with a high precision on the domain of definition, but also outside of the domain, with an acceptable precision for current purposes.

References

1. Box, G.E.P., Hunter, W.G., Hunter, J.S., *Statistics for experimenters: An Introduction to Design, Data Analysis and Model Building*, John Wiley & Sons, New York, 1978.
2. Cornell, J.A., *How to Apply Response Surface Methodology*, vol. 8, ASQC, Wisconsin, 1990.
3. Gudum, C., *Evaluation of thermal bridges by means of numerical simulation*, Nordic Symposium on Building Physics 2008, Copenhagen, Denmark, 16-18 June 2008.
4. Iacob, A., Lepadatu, D., Ciobanu, A.-A., *Parametric statistical analysis of thermal bridges in buildings*, Proceedings of International Conference DEDUCON – Sustainable Development in Civil Engineering, Iasi, 11 November 2011.
5. Ilomets, S., Kalamees, T., Paap, L., *Evaluation of the thermal bridges of prefabricated concrete large-panel and brick apartment buildings in Estonia*, Proceedings of 9th Nordic Symposium on Building Physics – NSB 2011, Volume 3, Tampere, Finland 29 May – 2 June 2011.
6. Janseens, A., Van Londersele, E., Vandermarcke, B., Roels, S., Standaert, P., Wouters, P., *Developments of limits for the linear thermal transmittance of thermal bridges in buildings*, Proceedings of 10th Thermal Performance of the Exterior Envelopes of Whole Buildings Conference, ASHRAE, Clearwater Beach, Florida, U.S.A., 2-7 December 2007.
7. Jaraminiene, E., Juodis, E., *Heat demand uncertainty evaluation of typical multi-flat panel building*, Journal of Civil Engineering and Management, Vol XII, No 1, 2006.
8. Lepadatu, D., Hambli, R., Kobi, A., Barreau, A., *Optimization of springback in bending process using FEM and Response Surface Methodology*, International Journal of Advanced Manufacturing Technology, 27, pp: 40-47, 2005.
9. Lepadatu, D., Hambli, R., Kobi, A., Barreau, A., *Statistical investigation of die wear in metal extrusion process*, International Journal of Advanced Manufacturing Technology, 28, pp: 272-278, 2006.
10. Mayer, R.H., Montgomery, D.C., *Response Surface Methodology process and product optimization using design of experiments*, Wiley, New York, 1995.
11. Montgomery, D.C., *Design and analysis of experiments*, 5th edition, Wiley & Sons, Inc., New York., 2001.
12. Munch-Andersen, J., *Improving Thermal Insulation of Concrete Sandwich Buildings*, Indoor and Built Environmeent, 18, 2009.
13. Ross, P.J., *Taguchi Techniques for Quality Engineering*, McGraw-Hill, Inc., USA, 1988.
14. Taguchi, G., Konishi, S., *Orthogonal Arrays and Linear Graphs*, Dearborn, MI, ASI press, 1987.
15. The European Parliament and the Council of the European Union, *Directive 2010/31/EU of the European Parliament and of the Council of 19 May 2010 on the energy performance of buildings*, Official Journal of the European Union, May 2010.

Intelligent Sensor Networks Used for the Assessment of Structural Health

Dragos Florin Lisman[1], Ludovic Gheorghe Kopenetz[2]
[1]*Department of Structural Mechanics, Technical University of Cluj-Napoca, Cluj-Napoca, 400114, Romania*
[2] *Department of Structural Mechanics, Technical University of Cluj-Napoca, Cluj-Napoca, 400114, Romania*

Summary

With recent developments in the field of wireless sensor networks the authors present in this paper a solution for complex monitoring systems, that can be used to perform continuous monitoring of different categories of bearing structures.

The system designed for the assessment of structural health is composed of the following main components: a data acquisition component, a data gathering component, a communication component, a storage component and a data interpretation and analysis component which also performs the computation and update of the structural model.

The data acquisition component is based on the use of a multitude of wireless sensors connected in network. There are several wireless sensor producers on the market today that supply sensors capable of acquiring information ranging from simple temperature, dust or humidity data to more complex sensors capable of detecting, cracks, crack propagation, linear displacements or image capturing sensors.

The system under testing uses such sensors and the main contributions of the research team are in customizing the hardware to deal with the time synchronisation of information received from several sensors, dissemination of sensor configuration information, storage of acquired data and the development of a software application able to interpret and present mandatory measures that have to be taken in order to maintain structural health.

The advantages of using a system based on wireless sensor networks range from the elimination of sensor wires and the associated installation costs to the possibility of using low-power, inexpensive nodes which in addition are able to provide redundancy in such a way that the failure of one sensor will have a very limited effect on the overall performance of the assessment system.

KEYWORDS: wireless, sensors, monitoring, structural health.

1. INTRODUCTION

On a global scale, a significant part of civil and commercial bearing structures are affected by certain degrees of deterioration. Due to the global crisis, it has become obvious to civil engineers the fact that there are insufficient funding solutions for immediate replacing or renovation of all affected structures. Thus, accurate information about the status of these structures is necessary in order to be able to optimize and prioritize the available resources. This information helps accurately classify which structures need replacement, which require immediate maintenance and which are in good condition and are normative compliant.

Integrating sensors into bearing structures is the main solution for performing periodical or continuous structural health monitoring. Structural health monitoring can be performed periodically or continuously based on the decision of structural engineers and experts. Both types of monitoring imply several activities like mounting the sensors, installing of power supplies or the connection of sensing devices to the mains of the structure or installing cable runs for the power supply and for the transmission of the data signals. On the long term, all the above mentioned activities can imply high installation and operation costs. Moreover, long bundles of wire cables or fiber optics are subject to periodic rupture or even connector failure. Wires also limit the number of sensors that can be mounted or there may be situations where cable runs cannot be mounted on certain parts or sections of the structure due to the structure's shape or its purpose.

Nevertheless, the integration of sensors into bearing structures has many benefits to the owners and users of the structures, including prediction of damages or catastrophic failures, improved emergency response, increased homeland security or reduced operation costs in the long term.

As a result, in the previous decade several private research companies, universities and international standardization institutions have started the development of wireless sensor networks. These networks are composed of devices called nodes having in their composition a processing unit, a wireless communication device and one or several sensors for data acquisition.

The recommended features of a wireless sensor network node are low power consumption, fast data acquisition capabilities, reliability, long term accuracy, reduced acquisition costs, very little or no maintenance over time and the possibility for remote configuration and programming. These features are not easy to implement because real-life structural monitoring applications and problems have different requirements. Selecting the appropriate sensors and the wireless communication protocol have a strong impact on the overall performance of a node and the lifetime of the energy source.

Nowadays a single integrated circuit is able to encompass a radio communication device, a processing unit and additional digital electronics. Very good example of such integrated circuits are produced by leading industry companies like Atmel, Texas Instruments or MicroChip [1], [2], [3].

According to the definition given in [4], a wireless sensor network is composed of a series of wireless nodes equipped with different types of sensors, placed in different locations on the structure, which communicate with one or several gateways using one or several different wireless communication protocols. A gateway or a basestation is the main collection point for the data sensed by the nodes. The data sensed by the nodes is transmitted directly or via other nodes to the gateway. In order to obtain small communication periods and thus lower energy consumption of nodes, the transmitted data is usually compressed. The data collected by the gateway is then fed as input to different software applications for further processing and information interpretation is performed by expert systems in conjunction with human experts in the structural engineering domain.

2. WIRELESS SENSOR NETWORKS PRINCIPLES

This chapter encompasses a brief description of the hardware components of a wireless sensor network node, the communication possibilities available, the energy supply options and power consumption related issues.

2.1. Node components

The basic hardware components that make up a wireless sensor network node are presented in Figure 1. and are compliant with the descriptions given in [4]. It can be observed that the components are modular and this architecture empowers the node's design with versatility and flexibility to requirements from different structural health monitoring applications.

The sensing devices are mounted on the prototyping board of the wireless node and can range from simple temperature, humidity, noise or dust sensors to more complex sensors able to detect cracks, crack propagation, linear displacements, accelerations or ultrasound sensors capable of distance measurement [5], [6]. The data acquired by the sensing devices is than fed into the conditioning module. This module is necessary because the sensed signal may be too weak or too noisy to be fed directly into the data storage devices. The most common circuits used for signal conditioning are conditional bridge circuits.

Multiplexing and amplifying circuitry is used in order to boost the conditioned signal which at the conditioning circuit's outputs can be as low as 10μV with

corresponding temperature drifts of 0.1µV/ºC. The most common circuits used at this point are precision operational amplifiers. Multiplexers are used in order to combine the inputs from several sensing devices and then feed them as input to the analog digital (A/D) converters.

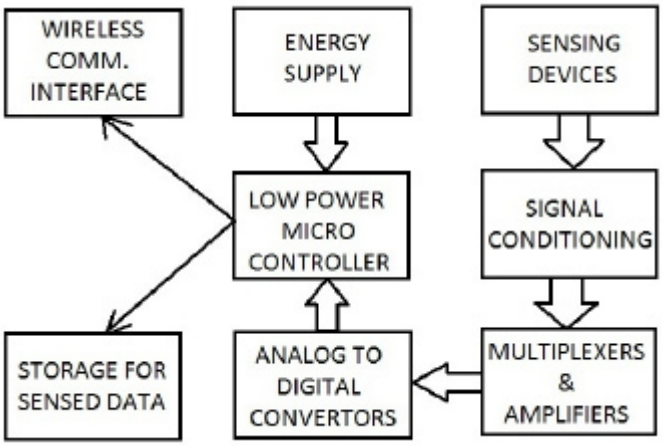

Figure 1. Node Components

The A/D converters are responsible for performing the digitization of the analog signals. The input signals are converted from an analog voltage range into a sequence of binary digits using several output channels of the A/D converters. Common resolutions for the A/D converters are 12, 14 or 20 bits.

The majority of nodes currently available on the market use 8-bit AVR RISC-based microcontrollers with operating frequencies between 8 - 16 MHz, capable of running in temperature conditions between -40ºC and + 85ºC which fit the majority of bearing structure monitoring scenarios. The microcontroller mainly has the following functions [7]:

- wireless network protocol management;
- sensor data acquisition management;
- power supply management;
- transmission of data from the sensor interface to the physical communication layer;
- read/write controller operations for the local storage media.

The microcontroller units are directly coupled with different types of wireless communication interfaces. These include the IEEE 802.15.4 compliant interface, GSM/GPRS interface, Bluetooth or IEEE 802.11 interfaces.

In addition, the nodes provide the possibility for local data storage by using a flash memory mounted on the board. In the majority of node implementations SD,

miniSD or microSD cards are used. These cards have capacities ranging up to a few GBs but they also have some strict timing constraints [8]. Due to these constraints some of the sensor data can be stored to the flash memories if the timing constraints are not too strong for the flash memory write delay to comply to. For example, the flash storage is suitable for temperature sampling which is performed once every few minutes as opposed to acceleration sampling which may take place several times a second.

From the point of view of the energy supply, several options are available including: batteries (Li-Ion or Li-polymer rechargeable), fixed or flexible solar panels, auxiliary 3V no-rechargeable batteries or the possibility of connecting an AC/DC adapter to the mains, depending on the monitoring application.

2.2. Wireless communication options

A wireless sensor networks usually has no or very little infrastructure. It is composed of a given number of nodes ranging from a few to tens or even thousands working together in order to obtain information about the bearing structure under monitoring. Several standards and protocols have been developed to sustain the specific requirements of wireless sensor networks communication including:

- IEEE 802.15.4/ZigBee standard compliant [2], [9];
- IEEE 802.11 b/g /Wifi standard compliant;
- GSM/GPRS;
- Bluetooth;
- RFID/NFC.

In the following subchapters each of the standards/protocols from the previous list are detailed along with the advantages and disadvantages of using them in real-life implementations. A feature offered by the majority of hardware and software suppliers for wireless sensor networks is that the nodes can be simultaneously equipped with two different communication adapters. Thus the node is able to integrate radios allowing communication combinations like: IEEE 802.15.4/ZigBee with GSM/GPRS, IEEE 802.15.4/ZigBee with IEEE 802.11 b/g /Wifi, IEEE 802.11 b/g /Wifi with Bluetooth, etc.

2.2.1. IEEE 802.15.4/ZigBee

IEEE 802.15.4 is the standard proposed by the Institute of Electrical and Electronics Engineers along with leading industry companies for usage in low rate wireless personal area networks also called LR-PANs [10]. The main focus points of this standard are low power consumption, low deployment costs and low complexity.

From the topology point of view, the nodes of the wireless sensor network can be organized as a tree of nodes, a mesh of nodes or simply peer-to-peer nodes as described in Figures 2 (a) and 2 (b).

The 804.15.4 standard states the protocols and functionality at the lower, hardware levels of communication. ZigBee encompasses the higher, software levels of communication built upon the lower 804.15.4 levels. Zigbee ensures simple, low cost and low power communication protocols able to form mesh networks connecting thousands of nodes together [11]. ZigBee compliant devices have a very low power consumption and can operate on a battery for several years. The communication frequencies used at the physical layer of the communication stack are 2.4 GHz, which is practically a worldwide license-free frequency band, 868 MHz and 900 MHz.

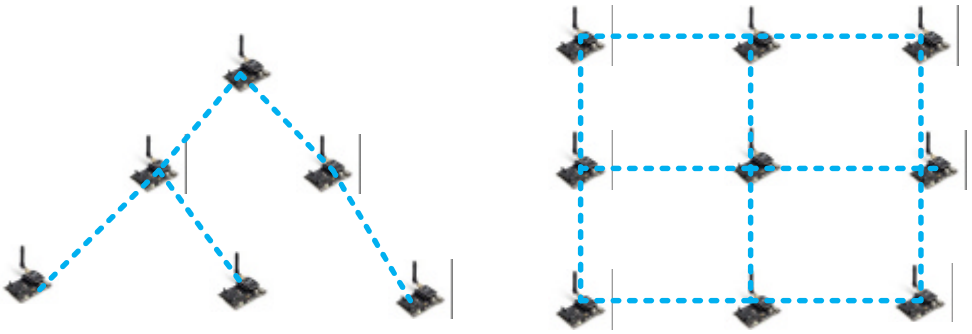

Figure 2. a) Tree node topology b) Mesh node topology

In line of sight conditions the communication range is from a few centimeters up to more than 10 km depending on the communication frequency and on the power of the dipole antenna. Lower distances between nodes require low power consumption in the range of 1 - 5mW, but for large distances of more than 4-5 km, power consumption tops to a few hundreds of mW [6], [11].

In terms of communication bandwidth, ZigBee ensures transmission rates starting from 20Kbps for the 868 MHz band, 40 Kbps for the 900 MHz band up to 250 kbps for the 2.4GHz band according to [4]. In addition, the standard provides the possibility to use the AES-128 encryption standard for the encryption of transmitted data. Thus, through encryption, the security of transmitted data is assured.

Currently, the IEEE 804.15.4/ZigBee standards are the most commonly accepted and employed standards in wireless sensor networks, especially for the low power consumption and due to the fact that nodes coming from sleep mode can achieve rapid synchronization to the network.

2.2.2. IEEE 802.11 b/g /Wifi

This is an older standard designed for local area networking between wireless personal computers or other wireless devices (e.g. smart phones) which is capable of relatively high transfer rates between the communication parties. The communication bandwidth ranges from 1Mbps up to 1Gbps (programmed for 2012 market release). The transmission range with simple dipole antennas is around 100m. By using high power directional high gain antennas higher distances can be obtained but with a considerable energy cost [11]. The requirement for time synchronization between 802.11 communicating nodes is performed by using periodic beacon transmissions [12].

Even if the transmission rates are appealing for wireless sensor networks, the main obstacles in the use of this technology on a large scale are high power requirements. Nevertheless, the technology still can be used for certain structural health monitoring applications, where energy supplies are not an issue, the distance between sensors is reduced and there is a strong requirement for high data rates. In addition, on top of the 802.11 communication stack, there are more security features that can be implemented in order to prevent any alteration of the transmitted data [13].

2.2.3. GSM/GPRS

This communication is based on the Global System for Mobile communication (GSM) standards and it uses a packet oriented mobile data service in 2G or 3G cellular networks called General Packet Radio Service (GPRS). Communication takes place in the quadband 850 MHz / 900 MHz / 1800 MHz / 1900 MHz typically used by GSM mobile phones. The data transmission rates are in the range 56 - 114 Kbps. These standards are considered to be suitable for long-distance communication between nodes.

This technology is suitable for communication of nodes which have to be placed at distances larger than the distances that can be covered by other technologies, but still in the rage of a mobile basestation [14], [15]. Its advantage for use in structural health monitoring applications is the fact that the GSM/GPRS node does not have to be permanently connected to other nodes through a communication link and it can come up when an event has occurred (e.g. a crack appeared) and at that point it can place a call to a central monitoring station or it can send a SMS containing the data to be reported. This is feasible in applications that are not time-sensitive and for which the delivery of the data can be delayed for the time needed to connect to the closest GSM basestation and place the call or send the SMS message [12].

The features that are typically offered by a GSM/GPRS node are:

- place or receive calls;
- send or receive SMS;

- placing x-tone missed calls;
- TCP/IP server;
- HTTP service;
- FTP service for sending or receiving files [6].

2.2.4. Bluetooth

This is a personal area network (PAN) proprietary open standard that has a lower power consumption than 802.11x. It was initially intended for short-range data transfers between personal computers and other digital peripheral devices such as PDAs (personal digital assistants) or mobile phones [16]. The typical transmission range is from a few meters up to 100 meters. In the case of higher transmission distances just a limited set of services offered by Bluetooth are available.

Bluetooth communication devices generally operate in the globally license-free ISM band (Industrial, Scientific and Medical) at frequencies around 2.4GHz and it is based on a master - slave where one master can communicate to up to 7 slaves in a piconet [17].

Data transmission rates for general Bluetooth are around 1Mbps with the possibility for some applications to reach a 3 Mbps rate. According to [16] and due to the limited number of slaves and the master - slave communication method, Bluetooth based sensor networks are appropriate for a niche of structural health monitoring applications, such as monitoring in urban terrains which need intensive data exchange during a few important time intervals and within a time frame of around 7 to 10 days.

A functioning example of a sensor network node implemented based on the Bluetooth technology was developed by the Computer Networks and Engineering Laboratory at ETH Zürich, Switzerland during a research project [18]. The 3rd hardware version of this node has been successfully used in application having more than 70 nodes.

2.2.5. RFID/NFC

This standard will be covered just briefly due to the limited communication scope which is in the range of 1 - 5 cm [6]. This technology is based on the ISO 14443A standard and is primarily used in wireless sensor networks intended for the logistics, location based services, access management and electronic prepaid metering.

2.3. Energy supplies and power consumption

One of the major concerns if note the major concern in designing feasible wireless sensor network deployments for bearing structure's health monitoring are the node

power consumption and the available options for power supply for the node. According to studies performed in [4] and [11], from the total power consumption of a node a percentage around 80% is spent by the wireless transmitter/receiver, around 4-5% by the sensing devices and the rest is consumed by the processing unit and on board electronics.

Generally, structural health monitoring applications are continuous or span over long periods of time (e.g. one or several years). Thus, it is desirable that the energy source is able to serve de node without servicing for the entire monitoring period. In addition, a proper operational scheme has to be designed for the hardware of the node and tuned algorithms have to be implemented at the operating system and application level in order to minimize power consumption.

The most important concerns are with the wireless transmission/reception part and the related algorithms, due to the fact that it is the most power consuming component of the node. The following actions must be considered during implementation [4]:

- Implementation of strict power management strategies and functioning modes (sleep mode, power-down mode, suspend mode);
- Reduction of transmitted/received data through the use of compression algorithms and through data reduction;
- Reducing the frequency of data transmissions;
- Reducing the wireless transceiver duty cycle;
- Transmission of data only when sensor events occur (e.g. transmit displacement data or temperature data only when an increase/decrease of the sampled data occurs);
- Reduce the administrative overhead of the transmitted data (reduce the amount of data that is not related to the sensed data).

Significant research has been performed on the topic of energy sources for wireless sensing nodes. In the typical scenario, when the energy source of a node is almost depleted, the node will shut down and will disconnect from the network. This can have a limited or significant impact on the structural health monitoring system depending on the node placement and the initial redundancy considered in the network design [19]. As a solution researchers have sought energy harvesting solutions besides energy conservation techniques and algorithms.

The typical energy source for a wireless node is a rechargeable or non-rechargeable battery. The most common rechargeable batteries used in the nodes are Li-Ion or Li-polymer. The second category is preferred due to lower manufacturing cost, adaptability to a wide variety of packaging shapes, reliability, and ruggedness. In addition, the self-discharge rate is lower at around 5% per month as compared to 8% for classical Li-Ion batteries.

Even if rechargeable batteries are used in the design, they need servicing at certain time intervals by either replacing the batteries or recharging them. By using energy

harvesting there exists a solution for online recharging. Energy harvesting involves the replenishing of the energy capacity of a nodes energy source. Research has been conducted on different methods like use of solar energy, vibration, thermal energy, acoustic noise or fuel cells [11], [20], [21].

The current mature energy harvesting technology is using solar cells and panels. There exist rigid solar panels capable of supplying 500mA at a voltage of around 7V and flexible solar panels capable of supplying 100mA at the same voltage. The acquisition cost is still high with prices starting from 20-25 Euros/pc. Even if it is a mature technology, solar energy harvesting has the main drawback that the results of the harvesting is proportional to the existing sunlight or to the existing artificial light.

3. WIRELESS SENSOR NETWORK'S ARCHITECTURE

The network architecture of a wireless sensor network depends greatly on the type of structural health monitoring application to be implemented. Several factors influence the architecture chosen for in situ deployment including but not limited to the type of structure under monitoring, structural dimension, structural materials or expose of nodes to natural elements.

In the following subchapters first a presentation of the most commonly met topologies for wireless sensor networks is detailed, followed by a description of node roles and details about the software architecture and its main components.

3.1. WSN topologies

One of the most common topologies used in civil engineering structural health monitoring applications is the star topology, where all the sensor nodes transmit information directly to a special station called gateway [22]. The gateway or the basestation acts a direct data sink which receives all the information from the wireless nodes and can be accessed using a variety of internet communication options including Wifi, GSM/GPRS or broadband technologies. A star topology is presented in Figure 3.

Another topology used in case of monitoring applications that need strong connectivity between sensing nodes is the mesh topology already presented on Figure 2(b). In this topology nodes are connected to one another, to the closest neighboring nodes as well as to one of several gateways (data sinks). Such topology ensure that the redundancy criteria are met, but at a higher cost, due to additional hardware and energy cost in terms of wireless communication volume.

In all topologies the data sink nodes or the gateways require a computing device with enough processing power and enough storage space. In addition, they must act as a remote gateway for the users of the structural heath monitoring system in order to allow remote connectivity, retrieval of data and data analysis software tools to run interpretation algorithms on the data. Last but not least, they must allow the structural expert to perform custom queries on the sensed data according to the criteria that he or she considers fit for the purpose of the monitoring.

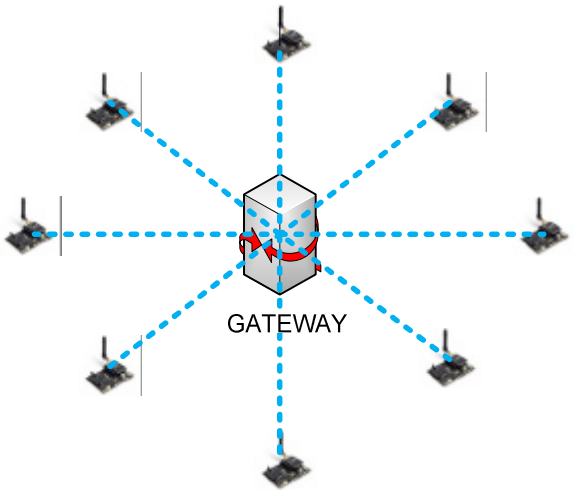

Figure 3. WSN star topology

Mesh topologies are especially appropriate for monitoring bridges and tunnels due to the fact that in these applications the primary concerns are to acquire data about the long-term changes in performance in a number of different locations on the structure. This requires a wireless sensor network composed of closely positioned nodes that sample data at a low time frequency of the order of minutes or even hours [23]. Due to the fact that in such monitoring application, nodes are closely positioned, it is not feasible to use wireless transmitters that need the power to communicate directly to the gateway. It makes sense using multi-hop communication inside a mesh topology whose nodes can communicate with one another as well as to the gateway in order to minimize the requirements in terms of transmission distance and thus reducing the overall energy consumption of the nodes.

3.2. Node types

In bridge or tunnel monitoring, as well as for other types of applications for bearing structures health monitoring, typically the following types of nodes are used:

- environmental nodes;
- deformation nodes;
- accelerations nodes [23];
- crack and crack propagation nodes [6], [25];
- inclinometer nodes [24].

3.2.1. Environmental nodes

Usually the steel wires and strands that compose the main cables of a bridge are exposed to the natural elements and it is important to have relative humidity information at the surface of the cables. This information can be obtained by directly mounting the sensors on the surface of the cables. In addition, environmental nodes are equipped with temperature sensors, particle and light sensors.

Humidity sensors can measure 0-100%RH with an accuracy of ±4%RH (at 25ºC, range 30 ~ 80%), <±6%RH (range 0 ~ 100) and a response time under 15s according to [25]. The temperature sensors can measure temperatures in the range between -40ºC and +125ºC with a stepping of 0.5ºC and an accuracy of ±2ºC (range 0ºC ~ +70ºC), ±4ºC (range -40 ~ +125ºC). These properties are sufficient to study temperature gradients across the cable length or at boundary regions. The light sensors have a spectral range between 400 - 700 nm and operate in environments with temperatures between -30ºC and +70ºC with a energy consumption closely to 0μA.

3.2.2. Deformation nodes

Deformation nodes are nodes equipped with sensors able to measure the amount of deformation of the monitored structural element. In [24] the research team presents a fiber optics based sensor capable of performing the measurement. The idea behind this sensor is that it differentially measures the time required by a laser impulse to travel through a fiber optic wrapped around the monitored structural element. If the structural element suffers deformation, the time needed by the signal to travel becomes longer.

Some advantages of this type of deformation measurement device are the facts that it is a minimally invasive measurement method, it does not suffer from electromagnetic noise and it can be used to measure the deformations of a wide range of elements, for example from a single 1 foot element up to an entire structure [24].

Supplementary, this type of node contains a temperature sensor in order to measure the instantaneous temperature in order to perform coordination to the amount of deformation at the measurement point.

3.2.3. Acceleration nodes

The majority of nodes can be equipped with an acceleration sensor. Acceleration sensors are capable of measuring accelerations in the range: ±2g (1024 LSb/g) / ±6g (340LSb/g) at frequencies of 40Hz/160Hz/640Hz/2560Hz [6]. Acceleration data is high-volume data and has to be stored immediately after sampling. Acceleration nodes are able to sustain a 500Hz sampling rate while writing the data on the microSD card without loses. This requires nodes designed to support bursts of high-rate data having strict reliability requirements.

The acceleration sensor in the case of a wireless node is a MEMS device (micro-electro-mechanical system) with dimensions in the scale of maximum 1 millimeter. These are low-power inexpensive alternatives to classical sensors very suitable for implementation in a energy-constrained wireless sensor node.

3.2.4. Crack and crack-propagation nodes

These nodes are equipped with sensors capable of detecting the appearance of cracks and measure the magnitude and 2D orientation of these cracks. Crack detection gages have lengths between 15 and 56 mm and widths between 3 and 6 mm [25]. The operation temperature typical to this type of sensor is between -195ºC and 120ºC.

The sensor consists of a small conductive strand with a very low resistance value embedded in a fiber-glass film. In the case of a crack development, the sensor shall break thus interrupting a closed electric circuit. This event will be signaled to the node's central processing unit. In order to mount such a sensor to a surface, it has be fixed using a special adhesive. The use of a protective coating is recommended in long term installations.

The crack-propagation sensor that is mounted on this type of node has the same operation principle, with the difference that it is composed of a small conductive strand which contains several parallel grid lines that break progressively with the propagation and enlargement of a crack's width. Several options are available for the distribution of the grids. There are be sensors having: 10-grid lines with 0.25 mm between grids, 20-grid lines with 0.25 mm between grids, 20-grid lines with 0.51 mm between grids, 20-grid lines with 2.03 mm between grids, 20-grid lines with 1.27 mm between grids or other formats depending on the specifics of the structural health monitoring application in terms of crack propagation data [25].

3.2.5. Inclinometer nodes

These nodes are equipped with sensors able to measure the inclination sustained by structural elements. These nodes are especially used in the case of bridge, tunnel or

road structural elements with relatively high success in determining the changes that appear at the relative position of structural elements.

3.3 The software of wireless sensor nodes

On top of the hardware of wireless sensor nodes runs a very compact operating system (OS). This is a distributed operating system and must be perceived as a operating system working on the entire network as a whole. Abstracting the capabilities of the hardware is a basic OS responsibility.

The majority of OSs are developed using the nesC programming language which makes them portable on many types of hardware platforms.

The basic services provided by the OS are:

- hardware abstraction;
- timers/alarms;
- memory management;
- sensor primitives;
- communication primitives.

One of the main goals of an hardware abstraction is to provide programmers with the facility of easy traversing the software/hardware boundary by allowing some software components to be replaced by hardware components with real hardware modules and vice versa.

Timers and alarms are used by applications running on top of the OS in order to get an event or a piece of data when the timer expires. Alarms are used to signal the applications running on top of the operating system about events that have occurred and must be processed immediately by the monitoring software applications.

The memory management function is responsible for the allocation of memory to the structural health monitoring applications running on top of the operating system. It is also responsible for the efficient allocation of memory in order to reduce memory waste. The fact that the memory resources of the node are reduced as compared to smart phones for example, has to be noted at this point.

The sensor primitives provide an abstract interface to the physical hardware sensors and the underlying node platform. At least five functions of this interface can be called by a monitoring application: sensor activation, sensor deactivation, get sensor value, configure sensor and get sensor status. In addition, when sensors are deactivated, the sensor API has support for turning off the power to the sensors, thus conserving energy of the sensor board.

Communication primitives are abstracted under the form of messages. Messages are preceded by a small identifier that is attached to each message, specifying the action that needs to be taken on the receiver's side when a given message has been

received followed by sensed data, timestamps and other data fields. Usually the nodes transmitting the information are the sensing nodes and the receivers of information are the sink nodes. Nevertheless, communication can take place in the other direction too, for configuration and administrative related tasks.

In the test setup used in our research, the structural health monitoring applications are developed directly on top of the operating system by making use of the operating system's functions. Still, there exists in other implementations of monitoring application another layer between the OS and the user applications. This layer is called a middleware layer and performs further abstractions on top of the OS's abstractions [24].

4. CONCLUSIONS

Intelligent monitoring of bearing structures by using wireless sensor networks proves to be a cost-effective solution that can be deployed on a wide range of infrastructure projects including but not limited to water-supply and aerial sewage infrastructure, bridges, tunnels, towers or road segments. They can supply civil engineers with real-time critical data on the health status and the performance degree of the monitored structures.

In the test phase our research team is implementing a structural health monitoring application on a sewage-pipe in Cluj County. The pipe is suspended using bearing cables. Monitoring is performed on the health of the bearing cables by obtaining information about relative humidity, accelerations and deformations. This is done by using three types of wireless sensing nodes: environmental, acceleration and deformation nodes.

Environmental nodes sample humidity, temperature and dust readings. The purpose is to analyze the daily, weekly and seasonal temperature readings and match them to the contractions of the bearing cables. Humidity readings are performed in order to determine the exposure of sustaining and connection elements and braces to corrosion. Relative humidity values above 60% accelerate corrosion processes.

The acceleration nodes are recording information about the vibrations induced in the bearing cables by wind and nearby traffic. The analysis of acceleration records will be done by a custom application and will help understand the dynamic behavior of the suspended bearing structure. From the theoretical point of view, the vibration response of the test structure is not random, but it is situated along some frequencies known as natural frequencies.

Deformation nodes supply an average value of the last 20 deformation readings. This average is performed due to irrelevant character of single samples. These tend to fluctuate. Elongation of the vertical sustaining cables is an indication of a

deterioration and will be automatically detected and signaled by a software application under development.

Using a combination of data supplied by environmental, acceleration and deformation nodes a monitoring application will be developed in the next research phase, which will, hopefully, be able to perform strain analysis on the bearing cables. Nevertheless, there is a wide research field left uncovered when discussing about structural heath monitoring applications based on intelligent networks composed of wireless sensing nodes.

References

1. ***, http://www.atmel.com/devices/ATMEGA128RFA1.aspx, viewed on 04/19/2012.
2. ***, http://www.ti.com/lsds/ti/analog/zigbee.page, viewed on 04/18/2012.
3. ***, http://www.microchip.com/stellent/idcplg?IdcService=SS_GET_PAGE&nodeId=2663, viewed on 04/17/2012.
4. Townsend, C. and Arms, S., *Wireless Sensor Networks: Principles and Applications*, Chapter 22, pp. 575-589, from *Sensor Technology Handbook*, Elsevier Newnes, Oxford, UK, 2005.
5. Basarna, C., Baydere, S., Bongiovanni G. and others, Research Integration: Platform Survey Critical Evaluation of platforms commonly used in embedded wisents research, Embedded WiSeNts - Project FP6-004400, 2006 available at: http://www.embedded-wisents.org/studies/wisents/download/survey.pdf, viewed on 02/15/2012.
6. ***, Libelium WaspMote technical guide (electronic version) available online at: http://www.libelium.com/documentation/waspmote/waspmote-datasheet_eng.pdf, viewed at 03/04/2012.
7. Arms, S.W., Newhard, A.T., Galbreath, J.H., Townsend, C.P., Remotely Reprogrammable Wireless Sensor Networks for Structural Health Monitoring Applications, ICCES International Conference on Computational and Experimental Engineering and Sciences, Medeira, Portugal, 2004.
8. ***, SD Association Homepage, https://www.sdcard.org/consumers/speed/, viewed on 03/03/2012
9. Jiang, X.D., Tang, Y-L, Lei, Y., Wireless Sensor Networks in Structural Health Monitoring Based on ZigBee Technology, Proceedings of the 3rd International Conference on Anti-Counterfeiting, Security and Identification in Communication (ASID'09), IEEE Press, Piscataway, NJ, USA, 2009, pp. 449 - 452.
10. Fasl, J. and Potter, D., Reliable Wireless Sensor Networks for Infrastructure Monitoring, Structural Health Monitoring: Proceedings of the 5th European Workshop on Structural Health Monitoring, DEStech Publications, Inc., Lanccester, PA, USA, 2010, ISBN: 978-60595-024-2, pp. 673 - 678.
11. Yick, J., Mukherjee, B., Ghosol, D., Wireless Sensor Network Survey, Elsevier B.V., Vol. 52, Issue 12, 2008, pp..2292 - 2330.
12. Lisman, D. F., Inter-Vehicle Communication Platform for Safety Applications - Communication Aspects, Diploma Thesis, Technical University of Cluj-Napoca, 2006.
13. Lisman, D. F., Securitatea Comunicatiei in Retele Vehiculare, Master's Thesis, Technical University of Cluj-Napoca, 2009. (in Romanian)
14. Jaman, G. and Hussain, S., Structural Monitoring using Wireless Sensors and Controller Area Network, Proceedings of the 5th Annual Conference on Communication Networks and Services Research (CNSR '07), IEEE Computer Society, Washington, DC, USA, 2007, pp. 26 -34.
15. Yan, B.Z. and Zhao, H.Y., A Low Cost GSM/GPRS Based Wireless Home Security System, *IEEE Transactions on Consumer Electronics*, May 2008, pp. 567-572.

16. Leopold, M., Dydensborg, M.B., Bonnet, P., Bluetooth and sensor networks: a reality check, Proceedings of the Sensys'03, Los Angeles, CA, USA, 2003.
17. Xiao, Y. and Pan., Y., *Wireless LANs & Bluetooth (Wireless Networks and Mobile Computing)*, Nova Science Publishers, Hauppauge, NY, USA, ISBN: 978-1594544323, 2005.
18. ***, BTnode Platform Official Website, http://www.btnode.ethz.ch/, viewed on 02/14/2012.
19. Lisman, D.F. and Kopenetz, L.G., Advanced In Situ Monitoring Techniques for the Behaviour of Heritage Structures, *Journal of Applied Engineering Sciences*, University of Oradea Publishing House, Oradea, Romania, Vol. 2(15), Issue 1, 2012.
20. Kim, S., Pakzad, S., Culler, D. and others, Wireless Sensor Networks for Structural Health Monitoring, SenSys '06 Proceedings of the 4th International Conference on Embedded Networked Sensor Systems, ACM, New York, NY, USA, 2006, ISBN: 1-59593-343-3.
21. Seah, W.K.G., Eu, Z.A., Tan, H.P., Wireless sensor networks powered by ambient energy harvesting (WSN-HEAP) - Survey and challenges, 1st International Conference on Wireless Communications, Vehicular Technology, Information Theory and Aerospace & Electronic Systems, Aalborg, Denmark, 2009, ISBN: 978-1-4244-4066-5
22. Fasl, J., Helwig, T., Wood, S., Samaras, V., Potter, D., Lindenberg, R., Frank, K., Evaluation of Wireless Devices for Monitoring Fracture - Critical Bridges, 7th International Bridge Engineering Conference, San Antonio, TX, USA, December 2010.
23. Hoult, N., Bennett, P.J., Stoianov, I., Fidler, P., Maskimovic, C., Middleton, C., Graham, N., Soga, K., Wireless sensor networks: creating 'smart infrastructure', *Proceedings of ICE,* Civil Engineering, 162, 2009, pp.136 - 143
24. Ceriotti, M., Mottola, L., Picco, G.P., Murphy, A.L., Guna, S., Corrà, M., Pozzi, M., Zonta, D., Zanon, P., Monitoring Heritage Buildings with Wireless Sensor Networks: The Torre Aquila Deployment, *Proceedings of the 8th ACM/IEEE International Conference on Information Processing in Sensor Networks (IPSN/SPOTS),* San Francisco, CA, USA, 2009.
25. ***, Libelium SmartCities technical guide (electronic version) available online at: http://www.libelium.com/documentation/waspmote/smart-cities-sensor-board_eng.pdf, viewed at 03/05/2012

Principles for design of wind turbine foundations. Case Study

Ana Nicuta, Razvan Mircea Chirila, Daniela Grigore
Faculty of Civil Engineering and Building Services, Technical University "Gheorghe Asachi" to Iasi, Code 70050, Romania,

Summary

Foundation for special constructions represent a particular interest considering that the current state of development in renewable energy regeneration problem for Europe and the entire world is a special problem. From the category of special construction are also the wind turbins that became very efficient for generating electricity without producing carbon dioxide emissions that affect the ozone layer and global warming. The foundations for such construction are classified in direct foundations – general raft foundation and indirect foundation through piles. The case study refers to the design of foundations for a wind turbine located in two different areas of Romania, with different geotechnical characteristics

KEYWORDS: wind turbine, foundations on piles, general slabs foundation

1. INTRODUCTION

Wind energy has been exploited on land ever since the first windmill was build in ancient Persia in the seventh century. Around the fourteenth century the Germans have used passive wind energy to remove water from the flooded fields with a so-called windmill [11].

But the widespread exploitation appeared only in the twentieth century alongside the modern windmills, wind turbines that can generate energy ranging from 250 to 300 KW. Modern wind turbins became very efficient and now generates electricity for thousands of homes in Europe and worldwide, without producing carbon dioxide emissions that affects the ozone layer and the global warming.

The country with the highest percentage of electricity developed from wind energy is Denmark, with about 20%, and the country that produces the biggest quantity of energy is Germany.

The total global capacity of wind turbines is around 75.000 MW. Most turbines produce energy 25% of the time and this number increases during the winter when the winds are getting stronger.

ISSN 2285-2735, Pages 252 - 261

2. TYPES OF WIND TURBINES

Wind energy is part of renewable energy. The aero-generator uses the wind's kinetic energy to drive the rotor shaft: it is converted into mechanical energy, which in turn is converted into electricity by a generator that is mechanically coupled to the wind turbine.

2.1. Vertical axis wind turbines

The turbine pylons with vertical axis are quite small, with a height ranging between 0,1 – 0,5 of the rotors height. This allows placing the entire energy conversion equipment (multiplier, generator), at the foot of the turbine, thus facilitating the maintenance operations.

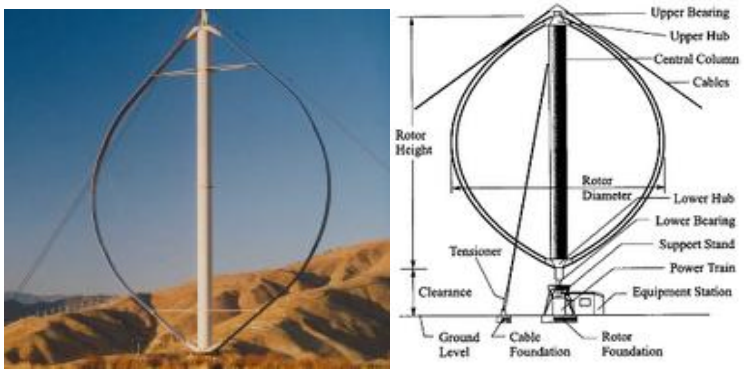

Fig.1. Types of wind turbins with vertical axis [13]

2.2. Horizontal axis wind turbines

The energy produced by the horizontal axis wind turbines is based on the principle of windmills. Most often, the rotor of these windmills have three blades with a certain streamlined profile, because in this way it achieves a good compromise between power ratio, cost and speed of rotation of the eolian transducer, as an aesthetic aspect improvement, compared with the rotor with two bladesb [10].

Horizontal axis wind turbines are mostly used because their aerodynamic performance is superior to the one of the vertical axis turbines, are less driven to significant mechanical stress and have a lower cost

There are two ways of positioning these horizontal axis turbines: upstream and downstream (Figure 2). The most widely used is placing the turbine axis upstream, with getting best results at high power.

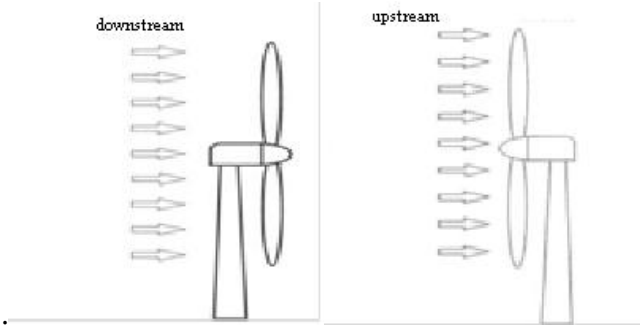

Fig.3. Scheme of horizontal axis wind turbine downstream and upstream

3. FOUNDATIONS FOR WIND TURBINE

The terrestrial wind turbines transfer the loads in to the ground through the foundation. Types of foundations for such constructions shall be chosen only after a detailed ground investigation has been made, through laboratory and in situ tests.

In preparation of the documentation for the geotechnical study it shall be take into consideration a more detailed site description in terms of geological, hydrogeological, climatic, seismic and framing development in the geotechnical category.

Land investigations provided by the geotechnical study should provide all the necessary data needed for designing in safety conditions, in compliance with the geotechnical design concept that ensures stability, strenght and durability of the construction.

The physical and mechanical characteristics of the ground where the wind turbines will be located, depending on the effort, usually governs the type of chosen foundation.

Before choosing the type of the foundation, the designer should check several important issues: the ground bearing capacity, the sliding and overturning stability, the resistance of the soil to degradation in terms of cyclic loads, compaction endings, differential compaction is more likely to develop because of the wind loads generated in the windmills, the possibility of soil erosion.

The foundations for such construction are classified as direct foundations – general raft foundation when the ground at the proposed foundation depth can support loads from the superstructure and indirect foundations – on piles, that are designed to transfer the loads in depth, to where the good ground foundation is located.

3.1. General slab foundations

Are surface foundations with varying sizes, with circular or octagonal shape in horizontal plane, with varying heights, depending on the size of the solicitations.

In calculating the raft foundation we must consider many factors from which the most important ones are the rigidity and foundation geometry, the size and distribution of loads, the deformation and strength characteristics of the ground and the execution phases.

The calculus follows the determination of contact pressures and deformations, bending moments and shear forces. In calculations, the raft foundation can be considered rigid or flexible.

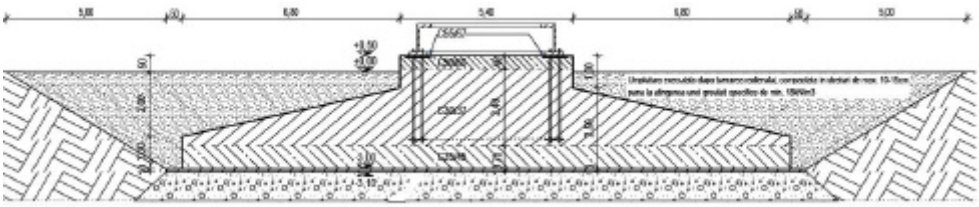

Fig.6. Example of general slab foundation

3.2. Indirect foundations through piles

Due to the important category of these types of buildings, large loads are transmitted to the foundation ground and the nature of the ground, force structure designers to choose many times the foundation through piles.

4. CASE STUDY

The case study refers to the design of foundations for a wind turbine located in two different areas of Romania.

The model for the wind turbine for which the calculus was made is VESTAS V90 – 1.8 MW VCS HH 105m [10]. The model characteristics are presented in Table 2.

The manufacturer provided data upon which the calcules is based. The data refers to a series of loads applied at the turbine base. The loads had extreme values, in oreder to observe the behaviour under worst circumstances.

Table 1. Loads on the foundation of the supratructure

Extreme loads	Mx [kNm]	My [kNm]	Fz [kN]
	75407	-2295	-3666

Tabel 2. Geometric characteristic of wind turbine

General information about the suprastructure (turbine)	
Diameter propeller	90.0 m
Number of blades	3
Length of blades	44.0 m
Height of tower	105.0 m
Diameter at the base of the tower	4.0 m
Suprastructure weight	360.0 t

The foundation selection was based on several parameters, as it follows [7]:

- The foundation's own weight caused permanent, constant loads these loads were procentually reduced by the construction-foundation assembly.

- The weight of the frost deposits determined cvasipermanent loads, with a slow variation; these loads had low procentual values. But if irregularities occur to the frost deposits, the rotor unbalances and dynamic loads occur on a regular basis, but with low percentages.

- Wind action determined random variable loads which happen on a regular incidence, resulting in intense wear stresses (the percentage of this occuring is dominant and has extreme values). Wind action depends on electrical conducting power and rotor influence on direct force applied on pile.

- Seismic action caused short term loads, which were equivalent to an isolated impulse, with a higher procentage. The seismic action, even if different than the wind action, causes similar effects which sum up to a horizontal oriented group.

The rotor unbalance caused damaging forces (the shattering of blades), which provided violent loads.

All these loads were transmited to the foundation base. The special efforts on the foundation ground were oriented on the axes, having an intensity that can be predicted and inclued as a general rule.

The foundation calculus was made by means of a hypothesis consideriing the efforts provided by the manufacturer as the load in exploitation regime for the turbine. A simplified model will be used, combining this hypothesis with the seismic effect. Modeling was performed using an AxisVM software.

The solution for this foundation was based upon the transmission of all the loads from the suprastructure through a slab foundation to a pile system located on each side of the slab.

Calculations and analysis of the interaction between ground foundation and infrastructure has allowed a comparison of the stress and displacement values for the two cases that were analyzed. The design of the wind turbine foundations has been made taking into consideration the force normatives and SR EN 61400-1:2006, that is identical to IEC61400-1.

The raft foundation was calculated considering a reinforced concrete slab with the thickness of 250 cm and an octogonal shape with the sides of 800 cm. The bed-load coeffienct k_s [1] had the following values: ks = 6,5 daN/cm^3 for location Galbiori (Constanta) and k_s = 8 daN/cm^3 for location Valea Lupului (Iasi).

4.1. Location: Galbiori, Constanta

Foundation for wind turbine is the raft generally type, disposed on the 16 bored piles, Ø1080 mm, embedded in the technical basis.

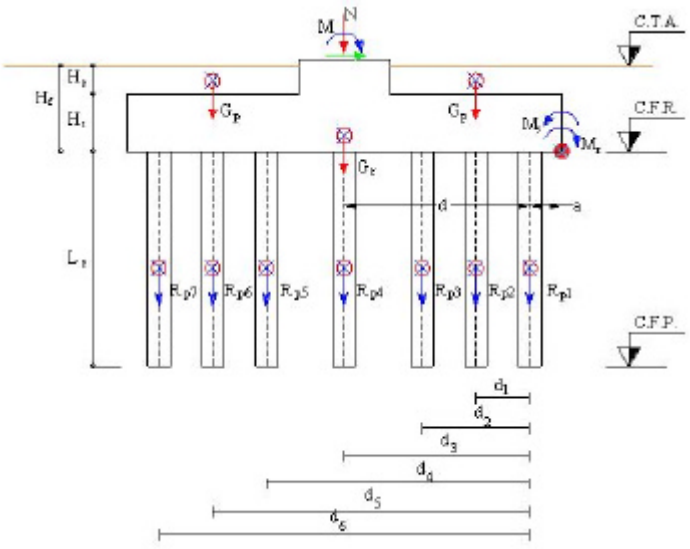

Fig.10 Cross section through the foundation

The factor of safety against overturning, is expressed: $M_s / M_r \geq 1,5$

$M_s / M_r = 281761,27 / 105754,1 = 2,66 \Rightarrow 2,66 > 1,5$

The calculation of bored piles was performed in according with [4], [5], [6], [7].

4.1.1. Ultimate compressive resistance from static load tests

$$\begin{aligned} R_{c;d} &= R_{b;d} + R_{s;d} = R_{b;k}/g_b + R_{s;k}/g_s \\ R_{c;d} &= 4561.025 \text{ kN} \end{aligned} \quad (2)$$

where:

$R_{c;d}$ - design value of the compressive resistance;

$R_{b;d}$ - design value of the base resistance;

$R_{s,d}$- design value of the shaft resistance.

$$R_{b;d} = R_{b;k}/g_b \quad (3)$$

where:

$R_{b;k}$ - characteristic values of the base resistance;

g_b - partial resistance factor for bored piles on base.

$$R_{s;d} = R_{s;k}/g_s \quad (4)$$

where:

$R_{s;k}$ - characteristic values of the shaft resistance;

g_s - partial resistance factor for bored piles on shaft (compression).

The caracteristic value may be obtained by calculating:

$$\begin{aligned} R_{b;k} &= A_b \cdot q_{b;k} \\ R_{b;k} &= 1570kN \end{aligned} \quad (5)$$

where:

A_b - area at the base pile;

$q_{b;k}$ - characteristic value of base resistance.

The characteristic values of the shaft resistance may be obtained by calculating:

$$\begin{aligned} &R_{s;k} = \sum A_{s;i} \cdot q_{s;i;k} = U \sum q_{s;i;k} \cdot l_i \\ &R_{s;k} = 3.14(20 \cdot 0.50 + 42 \cdot 3 + 54.50 \cdot 1 + 60 \cdot 4 + 64.8 \cdot 1.80 + 68.50 \cdot 1.20 + \\ &+70.60 \cdot 2.30 + 71.30 \cdot 0.70 + 77.80 \cdot 7.25 + 84.70 \cdot 2.0 \\ &R_{s;k} = 4945.75kN \end{aligned} \tag{6}$$

where:

$A_{s;i}$ - shaft area of the pile in contact with the soil;

U - pile cross – section perimeter;

l_i - the thickness of “i” layer, which is in direct with “i” layer;

$q_{s;i;k}$ - characteristic value of the shaft resistance to “i” layer.

4.1.2. Ground tensile resistance

General relationship for calculating:

$$F_{t;d} \le R_{t;d} \tag{7}$$

where:

$F_{t;d}$ - characteristic tensile value for the single pile corresponding to ULS;

$R_{t;d}$ - design value of the tensile resistance.

The characteristic value of tensile resistance may be obtained by calculating:

$$R_{t,d} = \frac{U \sum q_{s,k_2} \cdot l_i}{g_m \cdot g_{s_2}} = 4027.58kN \tag{8}$$

where:

q_{s,k_2} - characteristic values of shaft friction in the various layer obtained from values of ground properties;

U - pile cross – section perimeter;

l_i - the thickness of “i” layer, which is in direct with “i” layer;

g_{s_2} - values of the partial factor may be set by the National Annex;

g_m - values of the partial factor: g_m =2,4.

4.1. 3. Calculation of pressure on the slab foot

$$s = \frac{N+G}{A} + \frac{M}{W} = \frac{5746.9 + 276087.76}{763.96} + \frac{3138,8}{351.35} = 369.80\,kPa \quad (10)$$

4.2. Location: Valea Lupului, Iasi

The choice of the second location was made in order to highlight similar foundation types. These similarities provide a equal size, that would interact on soils with different characteristics. Therefore, on this location, the decision was to run the program with the same input data, the only difference being the elastic coefficient ks, which in this case has the value of 8 daN/ cm^3.

There has been made a tabular centralization of data to compare the values obtained on the first location.

Table 3. Comparasions between the two locations efforts

			Galbiori, Constanta ks= 6,5 daN/cm3	Valea Lupului, Iasi ks= 8 daN/cm3
Total displacement	ez (mm)	Min	-2.654	-0.867
		Max	0.405	0.058
Shear Forces	V (kN)	Min	121.00	62.30
		Max	1181.00	1024.60
Bending Moments	My (kNm)	Min	7540.70	7526.30
		Max	10355.5	9876.53
React.	Rz (kN/m2	Min	-212.30	-56.00
		Max	32.10	3.80

It ss observed a stress reduction of rafter surface for the Iasi area compared to the soil from Galbiori

5. CONCLUSIONSAND RECOMMENDATIONS

In this paper were used models for the design of wind turbine foundations, the special construction which have taken a major role in our country.

Diversity of sites within the territory of Romania requires additional research to determine the correct bearing capacity of the foundation land and choice for the optimal system of the foundation. The case study was performed for the same type of wind turbine, but on two different sites, which have different stratification, from our country.

Different versions of the type foundation have been used for VESTAS V90 -1.8 MW VCS HH 105m. wind turbine model.

The raft foundation on piles applied on both sites allowed an accurate comparation between strains and stresses, shown in Table 3. The foundation designed presented the same dimensions and geometrical features.

The researches performed had aimed to highlight the fact that wind power would be a key factor in achieving the purpose established by the European Union for the year 2020, and to provide less consume, with 20% energy obtained through pollutant emissions.

European Wind Energy Association estimates that wind power will have an amount ranging between 13% and 16% of the electricity consumed in the European Union until the year 2020.

Therefore, the expansion of this energetic industry in Romania demands us a better understanding the behavior of the wind turbine and its infrastructure in relation to the foundation soil.

References

1. Stanciu, A., Lungu, Irina, - *Fundatii*, Editura tehnica, Bucuresti, 2006
2. Botu, N., Musat, V. – *Geotehnica*, Editura Societatii Academice "Matei – Teiu Botez, Iasi, 2003
3. Lungu, Irina, Stanciu, A., Boti, N – *Probleme speciale de Geotehnica si Fundatii*, Editura Junimea, Iasi, 2002
4. NP 123:2010 Normativ privind proiectarea geotehnica a fundatiilor pe piloti
5. SR EN 1536 –Executia lucrarilor speciale.
6. SR EN 1997-1:2006 – Proiectarea geotehnica. Partea 1 – Reguli de proiectare.
7. SR EN 61400-1:2006 - Turbine eoliene. Partea 1: Conditii de proiectare
8. www.consoft.ro – Manual AXISVM
9. http://www.agp.ro
10. http://www.vestas.com/en/wind-power-plants.aspx#/vestas-univers
11. http://www.eoliene.eu/bazele-energiei-eoliene
12. www.wikipedia.com
13. www. visual.merriam-webster.com

Dynamic response of a wind turbine considering soil - structure interaction

Cerasela-Panseluta Olariu
Structural mechanics Department, Gh. Asachi University, Iasi, Romania

Summary

In our country wind turbine construction is extending. Due to the fact that Romania is located in a seismic area it is necessary to consider wind as well as the seismic action when analyzing the towers of wind turbines. An evaluation method of structural response under dynamic actions is the knowledge of the natural modes of vibration of the structure. This aspect becomes of a high interest in a wind turbine analysis because it is necessary to avoid entering the resonance range. In order to highlight the soil structure interaction effects are usually used two methods, namely the substructure method when the soil stiffness is modeled through springs and the finite element method which analyses the entire structure including the foundation soil. In this paper it is presented a dynamic analysis of a 70 meters tall wind turbine considering 4 different types of soils using the finite element method.

KEYWORDS: soil structure interaction, wind turbines, natural modes of vibration, resonance ranges.

1. INTRODUCTION

The new tendency of sustainability requires that all unconventional sources of energy should be exploited. Therefore all around the world new techniques of achieving energy are developed. The construction of wind turbines is accelerating in the last decade all over Europe, as well as in Romania. This growth of wind turbines construction has revealed some design and building difficulties because care need to be taken when dealing with some particularities of these structures.

One of the aspects that should be treated carefully during the functioning of a wind turbine is that it is necessary to avoid entering the resonance range. This implies the knowledge and control of the natural frequencies of vibrations of the tower which should not coincide with the rotor and blade-passing frequencies.

In order to control the natural frequency of the tower particular solutions for the tower as well for the foundations has to be chosen. In this situation considering a rigid base for the tower can outcome misleading results. Studies have proved that when soil stiffness is taken into account in analyses the natural frequencies of the structures differ (usually are smaller) from the case when a rigid base is considered [1]. Therefore in order to choose the best design solutions as to avoid the resonance range it is necessary to consider soil - structure interaction.

This paper presents some theoretical methods to appreciate the foundation soil stiffness for analyzing a wind turbine and a case study using finite element method to analyze the entire soil/foundation/wind turbine system.

2. THEORETICAL BACKGROUND

The International Standard IEC 61400-1 - Wind turbines - Part 1: "Design requirements" was published in order to ensure the safety of wind turbines against damage for the entire life span. In 2005 it was reevaluated and it became the European standard EN 61400-1: 2005. This standard provides safety requirements and specifies the essential design requirements to ensure the engineering integrity of wind turbine [2].

On the other hand, countries with experience in this area of construction like Denmark, Germany have developed national standard for wind turbine design. Guidelines for Design of Wind Turbines, 2002 - Denmark is an example of design guide based on accumulated experience and research in this field. [3,4]

In Romania the European standard was completed with national design requirements and in 2006 it became the national standard SR EN 61400-1:2006. Wind turbines. Part 1: Design requirements. This standard includes also other parts which deal with different aspects of the wind turbines design.

2.1. Wind turbine modeling

The tower of a wind turbine supports the nacelle and the rotor and provides the necessary elevation of the rotor to keep it clear off the ground and bring it up to the level where the wind resources are. Most large wind turbines are delivered with tubular steel towers, which are manufactured in sections of 20-30 m length with flanges at either end. The sections are bolted together on the site. The towers are conical, their diameters increase towards the base, and thereby increasing their strength towards the tower base, where it is needed the most, because this is where the load response owing to the wind loading is largest. The tower is usually

connected to its supporting foundation by means of a bolted flange connection or a weld (figure1)[3].

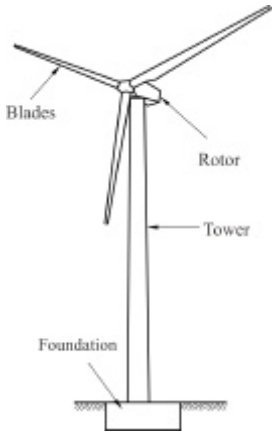

Figure 1. Main components of a wind turbine

On the entire life span of the wind turbine the tower has to withstand the operational vibrations. The rotor and blade-passing frequencies may cause increase of the forces acting on the tower which may lead to a highly insecure level of structural integrity.

The international design codes usually require that wind turbines should be designed for wind actions. On the other hand, in countries like Romania it is necessary to take into account apart from the wind action also the seismic action. When a wind turbine is to be designed for installation on a site which may be subject to earthquakes, the wind turbine has to be designed so as to withstand the earthquake loads.

Load calculations for a wind turbine structure are usually performed by means of a computer program based on an aeroelastic calculation procedure.

For analysis of the horizontal motions and accelerations, the wind turbine can be represented by a concentrated mass on top of a vertical rod. For a typical wind turbine, the concentrated mass can be taken as the mass of the nacelle, including the rotor mass, plus a part of the tower mass [5].

It is important to analyze the wind turbine tower for the earthquake-induced accelerations in one vertical and two horizontal directions. It usually suffices to reduce the analysis of two horizontal directions to an analysis in one horizontal direction, due to the symmetry of the dynamic system. The vertical acceleration may lead to buckling in the tower.

The way to avoid structural failures is to attain a natural frequency of the structure different from the operational frequency of the wind turbine. Usually the

operational frequency is smaller than the natural frequency of the tower. As the wind turbine blades start rotating their circular velocity is increasing and the induced vibration frequency increases. Depending on the power output capacity of the wind turbines, the blades rotate with rotational speeds that range from 30 to 60 rpm which correspond to some maximum operational frequencies from 0.5 to 1 Hz. Usually these operational frequencies are close to the natural frequency range of the soil-structure system [6].

A poor design decision can involve a maximum rotational speed that is very close to the natural frequency of the structural system resulting in a high likelihood of resonant amplification causing structural instability. Another poor design may have a rotational speed not very close to yet higher than the natural frequency of the structural system. In such cases, the structure would have to endure violent near-resonance vibrations as the operational frequency approaches the natural frequency while speeding up to and down from the maximum speed. This situation would result in very high dynamic forces which could cause immediate damage to the structure. Even if these dynamic forces do not exceed the structure’s strength capacity, fatigue-induced failures could also be encountered [8].

A sound design would avoid allowing the operational frequency to approach the vicinity of the natural frequency by a certain safety factor. According to different design codes a safety factor ranging from 5% up to 15% of the natural frequency is recommended [1, 2, 3, 4; 5].

2.2. Soil structure interaction for wind turbines

Wind turbines are usually supported by either a slab foundation or a pile foundation. Soil conditions at the specific site usually govern whether a slab foundation or a pile foundation is chosen. A slab foundation is normally preferred when the top soil is strong enough to support the loads from the wind turbine, while a pile supported foundation is used when the top soil is of a softer quality and the loads need to be transferred to larger depths.

The overall foundation stiffness is dependent on the strength and stiffness of the soil as well as on the structural foundation elements. The foundation stiffness needs to be determined as a basis for predicting the dynamic structural response to wind, wave and earthquake loading. The foundation stiffness is in general frequency dependent. This is particularly important when predicting dynamic response to earthquake [7; 11].

The finite element method provides a precise computational mean for soil structure interaction. The foundation soil can be modeled throughout finite elements in stead of providing a global stiffness of the soil. Although in this method the soil parameters considered are the elastic modulus and the Poisson’s ratio, the results are more realistic than using stiffness springs [6].

Various books are providing different equations to compute foundation stiffness depending on the shape, size and type of the foundation and on the soil properties. Table 1 presents some of these equations from three different sources to compute stiffness for a circular footing on stratum over bedrock (figure 2a.) and for circular footing embedded in stratum over bedrock (figure 2b.). There are also other equations to be used for other shapes of foundation and for pile foundations.

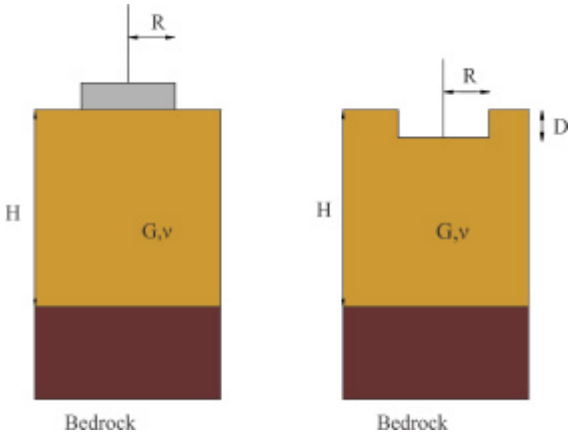

Figure 2. a. Circular footing on stratum over bedrock, b. circular footing embedded in stratum over bedrock

Table 1. Equations to compute stiffness for a circular footing on stratum over bedrock according to figure 2.a. [3, 9, 10]

Mode of motion	Circular foundation	
Source of references	Negoita and Fema 450	Guidelines for Design of Wind Turbines
Vertical	$k_z = \frac{4GR}{1-n}$	$k_z = \frac{4GR}{1-n}\left(1+1.28\frac{R}{H}\right)$
Horizontal	$k_x = \frac{32(1-n)GR}{7-8n}$	$k_x = \frac{4GR}{1-n}\left(1+1.28\frac{R}{H}\right)$
Rocking	$k_q = \frac{8GR^3}{3(1-n)}$	$k_q = \frac{8GR^3}{3(1-n)}\left(1+\frac{R}{6H}\right)$
Torsion	$k_t = \frac{16GR^3}{3}$	$k_t = \frac{16GR^3}{3}$

Guidelines for Design of Wind Turbines provide the following formula to compute the foundation stiffness for a circular footing embedded in stratum over bedrock (figure 2b) [3]:

$$k_z = \frac{4GR}{1-n}\left(1+1.28\frac{R}{H}\right)\left(1+\frac{D}{2R}\right)\left[1+\left(0.85-0.28\frac{D}{R}\right)\frac{D/H}{1-D/H}\right] \quad (1)$$

$$k_x = \frac{8GR}{1-n}\left(1+\frac{R}{2H}\right)\left(1+\frac{2}{3}\frac{D}{R}\right)\left(1+\frac{5}{4}\frac{D}{H}\right) \quad (2)$$

$$k_q = \frac{8GR^3}{3(1-n)}\left(1+\frac{R}{6H}\right)\left(1+2\frac{D}{R}\right)\left(1+0.7\frac{D}{H}\right) \quad (3)$$

$$k_t = \frac{16GR^3}{3}\left(1+\frac{8D}{3R}\right) \quad (4)$$

In figure 2 and in ale the equations the following notations were used:

G –shear modulus,
? –Poisson's ratio,
R – foundation radius,
D – embedment depth,
H – the width of the soil stratum to the bedrock.

3. CASE STUDY

In order to highlight the importance of taking in to account soil - structure interaction in a dynamic analysis for a wind turbine it was chosen a particular case. Therefore in this chapter there are presented the results from a dynamic analysis for a 70 meters tall wind turbine considering 4 different types of soils.

The entire soil – foundation - wind turbine structure was modeled using finite element method. The model used is presented in figure 3. The analysis was performed using the computational program Sap 2000. The tower was modeled through 'shell' finite elements having variable diameter and thickness along the height of the tower. It is a 67.6 m tall tubular steel tower with a range of diameter from 4.2 m at the base to 1.85m at the top. The mass of the tower is 85.15 tones and the weight of the rotor and the blades are 47 tones. The rotor and the blades were modeled as a concentrated mass at the top of the tower. Also along the entire height of the tower the weight from interior stairs and platforms was applied.

The foundation used for this model is a circular footing having a 16 meters diameter (D) and a 3 meters thickness. The foundation soil considered for the analysis was extended around the foundation at a length of 2D and in depth for 6D.

It is considered that the wind turbine is operating with variable speed range from nmin =5,5 rpm to nmax=29 rpm.

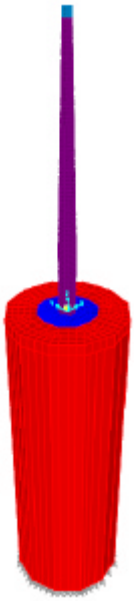

Figure 3. Model of the soil- foundation - wind turbine

Table 2 presents the characteristics of the 4 types of foundation soils used in the analysis. The names of the soils are given after their shear wave velocity. Also the soil classes correspond to the SR EN 1998-1:2004 standard.

Table 2. Foundation soils characteristics

Soil type	Shear waves velocity [m/s]	Soil class SR EN 1998-1:2004	Poisson's ratio , ?	Density, ? [N/m3]	Elastic modulus, E [N/m2]	Shear modulus, G [N/m2]	kx N/m3
V150	150	D	0.45	19620	4804940	1656875.9	3,5 *106
V300	300	C	0.4	20000	13757818	4913506	6 *106
V600	600	B	0.35	22000	23534400	8716444	35*106
V900	900	A	0.3	25000	50000000	19230769	70*106

From the dynamic analysis the natural frequencies of the tower considering the same type of foundation but different types of soils were determined. The variation range of the frequencies was considered to be at ±10%.

Table 3 presents these results obtained from the dynamic analysis.

Table 3. Natural frequencies and periods of vibration of the model

Mode of vibration	Type of soil	Frequency Hz	Frequency+10% Hz	Frequency - 10% Hz	Period of vibration s
1	V150	0,445	0.4895	0.4005	2,242
	V300	0,499	0.5489	0.4491	2,002
	V600	0,514	0,5654	0,4626	1.942
	V900	0,521	0,5731	0,4689	1.917
2	V150	1.5743	1,73173	1,41687	0,635
	V300	2.5212	2,77332	2,2690	0.396
	V600	3,084	3,3924	2,7756	0,324
	V900	3,243	3,5673	2,9187	0,308

The diagrams of resonance presented in figures 4 to 7 were realized using the following equations:

$$\frac{f_R}{f_{0,1}} \le 0.90 \text{ and } \frac{f_{R,m}}{f_{0,n}} \le 0.90 \text{ or } \frac{f_{R,m}}{f_{0,n}} \ge 1.10 \quad (5)$$

where: fR is maximum rotation frequency of the rotor in normal operation range;

f0,1 – first eigenfrequency of the tower;

fR,m – pass frequency of the m rotor blades;

f0,n – the n-th frequency of the tower..

The frequencies f_f 1- f_f 15 from the resonance diagrams were computed with the following relation:

$$f_f = \frac{i \cdot n}{60} \quad (6)$$

Where: i=1…15 and n= 1, 3, 5, 7, 9, 11, 13, 15, 17, 19, 21, 23, 25, 27, 29, 31.

It is necessary that the first frequency f_f1 avoid entering the variation range of the first frequency of the tower until the rotor reaches the speed of 29.18 rpm.

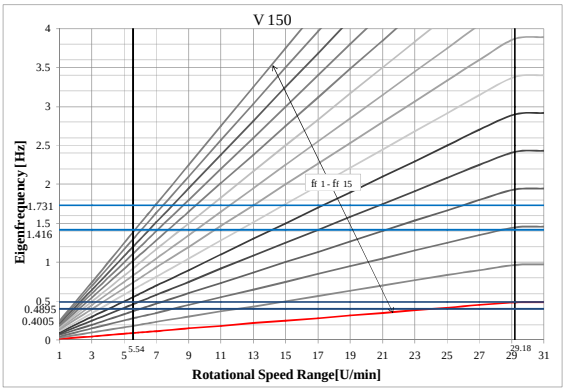

Figure 4. Diagram of resonance for model with soil V150

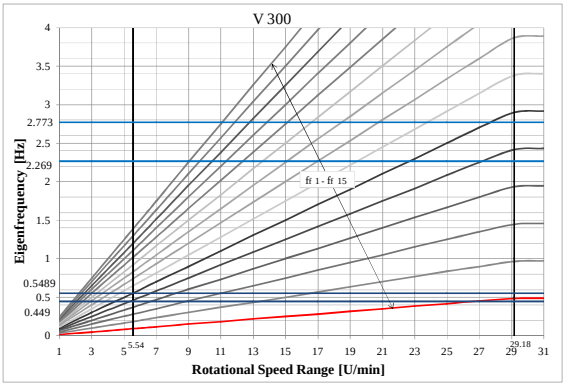

Figure 5. Diagram of resonance for model with soil V300

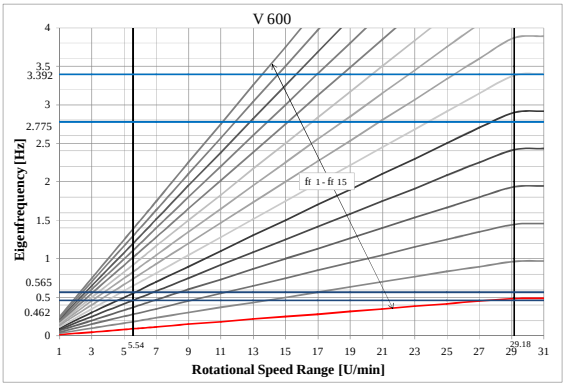

Figure 6. Diagram of resonance for model with soil V600

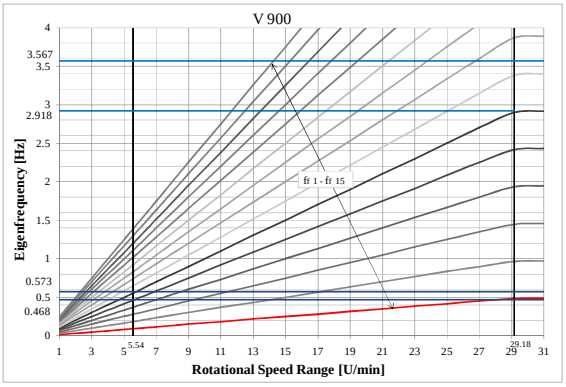

Figure 7. Diagram of resonance for model with soil V900

The resonance diagrams were performed in order to establish the minimum type of foundation soil on which this type of wind turbine can be placed.

From the resonance diagrams it can be noticed that the V150 type of soil is the most disadvantageous because the first operational frequency of the wind turbine is entering the resonance domain before the turbine reaches the maximum operational speed. Therefore the minimum type of soil to be used for this type of wind turbine and foundation system is V600 with the specific characteristics given in SR EN 1998-1:2004.

4. CONCLUSIONS

The natural modes of vibration and the frequencies of the entire soil - foundation-wind turbine system play an important role in wind turbine analysis. Based on this analysis it can be noticed that considering soil-structure interaction is a very important aspect in order to avoid entering the resonance range. Also by considering soil stiffness the entire system has smaller frequencies than considering the structure with a fixed base. This aspect is reflected in a lower limitation range of the tower’s frequencies which can imply a higher possibility for the operating frequency to coincide with the tower’s frequency. Therefore care must be taken when choosing the right foundation solution based on the type of soil it can be found on the construction site.

References

1. Olariu, C.P. Influenta deformabilitatii terenului de fundare asupra comportarii unor structuri de rezistenta, teza de doctorat , Universitatea Gh. Asachi, Iasi, 2011
2. The International Standard IEC 61400-1- Wind turbines - Part 1: Design requirements, 2005

3. Guidelines for Design of Wind Turbines, DNV/Ris? , Jydsk Centraltrykkeri, Danemarca, 2002.
4. Guideline for the certification of wind turbines, Germany, 2003.
5. Hau, E., Wind Turbines: Fundamentals, Technologies, Application, Economics; 2nd Edition Springer-Verl., Berlin, 2006;
6. Hartmann, F., Katz, C. - Structural Analysis with Finite Elements, Springer-Verl., Berlin, 2007;
7. Mohamed Al Satari, Saif Hussain, S.E – Vibration Based Wind Turbine Tower Foundation Design Utilizing Soil-Foundation-Structure Interaction, The 14th World Conference on Earthquake Engineering, Beijing, China, October, 2008
8. Pekka Maunu – Design of Wind Turbine Foundation Slabs, Master's Thesis Lulea University of Technology, Hamburg, 2008
9. NEHRP recommended provisions for seismic regulations for new buildings and other structures, Part 1-15, Fema 450, Washington, D.C., 2003.
10. Negoita, Al., s.a. - *Inginerie seismica*, Editura didactica si pedagogica, Bucuresti, 1985
11. Olariu, C.P.- Influenta deformabilitatii terenului de fundare asupra raspunsului dinamic al unei turbine eoliene. "Creatii universitare 2011", Al IV-lea Simpozion National Iasi, România, 2011.

Finite element analysis of bonding between carbon fibers reinforced polymeric composites (CFRP) and concrete

Ruxandra Oltean
Department of Civil and Industrial Engineering, "Gh. Asachi" Technical University, Iasi, Romania

Summary

Retrofit of reinforced concrete members using externally bonded fiber reinforced polymer composites (FRP) has become widely recognized. However, in many instances, the FRP strengthened element suffers a premature debonding failure between FRP and the concrete substrate before the concrete – FRP hybrid element reaches its bearing capacity. The FRP – concrete interface plays a major role in this strengthening method by providing effective stress transfer from the substrate to the FRP strips and guarantee the consistency of the hybrid systems made of FRP and concrete.

An experimental program has been carried out at the Technical University of Iasi, Romania to study the interfacial behaviour between carbon fibre reinforced polymer (CFRP) composite sheets and concrete as a preliminary required step to develop hybrid structures made of polymeric composites and traditional building materials.

In addition to the experimental work a finite element analysis was performed, using Ansys package software. Proper modeling of such hybrid structures require a significant effort made even assuming linear elastic behavior and problems exist when using finite elements to study the bonding between the FRP and the concrete due to the complexity of the materials. Therefore, most of the existing models in literature adopted a number of simplified assumptions. For example, the adhesive was often neglected and the bond layer was typically not modeled.

This paper focuses on predicting, by numerical modeling, the failure loads and stresses of concrete - CFRP hybrid elements utilizing three different CFRP plates.

The simulated results using the finite element analysis were found to agree well with experimental data from all sets of tests.

KEYWORDS: concrete; fiber reinforced polymers, bond, finite element analysis, strengthening.

1. INTRODUCTION

Since the beginning of structural restoration, architects and engineers have envisaged and actually applied a wide variety of repair or strengthening interventions to improve the structural response of the damaged concrete structures. Besides the usage of traditional techniques, modern techniques such as the application of FRP composites for strengthening are getting more attention nowadays. Modern practice in civil and structural engineering involves strengthening concrete structures by externally bonded FRP materials, which has become a common practice, widely recognized by modern design codes [1 – 6]. This type of reinforcing system has a significant number of advantages, such as lightness, noncorrosive, nonmagnetic, strong and highly versatile, FRP composite products being, in certain cases, the ideal materials for structural strengthening and rehabilitation [7 – 9].

The two general types of applications of externally bonded FRP composites on concrete substrate are generally known as contact-critical and bond-critical. In contact-critical applications, the load is transferred between FRP and concrete by contact stress across the interface, as in passive column confinement. In bond-critical applications, the load is transferred by shear stress as well as peeling-stress, as in flexural and shear reinforcements for beams [10]. Therefore the existing experimental work has been carried out using several set-ups, including single shear test [11 - 13], double shear tests [14 – 16] and beam tests [17] (Fig. 1). The current paper is concerned with the bond behavior in case of double shear test set-up using both experimental tests and the finite element (FE) analysis.

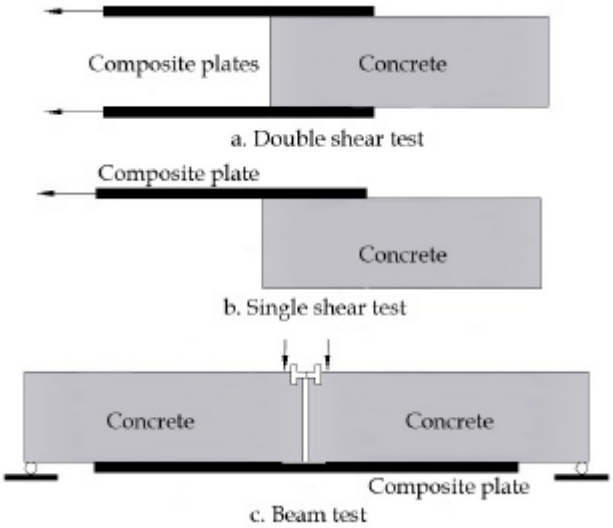

Figure 1. Bond test set-ups [17]

2. FINITE ELEMENT MODELING

Two identical CFRP plated concrete prisms 400 mm long and with a cross-section of 150 x 150 mm under tension were chosen as the benchmark specimen to be studied. Three simplified FE models with different types of CFRP reinforcement were built to analyze the bonding behavior using Ansys software package. For the first two models all components were assumed to be linear elastic, while for the third FE model the bilinear concrete behavior was considered. The materials properties of all components are given in Table 1 and the considered geometrical model can be observed in Figure 2. In order to reduce the solving time and to increase the precision the geometrical model was simplified using the symmetry of the elements, thus the simplified model is actually a quarter of the benchmark specimen.

Table 1. Properties of the constituent materials

Specimen series	C1	C2	C3
Type of CFRP plate	Sika Carbodur S1012	Sika Carbodur M1014	CFK 150/2000
Geometric characteristics (mm)	1.2x100	1.4x100	1.2x100
Density (kg/m^3)		1600	
Poisson's ratio		0.25	
Young's modulus (N/mm^2)	165000	210000	165000
Tensile strength (N/mm^2)	3100	3200	1000
Adhesive		Sikadur 30	
Density (kg/m^3)		1650	
Poisson's ratio		0.4	
Young's modulus (N/mm^2)		12800	
Tensile strength (N/mm^2)		25	
Compressive strength (N/mm^2)		75	
Concrete batch		Batch 1	
Density (kg/m^3)		2300	
Poisson's ratio		0.2	
Young's modulus (N/mm^2)		32000	
Tensile strength (N/mm^2)		2.2	
Compressive strength (N/mm^2)		31.6	

The FE modeling of all components was performed using 3D elements, solid elements. Namely, the specimens were modeled using 20 nodes solid elements, Solid 186, while for the interface area CONTA 174 were employed, elements which are currently used by Ansys in modeling the contact and slip between two surfaces. However, in this study perfect bond between materials was assumed. The

high strength of the epoxy used to bond the CFRP sheets to the concrete prisms supported the perfect bond assumption. More than that, the nodes of the CFRP solid elements were connected to those of adjacent concrete solid elements in order to satisfy the perfect bond assumption.

As an initial step, a fine FE mesh was employed especially in the area of CFRP bonding to the concrete substrate (Figure 3). In other words, the model was divided into a number of small elements, and after loading, stress and strain are calculated at integration points of these small elements [18].

The loading was applied taking into account the displacement control, thus it was imposed the ultimate value of the experimental displacement.

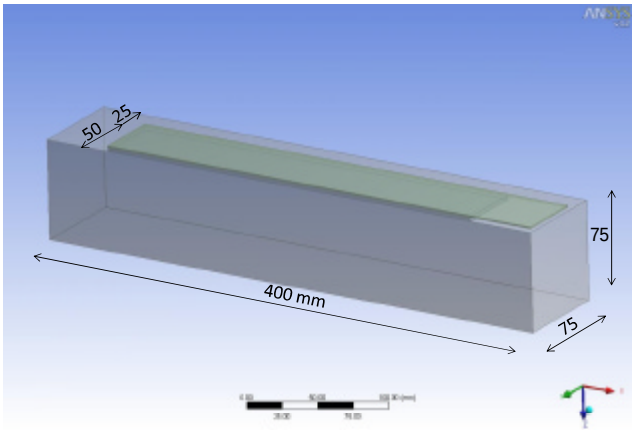

Figure 2. Simplified model

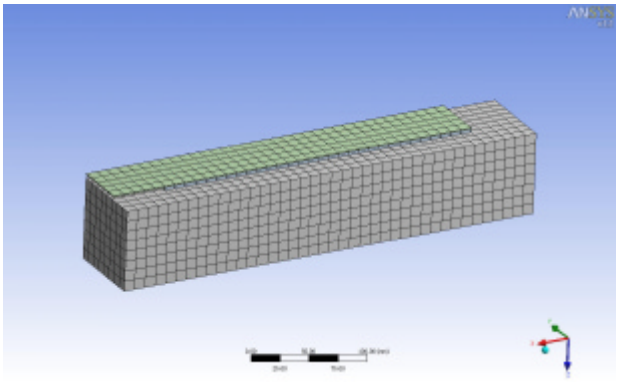

Figure 3. FE mesh

3. NUMERICAL RESULTS AND DISCUSIONS

This chapter presents the numerical results obtained after simulating the behavior of a CFRP – concrete hybrid system subjected to tension. Thus, in Table 2 are summarized the maximum values of the following parameters: total displacement, principal stresses, equivalent, normal and shear stresses, as well as the frictional stresses, evaluated on three FE models corresponding to the considered groups, namely C1, C2 and C3.

Table 2. Numerical results

	C1	C2	C3
Total displacement [mm]	0.17	0.24	0.30
Maximum principal stress [N/mm^2]	350.19	466.72	450.29
Equivalent stress [N/mm^2]	355.09	474.35	456.71
Normal stress [N/mm^2]	350.08	466.57	450.17
Shear stress in the composite[N/mm^2]	16.43	22.41	21.69
Frictional stresses [N/mm^2]	24.17	34.51	27.63

The above presented numerical results were obtained after performing a considerable number of iterations, describing in a satisfying manner the general behavior of a hybrid system, in terms of maximum normal stresses and ultimate loads (Figure 4, Figure 5).

The accuracy of the models and accordance to the experimental program can be also confirmed by the resemblance between the shear stresses – slip comparative curves (Figure 6).

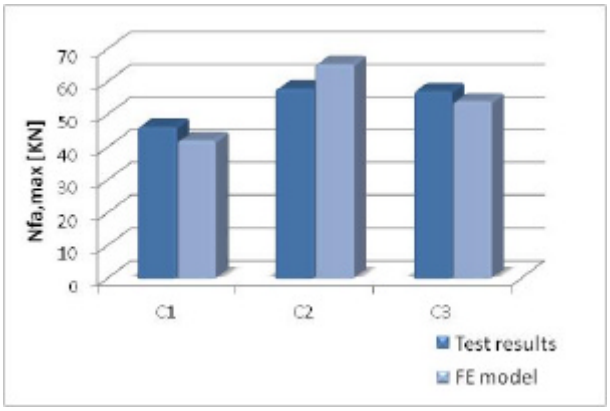

Figure 4. Experimental vs. FE analysis ultimate loads –

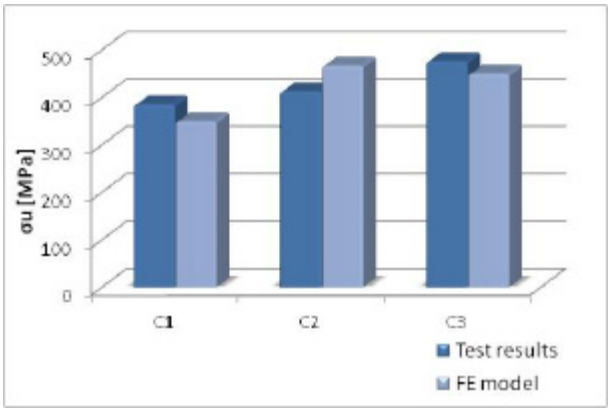

Figure 5. Experimental vs. FE analysis maximum normal stresses

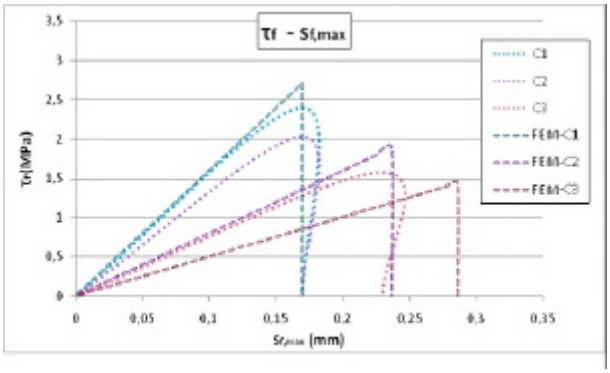

Figure 6. Experimental vs. FE analysis shear stresses – slip curve

4. CONCLUSIONS

Modern strengthening approaches are based on the idea that the strengthening should be light and removable and, if possible, it should not change the structural scheme or the construction; objective which can be achieved by using FRP composites. The FE analysis offers flexibility and precision, being possible to model different elements with complex geometry, having various loading schemes and boundary conditions. On this line, three FE models were carried out to establish the bonding behavior of a CFRP – concrete hybrid system. These models consisted in applying CFRP strips on two opposite sides of a concrete element, comprised of two identical prisms and subjected to tension. Analyzing the numerical results by comparing them to the experimental ones revealed a good correlation between the simulated structural behavior and the test results.

The FE analysis utilized in case of externally bonded FRP composites proved to be a powerful instrument in determining the general behavior of the considered element especially when the adhesive layer is included in the model.

References

1. JSCE, *Recommendations for upgrading of concrete structures with use of continuous fiber sheets. Technical Report*, Research Committee on Upgrading of Concrete Structures with Use of Continuous Fiber Sheets, Japanese Society of Civil Engineers, Japan, 2000.
2. Fib Bullettin 14, *Externally bonded FRP reinforcement for RC structures. Technical Report*, Federation Internationale du Beton, 2001.
3. ISIS, *Retrofitting concrete structures with fiber reinforced polymers*, ISIS, Canada, 2001.
4. ACI 440, *Guide for the design and construction of externally bonded FRP systems for strengthening concrete structures. Technical Report*, American Concrete Institute, 2002.
5. CNR – DT 200/2004, *Guide for Design and Construction of Externally Bonded FRP Systems for Strengthening Existing Structures. Materials, RC and PC structures, masonry structures*, National Research Council – Advisory Committee on Technical Recommendations for Construction, Rome, Italy, 2004.
6. CS 55, *Design guidance for strengthening concrete structures using fibre composite materials. Technical Report*, Concrete Society, UK, 2004.
7. Oprisan G., Munteanu V., Cozmanciuc C., Taranu N., Entuc I., *Particularities of structural response of confined reinforced concrete columns with composite membranes*, 9th International scientific conference VSU, Sofia, June 4-5, 2009, Vol. II, pp. 95-100, 2009.
8. Cozmanciuc C, Oltean R., Munteanu V., *Strengthening techniques of RC columns using fibre reinforced polymeric materials*, Bulletin of the Polytechnic Institute of Iasi, **LV (LIX)**, *3*, pp. 85-92, 2009.
9. Cozmanciuc C., Oprisan G., Taranu N., Munteanu V., Oltean R., Budescu M., *Structural behaviour response of eccentrically loaded reinforced concrete columns confined with carbon fibre reinforced membranes*, 11th International Scientific Conference VSU, Sofia, 2-3 June 2011, Vol. I, II – 198 – 203, 2011.
10. Mirmiran A., Shahawy M., Nanni A., Karbhari V., *Bonded Repair and Retrofit of Concrete Structures Using FRP Composites. Recommended Construction Specifications and Process Control Manual*, NCHRP Report 514, Washington-DC, USA, Transportation Research Board, 2004.
11. Yao. J., Teng J.G., Chen J.F., *Experimental study on FRP-to-concrete bonded joints.* Composites. Part B: Engineering, **36**, *2*, pp. 99–113, 2005.
12. Aiello M.A., Leone M., *Interface analysis between FRP EBR system and concrete.* Composites: Part B, **39**, pp. 618 – 626, 2008.
13. Resende Balseiro A.M., Rautenstrauch K., *Bond behaviour of CFRP to timber beams in the end-anchorage situation*. Scientific Report within Cost Action E34 – Wood Adhesion, Bauhaus, Germany, 2007.
14. Aiello M.A., Sciolti M.S., *Bond analysis of masonry structures strengthened with CFRP sheets*. Construction Building Materials, **20**, *1-2*, pp. 90 – 100, 2006.
15. Xiao J., Li J., Zha Q., *Experimental study on bond behaviour between FRP and concrete*. Construction Building Materials, **18**, *10*, pp. 745 – 752, 2004.
16. Aprile A., Spacone E., Limkatanyu S., *Role of bond in RC beams strengthened with steel and FRP plates.* J Struct. Eng, **127**, *12*, pp. 1445 – 1452, 2001.
17. Taranu, N., Oltean, R. Cozmanciuc, C., *Experimental investigation on bonding CFRP plates to concrete substrate*, Bulletin of the Polytechnic Institute of Iasi, **LVII (LXI)**, *3*, pp. 47 – 56, 2011.
18. Bathe, K.J., *Finite Element Procedures*, Prentice-Hall, Inc., Upper Saddle River, New Jersey, 1996.

Bond behavior between fibers reinforced polymeric (FRP) strips and concrete – An analytical and numerical investigation

Ruxandra Oltean[1], Ciprian Cozmanciuc[2]
[1]*Department of Civil and Industrial Engineering, "Gh. Asachi" Technical University, Iasi,, Romania*
[2]*Department* of Concrete Structures, Building Materials, Technology and Management, "Gh. Asachi" Technical University, Iasi, 700050, Romania

Summary

Reinforced concrete (RC) structures, due to aging, material degradation, settlements, and structural alterations, often need to be strengthened to re-establish their performance. In this frame, fibre reinforced polymer (FRP) composites in the form of bonded strips applied to the external surface can be a convenient strengthening solution.

In flexural and shear strengthening cases, debonding between concrete and externally bonded FRP usually corresponds to the ultimate limit state of strengthened RC elements. This type of failure either decreases the strength efficiency of FRP materials or causes a deficiency in member ductility.

Since the structural performance relies on bond between FRP and concrete, the characteristics of bond and methods to evaluate it are critical to understanding and evaluating FRP- concrete hybrid elements.

Numerous analytical models were developed onwards to predict the interface bond strength or local bond stress – slip curve influences peak flexural or shear strength of RC elements strengthened with externally bonded FRP composites, generally on the basis of pull tests setup.

An accurate analytic model is of fundamental importance in the modelling of FRP strengthened RC structures. In this paper, a review of existing bong strength models and bond – slip models is first presented.

Further research was being conducted to simulate bond behaviour of external FRP reinforcement and concrete substrate, considering the double shear test set-up. Three-dimensional models based on finite element analysis were realised, using Ansys software. These results are then compared with the ones obtained by analytical models. The simulated results shown that the model can describe the static FRP-to-concrete bond behavior with good accuracy and mesh objectivity.

KEYWORDS: concrete; fiber reinforced polymers, bond, finite element analysis, analytical models.

1. INTRODUCTION

FRP composites are being successfully used for strengthening of degraded RC structures. Bond of the external FRP reinforcement to the concrete substrate is of critical importance for the effectiveness of this technique, since it is the means for the transfer of stresses between concrete and FRP in order to develop composite action. Indeed, a number of failure modes in FRP – strengthened RC elements are directly caused by debonding of the FRP from the concrete substrate. Therefore, for the safe and economic design of externally bonded FRP systems, a complete understanding of the behavior of FRP – concrete interface needs to be developed and reliable bond-slip model established.

In various debonding failure modes, the stress state of the interface is similar to that in a shear / double shear test specimen in which a laminate is bonded to a concrete prism and is subjected to tension (Figure 1). As a result, a large number of studies, both experimental and theoretical, have been carried out on simple and double shear test on adhesive joints. Existing studies suggest that the main failure mode of FRP – concrete hybrid systems in shear tests is concrete failure under shear, occurring generally at a few millimeters from the concrete – to – adhesive interface [1]. The current paper aims to predict, through both analytical and numerical analysis the bond behavior of a FRP – concrete hybrid system in double shear test.

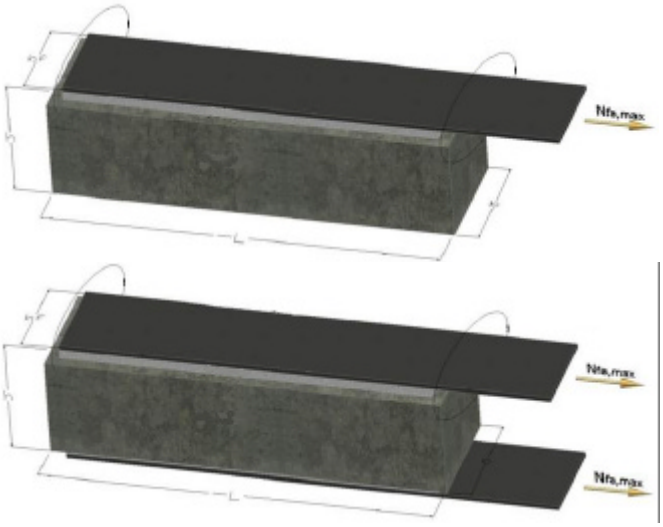

Figure 1. Single and double shear test setup

2. ANALYTICAL MODELS

2.1. Bond – slip models

Despite the difficulty in obtaining local bond–slip curves from pull tests directly, local bond–slip models for FRP to concrete interfaces have been developed based on strain measurements or load–slip curves.

Six local bond–slip models available in the existing literature are detailed below, where t (MPa) is the local bond (shear) stress, s (mm) is the local slip, $t_{\max}$ (MPa) is the local bond strength (i.e. the maximum bond/shear stress experienced by the interface), s_{peak} (mm) is the slip when the bond stress reaches $t_{\max}$, s_{ult} (mm) is the slip when the bond stress reduces to zero, k_b is the geometry factor, f'_c (MPa) is the cylinder compressive strength of concrete.

- Neubauer and Rostasy [2]

$$t_{\max} = 1.8 k_b f_{ctm} \tag{1}$$

$$s_{peak} = 0.202 k_b \tag{2}$$

$$k_b = \sqrt{1.125 \frac{2 - \frac{b_f}{b_c}}{1 + \frac{b_f}{400}}} \tag{3}$$

- Nakaba et al. [3]

$$t_{\max} = 3.5 f'^{0.19}_c \tag{4}$$

$$s_{peak} = 0.065 \tag{5}$$

- De Lorenzis et al. [4]

$$t_{\max} = 0.0182 \sqrt{n_f t_f E_f} \tag{6}$$

- Monti et al. [5]

$$t_{\max} = 1.8 k_b f_t \tag{7}$$

$$s_{peak} = 2.5 t_{\max} \left(\frac{n_f t_f}{E_f} + \frac{50}{E_c}\right) \tag{8}$$

$$s_{ult} = 0.33k_b \tag{9}$$

$$k_b = \sqrt{1.5\frac{2-\frac{b_f}{b_c}}{1+\frac{b_f}{100}}} \tag{10}$$

- Savoia et al. [6]

$$t_{\max} = 3.5 f'^{0.19}_c \tag{11}$$

$$s_{peak} = 0.065 \tag{12}$$

- Lu et al. [7 a, b]

$$t_{\max} = 1.5k_b f_{ctm} \tag{13}$$

$$s_{peak} = 0.195k_b f_{ctm} \tag{14}$$

$$s_{ult} = 2\frac{G_f}{t_{\max}} \tag{15}$$

$$k_b = \sqrt{\frac{2.25-\frac{b_f}{b_c}}{1.25+\frac{b_f}{b_c}}} \tag{16}$$

$$G_f = 0.308k_b^2\sqrt{f_{ctm}} \tag{17}$$

where,

E_c = elastic modulus of concrete;

G_f = fracture energy.

The model of Monti et al. [5] is comparable to that of Neubauer and Rostasy [2] but also gives the value of s_{ult}. The model of Savoia et al. [6] is similar to that of Nakaba et al. [3], and only the value of *s*peak changes. Only the models of Monti et al. [5] and Lu et al. [7 a, b] give the three parameters t_{max}, s_{peak},and s_{ult}, whereas, only the model of De Lorenzis et al. [4] considers t_{max} as a function of FRP stiffness. The other models consider t_{max} as a function of compressive or tensile strength of concrete, not depending on FRP stiffness [8]. Lu et al. [7 a, b] concluded that the model proposed by Chen and Teng [1] is the most accurate.

2.2. Bond strength predictions

Regardless the bond-slip model, the bond-strength of an FRP – concrete adhesive joint in terms of the interfacial fracture energy is given by Equation (18), which was developed by Holzenkämper [9] using a two-layered model.

$$P = b_f \sqrt{2 G_f E_f t_f} \tag{18}$$

Based on a series of tests, Neubauer and Rostásy [10] found that the fracture toughness could be calculated by:

$$G_f = c_f f_{ctm} \tag{19}$$

where, c_f was evaluated to 0.204 mm by a regression analysis of the test data. They further consider the effect of geometry of the specimen, and modified Holzenkämper's formula (Equation (18)) as:

$$P = \begin{cases} 0.64 k_b b_f \sqrt{E_f t_f f_{ctm}} \\ 0.64 k_b b_f \sqrt{E_f t_f f_{ctm}} \dfrac{L}{L_e}(2 - \dfrac{L}{L_e}) \end{cases} \tag{20}$$

where, $L_e = \sqrt{\dfrac{E_f t_f}{2 f_{ctm}}}$.

Monti et al. [5] conducted a parametric study using finite element analysis (FEA) in conjunction with experiments, and suggested the following formula for the bond capacity:

$$P = b_1 b_f \sqrt{\frac{E_f t_f t_{\max}}{3}} \tag{21}$$

where, ß$_1$ = the bond length factor $\begin{cases} = 1 & \text{– when } L > L_e; \\ < 1 & \text{- when } L < L_e. \end{cases}$

and $L_e = \sqrt{\dfrac{E_f t_f}{\sqrt{4 t_{\max}}}}$.

Täljsten [11] considered a three-layered model with a crack in the adhesive layer. In this way, he obtained:

$$P = b_f \sqrt{\frac{2E_f t_f G_f}{1+a}} \text{, with } a = \frac{E_f t_f}{E_c t_c} \tag{22}$$

where,

t_c = the height of the concrete prism

Wu et al. [12] used nonlinear interfacial constitutive laws to analyze a three-layered model and deduced a similar formula:

$$P = b_f \sqrt{\frac{2E_f t_f G_f}{1+b}} \text{, with } b = \frac{b_f E_f t_f}{b_c E_c t_c} \tag{23}$$

It may be seen that when $E_c t_c >> E_f t_f$ or $b_c E_c t_c >> b_f E_f t_f$, Equations (21) and (22) have a similar form as Equation (18). However, neither one calculate the interface fracture energy G_c.

Lu et al. [7 a, b] used new bond-slip models which are based on their earlier work of meso-scale finite element predictions, and suggested another similar model:

$$P = b_1 k_b b_f \sqrt{2G_f E_f t_f} \tag{24}$$

This definition follows Yuan et al. [13] equation for determining the effective bond length:

$$L_e = a + \frac{1}{2l_1} \ln\left[\frac{l_1 + \tan(l_2 a)}{l_1 - \tan(l_2 a)}\right] \tag{25}$$

where,

$$l_1 = \frac{t_{\max}}{s_{peak} E_f t_f}, \; l_2 = \sqrt{\frac{t_{\max}}{(s_{ult} - s_{peak}) E_f t_f}} \text{ and } a = \frac{1}{l_2} \arcsin\left[0.99\sqrt{\frac{s_{ult} - s_{peak}}{s_{ult}}}\right]$$

Chen and Teng [1] proposed a simple expression for calculating the ultimate bond strength as follows:

$$P = 0.427 b_1 k_b L_e b_f \sqrt{f_c'} \tag{26}$$

where,

$$k_b = \sqrt{\frac{2-\frac{b_f}{b_c}}{1+\frac{b_f}{b_c}}}, \qquad L_e = \sqrt{\frac{n_f t_f E_f}{\sqrt{f_{cm}}}}$$

f_c' = the concrete compressive strength determined on cylinders (in MPa)

ß$_1$ = the bond length factor $\begin{cases} = 1 & \text{– when } L>L_e; \\ \sin(\frac{p}{2}\frac{L}{L_e}) & \text{- when } L<L_e. \end{cases}$

All the models based on fracture mechanics require the knowledge of interface or adhesive fracture toughness. Efforts have been made to relate the interface fracture toughness to the tensile strength of concrete [1, 10, 14], but the proposed relations are empirical and the forms by different authors are quite diverse [15].

3. FINITE ELEMENT ANALYSIS

In this chapter using Ansys software package was simulated the bonding behavior of a double shear test setup. In this line, two identical carbon fibers reinforced polymeric (CFRP) laminates bonded on two concrete prisms 400 mm long and with a cross-section of 150 x 150 mm under tension were chosen as the benchmark specimen to be studied. Simplified FEA models with different three types of carbon fibers laminated composites were built, resulting in three groups of models, namely C1, C2 and C3. For the first two models it was assumed that all components are linear elastic, while for the third model the bilinear concrete behavior was considered, their properties being given in Table 1. The geometrical model was simplified using the symmetry of the elements, in order to reduce the solving time and to increase the precision, thus the simplified model is actually a quarter of the benchmark specimen (Figure 2).

A 3D FE modeling was realized, namely, the specimens were modeled using 20 nodes solid elements, Solid 186, while for the interface area CONTA 174 were employed. However, in this study perfect bond between materials was assumed. The high strength of the epoxy used to bond the CFRP sheets to the concrete prisms supported the perfect bond assumption. After meshing the specimen, the loading was applied taking into account the displacement control.

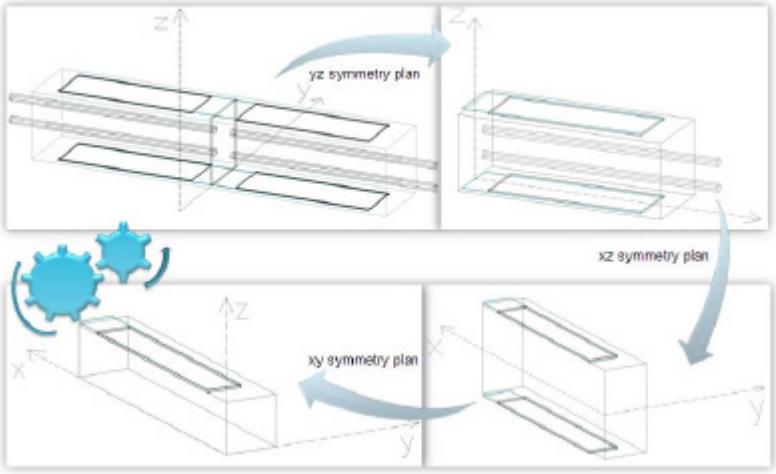

Figure 2. Reduced model obtained using symmetry plans

Table 1. Properties of the constituent materials

Specimen series	C1	C2	C3
Type of CFRP plate	Sika Carbodur S1012	Sika Carbodur M1014	CFK 150/2000
Geometric characteristics (mm)	1.2x100	1.4x100	1.2x100
Density (kg/m^3)		1600	
Poisson's ratio		0.25	
Young's modulus (N/mm^2)	165000	210000	165000
Tensile strength (N/mm^2)	3100	3200	1000
Adhesive		Sikadur 30	
Density (kg/m^3)		1650	
Poisson's ratio		0.4	
Young's modulus (N/mm^2)		12800	
Tensile strength (N/mm^2)		25	
Compressive strength (N/mm^2)		75	
Concrete batch		Batch 1	
Density (kg/m^3)		2300	
Poisson's ratio		0.2	
Young's modulus (N/mm^2)		32000	
Tensile strength (N/mm^2)		2.2	
Compressive strength (N/mm^2)		31.6	

4. COMMENTS AND RESULTS

In this section the authors present the numerical and analytical results obtained after simulating a double shear test setup for a hybrid CFRP – concrete element. Thus, in Figure 3 are illustrated the maximum loads corresponding to the considered series.

Regarding the bond – slip curve a summarized chart was realized for the presented analytical models (Figure 4), as well as for the simulated FEA models (Figure 5).

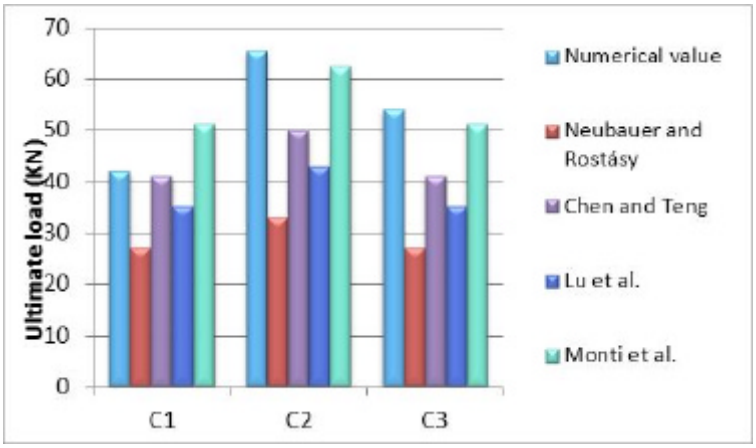

Figure 3. Numerical vs. analytical evaluation of ultimate load

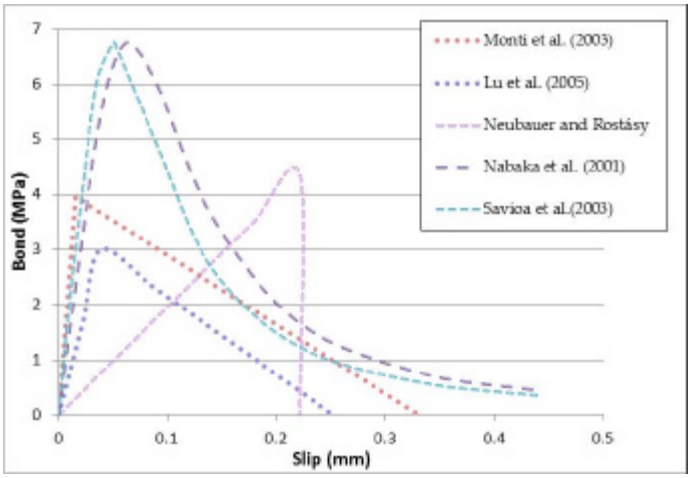

Figure 4. Bond – slip curve models

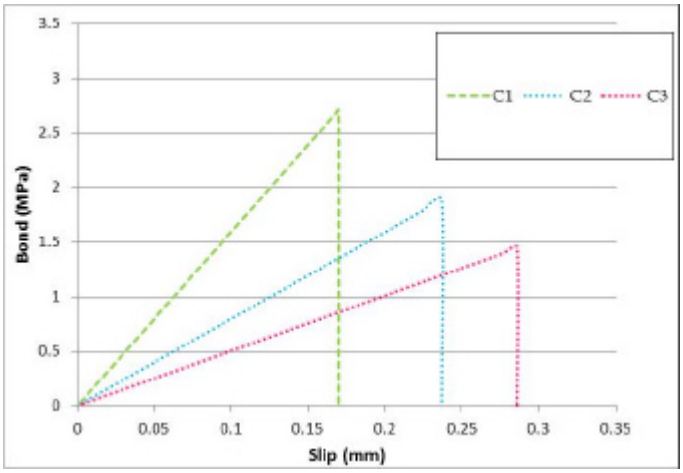

Figure 5. Numerical evaluation of the bond – slip curve

3. CONCLUSIONS

Clarifying the bond characteristics of the interface between concrete and externally bonded FRP strips is essential for designing externally bonded composite strengthening systems. Shear/ double shear tests are usually applied to obtain the bond characteristics of FRP – concrete interfaces in terms of overall or local interfacial bond properties. This paper analyses the analytical models showing how to obtain the main bond parameters necessary in engineering design and runs a numerical analysis for double shear tests of FRP – concrete interfaces.

Analyzing the results in terms of ultimate load one may state that the obtained numerical values are similar to the ones obtained using Monti et al. model. However, the numerical values overrate the values of the ultimate loads in two of the three studied cases.

References

1. Chen, J.F., Teng, J.G., Anchorage strength models for FRP and steel plates bonded to concrete, *Journal of Structural Engineering*, ASCE, Vol. 127, No. 7, pp. 784 – 791, 2001.
2. Neubauer, U., Rostasy, F. S., Bond failure of concrete fiber reinforced polymer plates at inclined cracks—Experiments and fracture mechanics model, *Proceedings of the 4th International Symposium on Fiber-Reinforced Polymer Reinforcement for Reinforced Concrete Structures*, SP-188, Americal Concrete Institute, Farmington Hills, Mich., pp. 369–382, 1999.

3. Nakaba, K., Kanakubo, T., Furuta, T., Yoshizawa, H., Bond behavior between fiber-reinforced polymer laminates and concrete, *ACI Struct. J.*, Vol. 98, No. 3, pp. 359–367, 2001.
4. De Lorenzis, L., Miller, B., Nanni, A., Bond of fiber reinforced polymer laminates to concrete, *ACI Mater. J.*, Vol. 98, No. 3, pp. 256–264, 2001.
5. Monti, M., Renzelli, M., Luciani, P., FRP adhesion in uncracked and cracked concrete zones, *Proceedings of the 6th International Symposium on FRP Reinforcement for Concrete Structures, FRPRCS-6*, World Scientific, Singapore, pp. 183–192, 2003.
6. Savoia, M., Ferracuti, B., Mazzotti, D., Nonlinear bond–slip law for FRP-concrete interface, *Proceedings of the 6th International Symposium on FRP Reinforcement for Concrete Structures, FRPRCS-6*, World Scientific, Singapore, pp. 163–172, 2003.
7. a. Lu, X. Z., Teng, J. G., Ye, L. P., Jiang, J. J., Bond–slip models for FRP sheets/plates bonded to concrete, *Eng. Struct.*, Vol. 27, pp. 920–937, 2005.
   b. Lu, X. Z., Teng, J. G., Ye, L. P., Jiang, J. J., Meso-scale finite element model for FRP plates/sheets bonded to concrete, *Eng Struct.*, Vol. 27, No. 4, pp. 564-575, 2005.
8. Pellegrino, C., Tinazzi, D., Modena, C., Experimental Study on Bond Behavior between Concrete and FRP Reinforcement, *Journal of Composites for Construction*, ASCE, Vol. 12, No. 2, pp. 180 – 189, 2008.
9. Holzenkämpfer, P., *Ingenieurmodelle des vverbundes geklebter bewehbrung für betonbauteile. Dissertation*, TU Braunschweig, 1994. (in German)
10. Neubauer, U., Rostásy, F. S., Design aspects of concrete structures strengthened with externally bonded CFRP plates, *Proceedings of 7th International Conference on structural faults and repairs*, Vol. 2, pp. 109-118, 1997.
11. Täljsten, B., Strengthening of concrete prisms using the plate bonding technique, *Internat J Fract*, 1996, Vol. 82, No. 3, pp. 253-266.
12. Wu, Z. S., Yuan, H., Niu, H. D., Stress transfer and fracture propagation in different kinds of adhesive joints, *J Eng Mech*, Vol. 128, No. 5, pp. 562-573, 2002.
13. Yuan, H., Teng, J. G., Seracino, R., Wu, Z. S., and Yao, J., Full range of FRP-concrete bonded joints, *Eng Struct*, Vol. 26, No. 5, pp. 553-565, 2004.
14. Taranu, N., Oprisan, G., Isopescu, D., Entuc, I., Munteanu, V., *Solutii compozite de realizare a structurilor ingineresti*, Editura Stef, 2006. (in Romanian)
15. Wu, Y., Zhou, Z., Yamg, Q., Chen, W., On shear bond strength of FRP-concrete structures, *Engineering Structures*, Vol. 32, pp. 897-905, 2010.

Computer aided optimization of a mixed structure

Ioana Olteanu[1] and Alexandru Stanila[2]

[1] *Department of Structural Mechanics, Gheorghe Asachi Technical University, Iasi, 700050, Romania*
[2]*Department of Civil and Industrial Engineering, Gheorghe Asachi Technical University, Iasi, 700050, Romania*

Summary

Modern architecture tends to propose structures with challenging shapes for the structural designer. These structures, beside their aesthetic properties, must fulfil some strength and stability requirements.

The technical content of the study refers to the structural configuration of an innovative flexible 5-storey building having the destination of a Students' Activity Centre, located in Iasi.

The structure has a pyramid shape with a centre core as structural system realized mainly of reinforced concrete. Radial disposed cantilevered floors, resembling with the branches of a tree, discharge on the centre core.

Several analyses were conducted in SAP2000 in order to find the most suitable configuration that satisfies strength, serviceability and stability requirements.

KEYWORDS: finite element analysis, mixed structure, structure optimization.

1. INTRODUCTION

Earthquakes effects from past years reveal the necessity to design considering the multi-hazard effect on structures. The studied project is located in Iasi, in an area where the most unfavorable situation is represented by the seismic action.

The earthquake effect is controlled by: structural deep central foundation with double function taproot system, central core made of concrete, flat plate frames and radial disposed cantilevered floors.

The architectural aspect of the building mimics the nature in plane and facades, layouts, elevation, and details of out-of-the-box architecture. The natural tree aspect integrates the building in the natural landscape.

The innovation of the structure consists of the challenge to realize a structure that satisfies the structural safety requirements and does not influence the environment conditions. Besides adopting reinforced concrete structural system, several ecological elements were considered, like special glazing curtain façade walls, special foundation, but they do not make the subject of the current paper.

The aims of structure modeling by FEM model are: to understand the global behavior of structure, to design each element and to optimize the overall behavior of the structure. Prescriptions from current regulations were considered.

2. STRUCTURE DESCRIPTION

2.1. Structure dimensions

The building central's core is 6.2 m x 6.2 m wide with a ground floor high of 4 meters and 3 meters high for the superior floors.

The surface of the first slab is 24.2 m x 24.2 m, the second slab have a surface of 19.7 m x 19.7 m, the third slab of 15.2 m x 15.2 m, the fourth one of 10.7 m x 10.7 m, and the last one of 6.2 m x 6.2 m.

The maximum high of the pyramid in top of the building is 2.3 meters.

2.2. Materials properties

The proprieties of the used materials are presented in table 1

Table 1. Material characteristics

No	Material	Density [daN/m^3]	Coefficient of elasticity [N/mm^2]	Poisson's coefficient [-]	Strength [N/mm^2]	
					reduction	expansion
1.	C 25/30	2500	32500	0.2	24.3	-
2.	S235	7850	270000	0.3	-	235

2.3. Structural system

The symmetrical geometry looking like a tree needed a specific structural conception in order to fulfill strength and stability requirements.

The configuration was for a flexible 5-storey building having the destination of a Students' Activity Centre. From structural point of view, the building has a central

core where the circulation function is located, that carries large, radial disposed cantilevered floors. As closing elements, translucent heat-saving panels were used.

The foundation is based on a rectangular foundation raft carried by four piles, placed on the corner of the main foundation raft, figure 1. The foundation raft dimensions are 21 by 21 m.

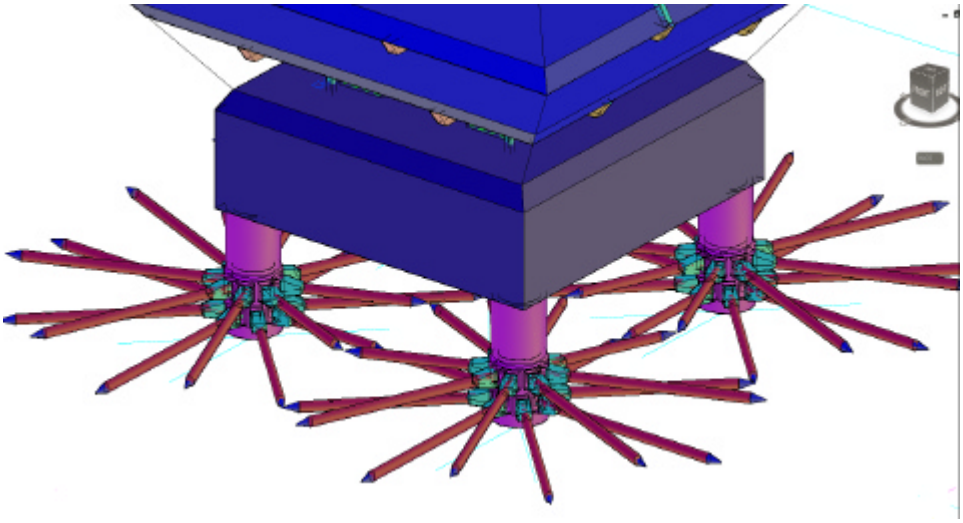

Figure. 1 Foundation detail

The central core is composed of four reinforced concrete columns having a L shape with the following dimensions 100 x 100 x 40 mm. The plan dimensions of the main central core are 6.2 x 6.2 meters as it can be seen in the Figure 2. The circulation core is enforced with structural walls of 15cm thickness.

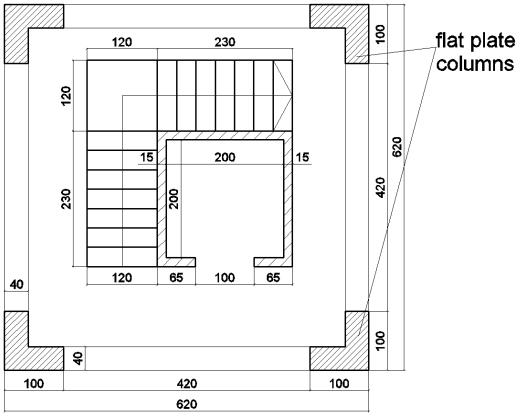

Figure. 1 Central core; horizontal and vertical section

In the final version, coffered slabs were adopted for the first and second floors of the structure in order to take over internal efforts. The contour beams are made of INP 400 steel profiles cross section. The slabs panels are 1.00 m x 1.00 m wide and the secondary beams that split the slab into panels have the section as presented in Figure 3.

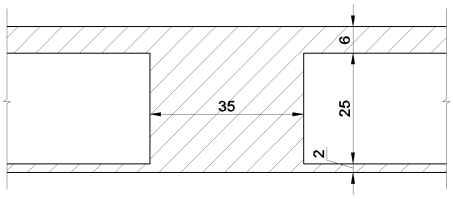

Figure 3 Coffered slab detail

The slabs over the second and the third floor are reinforced concrete, rested also on INP 240 steel profiles. The considered thickness of the slabs is 0.15 meters.

The last slab is also a 0.15 m reinforced concrete wide slab, which discharge on reinforced concrete beams of 0.3 x 0.4 m cross section.

All the slabs direct their load to the central core through principal reinforced concrete beam of 0.3 x 0.4 m cross section.

The biggest radial cantilever is of 9 m and in order to limit the vertical displacement of the slabs additional reinforced concrete columns were introduced. Reinforced concrete columns of 30 x 30 m were considered in the numerical simulation.

3. NUMERICAL SIMULATION

To understand the behavior of the structure and to design the elements, a model was made in FEM software SAP 2000, version 14.2. The program allows creating structural models rapidly and intuitively without long learning curve delays. Complex models can be generated and meshed with powerful built in templates.

Advanced analytical techniques allow for step-by-step large deformation analysis.

Eigen and Ritz analyses based on stiffness of nonlinear cases, buckling analysis, progressive collapse analysis, energy methods for drift control, base isolators and support plasticity. This finite element model had been developed to obtain the expected maximum stresses and the behavior of the structure under the load combinations detailed below.

The final structural model satisfies safety and stability requirements. For the considered model several analysis were performed in order to obtain the final results: modal analysis, static analysis and response spectrum.

3.1. Applied load

Beside the self weight of the structure, the taproot was also subjected to a 200 daN/sqm dead load and a 250 daN/sqm live load. The response spectrum analysis was performed using the normalized response spectrum from the Romanian seismic code, P100-1/2006, presented in figure 4.

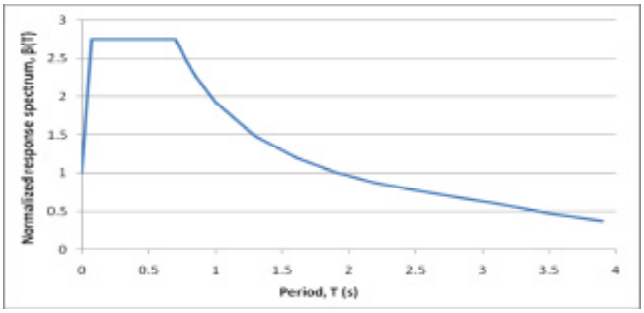

Figure 4. Considered response spectrum according to P100-1/2006

Other important parameters considered in the response spectrum analysis are: peak ground acceleration for Iasi a_g=0.2g, corner period, T_c=0.7s, importance factor for ordinary building, $?_I$=1.0 and a behavior factor of 6.15. The behavior factor is characteristic for a medium ductility and for frame and dual structural systems. The seismic action is applied on X axis, Y axis and on a 45 degree angle directions.

3.2. Considered combinations

Table 2. Considered combinations

Nr	Name	Dead	Live	RS x	RS y
0	C1 (modal analysis)	1	0.4	0	0
1	C2 (fundamental ULS)	1.35	1.5	0	0
2	C3 (seism x, ULS)	1	0.4	1	0
3	C4 (seism y, ULS)	1	0.4	0	1
4	C5 (seism 45, ULS)	1	1	0.707	0.707
5	C6 (characteristic, SLS)	1	0.4	0	0

Combinations for the Ultimate Limit States (ULS) and Serviceability Limit States (SLS) were considered, as showed in table 2. The combinations are according to CR0-2005 code.

3.3. Structural analysis results

3.3.1. Modal analysis results

The model analysis was performed considering masses from elements and gravitational loads, using C1 combination.

A comparison in terms of period, frequency and circular frequency between two versions of the structure was performed. The first version contains pre-stressed concrete columns only in the slab's corners; meanwhile the second version has pre-stressed columns on each façade in order to diminish the vertical displacement of the slab. Figure 5a shows that the first version has a period of 0.6225 s and that the slab over the ground floor vibrates significantly in vertical direction, in comparison with the second version for which the fundamental period is 0.26 s, almost 3 times smaller, and the characteristic vibration for mode 1 is torsion, figure 5b.

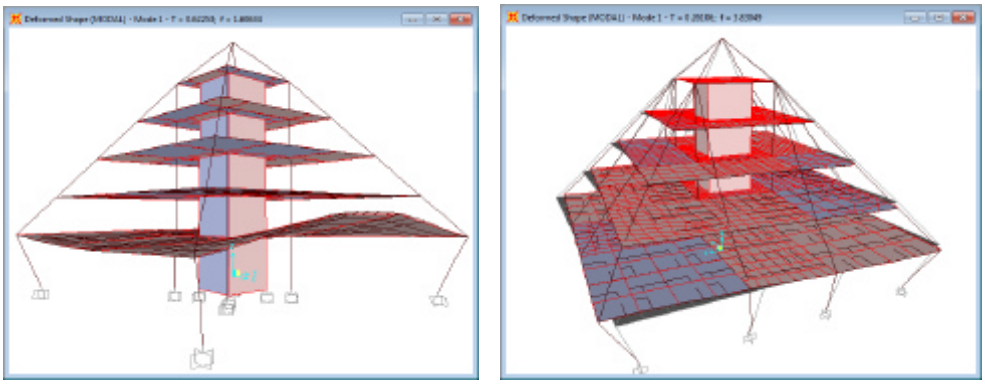

a. b.

Figure. 5 a. First mode of vibration for version 1; b. First mode of vibration for version 2

Table 3 presents complete results for the first 5 vibration modes for second structure, which was also considered in the rest of the analysis.

Table 3. Modal analysis results

Step number	Period [s]	Frequency [Hz]	Circular frequency [rad/sec]	Eigenvalue [rad2/s2)
1	0.261063	3.8305	24.068	579.25
2	0.181716	5.5031	34.577	1195.6
3	0.180717	5.5335	34.768	1208.8
4	0.176748	5.6578	35.549	1263.7
5	0.167240	5.9794	37.570	1411.5

3.3.2. Static analysis results

Considering the static combinations, C2 and C6, the following results were obtained for the slab in terms of stresses on the principal and secondary axis respectively, figure 6 and figure 7.

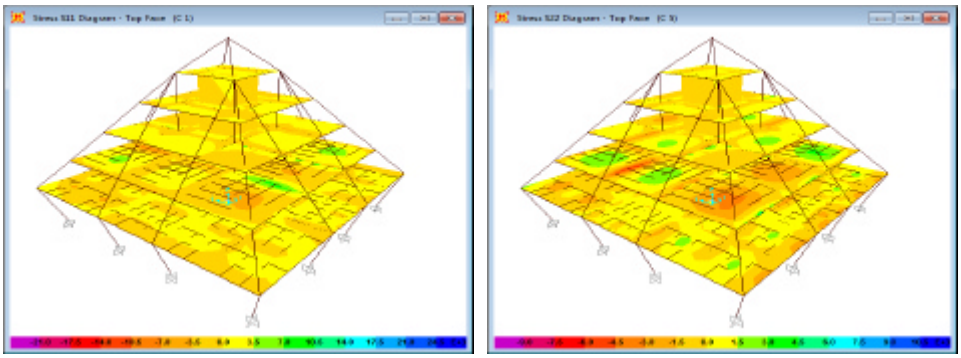

a. b.

Figure 6. Stresses on shells for C1 combination: a. S11 stresses; b. S22 stresses

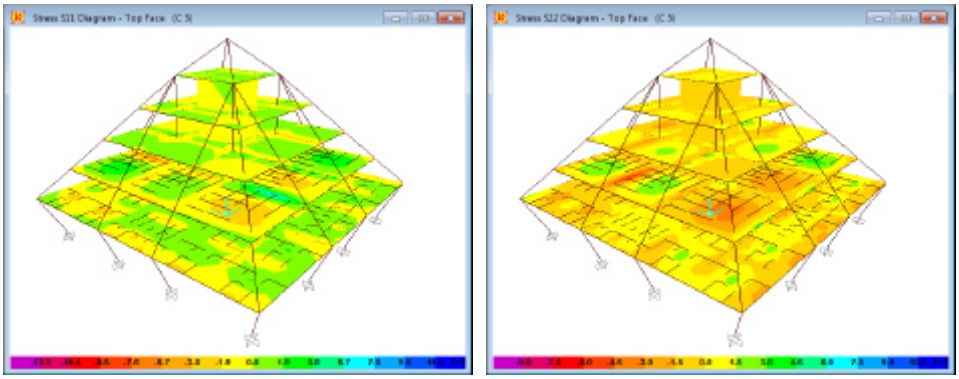

a. b.

Figure 7. Stresses on shells for C5 combination: a. S11 stresses; b. S22 stresses

Figure 8 presents the bending moment diagrams for a plane frame of the structure.

The performed analysis offer sufficient information in order to design and check the structural elements.

Considering the stresses which appear on the structural elements and comparing them with the material strength, it can be concluded that the selected cross section are enough to take over the internal efforts.

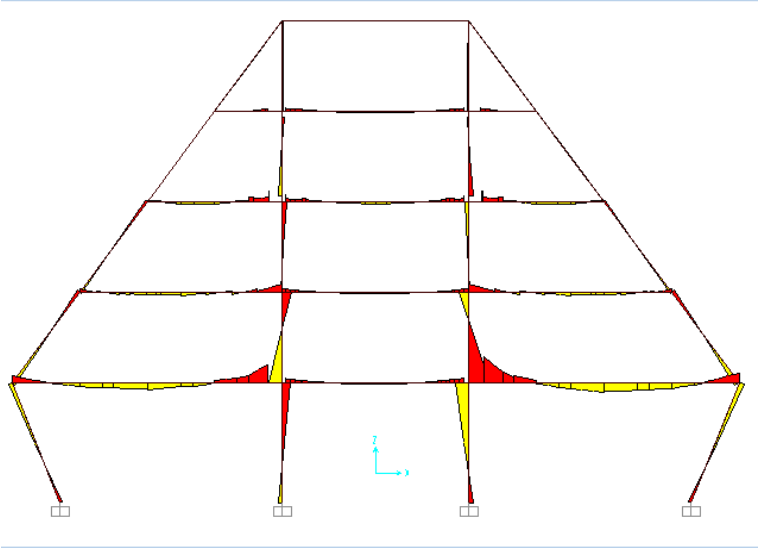

Figure 8. Bending moment diagram for C1 combination

3.3.3. Response spectrum analysis results

Antiseismic codes offer a wide variety of seismic analyses which can be applied on a structure. The analysis can be linear or nonlinear, static or dynamic. The most accurate one is considered the dynamic seismic analysis. Even though, researches in this field show that the response spectrum analysis can be considered a good approximation for the seismic analysis. Three seismic cases were considered – on X axis, on Y axis and on a 45 degree angle. Comparisons of the results for the stresses on both directions are made in the following figures.

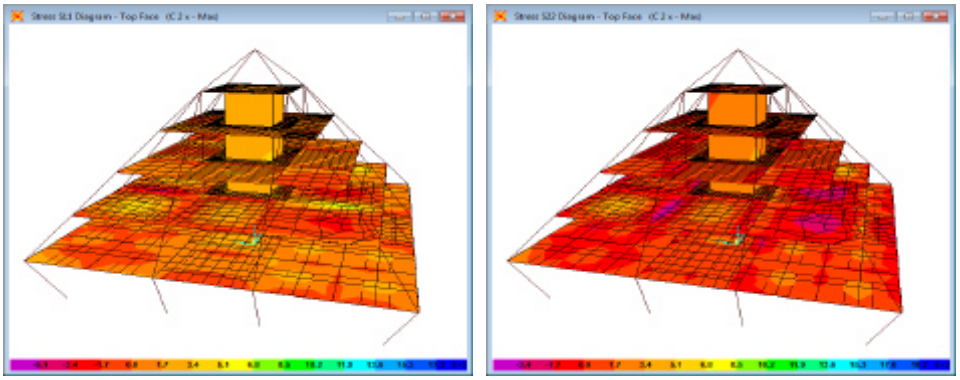

a. b.

Figure 9. Stresses on shells for C 2 combination: a. S11 stresses; b. S22 stresses

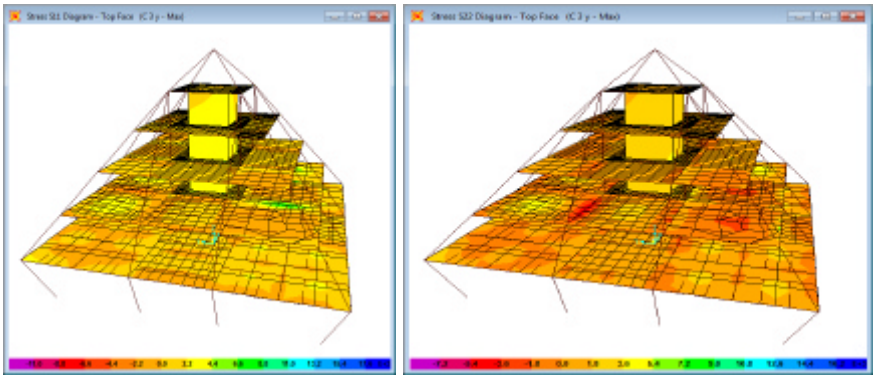

a. b.

Figure 10. Stresses on shells for C3 combination: a. S11 stresses; b. S22 stresses

Table 4 represents a synthesis of the maximum internal efforts for the structural elements, specifying the combination in which they occur.

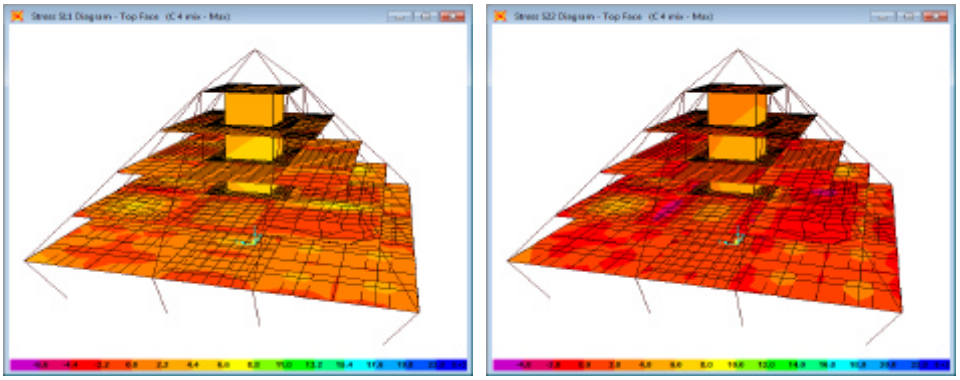

a. b.

Figure 11. Stresses on shells for C5 combination: a. S11 stresses; b. S22 stresses

Table 4. Maximum internal efforts

Maximum effort	Element	Combination	Magnitude
P (kN)	ground floor column	C4	-1483.841
V2 (kN)	ground floor beam	C2	-264.883
V3 (kN)	ground floor beam	C4	-683.439
M2 (kN*m)	ground floor column	C3	-581.0212
M3 (kN*m)	ground floor column	C2	-563.996
T (kN*m)	ground floor beam	C2	-28.2257

Table 4 is making a synthesis of the most loaded elements and the combination in which they appear. These values were considered for the checking of the elements.

4. CONCLUSIONS

The paper aim was to find the most suitable solution for the structural elements in order to satisfy seismic requirements from P100/2006. In order to do this, several analysis were performed.

The chosen solution is a mixed structure with a period of 0.26 s.

The structure satisfies two main conditions: aesthetical ones, from architectural point of view, and strength and safety ones from structural point of view.

References

1. Euro code 1 - EN 1991 parts 1-3, 1-4;
2. P100-1/2006 The Romanian Standard For Design Of Structures For Earthquake Resistance;
3. C107/1-3/2005 - Romanian standard for the calculus of the global thermal insulation coefficients for the civil residences;
4. CR0-2005 –Romanian standard – Design principles for structures in construction.

Numerical simulation approach to estimate the ground level wind action near a prismatic building

Radu-Aurel Pescaru, Georgeta Vasies, Hasan Ali Ahmad Akileh, Adrian Radu

Department of Civil and Industrial Engineering, "Gheorghe Asachi" Technical University of Iasi, Iasi, 700050, Romania

Summary

Buildings, with their shape or setting, have a strong influence on the wind flow in their proximity. The presence of large or high rise buildings can often modify the airflow, creating unpleasant and sometimes dangerous windy conditions at the pedestrian level around them.

Considering all these aspects mentioned above in many developed towns as Boston, San Francisco, Paris, Montreal, London, Tokyo e.a., city authorities require wind tunnel testing and numerical simulations of new built developments to estimate their impact to local wind environment. For already existing situations the city planners need some information, guidebooks, and practical means to control and manage the pedestrian level wind conditions.

The paper presents some results, regarding the pedestrian level wind environmental conditions around single rectangular shape buildings, from studies on numerical model of the structures. The researched was carried on at the Building Aerodynamics Laboratory of the Faculty of Civil Engineering and Building Services from Iasi, using a CFD analysis sub-program of the finite element program ANSYS 12.

KEYWORDS: wind activity; buildings; pedestrian level airflow; CFD analysis, numerical model.

1. INTRODUCTION

Wind is one of the most active climatic factors; in addition, both in Romania and throughout Europe, climate change caused an increase of the wind activity characterized by strong winds, frequent storms etc. Meanwhile, in the last 20 years, it is found in our country the expansion of urban areas and the agglomeration of

ISSN 2285-2735, Pages 301 - 309

existing ones with new high buildings of various shapes and sizes, resulting heterogeneous urban space geometry.

In this context the wind "flow" through the streets and generally at ground level becomes more mixed, and could adversely affect pedestrian comfort, dispersion of pollutants, snow accumulation etc. in open spaces, such as plazas, squares, and recreation grounds.

The urban expansion projects should take into consideration these adverse effects incompatible with the sustainable development. Therefore the ground level wind has to be estimated whether it may cause any intolerable consequence to pedestrian due to the construction of a proposed building or structure.

Studies regarding wind climate in built up areas are recommended to be completed in the phase of urban-development planning. This requirement is however difficult because every wind environment is unique due to the interaction of wind and the building form, local topology, predominant wind features. Especially the characteristics of wind instability and turbulence are difficult to estimate by conventional design means. Therefore specialists in wind engineering and building aerodynamics have developed different methods of prediction and assessment of the pedestrian level wind environment using experiments at model-scale in boundary layer wind tunnel (B. L. W. T.) reproducing the specific natural wind.

However the studies on physical models in boundary layer wind tunnel are generally not accessible or attractive to architects and design engineers for common projects, due to high additional costs imposed by the construction and maintenance of special testing equipments and of the tested building models. With the progresses in the computer science, the techniques of computational fluid dynamics (CFD) became an attractive alternative for wind studies developed on numerical models.

The paper presents a study aimed to provide information about ground level wind environment conditions for preliminary building design situation, using a commercial CFD. The numerical simulation in the study was developed under ANSYS_12 CFX , at the Building Aerodynamics Laboratory of our Faculty.

2. THE NUMERICAL SIMULATION APPROACH

In a numerical simulation, the size of a computing domain has to be determined as a first step [1]. Specifications from the literature suggest that the size of a domain must be a multiple of building dimensions [2]. For example the distance from the edge of the domain to any side of a building must be more than five times of the tallest building’s height [3].

Three prototypes of prismatic buildings were considered. Their base is 30 m x 30 m and the height is, in succession, 45 m (building no. 1), 60 m (building no. 2) and 75 m (building no. 3).

The initial input data for numerical simulation were the computational space dimensions, the building size and position; the upstream wind speed is 14 m/s and the turbulence intensity of 5%.

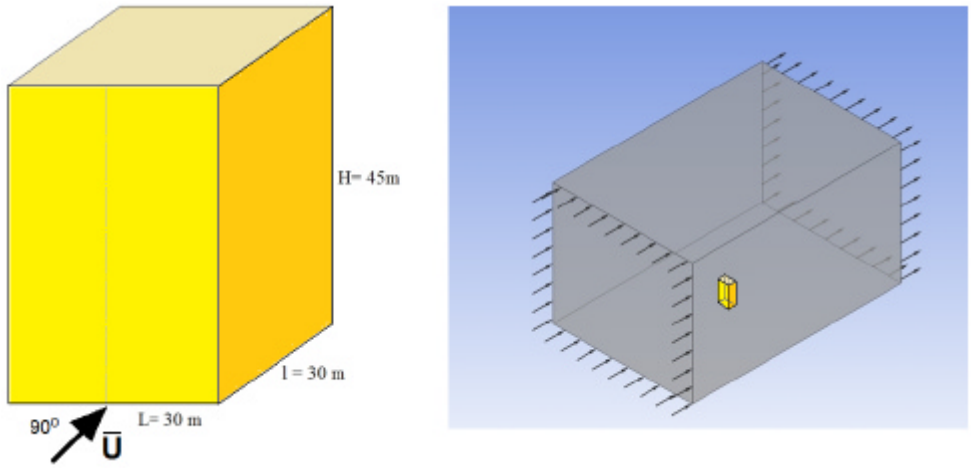

a. b.

Figure 1. a. - building No1, geometry and wind direction; b – the computational domain

The computer simulation study, using the CFD modelling, provided the following information:

- the power lines of air flow at ground level, or the flow pattern around the building, marked with collared fillets;
- the possibility to establish the wind flow velocity field (in m/s) and to represent it graphically as a coloured map, where different areas of equal speed has the same colour;
- the values of the wind induced dynamic pressure (Pa) in various points of interest situated at the ground level, or on the building surface.

The images below shows the flow lines of pedestrian level wind flow as derived from the numerical simulation, for each of the three types of buildings previously described (building no.1, building no. 2 and building no.3).

From the analysis of flow lines charts for the three types of prismatic shape building, with the base of 30x30 m and height of 45 m, 60 m and 75 m, results a thickening of the flow lines along the sides of buildings. This thickening reflects an increasing of the wind speed with the increasing of the building height.

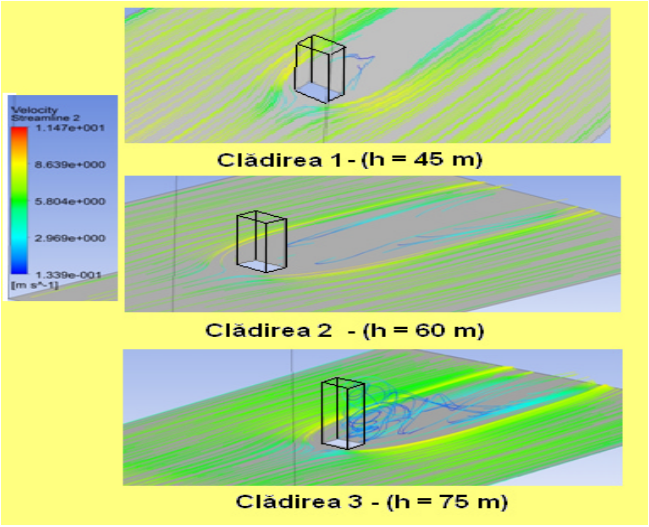

Figure 2. Flow stream lines at the ground level for the studied buildings

In case of building no.3, behind the structure corners from the downstream, can also be seen the presence of Von Karmán vortexes. These vortexes are stemming from the corners of the structure and are moving down to the trail of building wake. The presence of Von Karmán “vortex street” determine an acceleration of wind flow and increases the local turbulence, which can extend downstream up to a distance of about 1.5 H ... 2H, (where H is the height of the building).

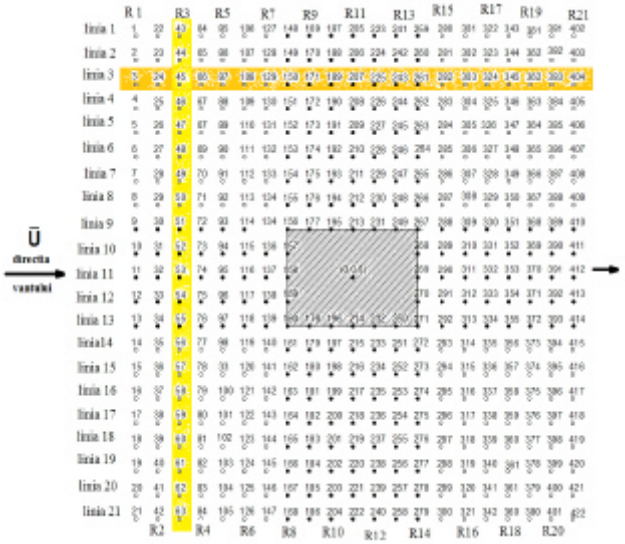

Figure 3. The building base and measurement points around the structure

Based on the results of the simulation for the three numerical models described above, was created a pivot table, figure 3, which shows the longitudinal component of pedestrian level wind speed values, measured in 422 points arranged in 21 columns (R1 R21 ....) and 21 lines (line 1 .... line 21) around the building base.

With wind speed values registered in the pivot table can draw graphs of the flow speed in different areas near the building. To save space are presented below only a few significant cases.

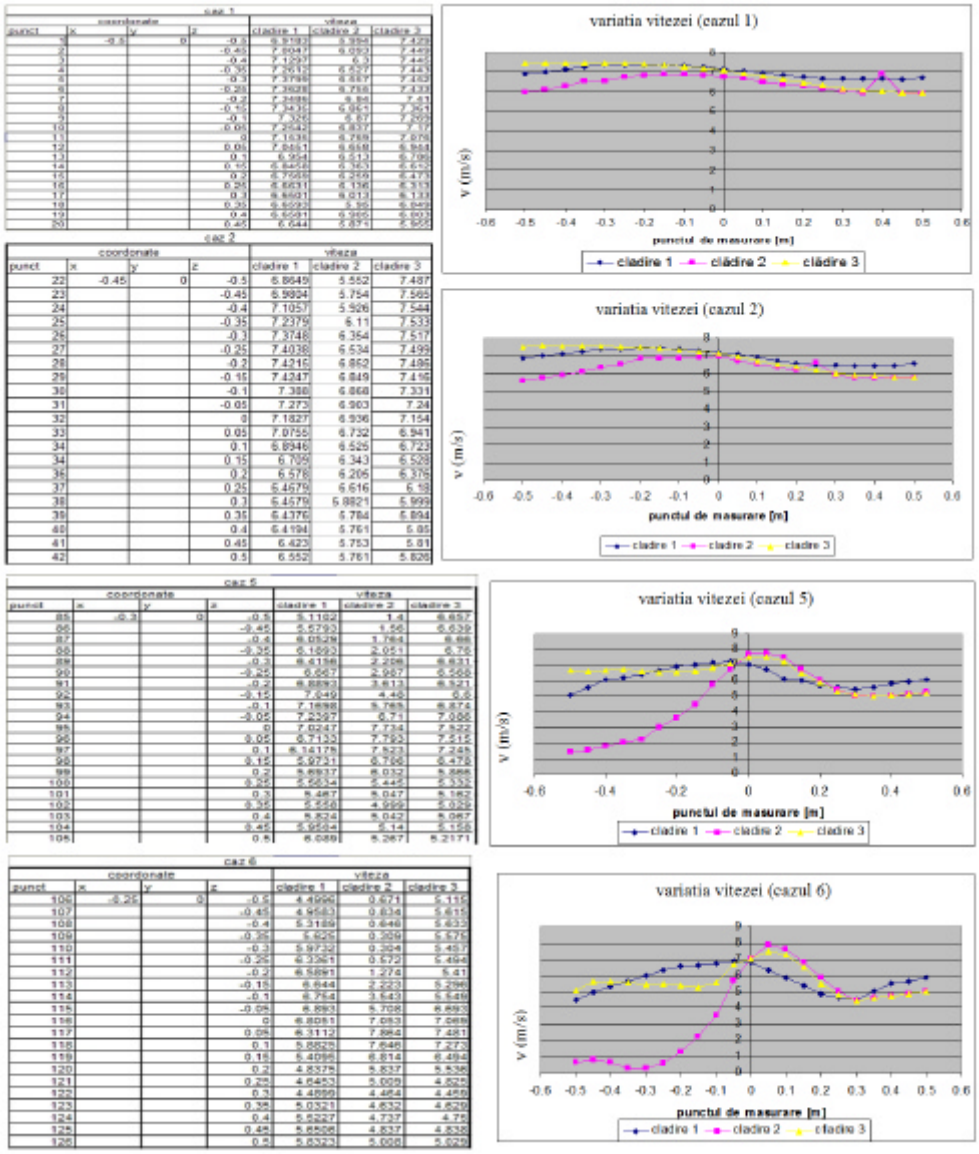

Figure 3. Spead values on columns (R1, R2, R5, R6)

3. THE WIND REDUCTION COEFFICIENT

The data obtained by CFD modelling can be used to calculate for each point by a Reduction Coefficient, Rc_{ij}, as proposed by WM Cornelis for windbreak screens in

his dissertation [4, 5]. The value of Reduction Coefficient reflects the reduction of the wind speed, and it is estimate using the equation:

$$Rc_{ij} = 1 - \frac{\bar{u}_{ij}}{\bar{u}_{0,ij}} \tag{1}$$

with :

i = height above the windbreak (in barrier height H),
j = distance from the windbreak (in barrier height H),
$\bar{u}_{ij}$ = arithmetic mean wind speed disturbed by the windbreak (m×s-1),
$\bar{u}_{0,ij}$ = arithmetic mean wind speed in absence of windbreak (m×s-1).

According to the value of the speed Reduction Coefficient can say that:

- if the value is positive and is close to 1 means that the area is heavily sheltered;
- if the value is close to 0, means that the wind speed on that area is similar to the speed free stream and the presence of the obstacle do not influence the flow;
- if value is negative results an acceleration of the flow on that area.

The values of the wind reduction coefficient can be plotted to create maps with sheltered or wind accelerated areas around the building.

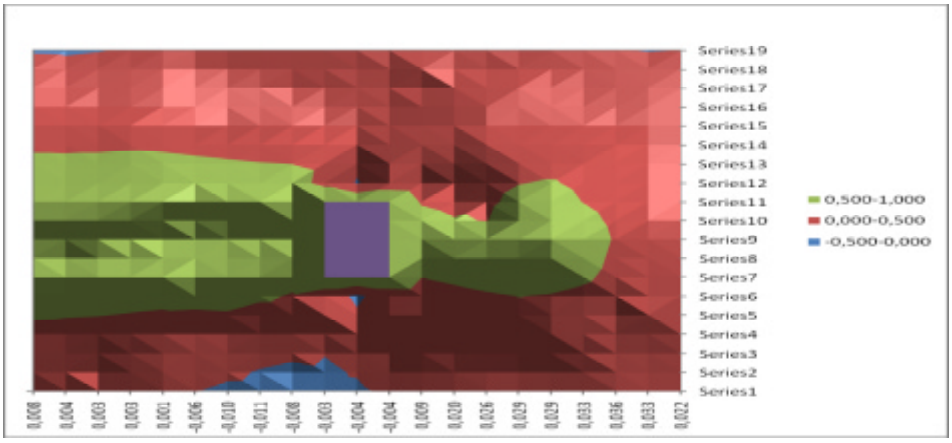

Figure 4. Reduction Coefficient map around building no. 1, H=45 m

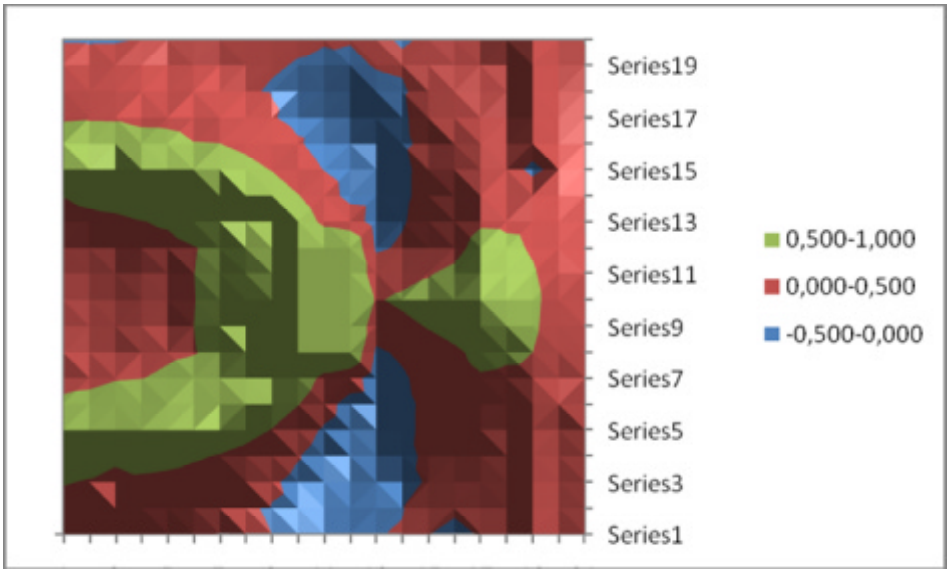

Figure 4. Reduction Coefficient map around building no. 2, H=60 m

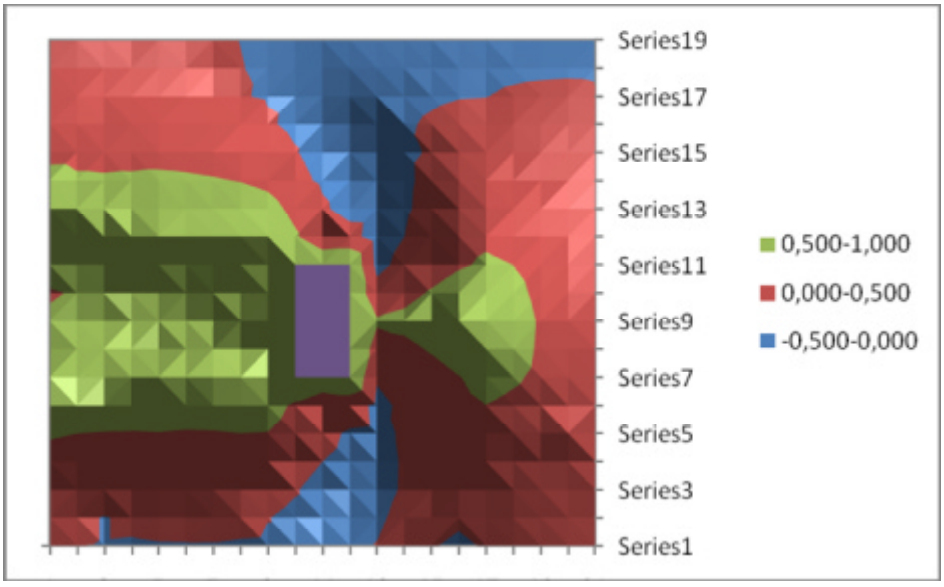

Figure 4. Reduction Coefficient map around building no. 3, H=75 m

For building no.2 (H = 60 m) can see the emergence of areas, starting at the downstream corner, where air velocity is increased reaching values up to 1,5 times the reference speed of the incident wind. This acceleration of flow due to Von

Karmán vortex is shaded downstream alternatively from the building corners, followed the general direction of the flow. In the case of building no. 3 (H = 75 m) the area covered by the trail of vortices expands significantly.

3. CONCLUSIONS

Conclusion extracted from this CFD wind application exercise is that although Computational Wind Engineering is still under development, techniques presented in the paper appear to be sufficient for external comfort assessment of pedestrian level wind environmental design.

It is important to make parallel researches for similar examples with boundary layer wind tunnel tests on physical models and with numerical simulations, any time when it is an opportunity, in order to validate an efficient CFD model for wind environmental design and to know the degree of errors that are critical in understanding, interpreting and presenting CFD results.

References

1. Baskaran A. and Kashef A. Investigation of airflow around buildings using computational fluid dynamics. *Engineering Structures* 1996, Vol. 18, No. 11, pp. 861-875.
2. Franke J., et al. Recomandation of the use CFD in wind engineering. *Proceeding of the International Conferinces on Urban Wind Enineering and Building Aerodybamics*, Belgia, 2004.
3. Hall R. C. Evaluation of modelling uncertainty – CFD modelling of near-field atmospheric dispersion, *Project EMU final report, WS Atkins Consultants Ltd*, UK, 1996.
4. Cornelis W.M. - A wind-tunnel study on the reduction coefficient of synthetic windscreens. *M.Sc. Thesis.* University of Ghent, Belgium. 96 p, (1994).
5. Pescaru, R.A, Akileh, H.A.A., Radu, A.,Laboratory measurements of wind velocity field behind windbreak screens, *Bul. Inst. Polit. Iasi*, t. LVII (LVII), f. 4, 2011

Seismic hazard of Romania: overview for the probabilistic approach

Elena Poida, Adrian Haiducu
Department of Structural Mechanics, Technical University of Civil Engineering, Bucharest, Romania

Summary

The seismic hazard analysis is concerned with getting an estimate of the strong-motion parameters at a site for the purpose of earthquake resistant design or seismic safety assessment. There are two main approaches for the seismic hazard analysis: Deterministic Seismic Hazard Analysis (DSHA) and Probabilistic Seismic Hazard Analysis (PHSA). In the deterministic method the seismic events are generated for a specific site considering information known such as seismic sources that could affect the area, historical earthquakes and geological conditions. The probabilistic approach takes into account the deterministic information and integrates the effects of all the earthquakes expected to occur at different sites during a specified life period, considering also the uncertainties and randomness involved.

A methodology to perform a probabilistic seismic hazard analysis for Romanian districts is presented in this paper. The Vrancea intermediate-depth earthquakes are considered as seismic sources and the specific attenuations relationships are presented. The results of this analysis are released through hazard maps and hazard curves representing the probability of exceeding different ground motion values at a site.

KEYWORDS: Seismic hazard, probabilistic analysis, Vrancea intermediate-depth earthquakes

1. INTRODUCTION

Romania is one of the world countries exposed to a persistent, periodical and severe seismic regime produced by various tectonic type sources: shallow or normal depth sources and intermediate depth sources. The intermediate depth sources $(70 \le H \le 170 \text{ km})$ are located in Vrancea region and affect 2/3 of the Romania territory, while the shallow sources contribute to local seismicity.

ISSN 2285-2735, Pages 310 - 318

The potential for dangerous, earthquake – related phenomena such as ground shaking, fault rupture or soil liquefaction are described by seismic hazard analysis.

The seismic hazard analysis is concerned with getting an estimate of the strong-motion parameters at a site for the purpose of earthquake resistant design or seismic safety assessment. There are two main approaches for the seismic hazard analysis: Deterministic Seismic Hazard Analysis (DSHA) and Probabilistic Seismic Hazard Analysis (PHSA).

In the deterministic method the seismic events are generated for a specific site considering known information such as seismic sources that could affect the area, historical earthquakes and geological conditions: "the earthquake hazard for the site is a peak acceleration of 0.35g resulting from an earthquake of magnitude 6.0 on the Balcones Fault at a distance of 12 miles from the site" [1].

The probabilistic seismic hazard approach, first addressed in 1968 by C. Allin Cornell in "Engineering Seismic Risk Analysis", takes into account the deterministic information and integrates the effects of all the earthquakes expected to occur at different sites during a specified life period, considering also the uncertainties and randomness involved: "the earthquake hazard for the site is a peak ground acceleration of 0.28g with a 10 percent probability of being exceeded in 50-year period" .

The result of the probabilistic seismic hazard analysis is the seismic hazard curve, representing the rate of probability of exceedance related to a ground motion parameter such as peak ground acceleration. The level of probability in building design codes is usually associated to a 50 year period.

The European seismic design codes consider two performance levels for buildings, Life Safety (LS) and Immediate Occupancy (IO) associated with two seismic hazard levels. This European approach was adopted in the new Romanian seismic code P100-1/2011, which considers a mean recurrence interval of 475 for high importance building and a mean recurrence interval for 100 years for the current buildings [2]. The reference return period of 475 years correspond to a 10 percent probability of being exceeded in 50 years and the return period of 100 years correspond to a 10 percent probability of being exceeded in 10 years [3].

If a series of seismic curves is developed for a range of different parameters (e.g., PGA, 1 sec spectral acceleration, 0.2 spectral acceleration, etc.) and values are extracted for a certain constant probability (say a 10% in 50 years probability of exceedance), then a design response spectrum may be created by plotting the parameter magnitude vs. period. A complete response spectrum, where each point has the same probability to being exceeded in a given period is called a uniform hazard spectrum (UHS). These spectra could then be used in a response spectrum analysis of the structure.

2. METHODOLOGY OF PROBABILISTIC SEISMIC HAZARD ANALYSIS

The probabilistic seismic hazard analysis (PSHA) of Romania is completed on seismicity, geology and attenuations characteristics available in the current scientific literature, using CRISIS2007 v7.2 computer code.

CRISIS2007 was developed at the Engineering Institute of the National University of Mexico (UNAM), by M. Ordaz, A. Aguilar and J. Arboleda and use as calculation base for the seismic hazard the standard probabilistic approach defined by Cornell in 1968. CRISIS allows the definition of two seismic models for the hazard assessment: Poisson and characteristic. The seismic sources are modeled as area sources, faults (modeled as lines in the space) or point sources and the seismic hazard assessment is computed through attenuation relations and seismic parameters defined by user.

Considering *?* a random variable describing the intensity of earthquake ground shaking at a site (in this analysis ?=S_a(T), the response spectral ordinate at vibration period T), CRISIS computes the annual exceedance rate of the value *?* (events per year), caused by earthquakes in the i-th seismic source, through the equation 2 obtained by discretization of the equation 1. The exceedance rate of value ?*, calculated with equation 2, is used in CRISIS for computing the seismic hazard curve.

$$?_i(?^*) = \sum_{i=1}^{N} ?_{0_i} \int_{M_{min_i}}^{M_{max_i}} \int_R P[? > ?^* | M, R] f_{M_i}(M) f_{R_i}(R) dM dR \quad (1)$$

$$?_i(?^*) = \sum_{i=1}^{N} ?_{0i} \sum_{M_{min_i}}^{M_{max_i}} \sum_R P[? > ?^* | M, R] f_{M_i}(M) f_{R_i}(R) \Delta M \Delta R \quad (2)$$

where: ?* is the certain value of the seismic ground motion parameter ? ;

$?_i$ is the annual probability of exceedance of selected ground motion parameter ?* , occur to the seismic source considered;

l_{0_i} is the rate of exceedance of reference earthquake in the seismic source i, corresponding to earthquakes with magnitude larger or equal with the minimum magnitude consider in the source *i*, (M_{min_i})

$f_{M_i}(M)$ si $f_{R_i}(R)$ are the probability density function for magnitude and source to site distance, considering that magnitude and distance are independent;

$P[g \geq g^* | M, R_i]$ is the probability of exceeding of a particular value, ?* , calculated with attenuation relations related to magnitude M and distance to site R;

$M_{max\ i}$ is the ground motion maximum magnitude considered in the seismic source *i*;

N is the number of seismic sources.

2.1. Magnitude recurrence

CRISIS admits two types of seismicity models. They essentially differ in the way in which the earthquake magnitude exceedance rate, ? (M) is described. The two models are: Poisson and characteristic. The Romanian hazard analysis is computed using the Poisson model. The earthquake magnitude exceedance rate is given by equation 3 and the probability density of the earthquake magnitude is given by equation 4, [4]:

$$?(M) = ?_0 \frac{e^{-ßM} - e^{ßM_{max}}}{e^{-ßM_{min}} - e^{ßM_{max}}} \tag{3}$$

$$f_{M\,i}(M) = b \frac{e^{-bM}}{e^{-bM_{min}} - e^{-bM_{max}}}, \quad M_{min} \leq M \leq M_{max} \tag{4}$$

Where: $?_0$ is the exceedance rate of magnitude M_{min};

ß is a parameter equivalent to the "b-value" for the source *i* (except that it is given in terms of the natural logarithm);

M_{max} is the maximum magnitude for the source.

2.2. Attenuation relations

The attenuation relations (predictive relationships) allow estimating the probability of exceedance of value ?* in the site during a ground motion with M magnitude and R source to site distance. Considering the seismic hazard parameter with a lognormal distribution with known magnitude and distance, the probability $P[?=?^*|M, R_i]$ is calculated with the equation 5, [4]:

$$P[? \geq ?^* | M, R_i] = 1 - F\left[\frac{\ln ?^* - \ln ?m(M,R)}{s_{\ln A}}\right] \tag{5}$$

where: Φ is the cumulative distribution function of the ground motion parameter;

?*m*(M,R) is the mean value of the ground motion parameter *?* (given the specific attenuation relation for magnitude M and site to source distance R)

$s_{\ln A}$ is standard deviation of natural logarithm of the ground motion parameter, ln ?

The equation 5 is represented in the Figure 1 as the area under the curve, for the case magnitude M is established, M=M* and the source to site distance is known, R=R*.

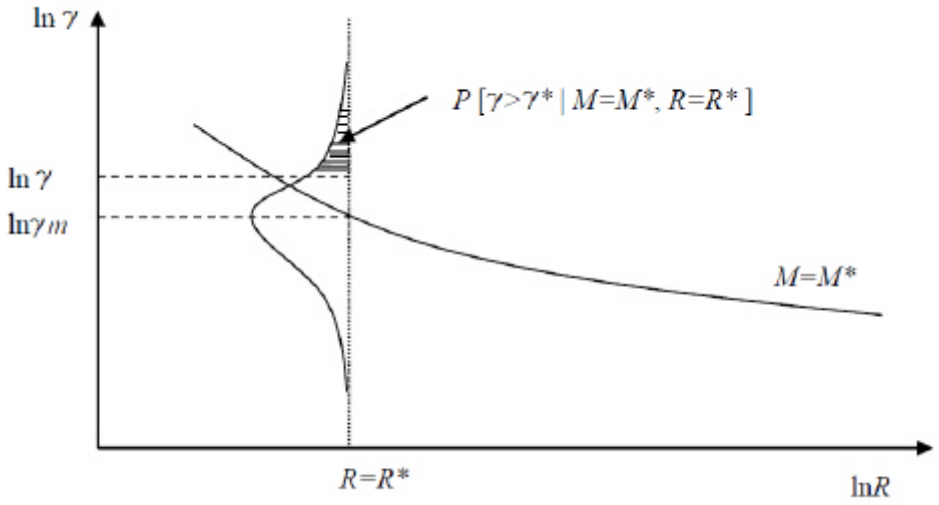

Figure 1. Estimate the exceedance of the ground motion parameter ?* using the seismic attenuation relation, in the case M=M* and R=R* [5]

3. COMPUTING THE SEISMIC HAZARD

3.1. Maps

For graphic identification of the site, CRISIS allows input of a map in *shape file* format (.*shp*) and mention of cities as reference points. A map for Romanian districts and cities, projected in World Geographic System 1985(WGS1984) was realized using the ArcGIS 3.3 software and input into CRISIS (Figure 2).

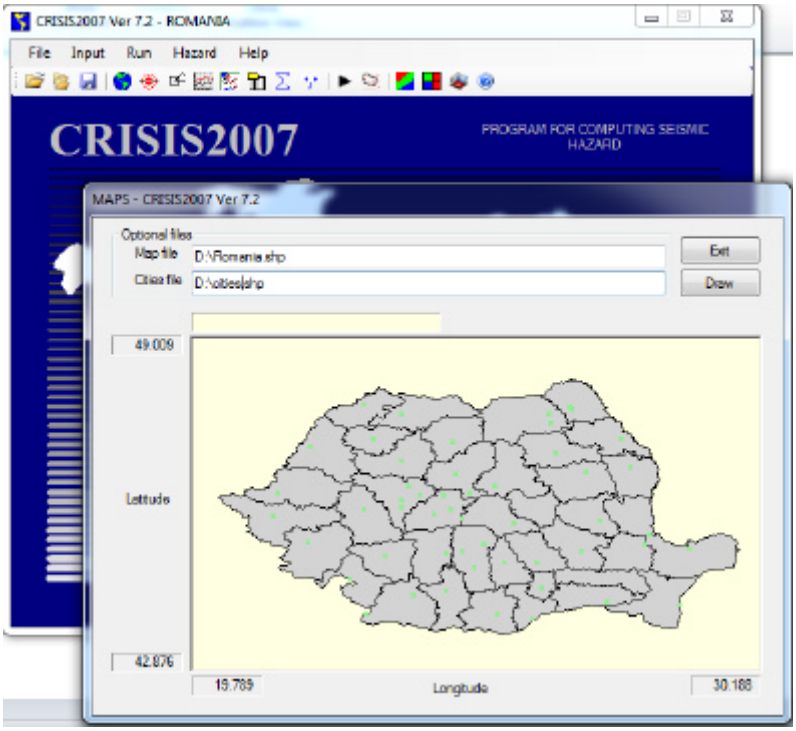

Figure 2. Romania district and cities input to CRISIS2007

CRISIS request the definition of the area for which the seismic hazard will be computed. In the current analysis the area of Ilfov district, including Bucharest city, was selected for validating the current results with the previews hazard analysis that have been completed for Bucharest city. The grid was defined with longitude and latitude increment of 0.05.Hazard will be computed at the nodes of this grid.

3.2. Vrancea seismic source

Vrancea seismic source is located to the Carpathian curvature and affect 2/3 of the Romania territory. Even though CRISIS admit a maximum number of seismic region of 400, in this analysis only the seismic region Vrancea was considered.

Vrancea source was modeled as point source and area source, considering an epicentral area of 40x80 sq. km. and the epicenter of the destructive ground motion of March 1977, the focal depth is between 60 and 170km (Figure 3). The seismicity of the source was selected as Poisson process.

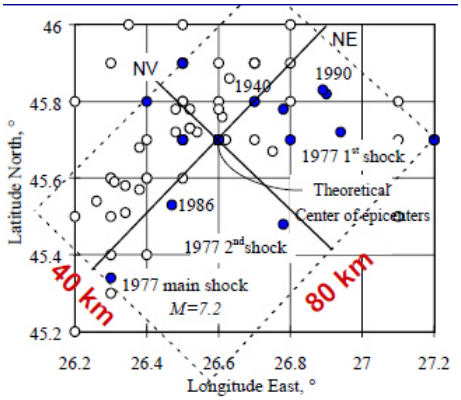

Figure 3. Epicenter position of Vrancea seismic source [6]

Taking into account the N45°E directionality of the seismic field produced by the Vrancea source, the attenuation analysis consider two orthogonal directions (the average direction of the rupture surface N45°E and the normal to this direction E45°S) [7]. The following type model is selected for attenuation analysis in Bucharest sector [7]:

$$\ln PGA = 1.685 + 1.181M_w - \ln R + 0.002R - 0.005h + e \qquad (6)$$

where: PGA is the peak ground acceleration at the site, M_W is the moment magnitude, R is the hypocentral distance to site, h the focal depth and ? is a random variable with zero mean and standard deviation $s_? = s_{\ln PGA} = 0.461$.

The main data for Vrancea seismic source input are: Expected value of maximum magnitude 8.1; Standard deviation of maximum magnitude 0.3; Maximum observed magnitude 7.8; Threshold magnitude M_0=5.0; Expected annual rate with magnitude ?(M0)=1.29; Expected value of ß=0.73[7].

3.3. Results

Table 1. The prediction of PVGA for different mean recurrence intervals of Ilfov district

Hypothesis for Vrancea seismic source	PGA(cm/s^2) 50 years	100 years	475 years
1.Point source 1977 earthquake location 26.3 long E, 45.3 4lat N, h=110km	254	275	397
2.Area source Source rupture area 40x80km^2 Horizontal, h=130km	192	232	326

CRISIS provides the results of the analysis graphic or through several output files. The graphic results for the current analysis are plotted in figure 4 and figure 5. The prediction of PGA for Ilfov district, considering different mean recurrence intervals are centralized in Table 1.

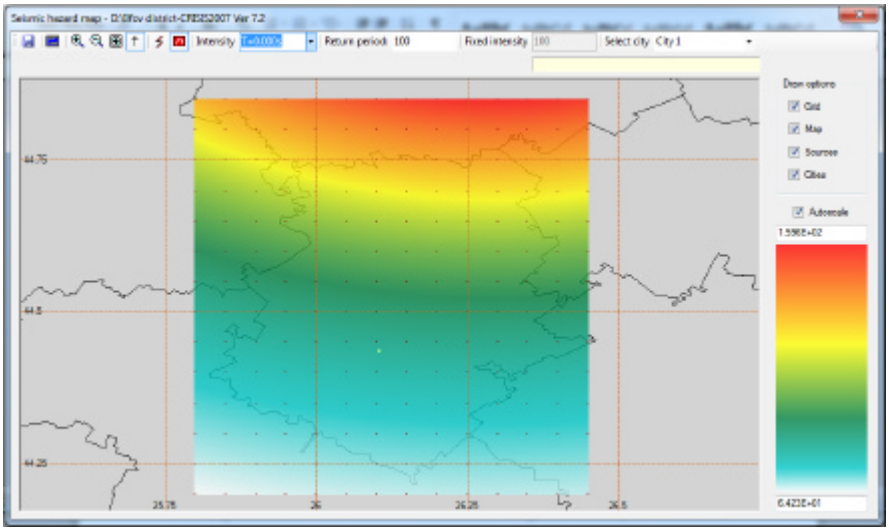

Figure 4. CRISIS2007 ver 7.2. Graphic output - Hazard map for Ilfov district

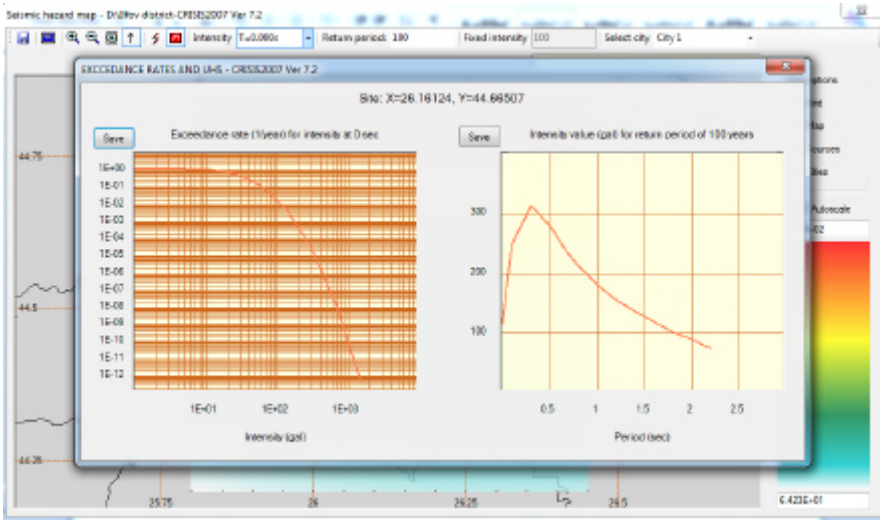

Figure 5. CRISIS2007 ver 7.2. Graphic output - Exceedance rate and UHS for Ilfov district

4. CONCLUSIONS

The seismic hazard analysis is concerned with getting an estimate of the strong-motion parameters at a site for the purpose of earthquake resistant design or seismic safety assessment. The probability seismic hazard analysis (PSHA) takes into account the deterministic information and integrates the effects of all the earthquakes expected to occur at different sites during a specified life period, considering also the uncertainties and randomness involved.

CRISIS computes seismic hazard using a probabilistic model that consider the rates of occurrence, attenuation characteristics and geographical distribution of earthquakes. Earthquake occurrence can be modeled either as a Poissonian process or as a Characteristic Earthquake process. Sources can be modeled as areas, lines or points, attenuation models are furnished by the user or built-in in. [4]

Romania is one of the world countries exposed to a persistent, periodical and severe seismic regime produced by various tectonic type sources: shallow or normal depth sources and intermediate depth sources. The intermediate depth sources are located in Vrancea region and affect 2/3 of the Romania territory, while the shallow sources contribute to local seismicity. For hazard analysis of the Romanian region the attenuation relations furnished by user should be considered. The results obtain with Crisis are validated through the preview hazard analysis studies. Crisis2007 is a powerful tool in computing a probabilistic hazard analysis.

References

1. FEMA 451, *Instructional Material Complementing FEMA 451 Design Examples–Seismic Hazard Analysis*, FEMA Publications Center, 2007
2. P100-1/2011, *Prevederi de proiectare pentru cladiri*, 2011. (in Romanian)
3. Solomos, G., Pinto, A., Dimova, S., *A review of the seismic hazard zonation in national building codes in the context of Eurocode 8*, EUR 23563EN, 2008.
4. Ordaz, M., Aguilar, A., Arboleda, J., *CRISIS 2007, ver. 7.2. Program for computing seismic hazard*, UNAM, Mexico, 2007.
5. Melendez, A., *Evaluation probabilista del riesgo sismico de edificios en zonas urbanas*, Tesis doctoral, Universitad Politecnica de Catalunya, 2011. (in Spanish)
6. Dubina, D., Lungu, D., *Constructii amplasate in zone cu miscari seismice puternice*, Editura Orizonturi Universitare, Timisoara, 2003. (in Romanian)
7. Lungu, D., et al, Synthesis report for the City of Bucharest, *RISK-UE An advanced approach to earthquake risk scenario with application to different European tow*n, 2004
8. Lungu, D., Vacareanu, R., Aldea, A., Arion, C., *Advanced Structural Analysis*, Conspress 2000
9. Vacareanu, R., Aldea, A., Lungu, D., *Structural Reability and Risk Analysis*, Conspress 2007
10. Aguilar, A., Pujades, L., Barbat, A., Lantada, N., A probabilistic model for the seismic risk of buildings. Application to assess the seismic risk of building in urban area, *9th US National and 10th Canadian Conference on Earthquake Engineering*, Toronto, 2010.

Maple 12 a Reliable Tool for Physics Learning

I. Radinschi[1], B. Aignatoiaei[2]
[1]*Department of Physics, "Gheorghe Asachi" Technical University University, Iasi, 700050, Romania*
[2]*Faculty of Automatic Control and Computer Science, "Gheorghe Asachi" Technical University University, Iasi, 700050, Romania*

Summary

In this work we explain and give examples how powerful algebra systems like Maple 12 gives the possibility to the students to improve their knowledge about physics phenomena. The applications are made using physical quantities from the Physics I course that is designated to the first-semester at the Faculty of Civil Engineering and Building Services of "Gheorghe Asachi" Technical University of Iasi, and have been developed with the aid of the Graphics package of Maple 12 program.

The Maple 12 program can be used for graphical representations at a high level. The students work in a simple manner with the program and draw the graphs for many physical phenomena. Moreover, this algebra system yields a very good environment for calculus, algebra, basic mathematics, differential equations, linear algebra, mathematical functions, packages, power series, physics, and also contains a student package that is very useful and "is designed to provide an introduction to the power of the full Maple system".

We present at the course some applications of the Maple 12 program that we have prepared in our PowerPoint presentation. After this, we give to the students the possibility to use it for some calculations and to make graphs. The program is useful at seminars for solving problems and can be also used in campus for a deeper understanding of the physical phenomena presented at the course of physics.

This tool enables our students to improve their learning process and obtain better results. The Maple 12 program becomes a more powerful tool for learning physics if it is used in connection with lectures, seminars and our Virtual Physics Laboratory.

In this paper we present examples of plotting 2d and 3d for some chapters of physics contained in our course of physics. We give examples of plotting physical quantities from Classical Mechanics and Waves chapters. For making the plots we use important physical quantities like the mechanical work, force, momentum, wave vector, period and pulsation.

KEYWORDS: Maple 12, physics, plots, graphs.

1. INTRODUCTION

Nowadays, the Maple 12 program [1] is considered as one of the most reliable products in term of technology that helps the students to improve their learning process.
We develop a method that takes into account the students knowledge and their performance in the use of Maple 12 program. After the implementation of the Maple 12 program in our Physics course, our students consider this an easy way of accessing this technology for their purposes. We point out that only a percentage of our students use this algebra system. This percentage is higher than last years. A greater percentage of students who have chosen to work with this computational program indicates an increasing of their interest for this type of learning.

With the aid of Maple 12 the students can make the connection between physical phenomena and mathematical formalism and graphical representations. Before using Maple 12 we used Maple 9.5 program [1], but now we choose the new version because of its improvements. The students can also use the Maple Calculator that is attached to the Maple 12 program. They can use it for graphs, data, variables, math and settings. Concerning the plotting, some of the many features introduced in Maple 12 [1] are “new abilities that include dual axis plots, polar plots, and specialized engineering plots such as frequency domain responses and root-locus plots”.

Our experience over the last decade in the use of computational programs [2]-[7] allows us to implement in our Physics course and seminars new algebra systems for improving the learning process.

2. MAPLE 12 A POWERFUL TOOL FOR PLOTTING

We present some applications of Graphics package of the Maple 12 program that we use at our Physics course. The plot and plot3d commands are used. We plot physical quantities from Classical Mechanics and Waves chapters [8].

2.1. Plotting the mechanical work, force and momentum

The commands in Maple 12 for plot and plot3d in the case of the mechanical work, force and momentum are given by

a) plot3d(F*r, r = 1 ...10, F = 1 ...10); and the graph is in Figure 1.

We have elementary mechanical work

$$L = F \cdot dr \tag{1}$$

and the mechanical work between two points A and B

$$L_{A \to B} = \int_A^B F \cdot dr \,. \tag{2}$$

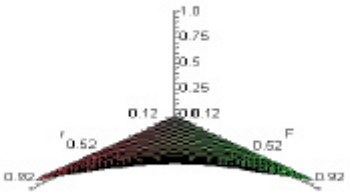

Figure 1. The plot3d for the mechanical work

The expression for the force is given by the second law of dynamics

$$\vec{F} = m\vec{a} \,. \tag{3}$$

b) plot3d(m*a, m = 1 ...10, a = 1 ...40); and the plotting is given in Figure 2.

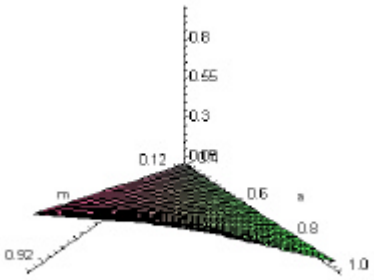

Figue 2. The plot3d for the force

The momentum has the expression

$$\vec{p} = m\vec{v} \,. \tag{4}$$

c) plot(1*v, v = 1 ...100); and the graph is presented in Figure 3. We choose for the mass the value m=1 (kg).

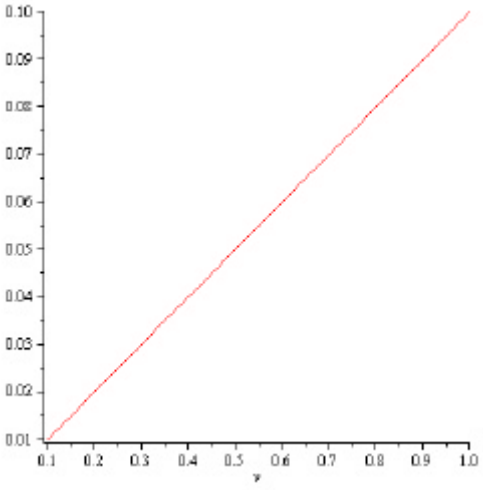

Figure 3. Plot for the momentum

d) plot3d(m*v, m = 1 ...7, v = 10 ...70000); and the plotting is given in Figure 4.

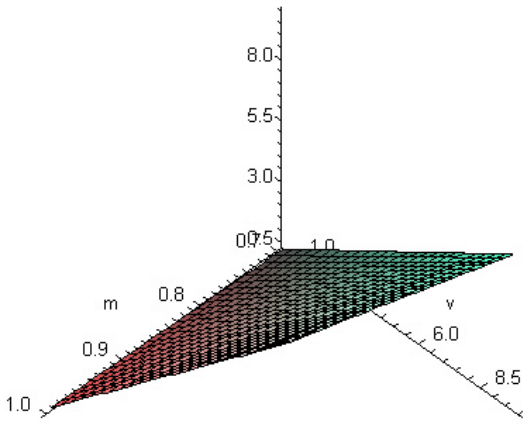

Figure 4. Plot3d for the momentum

2.2. Plotting the wave vector, period and pulsation

The wave vector is given by

$$k = \frac{w}{n}. \tag{5}$$

e) plot3d(w/n, w = 1 ...10, n = 1 ...100); and the graph is plotted in Figure 5.

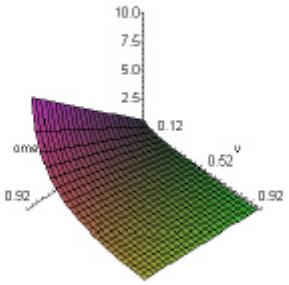

Figure 5. Plot3d for the wave vector

The period is

$$T = \frac{2p}{w}. \tag{6}$$

f) plot(2*Pi/w, w = 1 ...10); and the plotting is given in Figure 6.

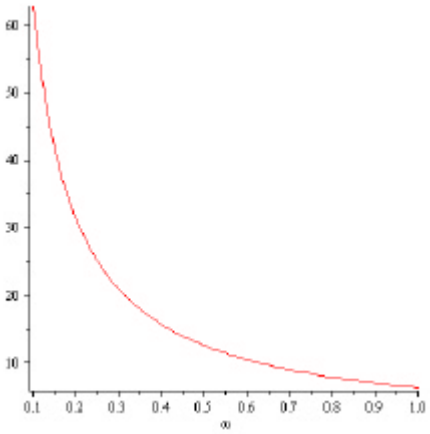

Figure 6. Plot for the period

The pulsation is given by

$$w = 2pn \ . \tag{7}$$

g) plot(2*Pi*n , n = 1 ...10); and the graph is presented in Figure 7.

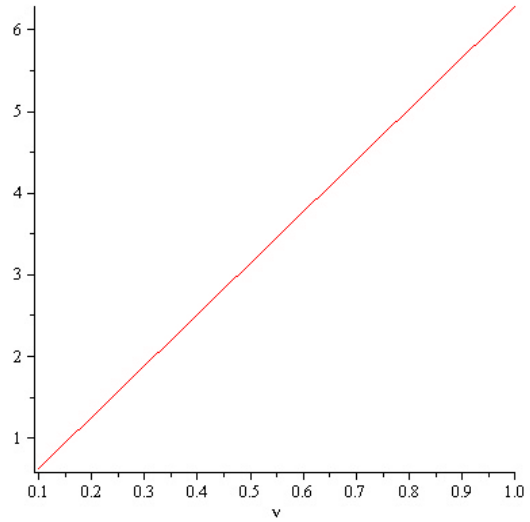

Figure 7. Plot for the pulsation

These are some examples of graphs developed in Maple 12. The students will also use other packages and performing calculations for seminars.

3. CONCLUSIONS

One of the newer versions of the Maple program, the Maple 12 provides new functions and packages presenting in this way many advantages. The program is a proper environment for calculus, plotting and animation.

When we implemented this algebra system in our Physics course we also give to our students the possibility to achieve a good training for using the program in the case they are beginners. In this case we started with simple applications and after this we introduced new problems to be solved. For the students who already know to work with Maple 12 we also offer some more advanced problems. In this way, all the students have made progresses at their levels of knowledge. We use the Maple 12 program in order to make plots for different important physical quantities and for physics laws. After they become more familiar with the program, the students have used it for solving equations and making other calculus improving

the learning process and preparing in a modern way for the seminars. The students will also be capable to develop their ability to learn physics without the guidance of the teacher. The program can be used outside class and this contributes to the improvement of the knowledge of physics laws and phenomena, and for the improving of the final mark at the exams.

References

1. http://www.maplesoft.com/
2. Radinschi, I., Ciobanu, B., *Physics Tests*, Junimea Publishing House Iasi, Romania, 2006.
3. Radinschi, I., Damoc, C., Aignatoaie, B., Cehan, V., *Improving the e-Learning of Engineering Physics with the Aid of Adobe Flash*, 8th International Symposium "Computational Civil Engineering 2010", Iasi, Romania, May 28, 2010, published in New computational concepts in civil engineering, editors Rodian Scinteie, Costel Plescan, "Matei - Teiu" Publishing House, Iasi, Romania, pp. 219-226, 2010.
4. Radinschi, I., Damoc, C., Cehan, A., Cehan, V., *Computer Simulations of Physics Phenomena Using Flash*, 5th International Conference on Hands-on Science Formal and Informal Science Education, October 13-17, 2008, Espaço Ciência, Olinda-Recife, Brazil, Edited by Manuel Filipe Pereira da Cunha Martins Costa (Universidade do Minho), José Benito Vazquez Dorrío (Universidade de Vigo), António Carlos Pavão (Espaço Ciência), Mikiya Muramatsu (Universidade de São Paulo), pp. 147-151, 2008.
5. Radinschi, I., Ciobanu, B., *Improving Civil Engineering Physics Teaching-Learning with Mathematica 5.1*, Proceedings of 5th International Symposium "Computational Civil Engineering 2007", CCE 2007, Iasi, Romania, May 25, pp. 180-190, 2007.
6. Radinschi, I., Frunza M., D., Ciobanu, B., *Online Virtual Model for Testing the Knowledge*, Proceedings of International Technology, Education and Development Conference INTED 2007 edited by IATED, Valencia, Spain, March 7-9, pp. 42-47, 2007.
7. Radinschi, I., Ciobanu, B., *Implementation of Computational Methods in Physics Learning*, Proceedings of 4th "International Symposium Computational Civil Engineering 2006", CCE 2006, May 26, Iasi, Romania, pp. 251-256, 2006.
8. Radinschi, I., Course of Physics, http://www.ce.tuiasi.ro/english/index.html

Optimization methods for steel girders using EUROCODE 3

Victoria E. Rosca, Elena Axinte, and Elena C. Teleman
Department of Civil and Industrial Engineering, "Gheorghe Asachi" Technical University of Iasi, 700050, Romania

Summary

Plate girders are used either on long spans where a rolled section would need to be spliced and as a result may be inefficient, or to support heavy loads. It is important to note that although plate girders may be lighter than other forms of compound beams, fabrication costs are likely to be much higher.

The design of a built-up steel girder is a tedious and time-consuming job for the designer. In common practice, steel plate girders are designed by a trail-and error approach due to the complexity of the design rules.

Standard optimal design formulation of steel plate girder respecting Class restriction is discussed. The design, resistance and deflection inequality constraints for steel built-up welded beams were defined in accordance with the European Standards Eurocodes (EN 1990; EN 1993-1-1; EN 1993-1-5) in order to satisfy the requirements of both the ultimate and the serviceability limit states.

Efficient procedures for minimum weight design of unstiffened steel plate girders using analytical and numerical approach are presented.

Analytical optimization method should prove useful to structural designers and is expected to advance existing design practices of steel beams.

The nonlinear optimization problem is formulated also on the basis of the current Eurocode 3 specification.

Results of numerical calculations for optimal shapes of three steel-grades and various beam length are presented.

By means of simple formulae derived above and using a simple spreadsheet program, it is possible to compare the characteristics of various length, steel grades and section Classes, which can be useful for designer.

KEYWORDS: steel beam, EC3, bending and shear, optimal design, nonlinear optimization.

1. INTRODUCTION

Optimization is the process of obtaining "the best" solution to a problem based on a given criterion. Structural optimization, therefore, is the process of obtaining the "optimum" solution to a structural problem. This optimization is obtained by using analysis and design theory and an optimum seeking method suited to the problem.

The optimization of girders has been extensively approached in the past by using minimum weight as the measure of effectiveness (Arora, 1997; Farkas & Jármai,1997, Bauer, 1994).

In this paper, the minimization method approach are initially briefly described. The procedure has been to minimize the cross-sectional area of the girder. This in turn minimizes the weight of the structure. Then the standard optimal design formulation of steel plate girder with Class restriction is discussed. Numerical implementation in a spreadsheet program like Excell using Solving Toolbox and the conversion of the design criteria in inequality constraints is illustrated.

The design, resistance and deflection inequality constraints for steel built-up welded beams were defined in accordance with the European Standards Eurocodes (EN 1990; EN 1993-1-1; EN 1993-1-5) in order to satisfy the requirements of both the ultimate and the serviceability limit states.

2. RESEARCH METHODOLOGY IN COST OPTIMIZATION OF PLATE GIRDERS

In this section, design of a welded plate girder is solving on the basis of the European Standards (EN 1993-1-1).

Formulation of an optimum design problem uses the following steps (Arora, 1997):

1) Identification and definition of independent variables;

2) Identification and definition of an objective function;

3) Identification and definition of constraints.

The dependent variables for the problem that can be evaluated once the design of girder is specified are identified as follows:

The objective is to minimize the total mass or equivalently, the cross-sectional area A of the girder. The independent variables consists of four design variables, depth (h), width (b), flange thickness (t_f) and web thickness (t_w), as shown in Figure 1.

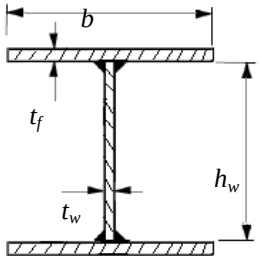

Figure 1 – Cross-section of plate girder

The objective function in the optimization problem is associated with a set of constraints. In the context of structural optimization, these constraints fall into two categories: behavior constraints that limit the plastic/elastic moment, shear force or stability conditions; and design constraints imposed on design variables to put practical limits on some dimensions of elements. Further, to simplify the formulation, it is necessary to introduce dependent design variables. These variables give rise to additional constraints, called equality constraints.

The mathematical programming can be expressed as follows:

$$\begin{aligned} &Min\ z\ =\ f(\boldsymbol{x}) \\ &\text{subjected to: } \begin{cases} h(\boldsymbol{x})\ =\ 0\,, & (\text{NLP}). \\ g(\boldsymbol{x})\ \le\ 0 \end{cases} \end{aligned} \tag{1}$$

where $\boldsymbol{x}$ is a vector of continuous variables, defined within the compact set X.

To find the mathematical formulation, two major steps are formulated (Arora, 1997; Farkas & Jármai,1997), namely:

a) To determine the major decision variables affecting the design of composite beams.

b) To formulate the objective of cost optimization of composite beams in optimization model.

3. DESIGN CONSTRAINTS DERIVED FROM EC3

Girders of the length L, depth h, simply supported and carry a concentrated force P_k at the middle span are considered in his paper.

The moment, shear, and concentrated load bearing resistances of beams whose plate elements are slender may be significantly influenced by local buckling

considerations. The moment, shear, and concentrated load bearing resistances of beams whose plate elements are slender may be significantly influenced by local buckling considerations. Because of this, beam cross-sections are classified as Class 1, 2, 3, or 4, depending on the ability of the elements to resist local buckling. Sections are classified by comparing the slenderness $? = (c/t)\sqrt{235/f_y}$ of each compression element with the appropriate limits of Table 5.2 of EN 1993-1-5. In this example, only cross-section of Class 1, 2 and 3 are considered.

The local web buckling constraint is expressed by

$$\lambda_w = \frac{h_w}{t_w} \le \lambda_{0w} \tag{2}$$

where limiting web slenderness has the following values

$$\text{for elastic design:} \quad l_{0w} \le 124e \tag{3}$$

$$\text{for plastic design:} \quad l_{0w} \le 83e \tag{4}$$

For the compression flange the limiting plate slenderness is:

$$\text{for elastic design:} \quad \lambda_{0f} \le 14\varepsilon \tag{5}$$

$$\text{for plastic design:} \quad \lambda_{0f} \le 10\varepsilon \tag{6}$$

For the moment resistance check of a beam that has adequate bracing against lateral buckling, the inequality:

$$M_{Ed} \le M_{c,Rd} \tag{7}$$

$$M_{c,Rd} = \begin{cases} M_{pl,Rd} = W_{pl}\dfrac{f_y}{\gamma_{M0}} & \text{for Class 1 and 2} \\ M_{el,Rd} = W_{el,min}\dfrac{f_y}{\gamma_{M0}} & \text{for Class 3} \end{cases} \tag{8}$$

must be satisfied, in which M_{Ed} is the maximum design moment, $M_{c,Rd}$ is the design section moment resistance, W is the appropriate section modulus (elastic or plastic, depending on section Class), f_y the nominal yield strength for the section, and $?_{M0} = 1$ the partial factor for section resistance.

For the shear resistance check, the inequality:

$$V_{Ed} \le V_{c,Rd} \tag{9}$$

must be satisfied, in which V_{Ed} is the maximum design shear force, and $V_{c,Rd}$ the design shear resistance. For a stocky web with $h/t_w = 72\varepsilon(235/f_y)$ and for which the

elastic shear stress distribution is approximately uniform (as in the case of an equal flanged I-section), the uniform shear resistance $V_{c,Rd}$ is usually given by:

$$V_{c,\,Rd} = h_w t_w \frac{f_y / \sqrt{3}}{\gamma_{M0}} \tag{10}$$

in which $f_y/\sqrt{3}$ is the shear yield stress and A_v is the shear area of the web defined in Clause 6.2.6(3) of EN 1993-1-1 [5].

The shear resistance of slender unstiffened webs for which $h/t_w > 72e$ decreases rapidly from the value in Equation (10) as the slenderness h/t_w increases. Neglecting the contribution of the flanges, for these.

$$\begin{aligned} V_{c,\,Rd} &= V_{bw,\,Rd}, \\ V_{bw,\,Rd} &\geq \eta h_w t_w \frac{f_y / \sqrt{3}}{\gamma_{M1}} \end{aligned} \tag{11}$$

where $V_{bw,Rd}$ is the design resistance governed by buckling of the web in shear, c_w is a factor for the shear area that can be taken as 1,2 for steels up to S460 and 1,0 otherwise, and g_{M1} (=1) is a partial resistance factor based on buckling. The buckling resistance of the web is given in EC3 as

$$V_{bw,\,Rd} = \chi_w h_w t_w \frac{f_y / \sqrt{3}}{\gamma_{M1}} \tag{12}$$

in which the web reduction factor on the yield strength $h_w t_w f_y/\sqrt{3}$ due to buckling is:

$$\chi_w = \begin{cases} \eta; & \bar{\lambda}_w < 0{,}83/\eta \\ 0{,}83/\bar{\lambda}_w; & \bar{\lambda}_w \geq 0{,}83/\eta \end{cases} \tag{13}$$

where the modified web plate slenderness for an unstiffned web, is:

$$\bar{\lambda}_w = \frac{h_w}{t_w} \frac{1}{37{,}4\varepsilon\sqrt{k_\tau}} \tag{14}$$

Since for unstiffned webs $k_\tau = 5{,}34$, the reduced web slenderness became:

$$\bar{\lambda}_w = \frac{1}{86{,}425\varepsilon} \frac{h_w}{t_w} \tag{15}$$

Thus, the constraints on shear can be rewritten as:

$$V_{bw,\,Rd} = \begin{cases} h_w t_w \dfrac{f_y / \sqrt{3}}{\gamma_{M1}} & \text{for} \quad \dfrac{h_w}{t_w} < \dfrac{71{,}733}{\eta} \\ 71{,}733 t_w^2 \dfrac{f_y / \sqrt{3}}{\gamma_{M1}} & \text{for} \quad \dfrac{h_w}{t_w} \geq \dfrac{71{,}733}{\eta} \end{cases} \tag{16}$$

With no web stiffeners the web should be sized to avoid the flange undergoing local buckling due to the web being unable to support the flange. This is known as flange induced buckling (EN 1993-1-5).

$$\frac{h_w}{t_w} \leq k \frac{E}{f_y} \sqrt{\frac{A_w}{A_{fc}}} \tag{17}$$

where f_y is the yield strength of the compression flange, A_{fc} is the effective area of the compression flange and A_w is the area of the web.

The parameter k takes values of 0,3 where plastic hinge rotation is utilized, 0,4 if the plastic resistance is utilized and 0,55 if the elastic resistance is utilized. Thus for rigid (continuous) design k = 0,3 unless the analysis is elastic with no redistribution. For simply supported beams k may be taken as 0,4.

Considering the serviceability limit state, the vertical defections is calculated and checked.

The total defections d_{max} subjected to the overall load and the defections subjected to the variable imposed load is:

$$\delta_{\max} = \frac{L^3}{384 \cdot 10^6 EI} \left(8P_k + 5q_k L\right) \quad [\mathrm{m}] \tag{18}$$

The allowable deflection ratio, e.g. for simply supported beams in buildings, according to EC3, is L/300. The deflection beam constraints $d_{max} \leq L/300$ can be expressed as:

$$I \geq I_o = \frac{C_w}{300} \tag{19}$$

where

$$C_w = \frac{5q_k L^3}{384E} + \frac{P_k L^3}{48EI} \tag{20}$$

4. ANALYTICAL OPTIMIZATION FOR OF THE GIRDERS WITHOUT CONSTRAINTS

4.1 Optimization of Classes 1 and 2

The moment is resisted by the complete section, when the moment capacity is given by that due to the flanges (Equation (21)) and the additional plastic capacity of the web:

$$M_{Ed} \le M_{c,Rd} \approx bt_f h_w f_{yd} + \frac{t_w h_w^2}{4} f_{yd} \tag{21}$$

where $f_{yd} = f_y/\sqrt{3}$ is the design strength of the flanges, t_f and b_f the thickness and width of the flange plates and h_w the distance between the internal faces of the flanges.

The cross-sectional area A is given by

$$A = 2bt_f + h_w t_w \tag{22}$$

Eliminate $b_f t_f$ between Equation (21) and (22) to give

$$A = \frac{2M_{Ed}}{h_w f_{yd}} + h_w t_w - 2\frac{t_w h_w}{4} = \frac{2M_{Ed}}{h_w f_{yd}} + \frac{t_w h_w}{2} \tag{23}$$

Defining the web slenderness ratio h_w/t_w (Equation (2)), then Equation (23) becomes

$$A = \frac{2M_{Ed}}{\lambda_w t_w f_{yd}} + \frac{\lambda_w t_w^2}{2} \tag{24}$$

For an optimum solution, $dA/dt = 0$, so Equation (24) becomes,

$$\frac{dA}{dt_w} = -\frac{2M_{Ed}}{\lambda_w f_{yd} t_w^2} + \lambda_w t_w = 0 \tag{25}$$

Optimal solution of the thickness is given now by

$$t_w = \sqrt[3]{\frac{2M_{Ed}}{\lambda_w^2 f_{yd}}} \tag{26}$$

and:

$$h_w = \sqrt[3]{\frac{2\lambda_w M_{Ed}}{f_{yd}}} \tag{27}$$

The area of the web, A_w is then given by

$$A_w = \sqrt[3]{\frac{4M_{Ed}^2}{\lambda_w f_{yd}^2}} \tag{28}$$

Using Equation (22), the flange area, A_f is given by

$$A_f = bt_f = \sqrt[3]{\frac{M_{Ed}^2}{\lambda_w f_{yd}^2}} \cdot \left[\sqrt[3]{\frac{1}{2}} - \sqrt[3]{\frac{1}{16}}\right] \tag{29}$$

or,

$$\frac{A_f}{A_w} = \frac{\sqrt[3]{\frac{M_{Ed}^2}{\lambda_w f_{yd}^2}} \cdot \left[\sqrt[3]{\frac{1}{2}} - \sqrt[3]{\frac{1}{16}}\right]}{\sqrt[3]{\frac{4M_{Ed}^2}{\lambda_w f_{yd}^2}}} = \frac{1}{4} \tag{30}$$

Thus the area of the web is equal four times that of a single flange.

4.2 Optimization of Classes 3

The moment is resisted by the complete section, when the moment capacity is given

$$M_{Ed} \le M_{Rd} \approx bt_f h_w f_{yd} + \frac{t_w h_w^2}{6} f_{yd} \tag{31}$$

where f_{yd} is the design strength of the flanges, t_f and b_f the thickness and width of the flange plates and h_w the distance between the internal faces of the flanges.

Eliminate $b_f t_f$ between Equation (22) and Equation (31) to give

$$A = \frac{2M_{Ed}}{h_w f_{yd}} + h_w t_w - 2\frac{t_w h_w}{6} = \frac{2M_{Ed}}{h_w f_{yd}} + \frac{2t_w h_w}{3} \tag{32}$$

Define the web slenderness ratio h_w/t_w (eqs. (2) and (3)), then Equation (32) becomes:

$$A = \frac{2M_{Ed}}{\lambda_w t_w f_{yd}} + \frac{2\lambda_w t_w^2}{3} \tag{33}$$

For an optimum solution, *dA/dt = 0*, so Equation (33) becomes,

$$\frac{dA}{dt_w} = -\frac{2M_{Ed}}{\lambda_w f_{yd} t_w^2} + \frac{4}{3}\lambda_w t_w = 0 \tag{34}$$

or,

$$t_w = \sqrt[3]{\frac{3}{2} \cdot \frac{M_{Ed}}{\lambda_w^2 f_{yd}}} \tag{35}$$

and

$$h_w = \sqrt[3]{\frac{3}{2} \cdot \frac{\lambda_w M_{Ed}}{f_{yd}}} \tag{36}$$

The area of the web, A_w is then given now by

$$A_w = \sqrt[3]{\frac{9 \cdot M_{Ed}^2}{4 \cdot \lambda_w \cdot f_{yd}^2}} \tag{37}$$

Using Equation (31), the flange area, A_f is given by

$$A_f = bt_f = \sqrt[3]{\frac{M_{Ed}^2}{\lambda_w f_{yd}^2}} \cdot \left[\sqrt[3]{\frac{2}{3}} - \frac{1}{6} \sqrt[3]{\frac{9}{4}} \right] \tag{38}$$

thus:

$$\frac{A_f}{A_w} = \frac{\sqrt[3]{\frac{M_{Ed}^2}{\lambda_w f_{yd}^2}} \cdot \left[\sqrt[3]{\frac{2}{3}} - \frac{1}{6} \sqrt[3]{\frac{9}{4}} \right]}{\sqrt[3]{\frac{9M_{Ed}^2}{4\lambda_w f_{yd}^2}}} = \frac{1}{2} \tag{39}$$

Thus the area of the web is equal twice that of a single flange.

4.3 Optimum Design of The Flanges

Thickness of the flange t_f must satisfy minimum requirements:

$$\begin{aligned} & t_w + 2 \text{ mm} \le t_f \le (2 \ldots 3) \cdot t_w \\ & 12 \text{ mm} \le t_f \le 30 \text{ mm} \end{aligned} \tag{40}$$

Shear lag in flanges may be neglected if $c < L_e/50$ where c is taken as the flange outstand or half the width of an internal element (Figure 1) and L_e is the length between points of zero bending moment. Where the above limit for c is exceeded the effects due to shear lag in flanges should be considered, accordingly EN 1993-1-5. Therefore, the wide of the flange is restricted to:

$$b \approx 2c \leq \frac{L_e}{25} \tag{41}$$

Dimensions of the flange are established now from optimum requirements:

$$\begin{aligned} b_f &\approx 2c \leq 2\lambda_f t_f \\ A_f &= bt_f = 2\lambda_f t_f^2 \\ t_f &\leq \sqrt{\frac{A_f}{2\lambda_f}} \end{aligned} \tag{42}$$

It should be noted that flange area of the girder must fulfill resistance conditions, Equation (8) thus,

$$b \approx \frac{M_{Ed}}{h_w t_f f_{yd}} - \xi \frac{t_w h_w}{t_f} \tag{43}$$

where ? is1/4 for Class 1 and 2 and 1/6 for Class 3.

5. OPTIMIZATION OF THE GIRDERS VIA NUMERICAL TECHNIQUES

The advantages of computer technology have been incorporated in the optimization of girder steel desig; most notably is the use of spreadsheets. Spreadsheets are user friendly and exceedingly powerful but are not being exploited as much as they could be in structural engineering design.

In structural optimization, various mathematical programming techniques have been extensively applied, with most of the applications based upon one of following algorithms. The method of moving asymptotes, sequential quadratic programming (*SQP*), penalty function methods or feasible direction methods. Many spreadsheet programs have the capability of solving constrained nonlinear problems. In the present work, the Solver tool of Microsoft Excell™ is used. No effort has been made to study the mathematical programming methods used in the structural optimization procedures and the nonlinear algorithm is used here essentially as a black box.

In this section optimization of the weight objective function associated with a set of constraints derived from EC3 requirements, is presented, i.e:

$$\min \quad G = (ht_w + 2bt_f) \cdot L$$

$$\text{subject to} \begin{cases} M_{Ed} \le M_{c,\,Rd} \\ V_{Ed} \le V_{c,\,Rd} \\ \text{if } \dfrac{V_{Ed}}{V_{c,\,Rd}} \ge 0{,}5 \text{ then } V_{Ed} \le V_{bw,\,Rd} \\ \lambda_w \le \lambda_{0w} \\ \lambda_f \le \lambda_{0f} \\ \delta_{\max} \le \dfrac{L}{300} \end{cases} \tag{44}$$

6. NUMERICAL EXAMPLES

A parametric study is presented to investigate the effects of beam spans on the cost optimization of steel girders. The optimization also considered different economic conditions: different structural steel grades, three defined spans, L = 15m, 18 m and 25 m, subject to a concentrated imposed load P_k = 104 kN (dead) and a dead weight q_k = 2,70 kN/m (Figure 2). In this formulation, bearing stiffeners, welded connections, and transverse stiffners are not taken into account.

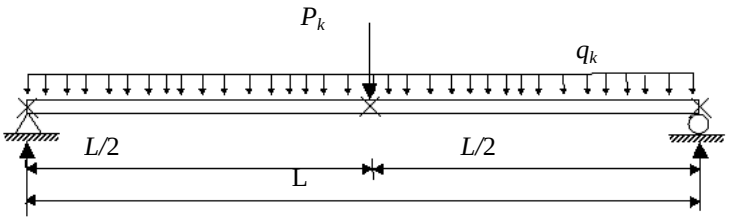

Figure 3 – Variable imposed load and the span of the girder

Characteristics of the optimum cross-section design are also compared with analytical solutions (Farkas & Jármai, 1997) with stress constraints and deflection constraints, respectively. Figure 2 and Figure 3 show differences about 20% for section Class 1 and 2 and 10% for elastic design (Class 3), when only stress constraints are active for analytical solution.

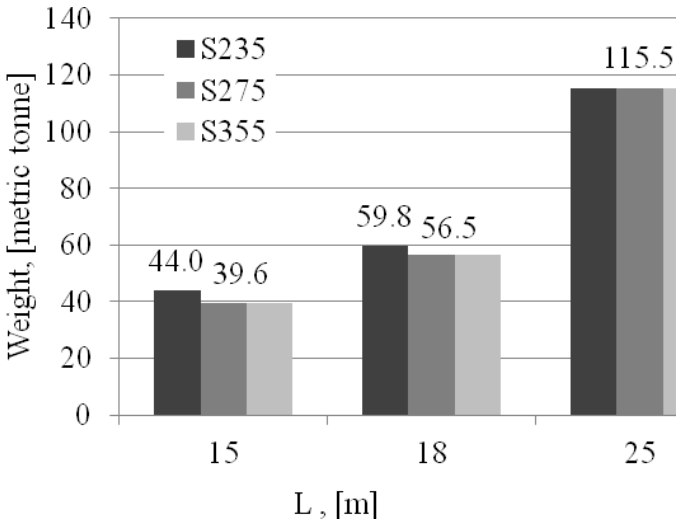

a.

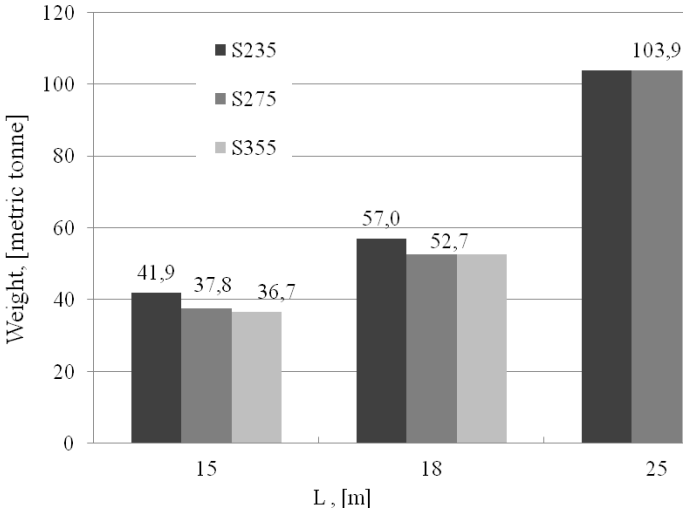

b.

Figure 2 – Minimum weight of optimized cross section in function of beam length and steel grade. *a*. –Class 1; *b*. –Class 2

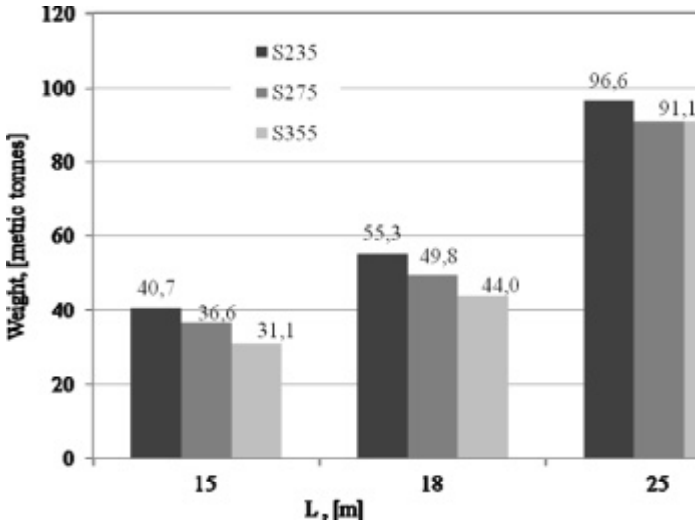

c.

Figure 3 – Minimum weight of optimized cross-section Class 3 in function of beam length and steel grade.

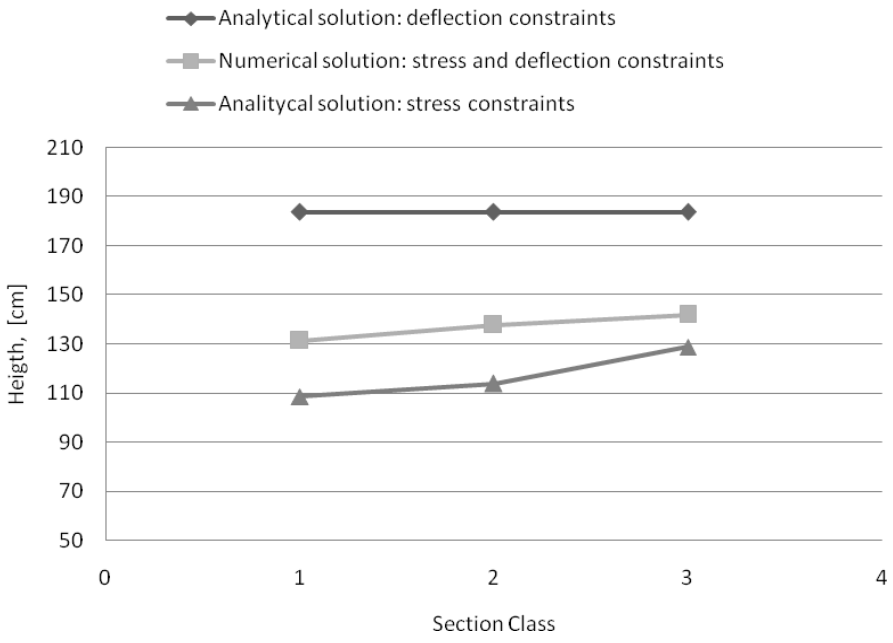

Figure 4 – Optimized height of welded *I* – beam for S235 steel grade

Note, however, that the optimum height values obtained by numerical solution using both constrains are smaller than the values for the case where only deflection constraint is included in the analytical formulation. Whenever, more constraints are imposed on the system, the optimum cost function value can be expected to increase.

Figure 4 summarizes numerical solutions of optimum design with four discrete variables formulations, for three Classes and steel grades, respectively. Duet tot la large span, for L =25 m, prevail deflection constraints and the optimum solution not depend on steel grade for Class 1 and 2. Active constraints are given by section 3.

7. CONCLUSIONS

Effective and simple methods of finding minimum (near minimum) weight of a structure, applying requirements from EC3 code, is presented. The paper proposes the cost optimization of *I* steel girders by means: (i) analytical method and (ii) numerical method. Analytical optimization method should prove useful to structural designers and is expected to advance existing design practices of steel beams. By means of simple formulae derived above and using a simple spreadsheet program, it is possible to compare the characteristics of various length, steel grades and section Classes, which can be useful for designer.

References

1. Arora J.S., *Guide to Structural Optimization.* ASCE Manuals and Reports on Engineering Practice, ASCE, New York, 1997.
2. Farkas, J, Jármai, K. *Analysis and Optimum design of Metal Structures*, A.A. Balkema, Rotterdam, Netherlands, 1997.
3. Bauer, J. A survey of methods for discrete structural design. *Computer Assisted Mechanics and Engineering Sciences*, vol. 1, 27–38, 1994
4. *** Basis of design and actions on structures, EN 1990.
5. *** Design of steel structures, Part 1-1: General rules and rules for buildings, EN 1993-1-1
6. *** Eurocode 3: Design of steel structures - Part 1-5: General rules - Plated structural elements, EN 1993-1-5.
7. *** Microsoft Excell 2007 Spreadsheet
8. Pacurar V., Aribert J.M., (Eds.) *Design of Steel Structures*, Tempus Phare Complem. Meas. Project 01198, Implem. of Struct. Eurocodes in Romanian Civil Engineering Standards, 1997.
9. Axinte E., Rosca V.E., Teleman E.C., *Elements for Steel buildings 2*, Ed. Academic Society "Matei Teiu Botez", Iasi, Romania, 2011. (in Romanian)

Some Considerations Regarding the Complex Eigenvalues in Structural Analysis

Octavian Victor Rosca
Structural Mechanics Department, Technical University"Gh. Asachi", Iasi, 700241, Romania

Summary

Most of the engineering problems in vibrations are leading to the eigenvalue problem, in the simple or generalized format. It is commonly accepted and convenient to use the real eigenvalues; therefore the matrices of the dynamic system are symmetric and positive defined. Moreover, in the case of the time history analysis the equations of motion are decoupled, based on the assumption that the damping is proportional (Rayleigh type) to the mass or stiffness or both. Under these circumstances the time responses obtained separately can be superimposed using the modal participations.

In the structural analysis there are situations when the eigenvalues and eigenvectors of non- symmetric matrices are requested, even of the complex matrices. Non- proportional damped structures are a part of these systems. The hypothesis of proportional damping is advantageous from the numerical point of view and the experimental tests show that this approximation leads in most cases to acceptable results. However it is not demonstrated yet the proportional behavior of the damping.

This paperwork deals with the numerical problem of the complex eigenvalues. A structural case study of a 3 storey frame tested on the master shaking table of the Laboratory of Earthquake Engineering from the Structural Mechanics Department of the Faculty of Civil Engineering and Building Services from Iasi it is presented.

The analysis conducted to the complex eigenvalues and modal shapes of vibration.

In the end the conclusions of the analysis and the computational effort are depicted.

KEYWORDS: Structural Analysis, Modal Analysis, Complex Eigenvalue Problem.

1. INTRODUCTION

Most of the engineering problems in vibrations are leading to the eigenvalue problem, in the simple or generalized format. It is commonly accepted and convenient to use the real eigenvalues; therefore the matrices of the dynamic system are symmetric and positive defined. Moreover, in the case of the time history analysis the equations of motion are decoupled, based on the assumption that the damping is proportional (Rayleigh type) to the mass or stiffness or both. The damping matrix C is then written as a linear combination of M and K ($C = \alpha M + \beta K$). Under these circumstances the time responses obtained separately can be superimposed using the modal participations.

In the structural analysis there are situations when the eigenvalues and eigenvectors of non- symmetric matrices are requested, even of the complex matrices. Non-proportional damped structures are a part of these systems. The hypothesis of proportional damping is advantageous from the numerical point of view and the experimental tests show that this approximation leads in most cases to acceptable results. However it is not demonstrated yet the proportional behavior of the damping.

Let us consider the solution of the Ndofs dynamic system in the linear vibration:

$$M\,\ddot{X} + C\,\dot{X} + K\,X = 0 \tag{1}$$

The solution can be written in the vector form:

$$x = q\,e^{st} \tag{2}$$

The substitution of (2) in (1) leads to the equation:

$$\left(s^2\,M + s\,C + K\right)q = 0 \tag{3}$$

that has to be provided with the zero determinant in order to obtain a non- trivial solution

$$\det\left(s^2\,M + s\,C + K\right) = 0 \tag{4}$$

The characteristic eq. (4) is also known as the quadratic form of the eigenvalue problem. The solution leads to 2 N eigenvalues and the corresponding 2 N eigenvectors (with N components). The general solution of the motion is obtained after the modal superposition of the 2 N solutions:

$$x = \sum_{i=1}^{2N} \xi_i\, q_i\, e^{s_i t} \tag{5}$$

where ξ_i are arbitrary constants that are find out from the initial coditions. The eigenvalues are obtained as complex conjugated pairs $s^m = \mu_m + i\,\nu_m$ si $s^*m = \mu_m - i\,\nu_m$ and the corresponding eigenvectors are written as $q_m = a_m + i\,b_m$ si $q^*m = a_m - i\,b_m$. The sollution that corresponds to the "m" DDOF is written:

$$x_m(t) = (c_m + i\,d_m)\,e^{(\mu_m + i\,\upsilon_m)\,t}(a_m + i\,b_m) + (c_m - i\,d_m)\,e^{(\mu_m - i\,\upsilon_m)\,t}(a_m - i\,b_m) \tag{6}$$

wher c_m and d_m are arbitrary constants. In order to obtain a damped oscillation in time it must that

$$\mu_m < 0 \tag{7}.$$

If all the roots of the eigenvalue problem are complex conjugated, then there will be N solutions of the type and the total response shall be provided by:

$$x = \sum_{m=1}^{N} x_m \tag{8}.$$

The eq. (6) can also be expressed in tthe exponent form:

$$x_m(t) = e^{\mu_m\,t}\left(v_m \sin \upsilon_m t + w_m \cos \upsilon_m t\right) \tag{9}$$

where:

$$v_m = -2\left(d_m a_m + c_m b_m\right) \tag{10.a}$$

$$w_m = 2\left(c_m a_m - d_m b_m\right) \tag{10.b}$$

and cm si dm are arbitrary constants that are calculated from the 2 N initial conditions. The final solution is of real type.

The quadratic eigenvalue can be transformed into a linear or standard problem. The transformation to the generalized (linear) form is presented. A displacement and velocity vector will be assembled, in a similar manner as that used in the state-space:

$$z = \begin{bmatrix} \dot{x} \\ x \end{bmatrix} \tag{11}$$

and the equations of motion are written:

$$\begin{cases} M\,\dot{x} - M\,\dot{x} = 0 \\ M\,\ddot{x} + C\,\dot{x} + K\,x = 0 \end{bmatrix} \tag{12}$$

or, in matrix format:

$$\begin{bmatrix} 0 & M \\ M & C \end{bmatrix}\begin{bmatrix} \ddot{x} \\ \dot{x} \end{bmatrix} + \begin{bmatrix} -M & 0 \\ 0 & K \end{bmatrix}\begin{bmatrix} \dot{x} \\ x \end{bmatrix} = \begin{bmatrix} 0 \\ 0 \end{bmatrix} \tag{13},$$

that leads to:

$$A\,\dot{z} = B\,z \tag{14}$$

where

$$A = \begin{bmatrix} 0 & -M \\ -M & -C \end{bmatrix} \tag{15}$$

$$B = \begin{bmatrix} -M & 0 \\ 0 & K \end{bmatrix} \tag{16}$$

and

It is selected a soution of the form $z = v\,e^{s\,t}$. The replacement in (14) leads to the generalized eigenvalue problem

$$B\,v = s\,A\,v \tag{17}$$

Just like in the case of undamped vibrations, the v_i vectors are orthogonal with respect A and B:

$$v_i^T A\,v_j = 0 \quad , \quad s_i \neq s_j \tag{18.a}$$

$$v_i^T B\,v_j = 0 \quad , \quad s_i \neq s_j \tag{18.b}$$

and are normalized over the A matrix, thus leading to:

$$v_m^T A\,v_m = 1 \quad , \quad m = 1, 2, \ldots, 2\,N \tag{19}$$

If we define the modal matrix V and the spectral matrix S of the 2 N eigenvectors v, like in the case of the standard eigen problem, we obtain:

$$V^T\,A\,V = I \tag{20},$$

$$V^T\,B\,V = S \tag{21}$$

The shift from the generalized problem to the standard one is performed by pre-product of B^{-1}

$$B^{-1}\,A\,v = \frac{1}{s}\,v \tag{22}$$

thus leading to:

$$D\,v = \gamma\,v \tag{23}$$

wher $D = B^{-1}\,A$ and $\gamma = 1 / s$. The D is the dynamic matrix and is defined thereby:

$$D = \begin{bmatrix} 0 & I \\ -K^{-1}M & -K^{-1}C \end{bmatrix} \tag{24}$$

where K-1 M is the dynamic matrix in the case of the free undamped vibrations.

2. CASE STUDY

It is considered the modal analysis of a 3 storey steel frame as depicted in the Figure no.1. For the dynamic model 3 translational DOFs are granted along the OX direction and numbered as shown. In order to simplify numerically the case study the masses, the storey stiffnesses and the damping coefficients are scaled and the system matrices are defined below.

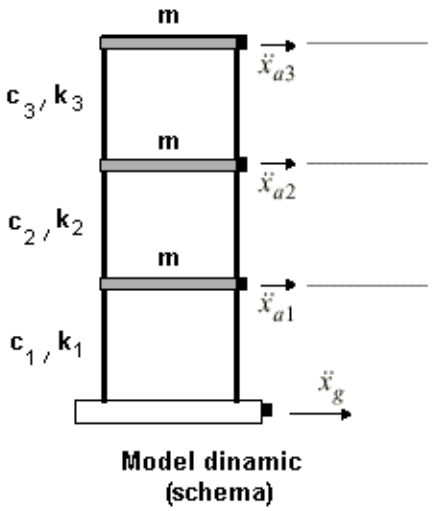

Figure 1

The mass matrix is considered diagonal, with equal uncoupled masses at each level. Masses are normalized to unit.

$$M = \begin{bmatrix} 1 & 0 & 0 \\ 0 & 1 & 0 \\ 0 & 0 & 1 \end{bmatrix} [/] \tag{25}$$

The stiffness matrix (scaled):

$$K = \begin{bmatrix} 398.6465 & -199.3233 & 0 \\ -199.3233 & 398.6465 & -199.3233 \\ 0 & -199.3233 & 199.3233 \end{bmatrix} [/] \quad (25)$$

The modal analysis in the field of real eigenvalues was performed by taking into account a stiffness proportional damping (i.e. $C = \beta K$, $\beta = 0.01$ (1%)). It resulted a proportional damping matrix:

$$C = \begin{bmatrix} 3.9865 & -1.9932 & 0 \\ -1.9932 & 3.9865 & -1.9932 \\ 0 & -1.9932 & 1.9932 \end{bmatrix} [/] \quad (26).$$

Using this model as basis, a non- proportional damping shall be added. We consider the first diagonal therm of C affected by an arbitrary coefficient (ex. ff = 8.5)

$$Cnp(1, 1) = ff * C(1, 1) \quad (27);$$

thus the non- proportional damping matrix becomes:

$$Cnp = \begin{bmatrix} 33.8850 & -1.9932 & 0 \\ -1.9932 & 3.9865 & -1.9932 \\ 0 & -1.9932 & 1.9932 \end{bmatrix} [/] \quad (28).$$

Now, by applying the complex eigenvalue process described in the previous chapter one obtaines:

- The complex spectral matrix:

$$\Lambda_{np} = \begin{bmatrix} -3.5787 + 22.5706i & 0 & 0 & 0 & 0 & 0 \\ 0 & -3.5787 - 22.5706i & 0 & 0 & 0 & 0 \\ 0 & 0 & -14.6445 + 8.7259i & 0 & 0 & 0 \\ 0 & 0 & 0 & -14.6445 - 8.7259i & 0 & 0 \\ 0 & 0 & 0 & 0 & -1.7091 + 7.0185i & 0 \\ 0 & 0 & 0 & 0 & 0 & -1.7091 - 7.0185i \end{bmatrix} \quad (29)$$

After sorting descending the diagonal elements and the computation of their modullus, one obtains:

- the circular frequency vector:

$$\omega_{np} = \begin{bmatrix} 7.2236 \\ 7.2236 \\ 17.0471 \\ 17.0471 \\ 22.8526 \\ 22.8526 \end{bmatrix} [rad/s] \quad (30).$$

- The complex modal matrix:

$$V_{np} = \begin{bmatrix} 0.0217-0.0368i & 0.0217+0.0368i & -0.0024+0.0550i & -0.0024-0.0550i & -0.0045+0.0102i & -0.0045-0.0102i \\ 0.0701-0.0365i & 0.0701+0.0365i & -0.0121+0.0138i & -0.0121-0.0138i & -0.0312-0.0183i & -0.0312+0.0183i \\ 0.0976-0.0348i & 0.0976+0.0348i & -0.0080+0.0007i & -0.0080-0.0007i & 0.0202+0.0084i & 0.0202-0.0084i \\ 0.2209+0.2151i & 0.2209-0.2151i & -0.4441-0.8260i & -0.4441+0.8260i & -0.2140-0.1371i & -0.2140+0.1371i \\ 0.1367+0.5545i & 0.1367-0.5545i & 0.0568-0.3083i & 0.0568+0.3083i & 0.5250-0.6383i & 0.5250+0.6383i \\ 0.0774+0.7443i & 0.0774-0.7443i & 0.1112-0.0809i & 0.1112+0.0809i & -0.2627+0.4259i & -0.2627-0.4259i \end{bmatrix} \quad (31)$$

The above matrix is computed for the standard problem of 2N order, $D_{np}\ v_{np} = \gamma_{np}\ v_{np}$ and the eigenvectors are transformed for the real system with N GLD.

- The complex shapes of vibration are:

$$X_{np} = \begin{bmatrix} 0.3165-0.2638i & 0.3165+0.2638i & 1.0000-0.0000i & 1.0000+0.0000i & -0.0364-0.3054i & -0.0364+0.3054i \\ 0.7560-0.1050i & 0.7560+0.1050i & 0.2608+0.2091i & 0.2608-0.2091i & 1.0000 & 1.0000 \\ 1.0000-0.0000i & 1.0000+0.0000i & 0.0198+0.1453i & 0.0198-0.1453i & -0.5999+0.0819i & -0.5999-0.0819i \end{bmatrix} \quad (32)$$

The complex modal shapes of the first and second mode of vibration are depicted in the complex space in the Figure No.2.

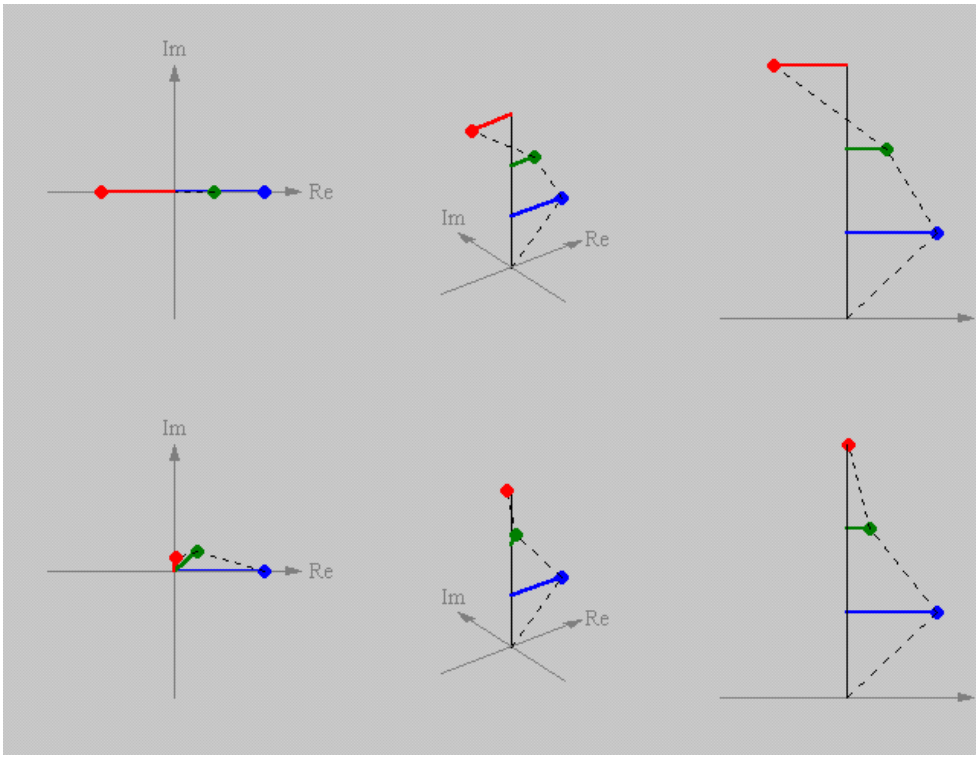

Figure 2 The complex modal shapes of vibration

3. CONCLUSIONS

This method is suitable for the solution of problems with non- proportional damping and it consumes a lot of operations. Broadly speaking, the solution of an eigenvalue problem consumes N3 operations (3rd order problem). The quadratic problem requires the solution of a 2N order system and it follows that the number of operations is 8 times bigger. In the case of a large eigenvalue problem, the performance of the solver is dramatically decreased. under these circumstances, a ballance between the costs and the Raileigh assumption might be useful, thus leading to good results, but not necessarily exact.

References

1. J. L. Humar, Dynamics of Structures, Prentice-Hall, N.J., 1990.
2. K. J. Bathe, Edward L. Wilson, Numerical Methods in Finite Element Analysis, Prentice-Hall Inc., Englewood Cliffs, New Jersey, 1976.
3. K.J. Bathe, Finite Element Procedures in Engineering Analysis, Prentice-Hall Inc., Englewood Cliffs, New Jersey, 1982.
4. J. H. Wilkinson, C. Reinsch, Linear Algebra, vol. II of Handbook for Automatic Computation, Springer Velrag New York, 1971.
5. J. H. Wilkinson, The Algebraic Eigenvalue Problem, Clarendon Press, Oxford, 1978.
6. P. Hood, “Frontal Solution Program for Unsymmetric Matrices”, Int. J. Num. Meth. Engng, 10, 379-399, (1976).
7. K. J. Bathe, EE. Wilson, “Large Eigenvalue Problems in Dynamic Analysis”, J. Engng Mech Div., ASME, 1972, 98, pp.1471-1485.
8. A. Perdon, G. Gambolati, “Extreme Eigenvalues of Large Sparse Symmetic Matrices by Rayleigh Quotient and Modified Conjugate Gradients”, Comput. Meth. Appl. Mech. Engng., 1986, 56, 251-254.
9. X. Wang, J. Zhou, “An Accelerated Subspace iteration Method for Generalized Eigenproblems” Comps. & Struct., 1999, 71, pp. 293-301.
10. Octavian V. Rosca, Ioan P. Ciongradi, “Metode numerice utilizate în programele de calcul automat al structurilor” Ed. Acad. Society “Matei-Teiu Botez”, Iasi, 2003.

URGENT1 - Software for planning and simulation of emergency evacuation using auto transport

Neculai Scîntei, Augustin-Ionu? Gavrila
"Gh.Asachi" Technical University, Iasi, 70050, Romania

Summary

The program URGENT1 was applied in a case study that simulated and planned decisions regarding population evacuation in emergency situations in a particular area. This program resolved the following problems: transportation plan, the making of the convoys, displacement itineraries, diagrams of population evaluation, it generated maps with information's regarding places, convoys, road segments, being of real use in training personnel that is responsible of population evacuation in cases of emergency.

KEYWORDS:emergency situation, population evacuation, simulation, deployment itinerary, evacuation diagrams, transport plans.

1. INTRODUCTION

Motto: "Human safety should be the supreme law."

Marcus Tullius Cicero

Population protection, of property and implementation of safety measures regarding the environment are the responsibilities of every human trough his actions.

Opportune and effective intervention is no longer possible trough the standard procedures that are based on approximate evaluations and experimental based decisions. In this case it is necessary to have knowledge in probabilistic evaluation regarding nature, content and quantity parameters of the phenomena that can produce calamity. Following this new parameters well based decisions can be made.

Intensified disasters and human crisis will lead to a raise in need of the *Inspectorate for Emergency Situations*, component of the National Emergency Situations Management system, to prevent and manage emergency situations, especially the capacity of the operative structures from within the system.

Prevention and risk reduction in the case of disasters, population and property protection against the negative effects of the emergency situations are a part of the specific activities of civil protection that must have permanently the capacity of a credible response, corresponding to the degree of danger in which the population is.

A strategic objective from the National strategy of civil protection in Romania is accomplishing preventively the measures of civil protection trough population evacuation, protection of property and cultural or archival values having in mind minimal destructive effect and/or military intervention. This objective can be accomplished through firm and opportune measures, enhancing the capacity of intervention of the forces and resources, trough the mobilization and requisition of resources and using the protection and intervention plans drawn in peace time, after reviewing and updating them.

This paper wants to be a stepping stone for the analysis, design and implementation of a integrated informatics system, capable to plan and simulate terrestrial transportation in the case of a disaster that requires population evacuation, material property moved from an affected area or one in the process to be affected, all being done well organized, and assuring their safety in an area with better conditions.

2. PLANNING AND ORGANIZING TRANSPORTATION ON THE TRAFFIC ROUTE IN EMERGENCY SITUATIONS

Traffic management of the transports is made having a good knowledge and operative skills on all the phenomena specific to these activities. The complexity of traffic management determines the replacement of the methods based on intuition and experience with scientific methods, all this being made for rationalizing the technical potential of execution transport missions in case of an emergency. Traffic management can have the following systemic approach: decisional subsystem – its role is regulatory in the system; operational subsystem of execution – which has the role of moving the decision in the action plan; information subsystem – which has the role to link the other two subsystems.

Organizing the evacuation procedure consists of: analysis of the emergency situation, prognosis regarding the evolution of the situation, determination of the destructive effects of the emergency, establishing first-aid emergency actions, recognition of the itinerary and areas where the evacuation is in effect, updating the evacuation plan and applying it, elaboration and transmission of the order/disposition of evacuation.

Traffic management on terrestrial routes will have as objective harmonizing the activities and correlation between decisional entities and execution ones.

The complexity and dynamic of the activities during an emergency situation imposes the amplification of collaboration between the decisional factors from the structure of the Ministry of Administration and Internal Affairs with other organs from state administration and public institutions with attributions in mobilization and evacuation.

3. SOFTWARE FOR PLANNING AND SIMULATION OF EMERGENCY EVACUATION USING AUTO TRANSPORT - URGENT1

Taking into consideration that lately there are more and more emergency situations, therefore more victims and affected areas, it is necessary to find more effective ways of intervention and saving population in dire situations through the evacuation in safer districts/areas using the advantages of modern techniques in planning, organizing, development and leading interventions.

The goal is making a software for optimized planning of population evacuation and rescue from a clearly marked area using traffic management in the given terrestrial transportation situation considering different degrees of emergency for affected districts. Taking into consideration that the railway infrastructure is underdeveloped in the endangered area it is considered that the model should contain only pedestrian evacuation with auto means of transportation using the national, regional and rural network of roads. Also the main concern is follow-through on every step of the evacuation regarding the support needed for the human decision factors with the purpose of ensuring the necessary information in taking decisions in respect to the given manpower and ways of intervention.

4. STRATEGIES, METRICS AND THE ALGORITHM OF EVACUATION

while(∃i=***UnsafeLocality**** so that ***ActualPopulation***[i]>0)
//*test **UnsafeLocality**: population*EmergencyDegreeEvacuation*(1-safety)>0
{
i=***ChooseUnsafeLocality***(strategy**, distance***, EstimateTime, ActualPopulation, VehicleCover)
//**: examples of **strategies**:
//**MaximumProfit**:
MaximalDistance/MaximalPopulation/MaximalEmergencyDegreeEvacuation...

```
//MinimumRegret: MinimalTime for evacuation of local population from selected area
//***distance – may be considered aproximate, on the shortest route possible,
//or taking into consideration degrees and
//time intervals to cover area arcs
  if(∃CoveringVehicles[i])
   {
    j=EvacuationPlanning(i);
    //considering:
    //time for loading, transport and unloading
    //anterior planning, degrees and intervals of occupancy
    //of road arches from the road network involved in evacuation
    EvacuationStart(i, j, SelectedPath, ComputedTimeIntervals, NecessaryStops)
   }
  else {
          j=ChooseSafeSource(AvailableVehicles,TimeIntervals,
          NeededSmallBusses,NeededBusses,NeededCoachBusses)
          SendHelp(j,i,way, TimeInterval, NeededSmallBusses,
NeededBusses,NeededCoachBusses)
          }
}
```

5. CASE STUDY

In this paper it was considered for exemplification a coded locality TF with a maximum degree of emergency evacuation and with a population of 13.573 people at which it is added the population of the nearby codified villages, 2.696 people.

Comparing the available auto transport capacities with the necessary of transport of the existing population in the locality TF at the initial moment T_0 it was decided to solicit help for supplementary transport capacity for a number of 1.020 people like this: from the codified locality VS – 370 places representing 5 small buses with 20 seats each, 3 buses with 40 seats each and 3 coach buses with 50 seats each from the coded locality RM – 650 places given by 10 small buses, 5 buses and 5 coach buses.

Following the diagram of the effective number of people situated in the coded locality TF it is observed that evacuation time, in minutes, of the 2.696 people from the nearby villages that are using for displacement pedestrians convoys and auto transport evacuation and the fact that the last convoy leaves at the minute 504.

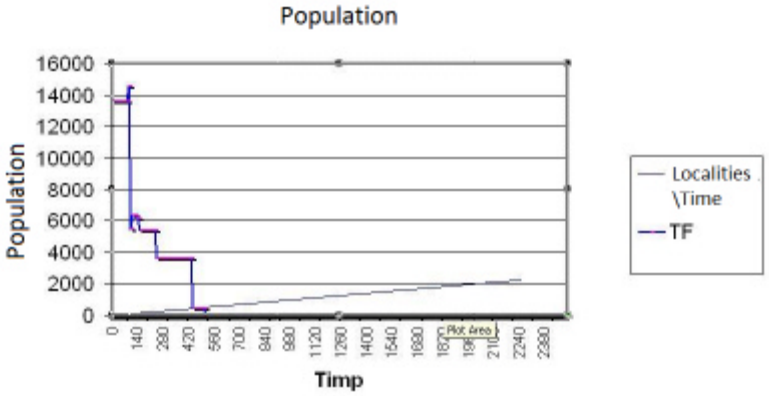

Figure 1. Diagram of the population evacuation development in TF coded locality

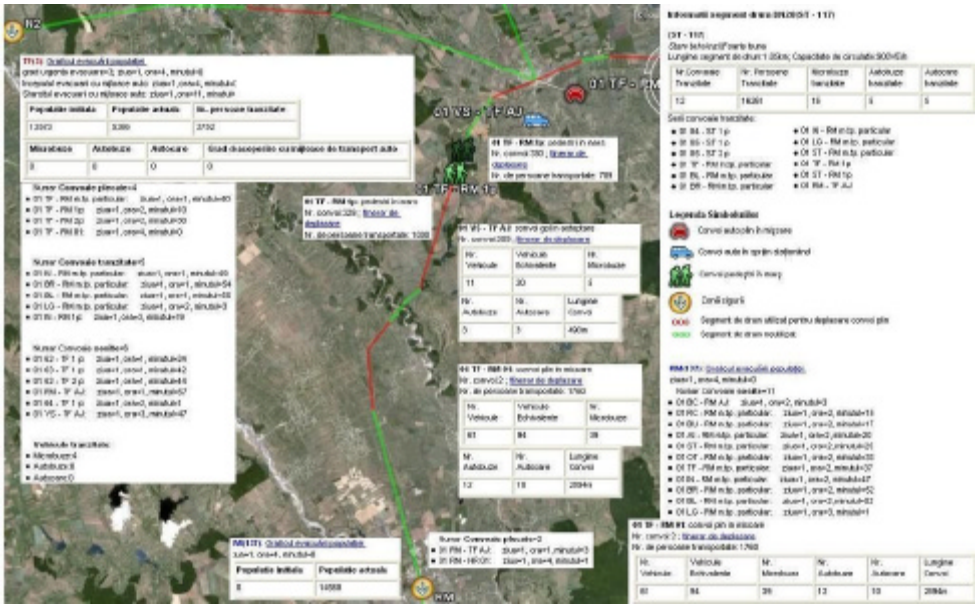

Figure 2. Population evacuation status in the given situation at minute 240

At minute 540 it is observed the 21 small buses convoy moving the last batch of 416 people from the coded TF locality; in this way at minute 561 the operation of evacuation with auto transport is finalized following that in the minute 663 the last pedestrian convoy, 01 TF – RM 02 p, to reach the safe coded locality RM.

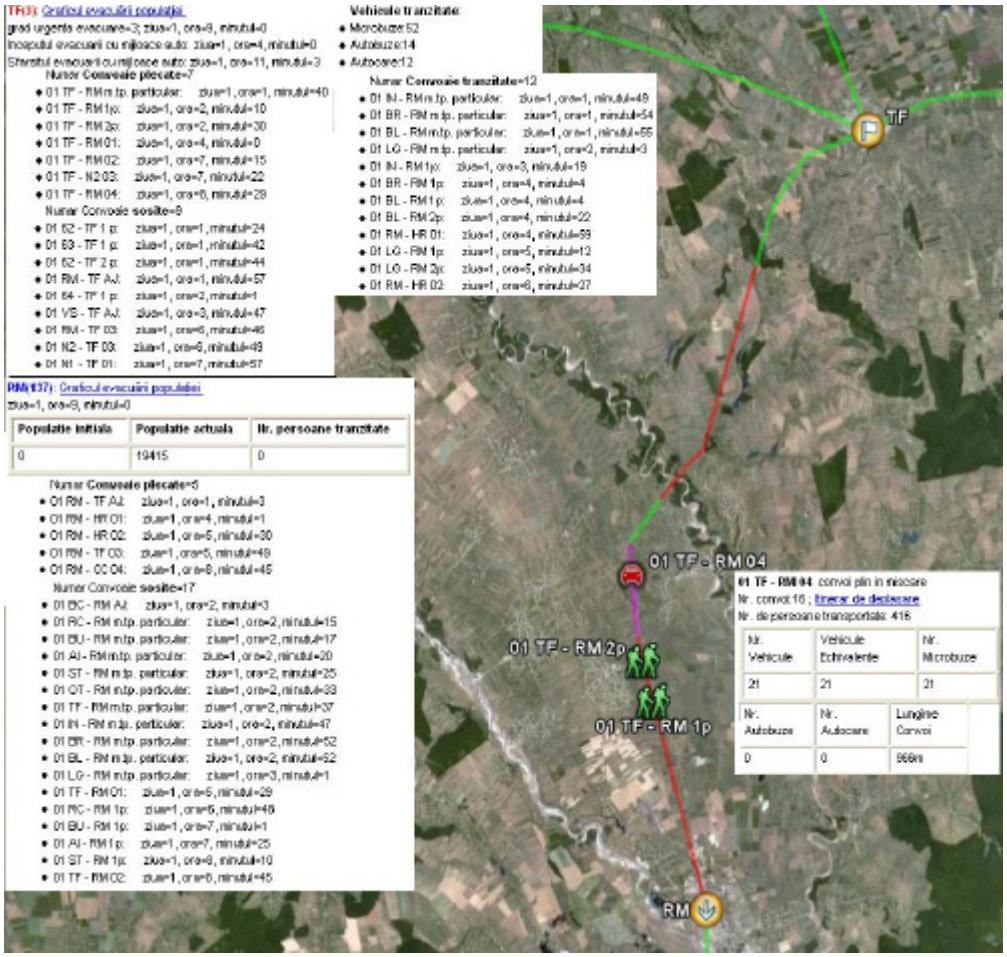

Figure 3. Population evacuation status at minute 540 in the given TF coded locality

6. CONCLUSIONS

The authors of this paper feel that the proposed goal was acquired, the design of a software for simulation, planning and optimization of risk and uncertainty condition decision making involving population evacuation using auto transport in emergency situations – URGENT1. This was made taking into consideration areas with different levels of danger, the terrestrial road system, the existing and supplemented road transportation using heuristics for time optimization in evacuating with minimal risk taking.

The software URGENT1 was applied at a given study case for simulating, planning and optimizing decision making regarding population evacuation in emergency situations from an area affected for one day and 17 hours with a positive result. This software resolved the following problems: transport plan, map generation with information's referring to areas, convoys, road segments – at 10 minutes interval having the possibility of being of real help for personnel training in evacuation techniques (extended – of material property also) in emergency situations.

The purpose of this software is to be used at institutional level and also at the level of local administration for the preparation of personnel and population in case of disaster. Using this resource will lead to economy to budgets both financial and material and mainly it would save human life.

References

1. Cascaval Petru, Cascaval Doina: *Modelare si simulare*. Iasi: Ed. Gh. Asachi, 2002. (in Romanian)
2. Croitoru Cornelius: *Tehnici de baza în optimizarea combinatorie*. Iasi: Ed. Univ. Al. I. Cuza, 1992. (in Romanian)
3. Hagiu Victor: *Managementul executiei proiectelor de constructii*.Iasi:Ed. Dosoftei. 2003. (in Romanian)
4. Ionescu Gh.Gh., Cazan Emil, Negruta Adina Letitia: *Modelarea si optimizarea deciziilor manageriale*. Cluj-Napoca : Ed. Dacia, 1999. (in Romanian)
5. Ionescu Tiberiu: *Grafuri-aplicatii*. Vol. I, Bucuresti: Ed. Didactica si Pedagogica, 1973. (in Romanian)
6. Ionescu Tiberiu: *Grafuri-aplicatii*. Vol. II, Bucuresti: Ed. Didactica si Pedagogica, 1974. (in Romanian)
7. Luban Florica: *Modelarea si simularea proceselor economice în transporturi.* Bucuresti: Ed. Academia de Studii Economice,1997. (in Romanian)
8. Lupescu Titus, Rosu Alexandru, Cerchez Mihu: *Programarea matematica cu aplicatii militare.* Bucuresti: Ed. Militara, 1965. (in Romanian)
9. Zarojanu Gh. *: Elemente de tehnica traficului rutier.* Iasi: Ed. Societatii Academice Matei – Teiu Botez, 2002. (in Romanian)
10. Andrei Neculai: *Modele, programe de test si aplicatii de programare matematica*. Bucuresti: Ed. Tehnica, 2003. (in Romanian)
11. Legea nr. 481 din 08.11.2004 privind protectia civila, cu modificarile si completarile ulterioare.
12. Hotarârea Guvernului României nr.547 din 09.06.2007 pentru aprobarea Strategiei nationale de protectie civila. (in Romanian)
13. Hotarârea Guvernului României nr.762 din 16.07.2008 pentru aprobarea Strategiei nationale privind prevenirea situatiilor de urgenta. (in Romanian)
14. Ordinul ministrului administratiei si internelor nr. 1184 din 06.02.2006 pentru aprobarea Normelor privind organizarea si asigurarea activitatii de evacuare în situatii de urgenta. (in Romanian)

Implementation of a Geotechnical GIS Database for 3D Modeling of the Layer Limit Surfaces

Ana-Luciana Tofan, Vasile Musat
Department of Roads, Railways, Bridges, and Foundations, Technical University "Gh. Asachi", Iasi, 700050, Romania

Summary

The existing plans and maps can be one of the methods for data acquisition needed for implementing a geotechnical GIS database. They contain a large amount of qualitative and quantitative information, available at different scales. Graphic data collection on plans and maps can be achieved by scanning, digitizing or automatic vectorization, processes in which the collected data are converted from analog to digital format.

The first stage of this work used information from 9 topographic plans at 1:1000 scale in analog (scanned) format, covering the center of Iasi, resulting the 3D terrain model, which is also the surface of the filling layer. In this sense, were through the stages of georeferencing, digitization, delimitation of the study area, entry of known rate points found on the scanned plans, ending with the implementation of 3D model and contour levels for the surface layer. Autodesk Map 3D, GTX and TopoLT platforms were used for these achievements.

Similarly, using the other stratification data, which has been classified as loess layer, water bearing layer, impermeable layer and lower layer, extracted from the existing geotechnical data of the boreholes performed on the study area, the steps of introducing corresponding rates were driven again, resulting the 3D models and contour levels.

KEYWORDS: GIS database; geotechnical data; Z-coordinate; 3D Model; contour levels.

1. INTRODUCTION

Currently, the Internet is known as the most efficient way through which large amounts of information circulating throughout the world with amazing speed and trough information technology were developed and develops data management systems with spatial location. The technology that purchases, integrates and

ISSN 2285-2735, Pages 355 - 367

provides spatial data is called "Geographic Information System" (GIS) and nowadays it is continuously growing, serving as a computerized tool for mapping and analysis of all elements that exist and events happen in the world. It integrates common database operations such as query and statistical analysis with unique advantages of maps for viewing and analyzing geographic spatial data.

Since maps are the most important way to represent graphic information, a GIS is combining their data, satellite images and aerial photos with alphanumeric databases containing information on graphical data. Geographic Information Systems allow to create maps, integrate information, visualize scenarios, solve problems with high difficulty and developing effective solutions in a new easy to use approach.

In order to obtain real-time spatially referenced data, it is necessary to achieve an integrated computerized support. This paper uses as a means of digital graphic data acquisition 1:1000 scale topographic plans, resulting from scanning and on-screen digitizing.

The main purpose of this paper is to present a method for integration of geotechnical data in a Geographical Information System to highlight changes in 3D surface models of stratification limits.

According to the specialized literature, a solution for solving this problem can be given by geostatistical methods, which can be used to better understand the spatial variations of soil characteristics (Akbarzadeh & Taghizadeh, 2010), by providing tools for analyzing spatial data and estimating unknown values (Isaaks & Srivastava, 1989).

Generally, these approaches using Geographic Information Systems technology involves difficulties when estimating 3D spatial variables due to loss of the Z-coordinate information (Choi & Park, 2006).

1.1. Study area

The considered study area for processing and synthesis of geotechnical data for 3D stratifications developing represents the part of Iasi with the highest occupancy of buildings, this forming the nucleus around which the city has been developed over time. The built background on the area under discussion incorporates both historical buildings, most of them being declared monuments (Palace of Culture, Three Hierarchs Church, Metropolitan Cathedral, National Theatre, Roznovanu Castle, Philharmonic Moldova, Union Museum, V. Alecsandri Museum, Natural Sciences Museum, Armenian, Barboi, Banu, Lipovenian Churches, etc.) and recent buildings (residential, administrative establishments, banks, hotels, family homes, public buildings and social services, catering, etc.).

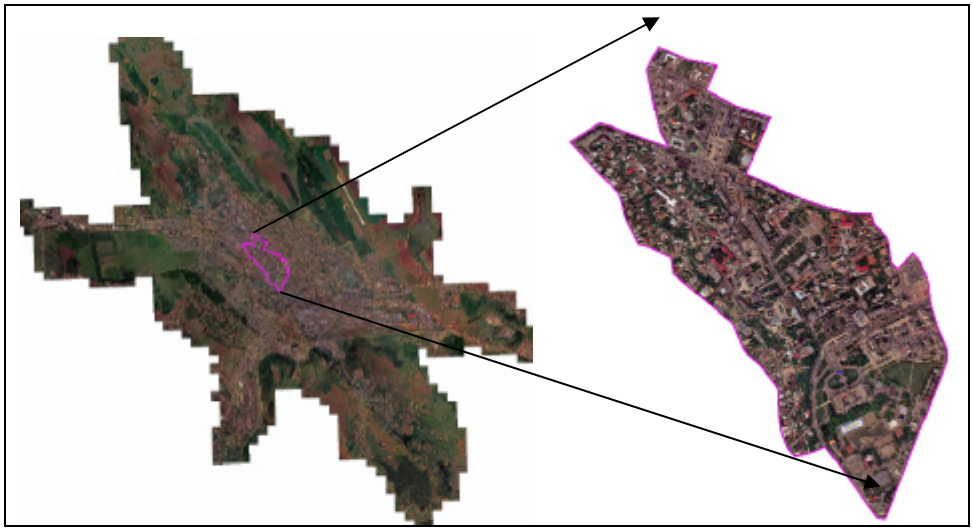

Figure 1. Location of study area in Iasi county

1.2. Sources for both graphic and alphanumeric data acquisition

This paper uses the following sources as means for digital graphic data acquisition:

a) orthophotomap of Iasi, air-photographed in 2005;

b) topographic plans in analog format at 1:1000 scale;

c) the layout of boreholes plans, according to geotechnical documentation;

d) boreholes stratification sheets, according to geotechnical documentation (figure 2).

The corresponding Z-coordinate for each layer were extracted in a first stage from the geotechnical boreholes sheets (insufficient), and for the 3D Model implementation of the filling layer surface, leveling network points whose rate is specified on the scanned maps and plans are used (figure 2.b).

However, for achieving the 3D Models of the other layer limit surfaces (loess layer, bearing water layer, impermeable layer, lower layer), the problem occurs in determining the Z coordinate of the points whose rate is known in the filling layer, but not known for the other layers and only the insufficient data from geotechnical boreholes sheets can be used.

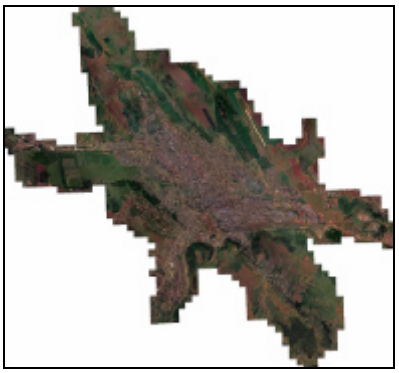

a)

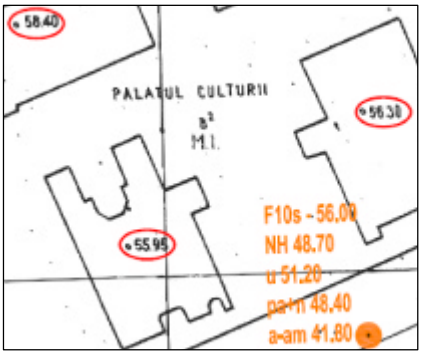

b)

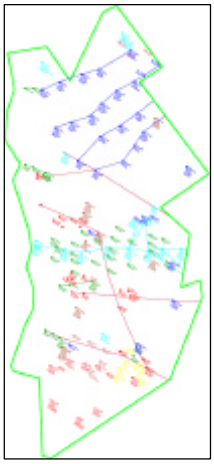

c)

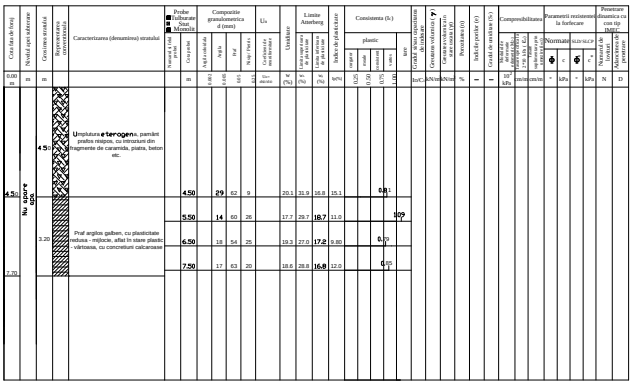

d)

Figure 2. Sources for data acquisition

2. IMPLEMENTATION OF GRAPHIC DATABASE

For the achievement of a GIS application, a series of steps must be covered such as: application design, data acquisition and processing, final product testing, analysis and interpretation of results.

From these, stages for acquisition and processing involve long time and high costs, so it is important to give special attention.

In the data acquisition phase, data sources are identified, content is analyzed, procedures for collection are established and data is collected. Data processing

involves the use of specialized GIS software functions for data cleaning, data integration and topologies establishment. (Bofu & Chirila, 2007)

Graphic information was taken using raster format topographic plans (trapezoids) at the scale 1:1000 (data acquisition from existing maps and plans), image air-photographed in 2005 (data acquisition from photogrammetry) and the layout of boreholes plans in accordance with geotechnical documentation.

2.1. GIS data acquisition

The existing maps and plans are the main source for the achievement of a GIS application and the graphic data can be obtained by scanning, digitizing and vectorization, the graphics being conversed from analog to digital format.

The achievement of graphic database involves obtaining the digital format for the analyzed study area through various stages. In this chapter are presented other methods different than those used in the paper for data acquisition such as:

2.1.1. Data acquisition from remote sensing

Remote sensing data is represented by satellite images obtained by collecting electromagnetic radiation transmitted by objects and transforming them into digital format. The main known data sources are the two remote sensing systems: the U.S. Landsat and SPOT of France.

2.1.2. Data acquisition from direct measurements

In this case, data are acquired by direct measurement, which can be performed with total station or GPS equipment. These type of works involves performing measurements in order to identify ownerships or large-scale plans to highlight the planimetric and elevation details. (Bofu & Chirila, 2007)

2.2. Achievement of digital graphic support of the study area by data processing

The 1:1000 scale topographic plans are obtained in analog format by scanning, so still must be processed with specialized software (Autodesk Map and RasterCad GTX Plus) to obtain digital format for the area. In this sense, several steps are performed as follows:

2.2.1. Calculation of the topographical plans cartographic elements

a. Inventory of existing database

Cadastral territory of the study area is placed within the municipality on a number of 2 plans at 1: 5000 scale, 5 plans at 1:2000 scale and 9 plans at 1: 1000 scale (table 1).

Table 1. Plans inventory of the study area

Scale	No	Name	Editing year	Edited by	Projection
1:5000	2	L-35-32-A-c-4-III L-35-32-C-a-2-I		I.P.T.A.N.A.	Local-Iasi
1:2000	5	L-35-32-A-c-4-III-3 L-35-32-A-c-4-III-4 L-35-32-C-a-2-I-1 L-35-32-C-a-2-I-2 L-35-32-C-a-2-I-4		I.P.T.A.N.A.	Local-Iasi
1:1000	9	L-35-32-A-c-4-III-3-d L-35-32-A-c-3-III-4-c L-35-32-C-a-2-I-1-b L-35-32-C-a-2-I-2-a L-35-32-C-a-2-I-2-b L-35-32-C-a-2-I-2-c L-35-32-C-a-2-I-2-d L-35-32-C-a-2-I-4-a L-35-32-C-a-2-I-4-b	1982/1983	I.P.T.A.N.A.	Local-Iasi

b. The connection scheme of the topographical plans

This scheme contains the plans shown in table 1 along with the (f , ?) geographical coordinates (figure 3).

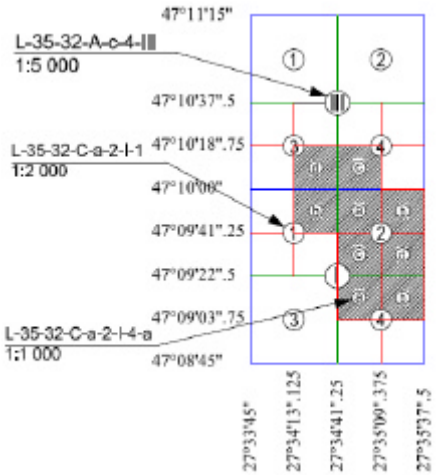

Figure 3. Connection scheme and (f , ?) geographical coordinates

c. The calculation of the (X, Y) stereo-70 coordinates

Based on the geographical coordinates of the topographic plans on Krasovski-1940 reference ellipsoid, it is necessary that they be transformed into rectangular coordinates in stereo-70 projection system applied to our country. This could be achieved using the formulas with constant coefficients as presented in a previous paper. (Tofan, 2011)

The calculus was performed for each 1NW, 2NE, 3SW and 4SE corners of 1:1000 scale topographic plans and are presented in table 3.

Table 3. Stereo-70 and geographical coordinates database

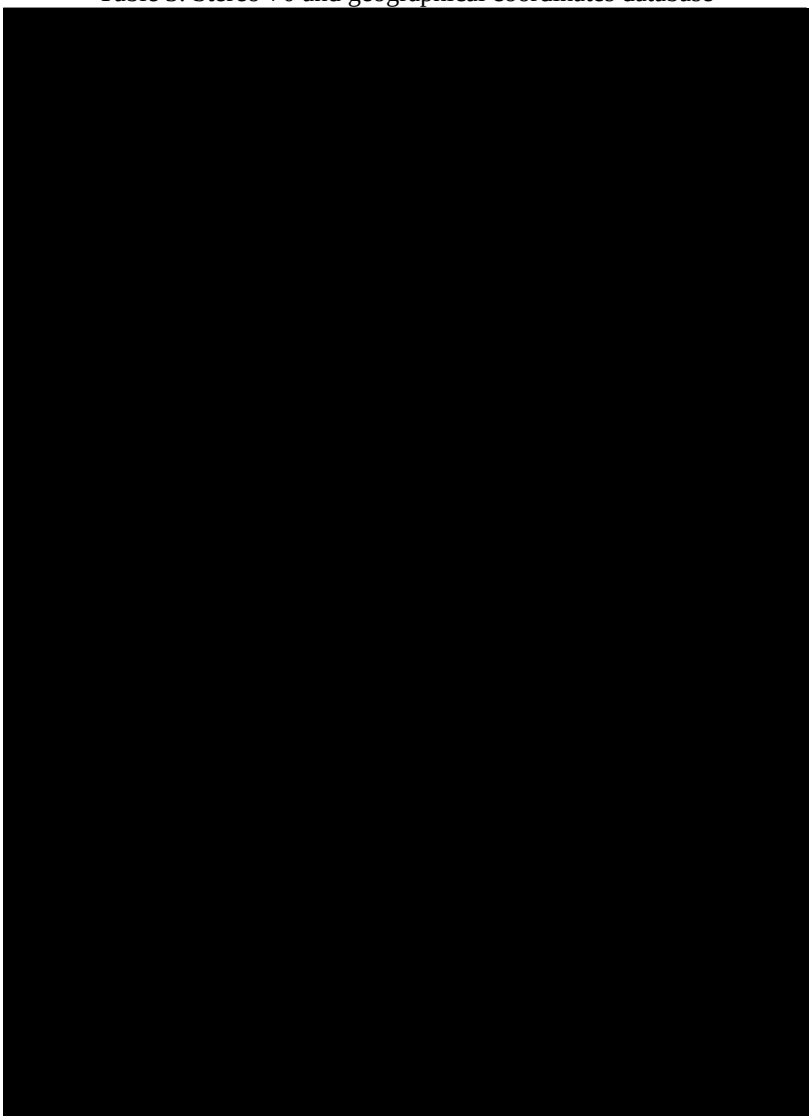

d. Attaching and georeferencing raster images

Raster images attaching and georeferencing were conducted in AutoCAD Map using the special functions in the Map menu.

Trapezoids scanned georeferencing is the process through which the images are brought into their spatial position and is of great importance in terms of accuracy and continuity of graphic information as support for future GIS application. Figure 4 shows in left the continuity of the scanned topographic plans obtained by georeferencing and in the right the detachment of the study area in digital format obtained by on-screen digitizing.

Figure 4. Graphic data processing for the achievement of digital format of the study area

In addition to the steps outlined above, the steps of defining name layers, on-screen digitizing, database defining for each digitized plan and projection system definition are detailed described in the mentioned paper. (Tofan, 2011)

3. IMPLEMENTATION OF ALPHANUMERIC DATABASE AND COUPLING IT WITH GRAPHICS BY DATA CONVERSION

Further, the alphanumeric data and 3D models of layer limits surfaces will be achieved by attaching TopoLT application to Autodesk Map platform.

The TopoLT specialized program provides tools for 2D and 3D applications with which you can create topographical or cadastral plans, 3D terrain model and contour levels, calculate volumes or georeferenced images can be inserted. Functioning of this program is possible for most CAD platforms (Autodesk, Bricscad, CADian, CMS IntelliCAD, progeCAD, ZwCAD), supporting Windows 98 / Me / NT / 2000 / XP / Vista / Windows 7 operating systems.

Under the Autodesk platform, but also for the other programs, TopoLT uses its drawing functions, plus specific program functions necessary to achieve topographical or cadastral plans in digital format. (http://topolt.com/)

3.1. Unknown rate point interpolation for each layer using known rate points

In this paper, Z coordinates of unknown points were determined by accessing the interpolation function from the TopoLT program menu. Thus, having the spatial coordinates (X, Y, Z) of a number of 470 points covering the study area and actually forming alphanumeric database, the next step is to convert and attach it to the graphics database.

The calculated rates for each layer (filling layer, loess layer, bearing water layer, impermeable layer, lower layer) were determined “on-screen” (in screen space) and the “.rtf” (rich text format) type files were downloaded accessing the function “Coordinates » Create coordinates table”. Based on them, the ".txt" type files containing PN (point name), X, Y, Z coordinates and code were created for each layer.

In this way, database can always be verified, completed or updated as new information regarding other performed boreholes in the study area are available.

After verifying, completing or updating the alphanumeric database, the next step is to couple it with graphics. This can be done by opening a new “.dwg” file and accessing the function “Coordinates » Draw points” from TopoLT menu, so all points with name, coordinates and code in accordance with those entered in the “.txt” type files are brought into screen space to visualize.

3.2. Coupling alphanumeric database with graphics

For 3D modeling and contour levels achievements, must first relate points of the ".txt" files with Autodesk platform. In this sense, five ".dwg" files were made, one for each surface.

Using the function "Coordinates »Draw Points" from TopoLT menu, must choose the ".txt "file corresponding to each layer. After making all settings and choosing the import method, click OK, and points will be visualized in the screen space. (http://topolt.com/)

To raise the other entities at their rate, "Transformations Lift-up to points elevations" function must be used.

3.3D MODELS AND CONTOUR LEVELS

Using the function “3D Model » Build 3D”, must select the points, delete points with elevation 0.000 m, select lines or polylines of forced change of the slope (breaking lines), select 3D model boundary (which is the outline of the study area) and models are generated automatically. Finally, a new window is shown where you can view the models, make renderings, choose the projection method, light intensity, quality of texture, whether smooth or not 3D objects, textures (http://topolt.com/). The resulting 3D models are presented in figure 5.

To visualize all the 3D models of each layer at once, they have to be brought in a single “.dwg” file using the commands “Edit » Copy”, “Edit » Paste to original coordinates” and “3D Model » View 3D model” (figure 6).

The contour levels are also automatically generated for each layer based on fairness, colors and thicknesses chosen in Program Options (figure 7) by accessing the function “3D Model » Draw contour levels” (http://topolt.com/).

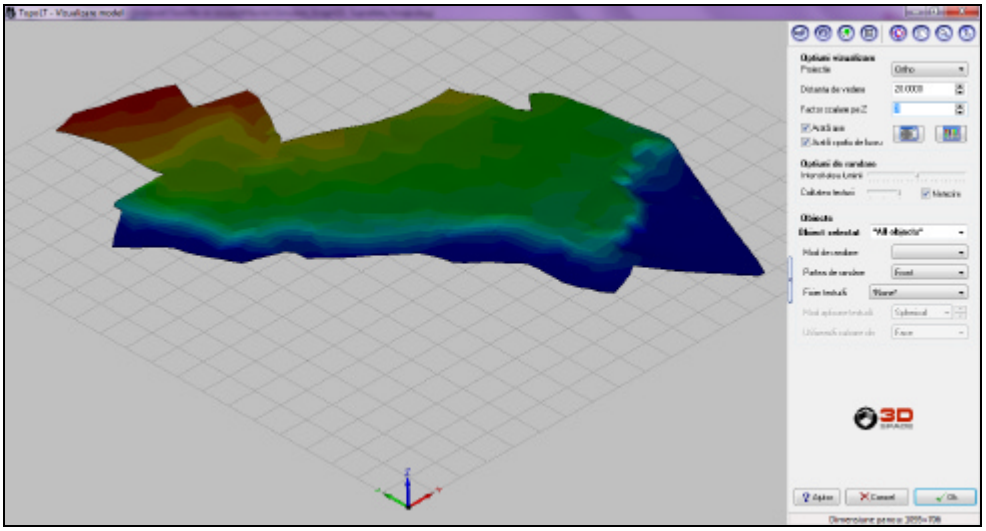

FILLING LAYER

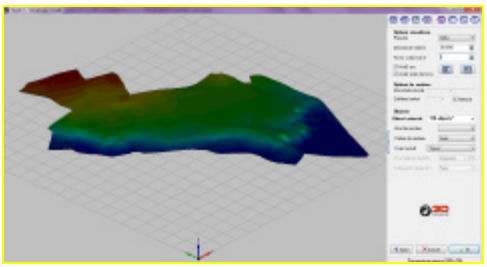

LOESS LAYER

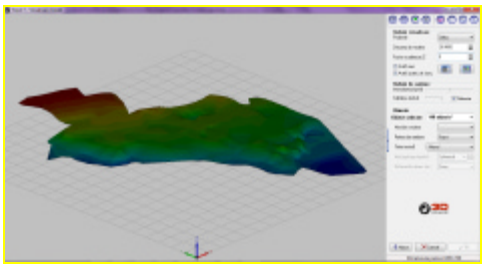

WATER BEARING LAYER

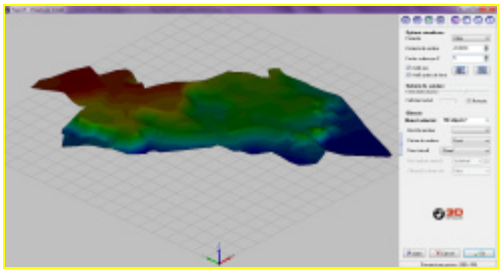

IMPERMEABLE LAYER

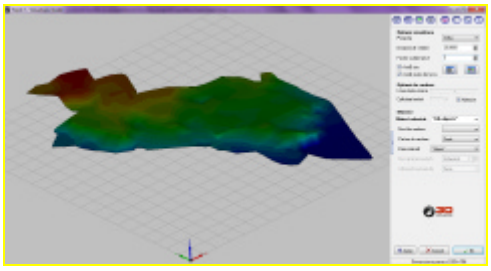

LOWER LAYER

Figure 5. 3D Models of the layer limit surfaces

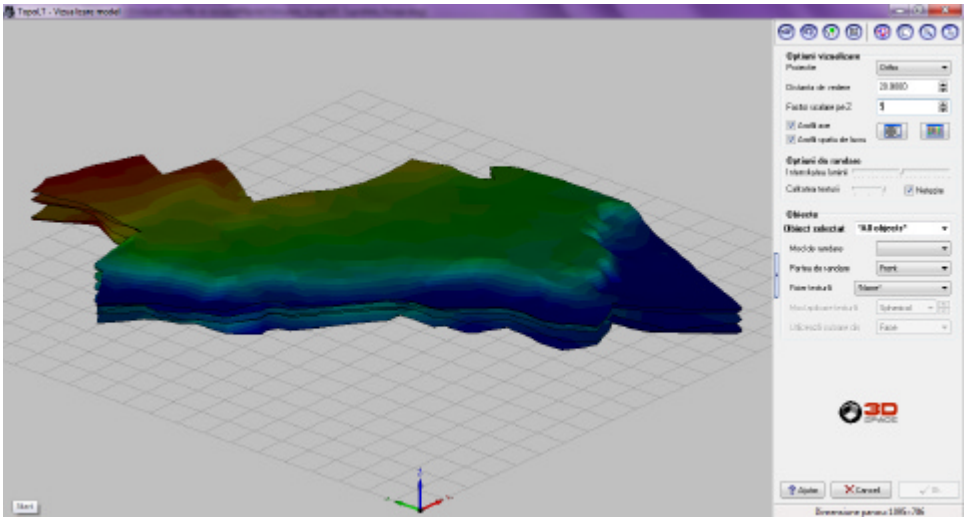

Figure 6. The 3D Model view of all the layer limit surfaces

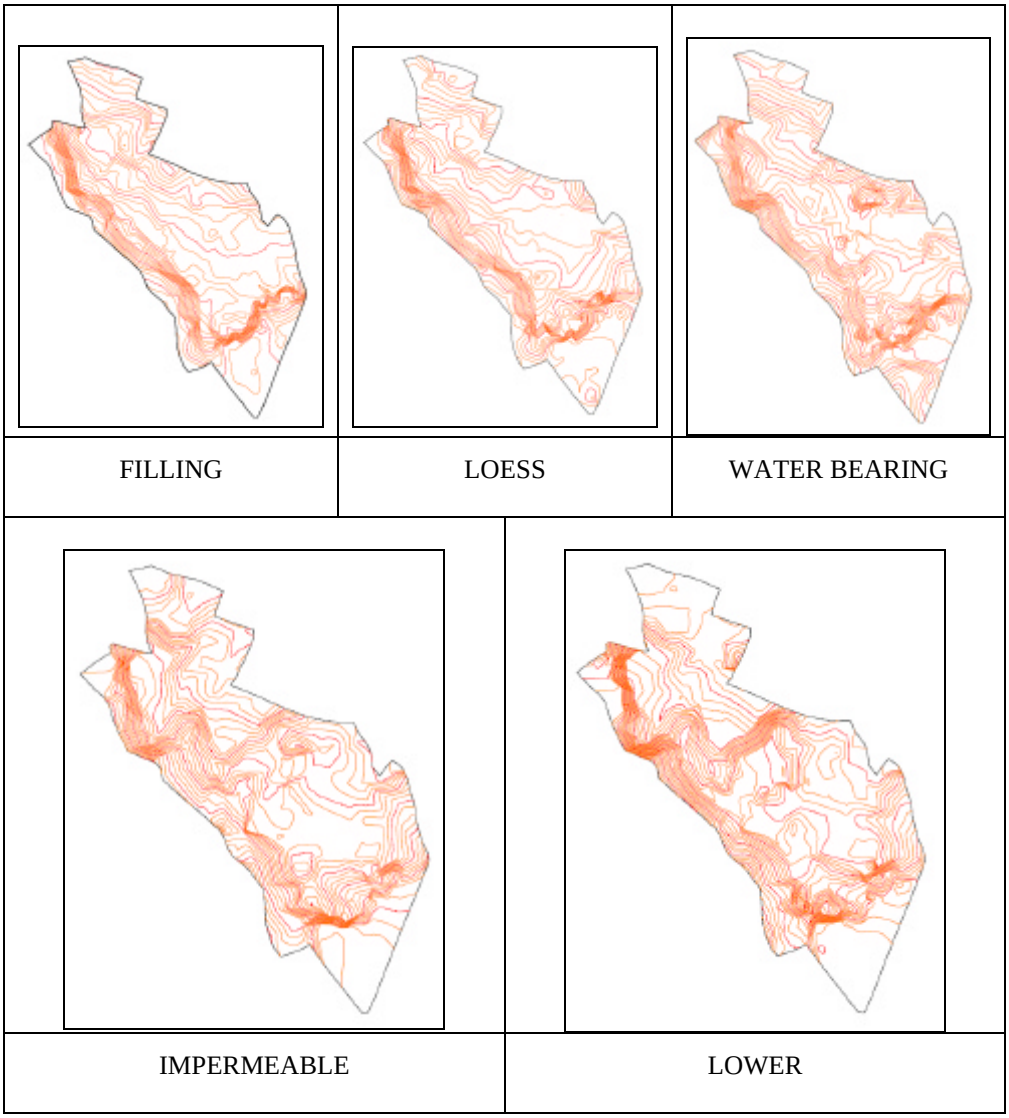

Figure 7. Contour levels of the layer limit surfaces

4. CONCLUSIONS

A system through which is collected, stored, handled, processed, analyzed and visualized all the necessary data at any time determines also a better organization of the existing information for a particular study area.

Such a system can also be achieved for geotechnical engineering by Geographical Information Systems technology, this paper presenting a way to implement a database containing information from scanned maps and plans, as well as from boreholes sheets, to 3D modeling and corresponding contour levels implementation of the layer limit surfaces.

Also these results can be used in establishing the points for factor of ground condition that is taken into account when estimating geotechnical risk.

References

1. Akbarzadeh, A., & Taghizadeh, M. R. (2010). Distributia spatiala a unor proprietati ale solului prin utilizarea metodelor geostatistice în regiunea Khezrabad (Yazd) din Iran. ProEnvironment 3 (2010) , 227-236.
2. Bofu, C., & Chirila, C. (2007). Sisteme Informationale Geografice. Cartografierea si editarea hartilor. Iasi: Editura Tehnopress.
3. Choi, Y., & Park, H.-D. (2006). Integrating GIS and 3D geostatistical methods for geotechnical characterization of soil properties. IAEG 2006 Paper number 532 , 1-8.
4. http://topolt.com/ . (n.d.).
5. Isaaks, E. H., & Srivastava, R. M. (1989). Applied Geostatistics. New York.
6. Tofan, A.-L. (2011). Integrarea datelor grafice pentru un areal din zona centrala a municipiului Iasi într-un Sistem Informational Geografic în vederea evaluarii si monitorizarii riscului geotehnic. Al IV-lea Simpozion National "Creatii universitare 2011" .

Numerical Evaluation of the Seismic Behavior of a Load-Bearing Masonry Condominium Structure Specific for Romanian Urban Areas

Ana-Maria Toma[1], Gabriela M. Atanasiu[2], and Ionut-Ovidiu Toma[2]
[1]*Department of Graphical Communication, "Gheorghe Asachi" Technical University of Iasi, Iasi, 700050, Romania*
[2]*Department of Structural Mechanics, "Gheorghe Asachi" Technical University of Iasi, Iasi, 700050, Romania*

Summary

The paper presents preliminary results related to the numerical evaluation of the seismic behavior of a load-bearing masonry condominium structure widely met in the Romanian urban areas by means of SAP2000 computer software. The numerical model follows closely the geometry and the loading conditions of a real structure. The seismic behavior was analyzed from the point of view of the fundamental period of vibration, by means of the degradation coefficient, and lateral displacements at the level of each floor. The model was subjected to various earthquake scenarios all of which took place during the life-time of the structure. The obtained results show that there are minor degradations in the structure and, therefore, the safety of the occupants is not jeopardized.

KEYWORDS: non-linear time history analysis, masonry structure, seismic behavior, degradation coefficient.

1. INTRODUCTION

An increase in the number of natural disasters occurring all over the world has been recorded for the past decade. Natural disasters are extreme geological, meteorological or hydrological events that exceed the ability of a community to cope with that specific event. They result, more often than not, in great human, property, and environmental losses, along with social and economic disruptions [1].

Assessing the impact of a natural disaster upon a community is important for many reasons [2-4]. One of the reasons is that the information about disaster impacts can be used to identify specific segments of the community that have been affected or might be affected in the future. Additionally, decision makers can develop disaster impact scenarios before they even occur in order to assess the potential

consequences [5-9]. Due to the increased public awareness to the effects of natural disasters, with particular focus on earthquakes, great emphasis is being placed on the role of disaster mitigation and vulnerability assessment in planning for sustainable development. Communities can use risk and vulnerability assessment results to reduce the impacts from hazards through the development or revision of emergency response, disaster recovery and hazard mitigation strategies [4, 6, 10].

Evaluating the seismic hazard in a region is of critical importance in the field of structural engineering. Although the first scientific efforts in earthquake parameter prediction date back to 67 years, advances made in this field can best be described as sporadic, as described by Panakkat and Adeli, 2008 [11].

Buildings have partially or totally collapsed during recent earthquakes in Turkey 1999, India 2001, Italy 2009, Haiti 2010, Chile 2010 and Japan on March the 11th, 2011. Many of these collapses occurred in older buildings designed according to what nowadays are considered inadequate design standards. Others have been attributed to mistakes made during the design and execution stages. However, several of the collapses took place in buildings that were designed and constructed in accordance with modern seismic design principles. Therefore, as demonstrated by the on-site investigations, it is possible that many of the observed collapses have been the result of deficiencies in our knowledge of the regional seismic hazard, the behavior of structural materials under dynamic loads, and the post-elastic behavior of structural systems [12].

Therefore, from the structural engineering point of view, it is important to assess the behavior of a building during seismic excitations in order to determine whether or not supplementary measures should be taken before such an event occurs in order to prevent the possible collapse of the building. The assessment can be performed either by means of experimental works on scaled down [13] or full-scale models mounted on shaking tables [14, 15] or by means of numerical simulations using advanced software packages. Numerical simulations by means of the Finite

Figure 1. Load-bearing masonry structure

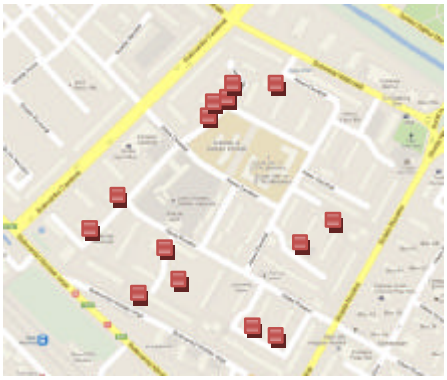

Figure 2. Selected urban sample

Element Method have become a valuable and important tool in the field of Civil Engineering. The application of suitable mathematical algorithms and nonlinear material models allow for the identification of the damage and possible failure modes of a structure subjected to any type of loading scenario [16-20].

The paper presents partial results from the numerical evaluation of the seismic behavior of a load bearing masonry condominium largely used in the Romanian urban areas. The structure is a four-story high load bearing masonry structure, Figure 1, built during the late 1960s and it is a typical condominium type of structure for the city of Iasi and other urban areas in Romania. The selected urban sample is presented in Figure 2. The model was subjected to different earthquake scenarios, all of which took place during the life-time of the structure, and the behavior was investigated from the point of view of the degradation coefficient [21] and peak lateral displacements at each storey level. The paper brings its contribution to the pre-disaster mitigation which is essential to the long-term sustainable development of communities. Risk assessment is an integral part of disaster mitigation. It provides critical information on the characteristics of potential disasters in a region and allows planners to identify and prioritize mitigation opportunities [22, 23].

2. NUMERICAL MODEL

2.1. Geometry, Sections and Materials

A 3D view of the numerical model is shown in Figure 3. It has been generated by means of the performant computer software SAP2000 v.14 [24] following the specifications of Project 1497/1966 [25]. Linear beam elements were used to model the beams and the monolith concrete columns between the masonry panels. The walls and the stair-case, Figure 4, were modeled by means of *Shell Layered / Nonlinear* elements.

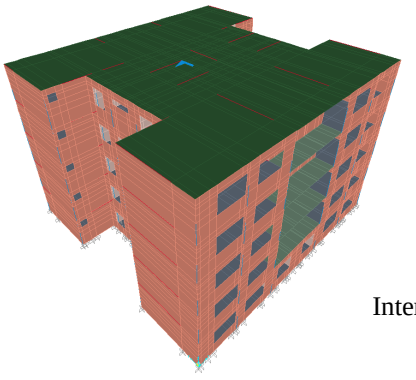

Figure 3. 3D view of the model

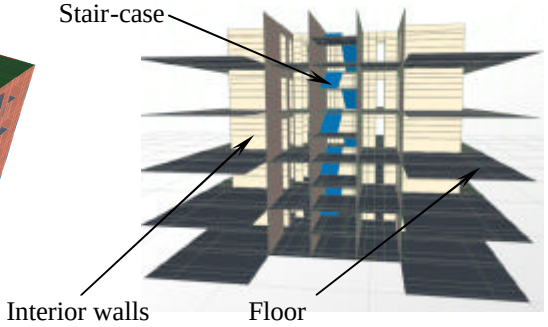

Figure 4. Details of the numerical model

Since floors are generally considered to have an infinite rigidity, only translational degrees of freedom were allowed in the numerical model. All other rotational degrees of freedom were restrained. Additionally, the floors were assumed to behave elastically and were, therefore, modeled using *Thin Shell* elements.

The loggias, floors, stairs and the terrace were made of reinforced concrete class C8/10. The interior and exterior walls were made of masonry. The masonry was modeled as an equivalent concrete material with a mass per unit volume of 1845 kg/m^3 and a design compressive strength of 6.1 MPa [26].

2.2. Loading Scenarios

The static loads, except the self weight which is automatically computed by the program, where defined as *Superdead* loads and their design values were selected in accordance to STAS 10101/1-78 [27]. The effect of the snow was also taken into account according to the code prescriptions [28].

The load combinations were defined following the guidelines from CR0-2005 design code [29] both for the fundamental and the special group of loads. In the case of load combination taking into account the effect of the earthquakes, several earthquake scenarios were considered by means of their accelerograms. The considered earthquakes were Vrancea 1977, 1986, 1990 and 2004. All the recordings of the accelerograms were for the city of Iasi [30] with the sole exception for the 1977 earthquake. In this case, the recording made in Bucharest at the headquarters of the Romanian Institute for Building Research was considered [31].

The identification data for each earthquake is presented in Table 1 whereas Table 2 outlines the characteristics of each recording used in the numerical model.

Figure 5 shows the time-history in terms of ground acceleration for the first earthquake from 1990, depicting both the longitudinal and the transversal components. The recording was done at the IAS2 station, as mentioned in Table 1.

Table 1. Identification data for each earthquake scenario considered

	Location	Depth [km]	Earthquake code	Code of recording station	Date	Magnitude [Mw]	PGA [m/s^2]
1	Vrancea, Romania	109	771	INC1	1977.03.04	7.5	1.95
2		133	861	IAS2	1986.08.30	7.3	1.46
3		91	901	IAS2	1990.05.30	7.0	1.26
4		91	902	IAS2	1990.05.31	6.4	0.46
5		100	041	IAS4	2004.10.27	6.0	0.66

Table 2. Characteristics of the recorded earthquakes

	Earthquake Code	Duration [s]	Peak Ground Acceleration (PGA) values			
			Longitudinal component [m/s^2]	Time stamp [s]	Transversal component [m/s^2]	Time stamp [s]
1	771	40.14	1.62	5.58	1.95	6.12
2	861	21.15	0.641	20.385	1.46	19.93
3	901	31.18	1.262	14.33	1.095	14.61
4	902	26.45	0.389	12.025	0.458	0.52
5	041	73.09	0.582	22.72	0.658	22.81

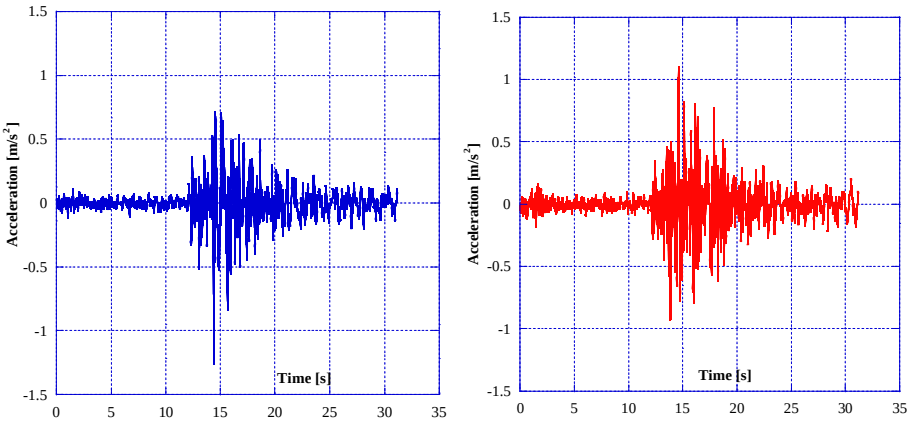

Figure 5. Sample of the first 1990 earthquake recording made at the IAS2 station: longitudinal component (left); transversal component (right)

The non-linear time history analysis was performed by using the Hilber-Hughes-Taylor time integration method [32]. This is an implicit method that allows for energy dissipation and second order accuracy both of which are not possible with the regular Newmark method. As presented in the literature [33], the method preserves the stability and numerical damping properties of the trapezoidal method while achieving a second order accuracy when used in conjunction with the second order differential equations.

3. RESULTS AND DISCUSSIONS

3.1. Degradation Coefficient

The coefficient of degradation, as defined in the scientific literature [21], depends of the natural period of vibration of the structure in its initial state, T_0, and in its degraded state, T_{degr}. The classification of the structures depending on the

coefficient of degradation has been made according to the reference intervals [8, 21].

Figure 6 presents the change in the fundamental period of vibration of the considered structure after being subjected to each earthquake scenario. The cumulative damage of the structure, evaluated by the change in the fundamental period of vibration, is shown to increase with each earthquake scenario that the structure is subjected to. Figure 7 shows the displacement distribution in the X direction corresponding to the fundamental mode of vibration, T_0 = 0.171807 seconds. It can be observed that, although the in-plane shape of the structure is a symmetric one, the first mode of vibration is not a translational one but it exhibits some rotation as well. This is caused by the fact that the stiffness is not symmetrically distributed over the floor surface due to the presence of the stair case. Hence, one half of the building exhibits positive translation, shown in blue with a maximum value of u_x = 0.1877 mm, whereas the other half is characterized by a negative displacement, shown in red with a minimum value of u_x = - 0.2063 mm. However, the difference between the extreme positive and negative values of displacements is so small that the torsional effect induced by the presence of the stair case can be neglected in this case.

Table 3 summarizes the obtained results from the numerical analysis in terms of values for the degradation coefficient. This, in turn, falls within a certain reference interval that indicates the degradation state of the considered structure. Even after all earthquake scenarios, the structure shows only minor degradations. This is very important since the collapse of the structure is prevented. As it is well known, collapse prevention is one of the objectives of a performance-based design [34, 35]. One of its key features is the assurance of an adequate safety margin against collapse under the expected maximum seismic load [36].

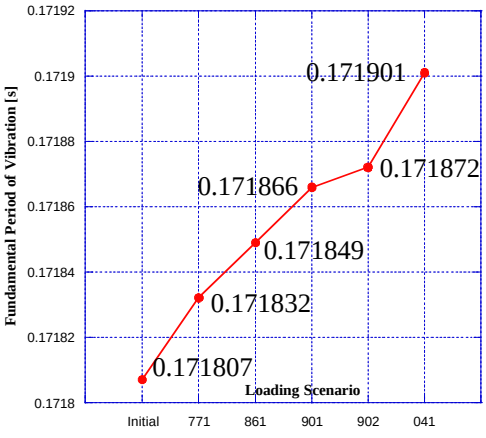

Figure 6. Variation of T for different earthquake scenarios

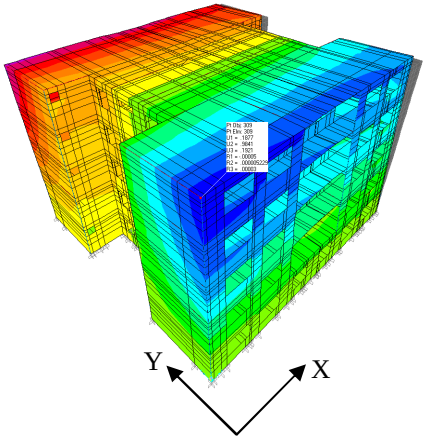

Figure 7. Displacements in x direction for the first mode of vibration

3.2. Extreme Storey Displacements

Figure 8 presents the extreme values of the recorded storey displacements in both X and Y directions. It can be observed that for the first considered earthquake scenario, 771, de extreme values of the displacements in both X and Y directions are the same. However, following the next scenario, the displacements in Y direction become slightly larger, by as much as 12%.

The general observation is that the values of displacements in Y direction are on average 19% larger compared to those in X direction. The percentage is lower for early earthquake scenarios and increase with the number of earthquakes the structure is subjected to. It should be pointed out that the maximum measured value of the displacement at the top of the structure was 3.24 mm. Such a small value of the peak displacement could be explained by the high stiffness of the structure and by the fact that only minor degradations occurred in the model after being subjected to all scenarios, Table 3.

Table 3. Degradation coefficient and degradation state

Earthquake Scenario	Fundamental Period of Vibration [sec]	Degradation Coefficient [21]	Degradation State [8]
771	0.171832	1.455×10^{-4}	Minor Degradations
861	0.171849	2.444×10^{-4}	
901	0.171866	3.433×10^{-4}	
902	0.171872	3.782×10^{-4}	
041	0.171901	5.468×10^{-4}	

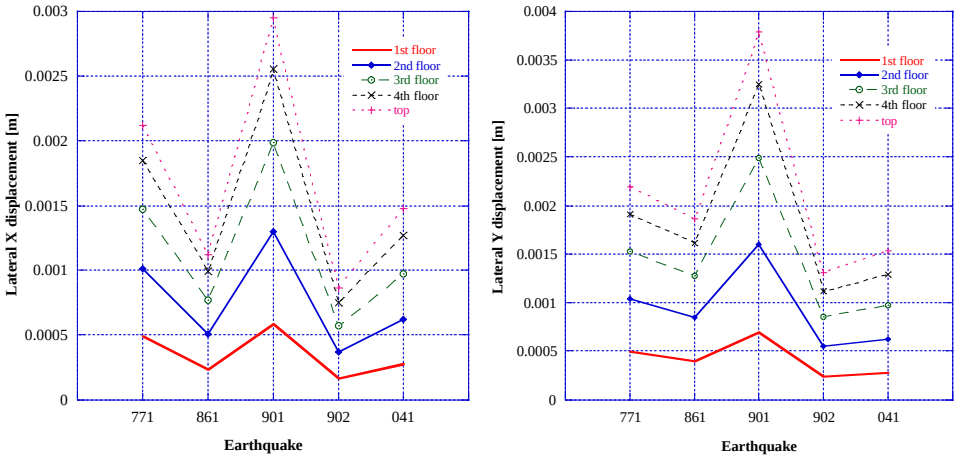

Figure 8. Extreme storey displacements in X and Y directions

3. CONCLUSIONS

The paper presents a numerical assessment method of the seismic behavior of a load bearing structure that is widely met in the Romanian urban areas. The method is based on the non-linear time history analysis of the considered model. The considered earthquake scenarios are based on the seismic actions recorded during the life time of the real structure. The seismic behavior is analyzed from the point of view of the degradation coefficient and the extreme values of the lateral displacements corresponding to each storey.

Based on the obtained results for the degradation coefficient is can be concluded that even though the structure suffered minor degradations produced by the earthquakes during its life time, those degradations do not endanger the life of inhabitants.

The analysis of the maximum storey displacements in both in-plane directions confirm that the structure did not exhibit large lateral displacements and, as a result of that, the degradations should not be important. The maximum recorded value at the top of the structure is 3.24 mm, being lower that the limit value prescribed by the design codes [37].

References

1. Geis, D.E., By Design: The Disaster Resistant and Quality-of-Life Community, *ASCE Natural Hazard Review*, vol. 1(3), pp. 151-160, 2000.
2. Maksud Kamal, A.S.M., Earthquake Risk Assessment and Corresponding Contingency Plans of the Major Cities of Bangladesh, *Proceedings of the 8th International Conference on Urban Earthquake Engineering (8CUEE)*, Tokyo, Japan, paper ID: 12-291, 2011.
3. Luna, R., Hoffman, D., Lawrence, W.T., Estimation of Earthquake Loss due to Bridge Damage in the St. Louis Metropolitan Area. I: Direct Losses, *ASCE Natural Hazard Review*, vol. 9(1), pp. 1-11, 2008.
4. Faccioli, E., Seismic Hazard Assessment for Derivation of Earthquake Scenarios in Risk-UE, *Bulletin of Earthquake Engineering*, vol. 4, pp. 341-364, 2006.
5. Lindell, M.K., Prater, C.S., Assessing Community Impacts of Natural Disasters, *ASCE Natural Hazard Review*, vol. 4(4), pp. 176-185, 2003.
6. Odeh, D.J., Natural Hazards Vulnerability Assessment for Statewide Mitigation Planning in Rhode Island, *ASCE Natural Hazard Review*, vol. 3(4), pp. 177-187, 2002.
7. Atanasiu, G.M., Toma, A.M., Managing the Seismic Risk of Some Residential Buildings of Romanian Urban Infrastructure, *Proceedings of the 14th European Conference on Earthquake Engineering (14ECEE)*, Ohrid, Republic of Macedonia, paper ID: 439, 2010.
8. Toma, A.M., Atanasiu, G.M., Seismic Risk Evaluation Based on Digital Mapping of a Romanian Urban Area, *Proceedings of the 8th International Conference on Urban Earthquake Engineering (8CUEE)*, Tokyo, Japan, paper ID: 12-124, 2011.
9. Toma, A.M., Atanasiu, G.M., Toma, I.O., GIS-Based Seismic Risk Evaluation of Tall Residential Buildings of Romanian Urban Areas – Case Study for the City of Iasi, *Proceedings of the International Conference on Engineering UBI2011 – Innovation and Development*, Covilha, Portugal, 2011.

10. Meli, R., Alcocer, S.M., Implementation of Structural Earthquake-Disaster Mitigation Programs in Developing Countries, *ASCE Natural Hazard Review*, vol. 5(1), pp. 29-39, 2004.
11. Panakkat, A., Adeli, H., Recent Efforts in Earthquake Prediction (1990-2007), *ASCE Natural Hazard Review*, vol. 9(2), pp. 70-80, 2008.
12. Villaverde, R., Methods to Assess the Seismic Collapse Capacity of Building Structures: State of the Art, *ASCE Journal of Structural Engineering*, vol. 133(1), pp. 57-66, 2007.
13. Toma, I.O., Budescu, M., Albu, G., Seismic Behavior of an Experimental Model Made of Thin-Walled Cold Formed Steel Profiles – Hardell Structures, Bulletin of the Polytechnic Institute of Iasi, Construction. Architecture Section, Tome LV(LIX), pp. 67-78, 2009.
14. Moon, F.L., Yi, T., Leon, R.T., Kahn, L.F., Testing of a Full-Scale Unreinforced Masonry Building Following Seismic Strengthening, *ASCE Journal of Structural Engineering*, vol. 133(9), pp. 1215-1226, 2007.
15. Di Ludovico, M., Manfredi, G., Mola, E., Negro, P., Prota, A., Seismic Behavior of a Full-Scale RC Structure Retrofitted Using GFRP Laminates, *ASCE Journal of Structural Engineering*, vol. 134(5), pp. 810-821, 2008.
16. Konstantinidis, K., Kappos, A.J., Izzuddin, B.A., Analytical Stress-Strain Model for High-Strength Concrete Members under Cyclic Loading, *ASCE Journal of Structural Engineering*, vol. 133(4), pp. 484-494, 2007.
17. Palermo, D., Vecchio, F.J., Simulation of Cyclically Loaded Concrete Structures Based on the Finite Element Method, *ASCE Journal of Structural Engineering*, vol. 133(5), pp. 728-738, 2007.
18. Kim, U., Leon, R.T., Galambos, T.V., 3-D Nonlinear Dynamic Behavior of Steel Joist Girder Structures, *Engineering Structures*, vol. 31, pp. 268-274, 2009.
19. Ivorra S., Pallares, F.J., Adam, J.M., Dynamic Behavior of a Modern Bell Tower – A Case Study, *Engineering Structures*, vol. 31, pp. 1085-1092, 2009.
20. Grange, S., Kotronis, P., Mazars, J., Numerical Modelling of the Seismic Behavior of a 7-Story Building: NEES Benchmark, *Materials and Structures*, vol. 42(10), pp. 1433-1441, 2009.
21. DiPasquale, E., Cakmak, A.S., Seismic Damage Assessment Using Linear Models, *Soil Dynamics and Earthquake Engineering*, vol. 9(4), pp. 194-215, 1990.
22. Talaslidis, D.G., Manolis, G.D., Paraskevopoulos, E., Panagiotopoulos, C., Pelekasis, N., Tsamopoulos, J.A., Risk Analysis on Industrial Structures under Extreme Transient Loads, *Soil Dynamics and Earthquake Engineering*, vol. 24(6), pp. 435-448, 2004.
23. Romeo, R.W., Bisiccia, C., Risk-Oriented Microzoning Study of an Urban Settlement, *Soil Dynamics and Earthquake Engineering*, vol. 26(10), pp. 899-908, 2006.
24. Computers and Structure Inc., SAP2000 Integrated Software for Structural Analysis & Design, Berkeley, California, USA (2005), available at: http://www.csiberkeley.com/products_SAP.html
25. Project no. 1497/1966 – Blocuri de locuinte P+4 cu pereti structurali din zidarie de caramida, *ICPROM Iasi archives*. (in Romanian).
26. CR6-2006, Cod de proiectare pentru structuri din zidarie, *National Institute for Research and Development in Construction – INCERC*, 2006 (in Romanian)
27. STAS 10101/1-78, Actions upon structures. Technical Weights and Dead-Loads, *Romanian Association for Standardization (ASRO)*, 2010. (in Romanian)
28. CR1-1-3-2005, Cod de proiectare: Evaluarea actiunii zapezii asupra constructiilor, *Universitatea Tehnica de Constructii Bucuresti*, 2005. (in Romanian)
29. CR0-2005, Cod de proiectare: Bazele proiectarii structurilor în constructii, *Universitatea Tehnica de Constructii Bucuresti*, 2005. (in Romanian)
30. Borcia, I. S., Procesarea înregistrarilor miscarilor seismice puternice specifice teritoriului României, *Ph.D. Thesys*, *Universitatea Tehnica de Constructii Bucuresti*, 2006. (in Romanian).
31. National Institute for Research and Development in Construction, Urban Planning and Sustainable Spatial Development, URBAN-INCERC, http://www.incerc2004.ro/accelerograme.htm (last accessed, March 2012).
32. Hilber, H.M, Hughes, T.J.R, Taylor, R.L., Improved Numerical Dissipation for Time Integration Algorithms in Structural Dynamics, *Earthquake Engineering and Structural Dynamics*, vol. 5, pp. 282-292, 1977.

33. Negrut, D., Rampalli, R., Ottarsson, G., Sajdak, A., On the Use of HHT Method in the Context of Index 3 Differential Algebraic Equations of Multibody Dynamics, *Journal of Computational and Nonlinear Dynamics*, vol. 2(1), pp. 73-86, 2007.
34. Fajfar, P., A Nonlinear Analysis Method for Performance Based Seismic Design, *Earthquake Spectra*, vol .16(3), pp. 573-592, 2000.
35. Moehle, J.P., Nonlinear Analysis for Performance Based Earthquake Engineering, *The Structural Design of Tall and Special Buildings*, vol. 14(5), pp. 385-400, 2006.
36. Ghobarah, A., Performance-Based Design in Earthquake Engineering: State of Development, *Engineering Structures*, vol. 23(8), pp. 878-884, 2001.
37. P100-1-2011, Seismic Design Code P100 – Part I – Design Specifications for Buildings, *Universitatea Tehnica de Constructii Bucuresti*, 2011. (in Romanian)

Numerical simulation of wind action on solar panels inclined with 30º and different wind directions

Georgeta Vasies, Elena Axinte, Claudiu Romila, and Adrian Radu
Technical University Gh. Asachi" Iasi, Faculty of Construction & Building Services. 43 Dimitrie Mangeron Str., 700050, Iasi, Romania

Summary

Solar panels are increasingly being used to convert solar energy into thermal energy (solar collectors) and electricity (photovoltaic panels). In the last decade, their number has increased considerably. Therefore, more research on these systems is needed, especially in the aerodynamic domain. The wind represents the main action that determines the design of support systems for solar panels, wherever they are located, on flat roofs, pitched roofs or at ground level. Computational Fluid Dynamics (CFD) simulations can be performed in order to estimate the wind pressure on solar panels. In this study, the wind pressure on 12 solar panels in an arrayed configuration, mounted on ground level, with an angle of 30º and seven wind directions (0º, 30º, 45º, 60º, 90º, 135º, 180º) have been analyzed with the computer code ANSYS 12 CFX.

KEYWORDS: wind action, solar panels, wind degree, numerical simulations and pressure distribution.

1. INTRODUCTION

The techniques for capture and conversion of solar energy are in continuous development. Installation of solar plant involves important financial resources and the economic criteria that have an important role in design of supporting systems [1]. The determination of wind forces on the support systems of solar panels is the subject of many research studies. The behavior of solar arrays immersed in an aerodynamic field has made the subject of several studies in the wind tunnel with atmospheric boundary layer and numerical simulations using specialized software of fluid flow. In the last decade numerous studies were performed in order to determine pressure distributions and wind forces of size on solar panels located on flat and pitched roofs, building envelope or at ground level. Design of the anchoring systems must be done so that the extreme values of wind will not affect

ISSN 2285-2735, Pages 378 - 392

the integrity of the solar panels. The main problem in designing of the anchoring systems is to determine the correct uplift forces and pressure field, and the solutions to reduce them.

In case of solar panels located at ground level, the assessment of the wind loads proves to be an easer task than for panels installed on the roof top.

a. b.

Figure1. Solar panels installed at ground level: a. in a solar array configuration; b. in consecutive rows

In this study, wind action on twelve solar panels arranged in a 4x3 array, placed at ground level was analyzed. In the Romanian standard SR EN 1991-1-4:2006 the procedure for evaluating the wind loads on publicity boards is presented, but it cannot be extended to solar panels installed on ground level because publicity boards have a vertical position and wind acts perpendicular on their surface while solar panels are tilted under a particular angle. In Romania, due to the sunlight conditions, it is recommended that the solar panels should be disposed at an angle tilted between 30º and 40º to the plane of the ground. Also, in the scientific literature, is recommended that solar panels should be facing south direction with small deviations to southeast and southwest. This study aims to determine the loads produced by wind action on a solar panels array under different angles of attack.

2. SOLAR PANELS DISPOUSED AT GROUND LAVEL

At ground level, the air flow disturbance is not only a consequence of solar panels presence, but it is also influenced by location (open field, bordering area and neighborhood buildings) and terrain topography [2]. Intensity of wind loads depends of the arrangement of solar panels (in consecutive rows or isolated solar arrays), the incidence of wind and the distance between panels rows/arrays. Wind speed decreases at the lower part of the atmospheric boundary layer (figure 2), but

when turbulence intensity is large enough and when wind speeds high, damages can occur on anchoring systems of solar panels.

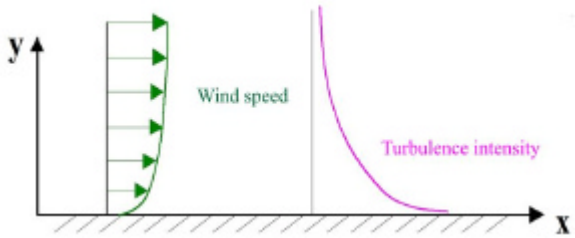

Figure 2. Profile of wind velocity and turbulence in atmospheric boundary layer

In order to determine the average wind speed and the velocity profile, the influence of orography and roughness factors (specific for each terrain type), is fundamental. In urban and suburban areas, it is interesting to see how roughness characteristics change the air flow conditions. According to roughness conditions (different types of vegetation and constructed areas) Roumanian standard SR EN 1991-1-4:2006 divides ground surface in five categories of exposure [5]:

Table 1. Terrain categories and terrain parameters (SR EN 1991-1-4:2006)

Terrain category		z_0 (m)	z_{min} (m)
0	Sea or coastal area exposed to the open sea	0.003	1
I	Lakes or flat and horizontal area with negligible vegetation and without obstacles	0.01	1
II	Area with low vegetation such as grass and isolated obstacles (trees, buildings) with separations of at least 20 obstacle heights	0.05	2
III	Area with regular cover of vegetation or buildings or with isolated obstacles with separations of maximum 20 obstacle heights (such as villages, suburban terrain, permanent forest)	0.3	5
IV	Area in which at least 15 % of the surface is covered with buildings and their average height exceeds 15 m	1.0	10

Velocity variation with height can be better observed from the velocity profiles proposed by Davenport [3] for three different types of terrain roughness (figure 3).

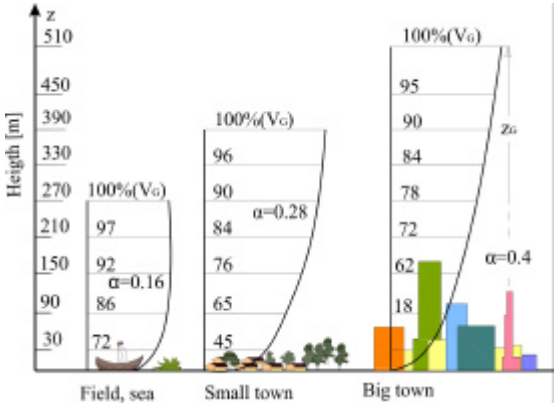

Figure 3. Ideal velocity profile established by Davenport for characterizing the boundary layer of Earth’s atmosphere

3. CFD SIMULATION CASES

In the present study, CFD techniques have been used to investigate the aerodynamic features of a stand-alone ground mounted solar panels modules, arranged in a 4x3 array. The pressure distribution was evaluated for the entire array and also for every individual solar panel. Seven different incidence angles of attack were considered, listed in Table 2. The solar array has 17.641 sqm and it is compose by twelve solar panels (figure 5a) with: 1.482 m length, 0.992 m width and 0.045 m thickhness.

Table 2. CFD simulation cases

Cases	Panel type	Panel inclination	Angle of attack
Case 1	Arrayed	30º	0º
Case 2	Arrayed	30º	30º
Case 3	Arrayed	30º	45º
Case 4	Arrayed	30º	60º
Case 5	Arrayed	30º	90º
Case 6	Arrayed	30º	135º
Case 7	Arrayed	30º	180º

The numerical simulation was developed using ANSYS 12 CFX code. The solar array is immersed in the computational domain (figure 4), whose minimum

dimensions respect the specifications from the scientific literature [4]. The solar array is lifted at 0.6m height above the ground level. On the surface of the array, the pressure is measured in 144 points for each face, arranged in 9 lines (figure 5 b). Overall resultant pressure has also been calculated.

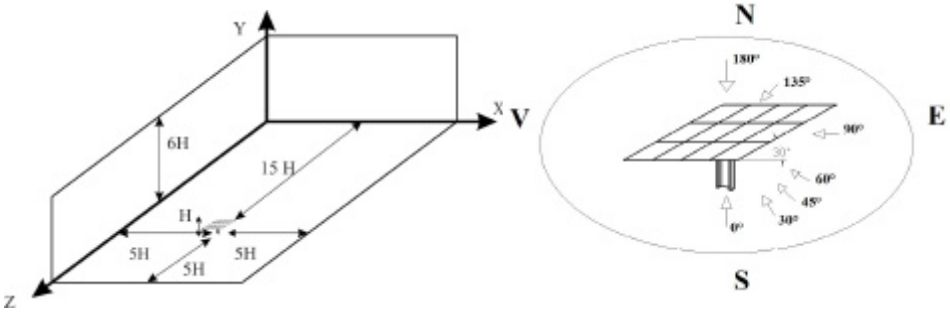

Figure 4. Computational domain and angles of attack

During the numerical simulation season, the considered wind speed was of 18 m/s and the turbulence intensity 10 % for all the seven analyzed cases. The pressures values on both faces of the exposed solar panels array were registered.

4. RESULTS AND DISCUSSIONS

In the analyzed cases a global analysis for determining the average pressure on solar array, and a local analysis for determining the critical panels of solar array have been made. Angle of attack which produces the largest wind loads has been determined by comparing the results.

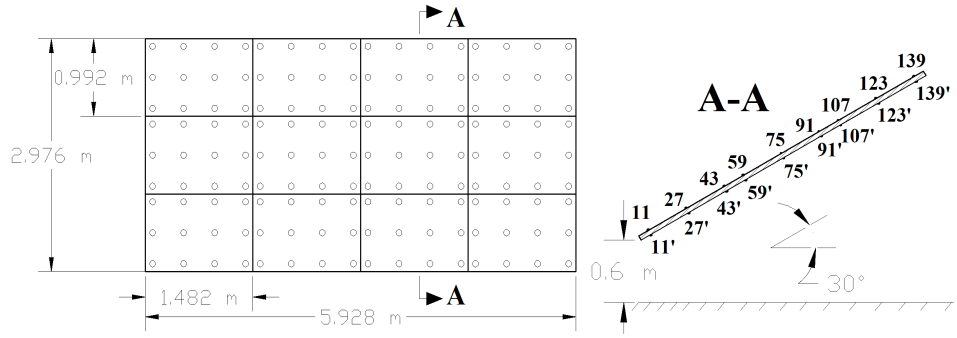

a. b.

Figure 5. Pressure points distribution on the surface of the solar array

4.1 Case 1: Wind angle of attack at 0º

The highest pressures occur on surfaces of panels 9, 10, 11 and 12, that are positioned on the top of the solar array (figure 6 and 8). Panel number 2 is the least loaded, with a mean pressure oh -23.7 Pa and the most loaded is panel number 12 with a mean pressure of -177.85 Pa (figure 7). The mean pressure on surface of solar array is -103.25 Pa.

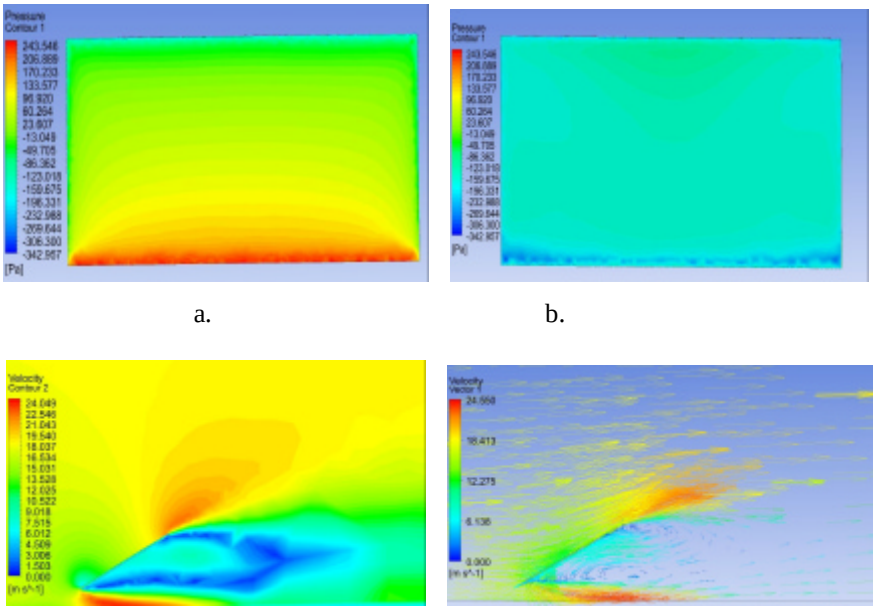

a. b.

c. d.

Figure 6. Pressure distribution on upper face (a.) and underside face (b.) of solar array, velocity contour (c.) and velocity vectors (d.) for an angle of attack of 0°

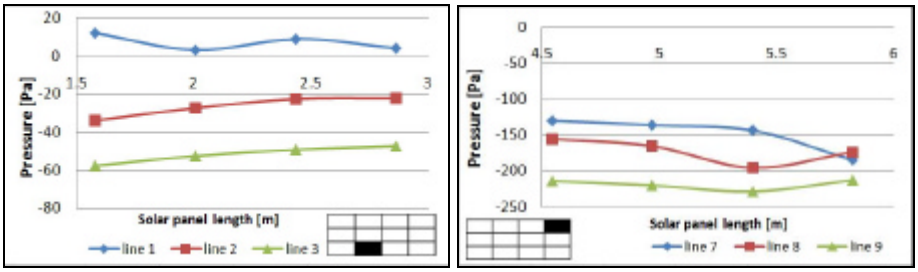

a. b.

Figure 7. Pressure variation on panels 2 and 12

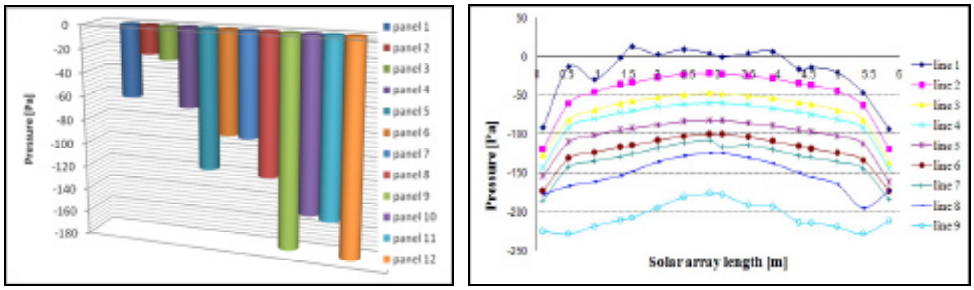

a. b.

Figure 8. Mean pressure on: a. panels of solar array; b. solar array surface

4. 2 Case 2: Wind angle of attack at 30 º

When the wind angle is at 30º, the left part of the solar array is more loaded than right one (figure 9). Like in the previous case, pressure values are negative on entire solar array with a mean value of -112.33 Pa (figure 11).

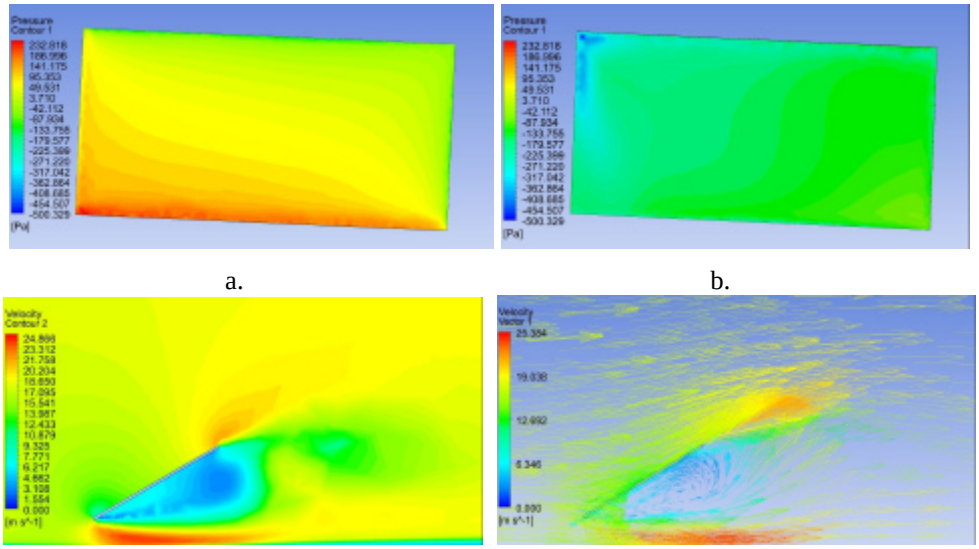

a. b.

c. d.

Figure 9. Pressure distribution on the upper face (a.) and the underside face (b.) of solar array, velocity contour (c.) and velocity vectors (d.) for an angle of attack of 30°

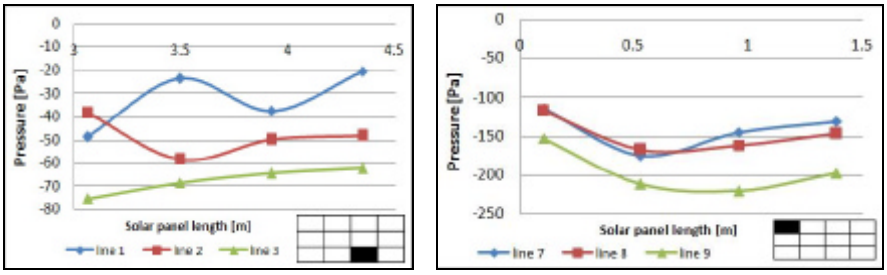

a. b.

Figure 10. Pressure variation on panels 3 and 9

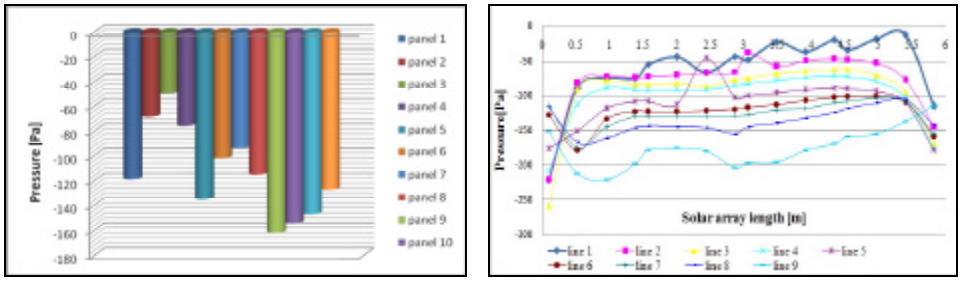

a. b.

Figure 11. Mean pressure on: a. panels of solar array; b. solar array surface

Panel number 9 is the most loaded, with a mean pressure of -161.99 Pa, followed by panel 10 with a mean pressure of -154.15 Pa. Panel number 3 is the least loaded, with a mean pressure of -49.68 Pa (figure 10).

4.3 Case 3: Wind angle of attack at 45º

Like in the previously analyzed cases, over the entire surface of the solar array negative pressure have been found (figure 12 and 14 b). The mean pressure obtained for the solar array is -118.88 Pa. The suctions developed on the left side are up to 45% higher that the values of the right one. Panel number 1 is the most loaded, with a mean negative pressure of -291.35 Pa. The least loaded is panel number 4, with a mean pressure of -69.1 Pa (figure 13).

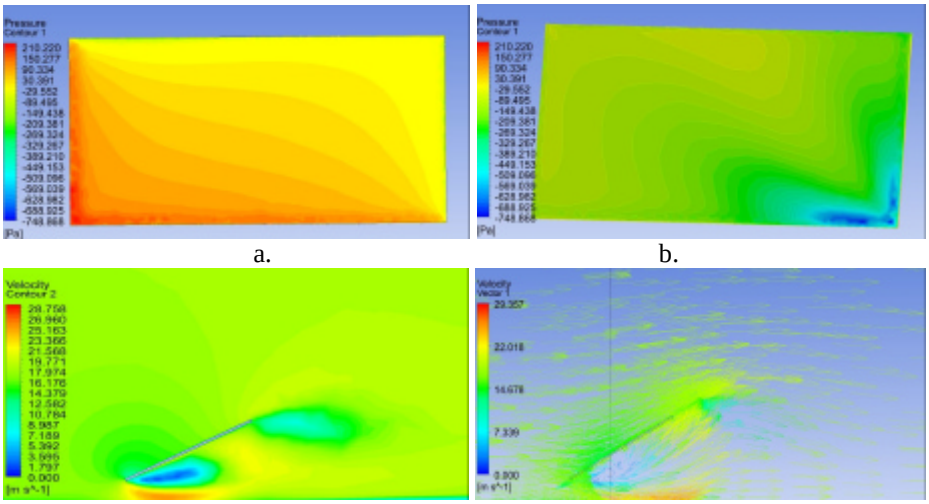

a. b.

c. d.

Figure 12. Pressure distribution on the upper face (a.) and the underside face (b.) of solar array, velocity contour (c.) and velocity vectors (d.) for an angle of attack of 45°

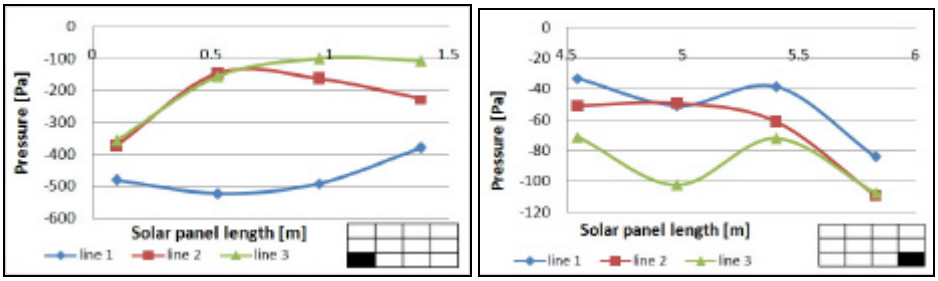

a. b.

Figure 13. Pressure variation on panels 1 and 4

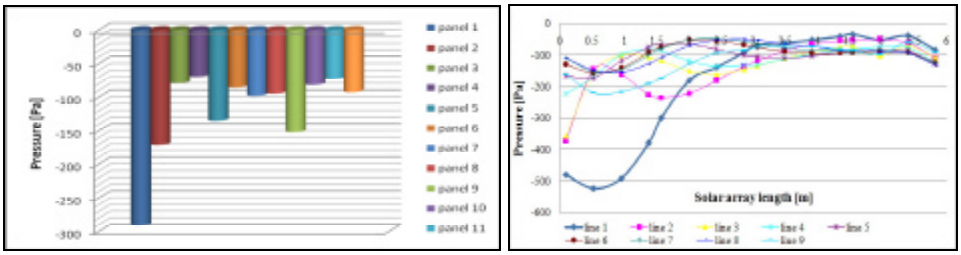

a. b.

Figure 14. Mean pressure on: a. panels of solar array; b. solar array surface

4.4 Case 4: Wind angle of attack at 60°

The pressures obtained in all analyzed points are negative, the measured mean pressure on solar array being -96.13 Pa (figure 17). The left one is again more loaded than the right one (figure 15). The least loaded are panels number 11 respectively 12 and the most loaded is panel one (figure 16).

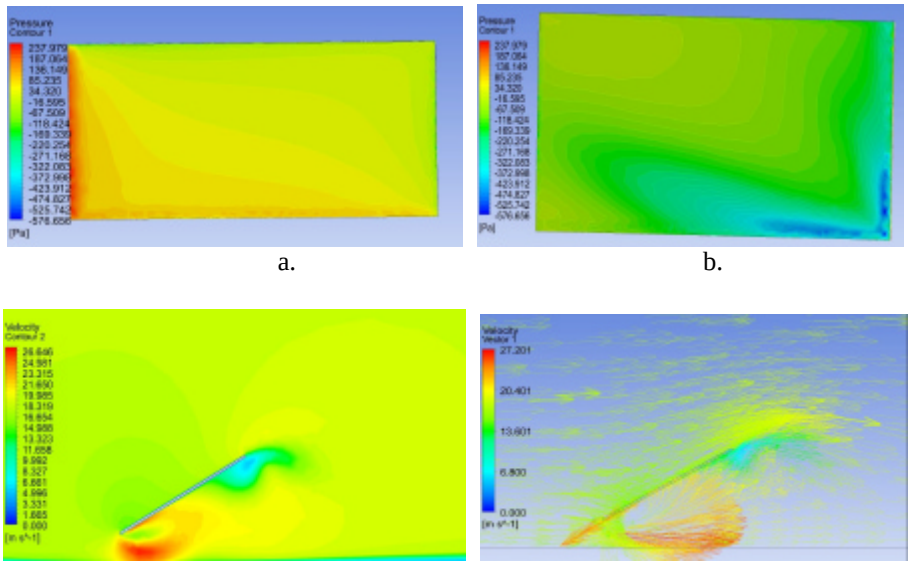

a. b.

c. d.

Figure 15. Pressure distribution on the upper face (a.) and the underside face (b.) of solar array, velocity contour (c.) and velocity vectors (d.) for an angle of attack of 60°

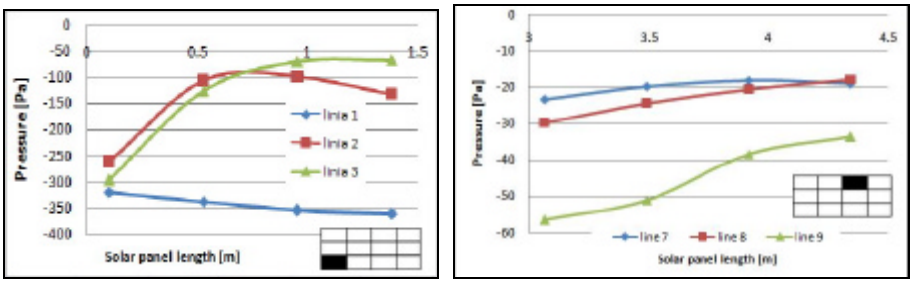

a. b.

Figure 16. Pressure variation on panels 1 and 11

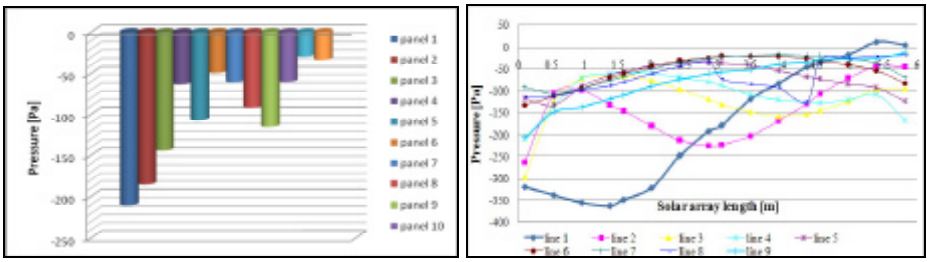

a. b.

Figure 17. Mean pressure on: a. panels of solar array; b. solar array surface

4.5 Case 5: Wind attack angle at 90°

The solar array has the smallest loads when the attack angle is at 90º (figure 18). The resultant pressures are both positive and negative, according to the position on solar panels in the array (fig. 20). The pressures developed on the left side (panels 1, 5, and 9) and on the right side of solar array (panels 4, 8, 12) are entirely negative, while the pressures developed on central panels have positive values. Though, the mean pressure on solar array has a negative value of -2.26 Pa. The biggest negative pressure (-18.74 Pa) was found on panel number 5, and the lowest negative pressure (-4.64 Pa) on panel number 10 (figure 19).

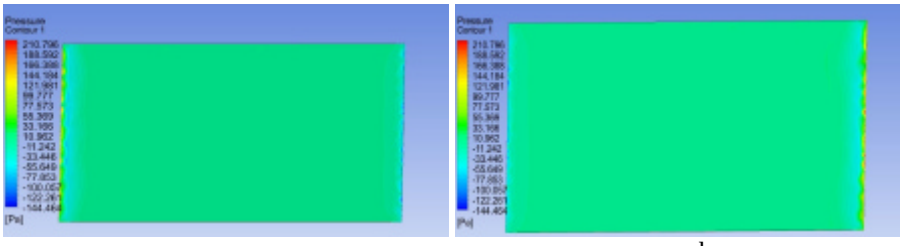

a. b.

Figure 18. Pressure distribution on the upper face (a.) and the underside face (b.) of solar array, velocity contour (c.) and velocity vectors (d.) for an angle of attack of 90°

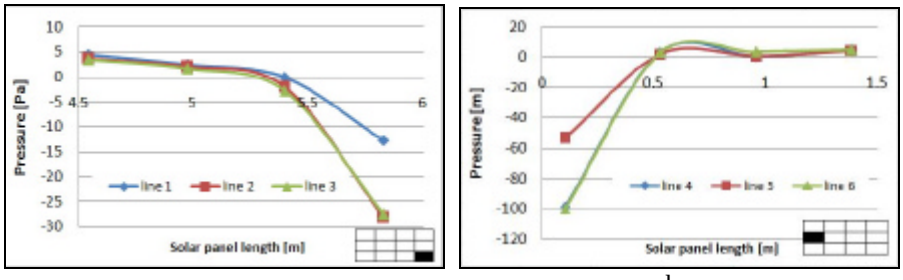

a. b.

Figure 19. Pressure variation on panels 4 and 5

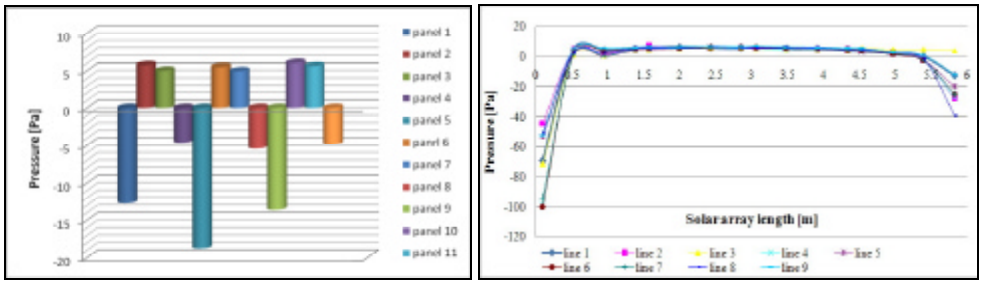

a. b.

Figure 20. Mean pressure on: a. panels of solar array; b. solar array surface

4.6 Case 6: Wind angle of attack at 135º

For an attack angle of 135º, the mean pressure on solar panels has both positive and negative values. Negative pressures appear on panels positioned on the extremities, while the pressures on central panels are positive (figure 21 and 23). The mean pressure on solar array surface is -62.8 Pa. Panel number 12 (figure 22) has the highest mean negative pressure (-257.89), and panel number 7 has the lowest positive pressure (16.25Pa).

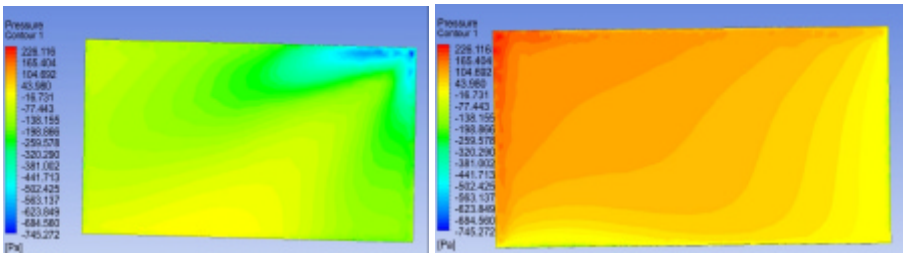

a. b.

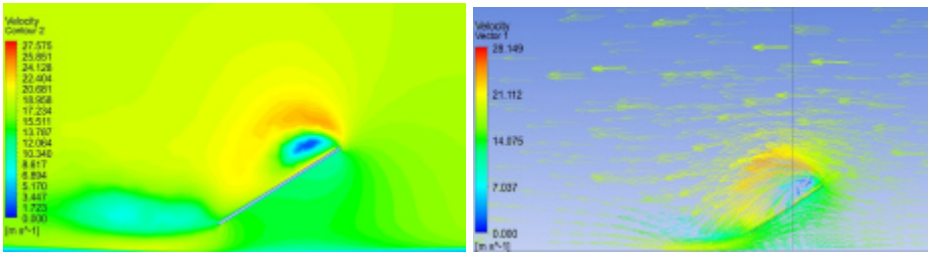

c. d.

Figure 21. Pressure distribution on the upper face (a.) and the underside face (b.) of solar array, velocity contour (c.) and velocity vectors (d.) for an angle of attack of 135°

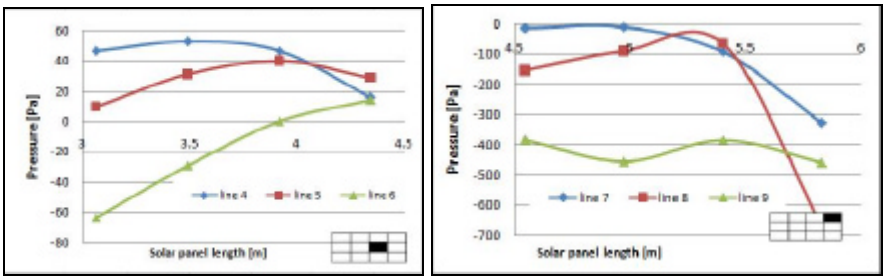

a. b.

Figure 22. Pressure variation on surface of panels 7 and 12

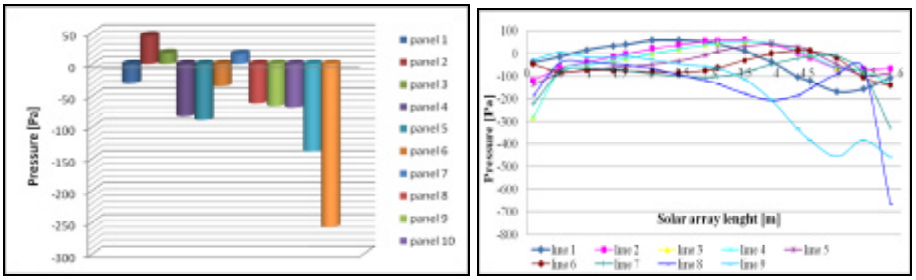

a. b.

Figure 23. Average pressure on: a. panels of solar array; b. solar array surface

4.7 Case 7: Wind angle of attack at 180º

The mean pressure measured on the solar array surface has a negative value (-39.7 Pa). The most loaded panel is panel number 1, with a value of mean negative pressure of -140.95 Pa (figure 22a). The least loaded panel is number 6, with a mean pressure of 1.77 Pa (figure 22b). The resultant pressures at the lowest and lateral sides of solar array are negative, while in the central zone, positive pressures are obtained.

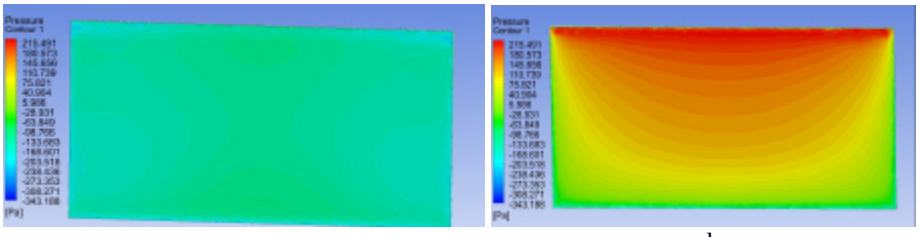

a. b.

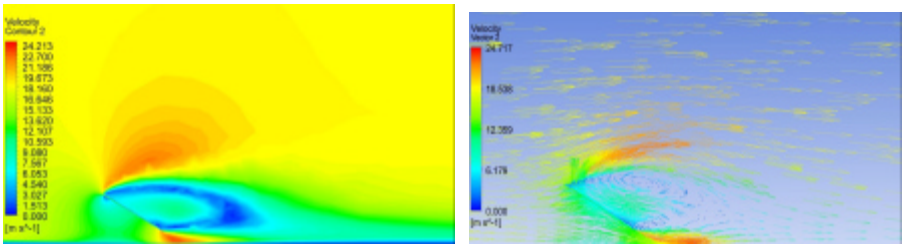

c. d.

Figure 24. Pressure distribution on the upper face (a.) and the underside face (b.) of solar array, velocity contour (c.) and velocity vectors (d.) for an angle of attack of 180°

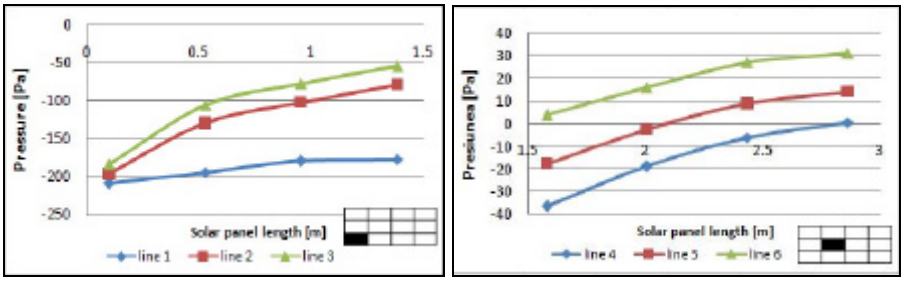

a. b.

Figure 22. Pressure variation on panels 1 and 6

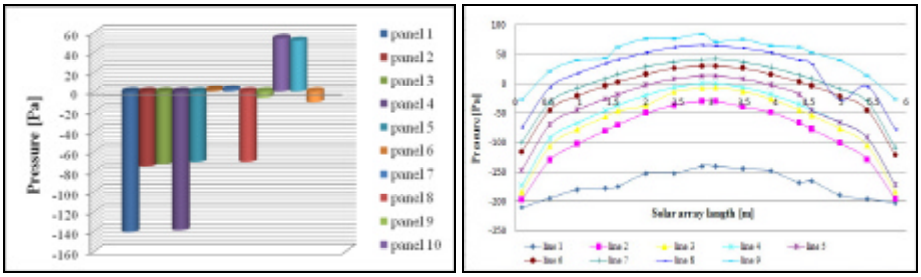

a. b.

Figure 23. Mean pressure on: a. panels of solar array; b. solar array surface

5. CONCLUSIONS

Wind direction has a major influence on the pressure distribution on solar arrays. Suctions have higher values for wind directions of 30º, 45º, 60º and 135º, when the incidence angles create conical vortices on surface of solar array. These vortices

appear in pairs, one on each edge of solar array. The center of each vortex is at the area where high suctions occur. The obtained results for each analyzed case where used to make a comparison between mean pressures developed on each panel of the solar array. A global analysis was performed; the mean pressure was compared for each considered attack angle. The biggest suctions appear for an attack angle of 45º respectively 30º.

References

1. Vasies, G., Axinte, E., Teleman, E.C., *Numerical simulation of wind action on solar panel placed on flat roofs with and without parapet*, Buletinul Institutului Politehnic din Iasi, Sectia Constructii. Arhitectura, Tomul LVIII (LXII), Fasc. 1, Editura Politehnium, ISSN 1224-3884 (p), ISSN 2068-4762 (e), p 139-155, Iasi, 2012.
2. Bitsuamlak, G.T., Dagnew A.K., Erwin J., *Evaluation of wind loads on solar panel modules using CFD*, The Fifth international Symposium on Computational Wind Engineering (CWE2010), Chapel Hill, North California, USA, May 23-27, 2010.
3. Radu, A., Radu, V., *Aerodinamica constructiilor. Îndrumator pentru lucrari de laborator la Constructii civile si industriale*, Ed. Institutului Politehnic, Iasi, 1981.
4. Franke J. et al., *Recommendations of the Use CFD in Wind Engineering*. Proc. of the International Conference on Urban Wind Engineering and Buildings Aerodynamics, Belgium, 2004.
5. ***SR EN 1991-1-4:2006, Eurocod 1: Actiuni asupra structurilor. Partea 1-4: Actiuni generale-Actiuni ale vântului.

Wind action on solar panels placed on flat roofs with parapets

Georgeta Vasies, Elena Axinte, and Elena Carmen Teleman
Technical University Gh. Asachi" Iasi, Faculty of Construction & Building Services. 43 Dimitrie Mangeron Str., 700050, Iasi, Romania

Summary

Wherever they are located, on flat roofs, pitched roofs or at ground level, the wind represents the main action that determining the design of support systems for solar panels. Increasing the number of solar panels used in the world, determine behavior research on these systems in the aerodynamic field. In the specialty literature is recommended orientation of solar panels to south, south-east, respectively south-west, for benefit of a better sunlight. In Romania the dominant wind direction is from north, north-east or north-west, in which case the wind blows behind the field of panels. It is aimed the highlight of shielding effect produced by the building, respectively by building and parapet on the pressure distribution on the solar panels surface. Numerical simulations are performed in ANSYS 12 CFX, for an incidence wind angle of 135 º.

KEYWORDS: wind direction, solar panels, CFD simulation, flat roof, shielding effects

1. INTRODUCTION

The techniques for capture and conversion of solar energy are in continuous development. Determination of wind forces on the support systems of solar panels is the subject of many research studies. The behavior of solar arrays immersed in aerodynamic field, makes the subject of several studies in wind tunnel with atmospheric boundary layer and numerical simulations using specialized software in fluid flow. In the last decade numerous studies was performed for determinate the pressure distributions and the size of wind forces on solar panels located on flat roofs, pitched roofs, building facades or at ground level.

Wood, Denoom and Kwok [1] investigated the behavior of solar collectors located on the flat roof, parallel with the roof line. In their studies the distance between roof and collectors and the distance between rows of collectors was varied, proving that none of these parameters have a considerable influence on the pressure distribution. The experiments showed that the distance between solar modules and

ISSN 2285-2735, Pages 393 - 401

roof edges, orientation of panels toward the wind direction and the shape and size of the building, can influence or even change the wind loads on solar collectors placed on flat roofs. Blackmore [2] using his studies, has published a design code for solar panels placed on flat roofs, but he did not consider the maximum pressure that occur for different wind angles. In Romania, Radu, Axinte and Theohari [3] have made studies on solar collectors located on flat roofs, using a wind tunnel with open circuit. The collectors were arranged in compact group and two distinct groups and the pressure distribution was analyzed for the main wind directions. The net pressure was determined for each collector and for each row of panels was calculated the average pressure. Also was showed the shelter effect produced by the first row of collectors. Radu and Axinte [4] have investigate the effect of the parapet on collectors modules placed on roof top, showing that it's presence reduces the both pressure and suction in the corner areas of the flat roof. The collectors have been placed on the flat roof of a five story building, reduced to the scale of the model. The height and the permeability of the parapet were varied. The experiments demonstrated that the presence of parapet reduces the pressure up to 45% and the uplift forces up to 25 %, for the first row of collectors. Making comparison between various situations, the authors concluded that the reduction of pressure and wind forces is dependent by the building height; if the height increases, this reduction become insignificant. Solar panels exposed to wind action involves issues such as determining the influence of air flow on energy efficiency and designing the support systems for satisfy the requirements in service with minimal use of materials [5]

Since the wind tunnel experiments and full-scale measurements require time and significant financial resource, in wind engineering has developed the numerical simulation of wind action, based on computational fluid dynamics. Increased processing speed of computers has led the development of specialized computers programs in fluid flow and numerical simulation results are often comparable with data collected in the wind tunnel experiments.

3. NUMERICAL SIMULATION USING ANSYS CFX

The numerical simulation in the study presented here was developed using ANSYS 12 CFX. The building is immersed in the computational domain, its minimal dimensions respecting the specifications from the literature [6]. Solar panels rows are arranged in compact group on the flat roof of a building with parapets (figure 1). The rows have 27.5 m length, 1.58 m height and 0.008 m thick and are titled by 35° to the roof plan. The distance between two rows of panels is 1.0 m and the distance from the roof edge to the first row is 3.0 m. Numerical simulation was done considering the wind angle by 135°. Solar panels are facing to south, while the wind direction is northeast (figure 2).

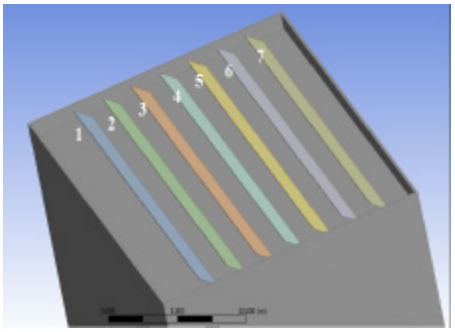

Figure 1. Arrangement of solar panels on flat roof

The building equipped with solar panels on the roof is a regular one, 30 m x 20 m in plane dimensions and 15 m height; an attic of 1.0 m is placed on the roof perimeter. The solar panels are lifted at 0.2m height from the level of the roof and situated in consecutive rows, respecting the recommendations from the scientific literature [7]: the distance between these rows and the edge of the attic is about $e/10$, where:

$$e = \min(b, 2h) \tag{1}$$

The significance of the symbols being:

b - the dimension of the face normal to the wind direction,

h - height of the building.

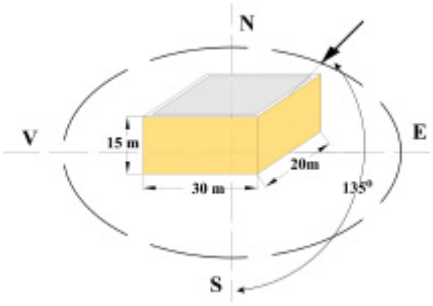

Figure 2. Dimensions of the building and the wind action angles

During the numerical simulation season, the wind speed considered is 14 m/s and the turbulence intensity is 10 %. As a result of the numerical simulation for the two analyzed cases, the pressures coefficients on both faces of the exposed solar panels were registered.

4. DISCUSSIONS AND RESULTS

In the case of the plane solar panels mounted on supports the local pressure coefficients will act on both faces of the panel and the resultant of the normal component will be obtained with the sum[4]:

$$c_{LR} = \pm c_{ns} \pm c_{ni} \tag{3}$$

where c_{ni} is the pressure coefficient on the in wind surface of the panel and c_{ns} is the pressure coefficient from the leeward face (Fig. 3 b).

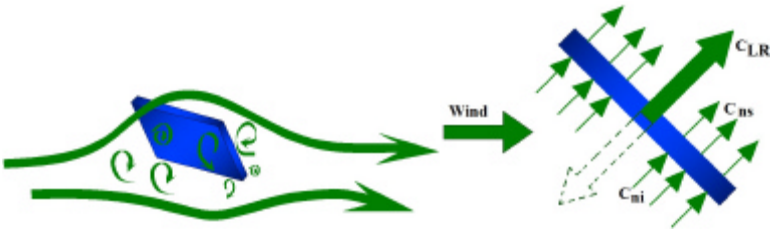

Figure 3. The air flow around the plane surface of the solar panel and the computation of the coefficient c_{LR}

The Romanian wind standard does not give information available for design of solar panels systems.

4.1 Analysis of the results obtained during the numerical simulation

For every row of solar panels, the pressure produced by wind action was measured in 45 points, placed in 5 lines respective 9 columns, according to figure 4.

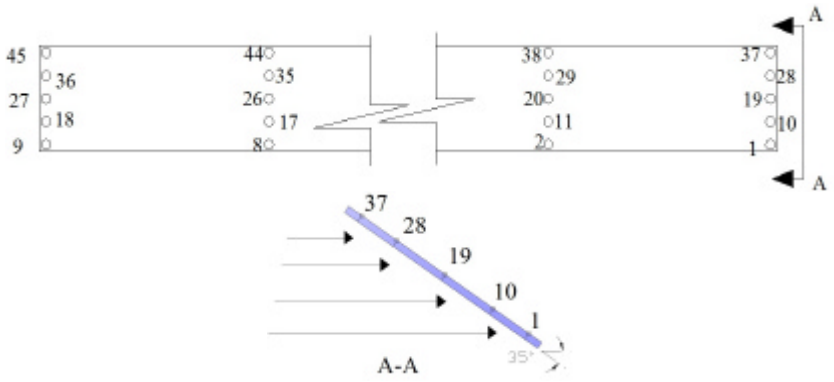

Figure 4. Distribution of the points on the surface of the solar panels where the local wind pressure was measured

For each point was measured the pressure values on both sides of the solar panels and calculated the resulting pressure. With the values obtained in every point, graphics were traced and has been made observations regarding pressure variations on every row of solar panels. The resultant pressures in all points analyzed is negative. The mean pressure values obtained from the 45 points located on each side of panel’s rows are entirely negative. The lower suction appears in the points of first row of solar panels and increasing gradually until the penultimate row.

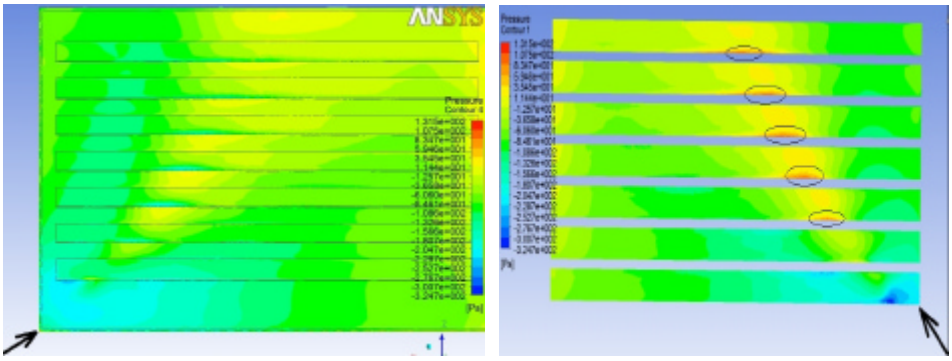

a *b*

Figure 5. Pressure distribution on solar panels face: a - upper (active) face, b - underside (exposed) face

The negative pressures measured in the first column of rows number 1, 2 and 3 (right side) are double compared with negative pressure values measured on the panels located in the left side of this rows (column 9). Starting with row number 4, the pressures measured on left side grow, compared with values measured on right side. The difference gets up to 60 % higher in case of the sixth row and 110 % higher in case of the last row of solar panels.

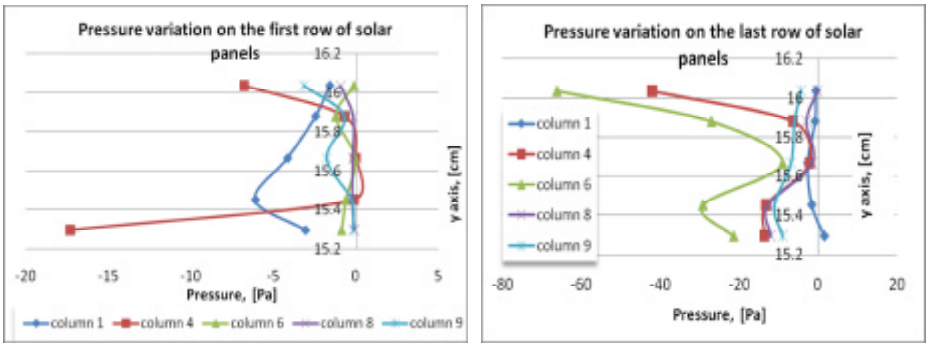

Figure 6. Pressure variation on the first and last rows of solar panels

Positive pressure, lower in value, appear in the central area of the solar panels group. These positive values appear in points 7 and 16 on the third row, in points 6 and 15 on the fourth and fifth row, respectively in points 5 and 14 on the last row of solar panels. The positive values appear only on active face of solar panels, while the resultant pressure is negative.

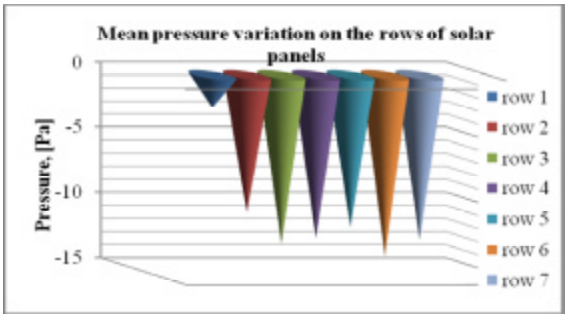

Figure 7. Mean pressures variation on the rows of solar panels

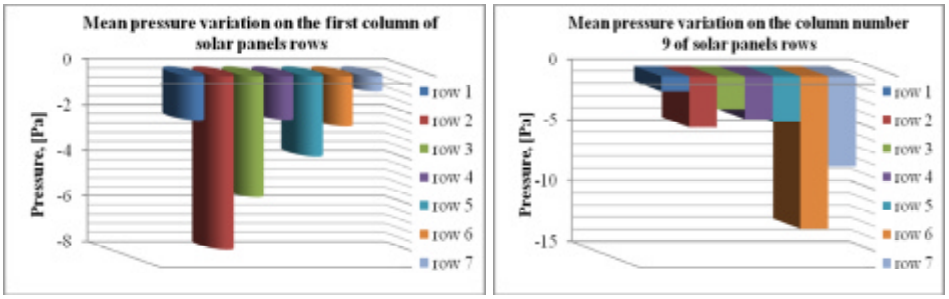

Figure 8. Mean pressure variation on the first and last column of solar panels rows

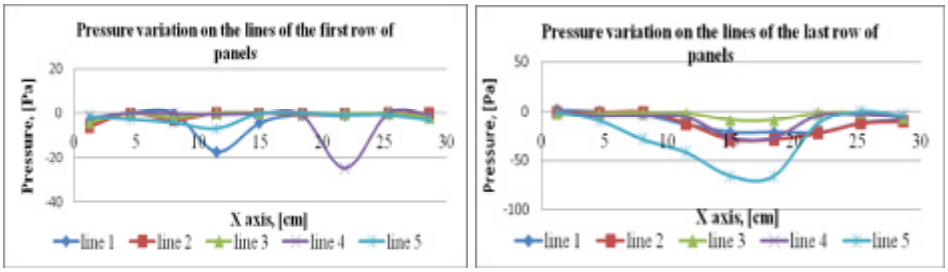

Figure 9. Pressure variation on lines of first and last rows of solar panels

4.2 Discussions

Wind direction has a major influence on the pressure distribution on flat roof surface and also on faces of solar panels arrays. Local suctions are more intense for wind direction of ±45° and that wind acts from N-E direction, behind the solar arrays, leads to negative pressure on both sides of panels. Considering the incidence angle of 135°, would create conical vortices (delta-wing vortex) at the roof level. These vortices are usually in pairs, one on each roof edge, and the center of each vortex is an area where high suctions occurring.

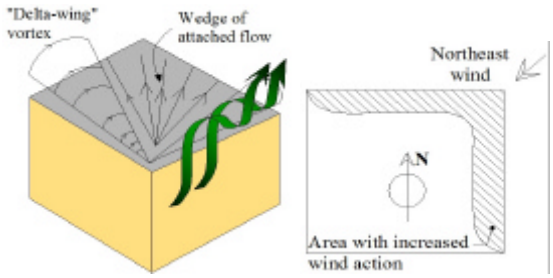

a. b.

Fig. 10 – Development of conical vortexes for angle of incidence wind between 30° and 60° (by Cook, 1985) and their action area

Conical vortexes action leads to development of high uplift forces, which means a biggest load on support systems of solar panels.

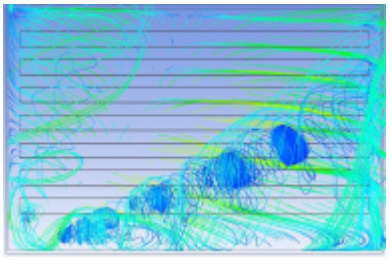

Fig. 11 – Streamline on roof level

The shape and size of the building have a big influence in pressure distribution on solar panels mounted on building roof. Placement of solar panels on the roof top favors the appearance of local turbulence with changes of pressure distribution and reduces uplift force by down force. Though, wind incidence can create wake vortexes and then suction effects are more obvious. By their position, solar panels can shield each other, phenomenon amplified by attic presence.

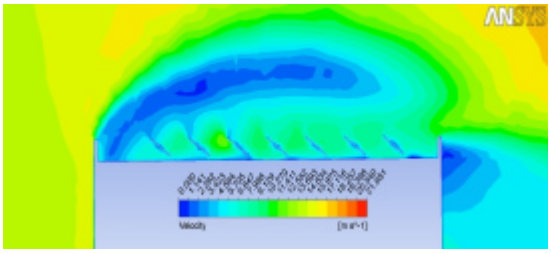

a

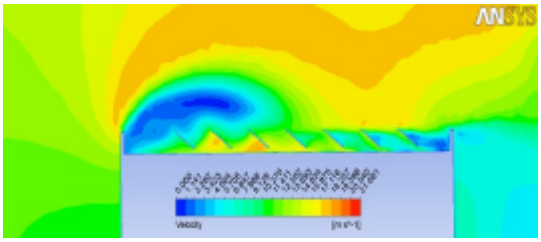

b

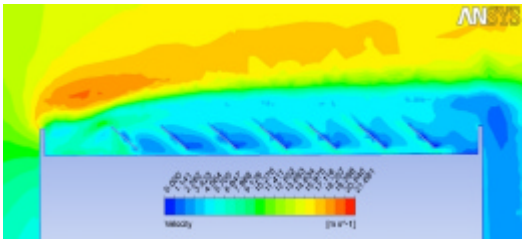

c

Figure 12. Velocity counter in: *a* - right extremity, *b* - central zone, *c* - left extremity of solar panels rows, for building with parapet

5. CONCLUSIONS

Oblique direction of wind action is an unfavorable case, generating high intensity of uplift forces in the corner areas of the flat roof, forces which bring an additional load on support systems of solar panels. Placement of solar panels to a height of 20 cm above the roof level, allows infiltration of streamlines under rows of solar panels. In the middle of the roof, where conical vortexes influence is lower; on active face of solar panels appear positive values of pressure. Building height has an important role in the pressure distribution on the roof and panels arrays.

Presence of the parapet helps to mitigate the wind loads, and increase the shelter effect.

References

1. Wood G.S., Denoon R.O., Kwok K.C.S., *Wind Loads on Industrial Solar Panel Arrays and Supporting Roof Structure*. Wind & Structure, 4, *6*, 481-494 , 2001.
2. Blackmore, P., BRE Digest 498, Wind loads on roof-based photovoltaic systems, 2004
3. Radu A., Axinte E., Theohari C., Steady wind pressures on industrial solar collectors on flat-roofed buildings, Journal of Wind Engineering and Industrial Aerodynamics vol. 23, pp 249-258, 1986
4. Radu a., Axinte E., Wind forces on structures supporting solar collectors, Journal of Wind Engineering and Industrial Aerodynamics vol. 32, pp 93-100, 1989
5. Axinte E., Modelarea fizica a interactiunii vant-structura pentru proiectarea captatoarelor solare, teza de doctorat, Universitatea Tehnica "Gheorghe Asachi", Iasi, 1988
6. Franke J., et al., Recomandation of the use CFD in wind engineering, Proceeding of the International Conferinces on Urban Wind Enineering and Building Aerodybamics, Belgium, 2004
7. *** SR EN 1991-1-4/2006, Eurocod 1: Actiuni asupra structurilor. Partea 1-4: Actiuni generale-Actiuni ale vantului

Multidirectional energy dissipative columns

Vasile-Mircea Venghiac
Department of Structural Mechanics, "Gh. Asachi" Technical University, Iasi, 700050, România

Summary

The Slimdek composite flooring system was created and is widely used in Great Britain where there is no seismic activity. In recent years, countries situated in seismic areas showed great interest in this type of composite flooring system. This raises the problem of energy dissipation. Plastic hinges cannot develop in the beams due to the fact that they are encased in concrete. Thus, the behaviour of the Slimdek flooring system is similar to the behaviour of flat slabs. In order to absorb the seismic energy, multidirectional dissipative columns are proposed. These columns show great potential for energy dissipation in new or existing buildings with Slimdek composite floors or flat slabs.

KEYWORDS: yielding steel damper, energy dissipative column, cyclic loading, Slimdek, composite floor.

1. INTRODUCTION

The Slimdek composite floor was conceived and is widely used in Great Britain. It consists of encasing asymmetric section beams in concrete by placing the steel decking on the bottom flange of the beams as shown in figure 1.

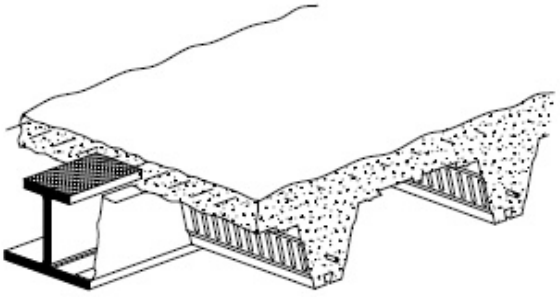

Figure 1. Slimdek composite flooring system [4].

The floors can reach up to 9 m spans without the need of secondary beams. This type of composite flooring system presents many advantages, as the following:

- Reduced height of the structural system. This reduces the cost of claddings;
- Ease of service integration. The services can be accommodated within the thickness of the slab, between the ribs of the decking;
- Good fire resistance. A fire resistance of 60 minutes can be achieved without any supplementary fire protection [3].

Countries in seismic areas, such as New Zeeland, showed great interest in this type of composite floor. Plastic hinges cannot develop in the beams of the Slimdek composite floor, making this system similar to flat slabs. The seismic energy must be absorbed by using damping devices. There are many types of dampers available, such as ADAS (Added Damping and Stiffness), TADAS (Triangular plate Added Damping and Stiffness), DFMD (Dual Function Metallic Damper), Pall, Damptech, Sumitomo etc.

2. OBJECTIVES AND SCOPE OF WORK

The author proposes a new type of metallic damper called “multidirectional energy dissipative column” or MDC. This type of device has the advantage of absorbing the seismic energy within the column, without the need of additional braces which can obscure the window area.

The main objective is to investigate the capacity of energy dissipation of the proposed device. The hysteretic behaviour of the device is also analyzed.

3. MDC MODELS

Unlike “energy dissipative columns” analysed before [5-7], the MDC device is capable of dissipating the seismic energy on all directions. It consists of using a circular hollow section with dissipative elements placed at each end of the column. The dissipative elements are made of circular hollow sections with different types of holes. The size, shape and position of the holes are designed so that the plastic stresses would appear on the whole dissipative element in order to achieve good energy dissipation.

Eight models are considered with different types of holes in the dissipative element (figure 2), as follows:

- Model MDC1: 24 slits (10x200 mm);

- Model MDC2: 24 slits (10x30 mm) on 5 rows;
- Model MDC3: 24 circular holes (Ø10 mm) on 8 rows;
- Model MDC4: 24 circular holes (Ø15 mm) on 8 rows;
- Model MDC5: 24 circular holes (Ø20 mm) on 8 rows;
- Model MDC6: 24 circular holes (Ø20 mm) on 8 rows with cross layout;
- Model MDC7: 24 circular holes (Ø20 mm) on 10 rows;
- Model MDC8: 24 circular holes (Ø20 mm) on 15 rows.

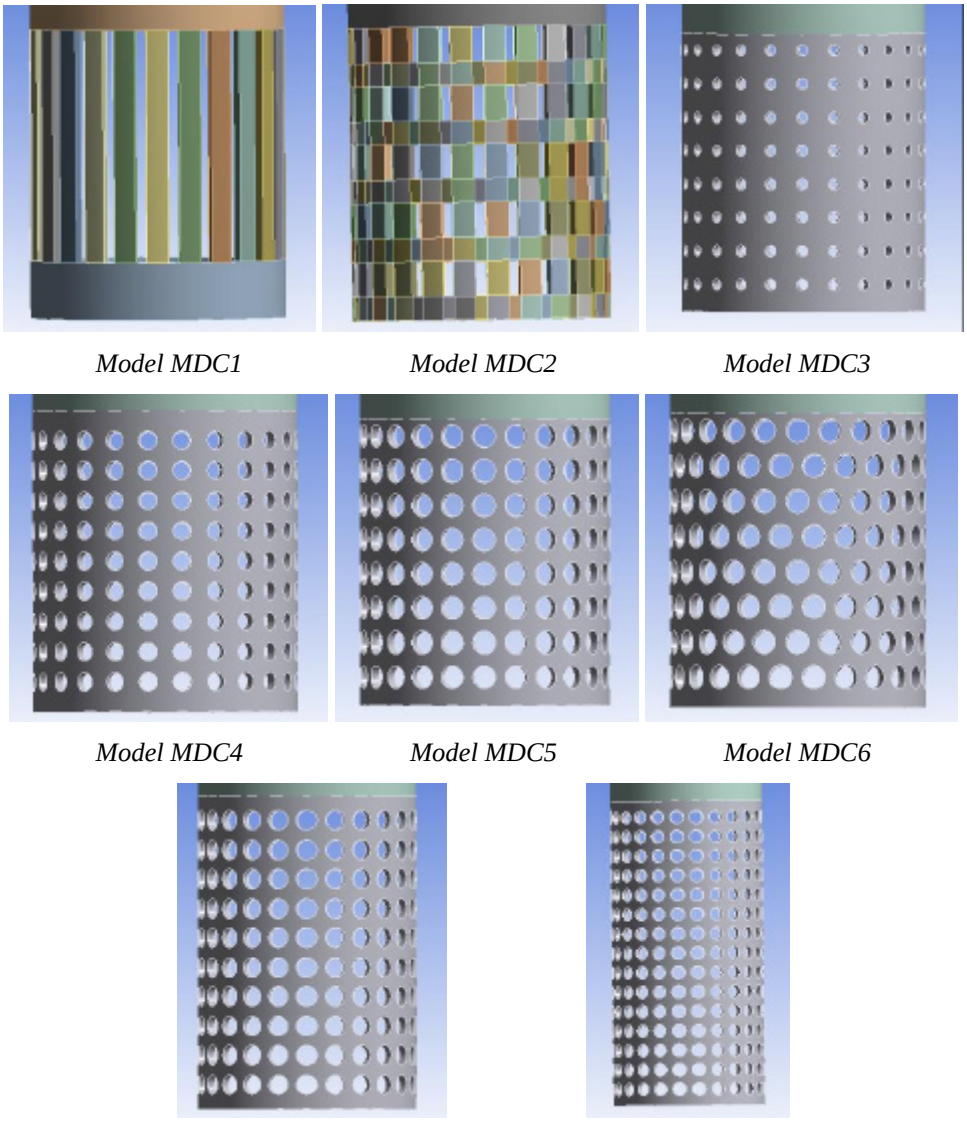

Figure 2. MDC models in ANSYS [1].

The program used for the analysis is ANSYS v12. The considered models have the following characteristics:

- the circular hollow section is 219.1x8 mm [2];
- the height of the column is 3.00 m;
- the steel grade is S235;
- the action is an imposed displacement of 25 mm according to the graph shown in figure 3.

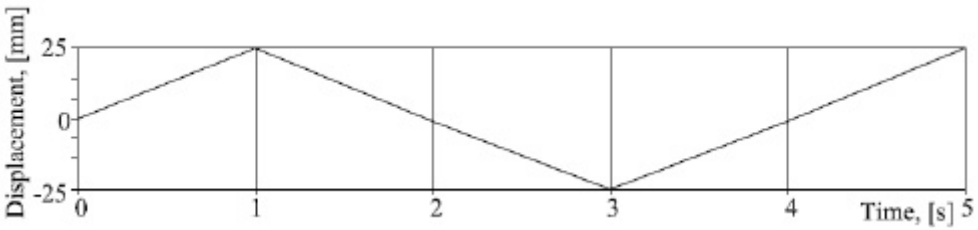

Figure 3. Imposed displacement.

4. RESULTS

The hysteretic loops for models MDC1 and MDC2 are presented in figure 4. Model MDC2 has a better energy dissipation capacity and also a bigger rigidity. The disadvantage of this model is the difficulty of creating the slits.

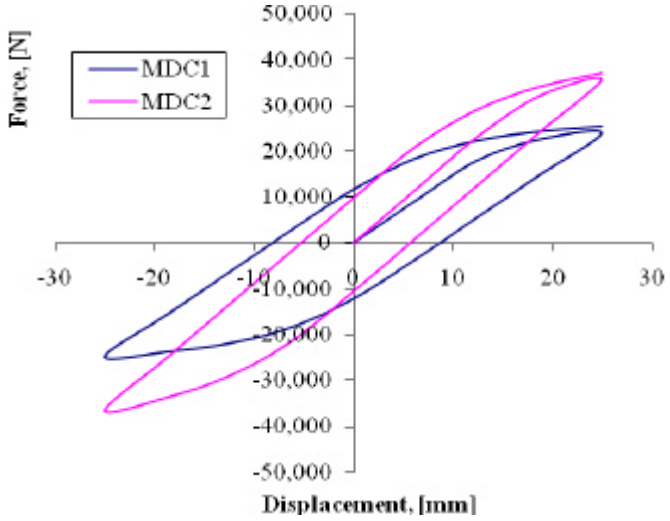

Figure 4. Hysteretic loops for models MDC1 and MDC2.

Models MDC3, MDC4 and MDC5 differ in hole size. The hysteretic loops are presented in figure 5.

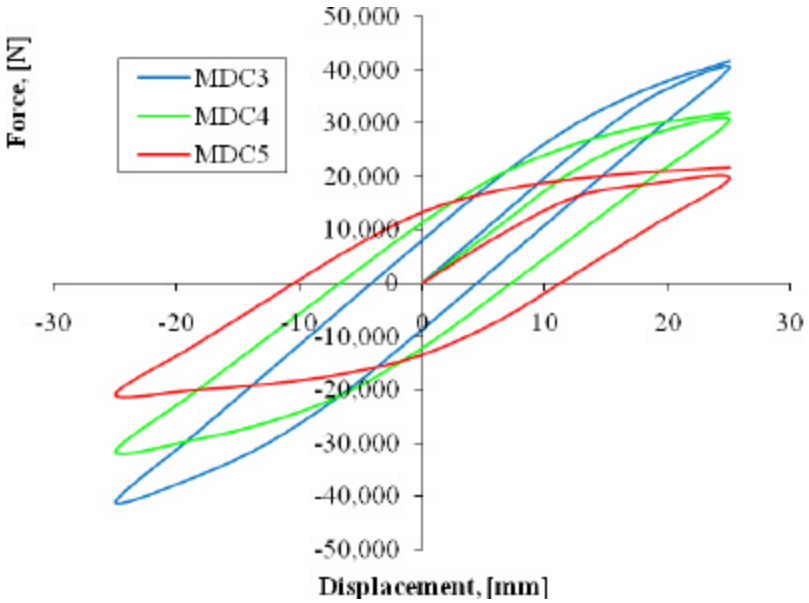

Figure 5. Hysteretic loops for models MDC3, MDC4 and MDC5.

Models MDC5 and MDC6 have different types of hole layouts. By analyzing their hysteretic loops (figure 6) it can be concluded that model MDC5 has a better energy dissipation capacity. Also, the different hole layouts have no influence on the rigidity of the element.

Models MDC5, MDC7 and MDC8 differ by the dissipative element length. The hysteretic loops in figure 7 outline the fact that plastic deformations are better distributed on a shorter dissipative element. Also, the rigidity of the device is decreased by increasing the length of the dissipative element.

The equivalent stresses (von-Misses) of the MDC models are presented in figure 8 and the values of the total dissipated energy for each model are presented in table 1.

Table 1. Total dissipated energy

Model	MDC1	MDC2	MDC3	MDC4	MDC5	MDC6	MDC7	MDC8
Total dissipated energy [J]	1111.7	1183.6	1178	1234.1	1147.5	1092.5	1080.9	956.7

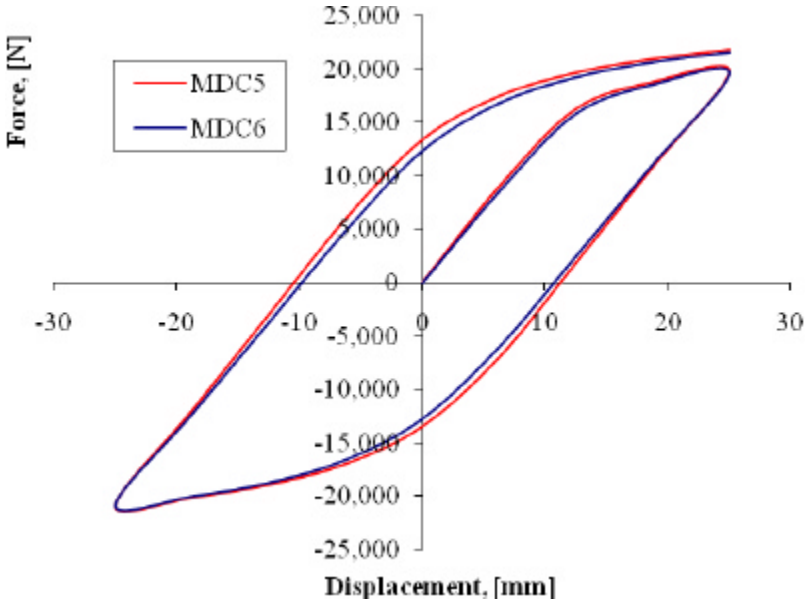

Figure 6. Hysteretic loops for models MDC5 and MDC6.

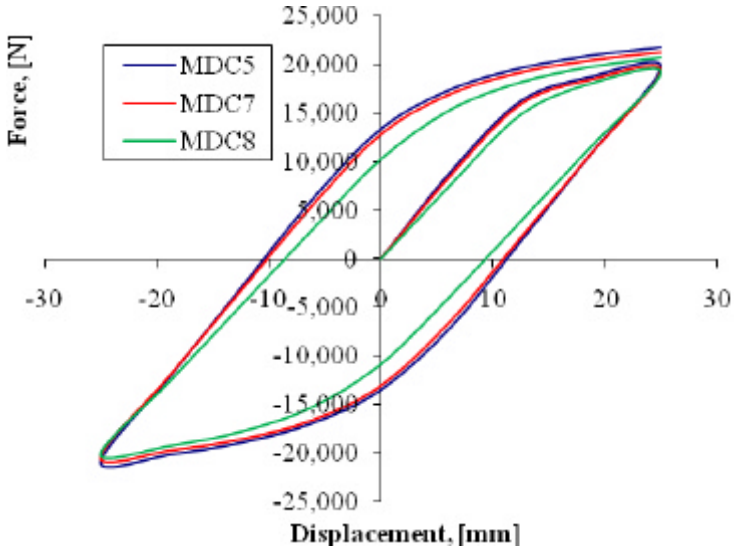

Figure 7. Hysteretic loops for models MDC5, MDC7 and MDC8.

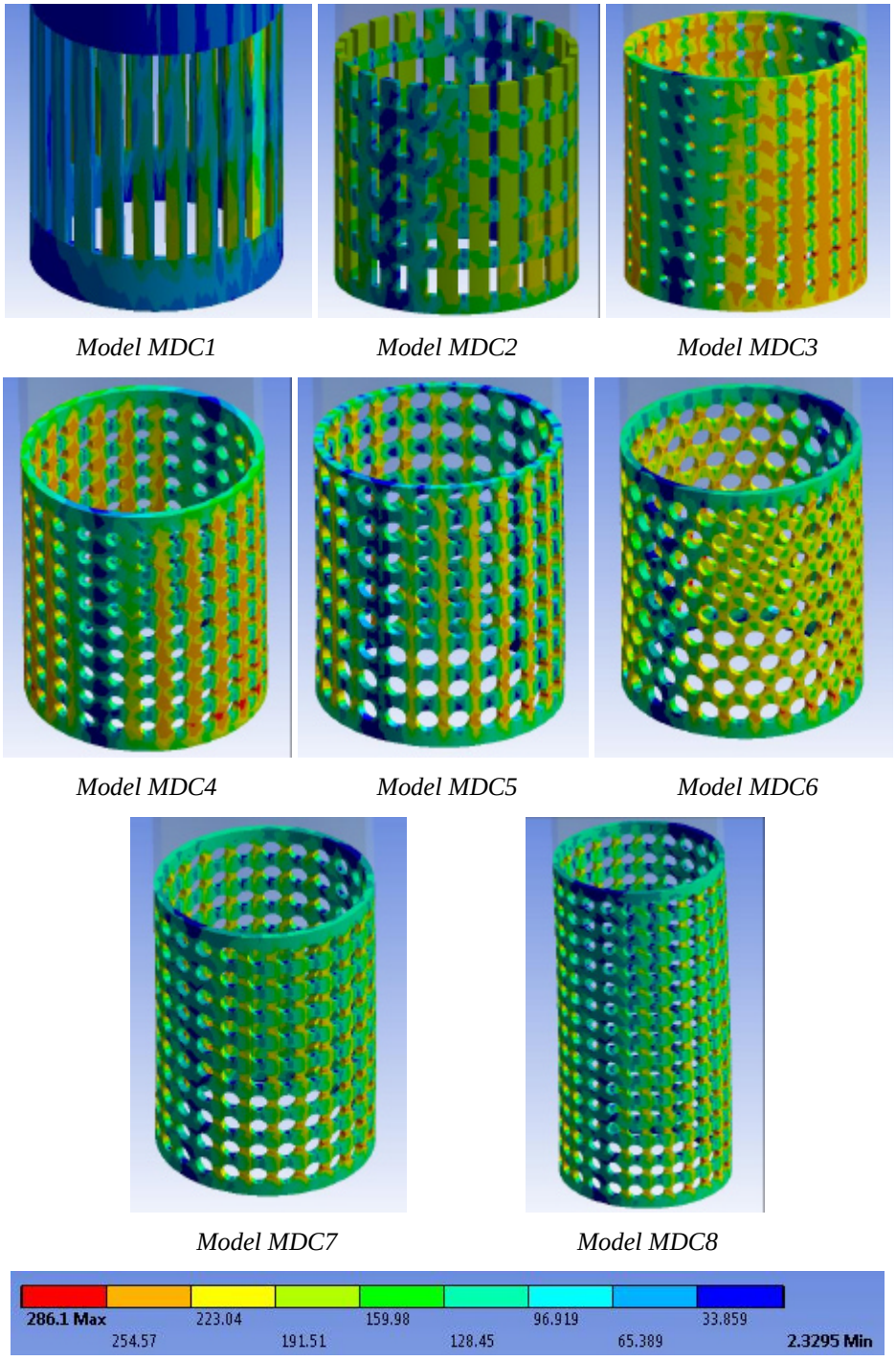

Figure 8. Stresses in MPa in the dissipative elements of the MDC models [1].

5. CONCLUSIONS

The multidirectional energy dissipative columns show great potential for energy dissipation at structures with Slimdek composite floors. The shape of the hysteretic loops of all MDC models analyzed in this paper is symmetric, which means that the behaviour of these devices is stable and predictable in time. These devices can be used either as earthquake dampers or as wind dampers. The variety of hole shapes and sizes allows the structural engineer to fully control the rigidity and energy dissipation capacity of the MDC device.

References

1. ANSYS, User's Manual Revision 11, ANSYS, Inc., Canonsburg, PA, 2009.
2. DIN EN 10210-2. *Hot finished structural hollow sections of non-alloy and fine grain steels – Part 2: Tolerances, dimensions and sectional properties*, Beuth Verlag, Berlin, Germany, 2006.
3. Hicks, S. J., Lawson, R. M., Rackham, J. W., Fordham, P. *Comparative structure cost of modern commercial buildings – Second Edition*, The Steel Construction Institute, UK, 2003.
4. Rackham, J.W., Couchman, G.H., Hicks, S.J. *Composite Slabs and Beams using Steel Decking: Best Practice for Design and Construction (Revised Edition)*, The Steel Construction Institute and The Metal Cladding & Roofing Manufacturers Association, ISBN: 978-1-85942-184-0, UK, 2009.
5. Venghiac, V.M., Budescu, M. *Optimization methods of energy dissipative columns*, Buletinul Institutului Politehnic din Iasi, Sectia Constructii. Arhitectura, Tomul LVII, Fasc. 4, ISSN 1224-3884, pp. 33-41, 2012.
6. Venghiac, V.M., Ciongradi, I.P., Budescu, M. *Steel structures with composite floors and energy dissipative columns*, Proceedings of The 8th International Symposium „Computational Civil Engineering 2010 – New Computational Concepts in Civil Engineering", Editura Societatii Academice „Matei – Teiu Botez", ISBN 978-973-8955-87-5, pp. 459-466, Iasi, 2010.
7. Venghiac, V.M., Melenciuc, S.C., Ciongradi, I.P., Budescu, M. *The influence of solid dry friction damping at columns with compound sections*, Buletinul Institutului Politehnic din Iasi, Sectia Constructii. Arhitectura, Tomul LVII, Fasc. 1, ISSN 1224-3884, pp. 47-54, 2011.